A Combined Material and Structural Approach to Fatigue Failure Analysis of Bolted Thick Composite Laminates

Hamid Hamidi

A Thesis

In the Department of

Mechanical, Industrial and Aerospace Engineering

Presented in Partial Fulfillment of the Requirements

For the Degree of

Doctor of Philosophy (Mechanical Engineering) at

Concordia University

Montréal, Québec, Canada

May 2019

CONCORDIA UNIVERSITY

SCHOOL OF GRADUATE STUDIES

This is to certify that the thesis prepared

By: **Hamid Hamidi**

Entitled: **A Combined Material and Structural Approach to Fatigue Failure Analysis of Bolted Thick Composite Laminates**

and submitted in partial fulfillment of the requirements for the degree of

Doctor of Philosophy (Mechanical Engineering)

Complies with the regulations of the University and meets the accepted standards with respect to originality and quality.

Signed by the final examining committee:

______________________ Chair
Dr. Zhibin Ye

______________________ External Examiner
Dr. Ramesh Talreja

______________________ External to Program
Dr. Khaled E. Galal

______________________ Examiner
Dr. Martin Pugh

______________________ Examiner
Dr. Farjad Shadmehri

______________________ Thesis Co-Supervisor
Dr. Suong Van Hoa

______________________ Thesis Co-Supervisor
Dr Rajamohan Ganesan

Approved by: ______________________
Dr. Ivan Contreras, Graduate Program Director

August 27, 2019 ______________________
Dr. Amir Asif, Dean,
Gina Cody School of Engineering and Computer Science

Abstract

A Combined Material and Structural Approach to Fatigue Failure Analysis of Bolted Thick Composite Laminates

Hamid Hamidi, PhD

Concordia University, 2019

Most of the existing works on fatigue of long fiber composite laminates approach the problem from the material point of view. These works have also been mainly on thin laminates. This is because the laminates (particularly unidirectional laminates) are considered to be homogeneous and uniform. This may or may not be true because of the heterogeneous nature of the composite (consisting of fibers and matrix and interface), and the significant variability which gives rise to random spatial variation in the properties. A composite laminate is actually both a structure and a material. For thin laminates, the structural aspect is usually scanned over and only the material aspect is focused on. This gives rise to the expectation that the laminate should behave as a material (with good homogeneity and with little variability). This has resulted in failure of many failure criteria.

The importance of the structural aspect is more evident for the case of thick laminates, subjected to flexural loading while being constrained by bolts. To study the fatigue behavior of such materials (and structures), both the structural aspects and the material aspects must be taken into consideration. This is the subject of study of the present research. A combined material and structural approach, namely, the application of coupon level material properties (material level) into the 3D finite element model (structural level) is introduced and applied. By doing this, it examines the behavior of thick unidirectional glass/epoxy laminates subjected to flexural loads while being constrained by bolts. Both theoretical and experimental studies are carried out to validate each other. The theoretical part consists first of structural analysis which provides the

locations of potential failure. This is followed by the application of fatigue failure criteria at these locations. Good correspondence is seen between the experimental and the theoretical results.

The agreement between the results of experiments with those of developed fatigue progressive damage modeling (FPDM) shows that the combined material and structural approach is suitable to study the fatigue behavior of thick composite laminates subjected to bolt loads.

Keywords: Fatigue; Thick Composite Laminates; Finite Element Analysis; Fatigue Progressive Damage Modeling (FPDM)

Acknowledgment

I would like to express my deep gratitude to Professor Suong Van Hoa and Professor Rajamohan Ganesan, my research supervisors, for their patient guidance, enthusiastic encouragement and useful critiques of this research work.

Special thanks to Professor Hoa whose willingness to give his time so generously was truly helpful from the beginning to the end of this work. The door of his office is always open to his students. I have been so lucky to get the chance for being supervised by Dr. Hoa as the most professional and caring professor of my whole life.

My grateful thanks are also extended to Professor Ganesan, for his invaluable advice and assistance in conducting the project in the right direction, for his help in doing the computational analysis and critical review of the thesis.

I would also like to thank my examining committee members, Dr. Ramesh Talreja, Dr. Khaled E. Galal, Dr. Martin Pugh and Dr. Farjad Shadmehri for their helpful comments.

This research has been conducted by financial supports of Natural Sciences and Engineering Research Council of Canada (NSERC), Le Consortium de recherche et d'innovation en aérospatiale au Québec (CRIAQ) and Bell Helicopter Textron Inc.

Also, many thanks for all members of Concordia Center for Composites (CONCOM) for their help in completing my work. I wish to thank all friends in particular Dr. Alireza Gorjipoor, Mr. Jeffrey Fortin Simpson, Ms. Wendy Xiong, Dr. Hamidreza Yazdani Sarvestani, Dr. Iosif Daniel Rosca, Dr. Yasser Mahmoud Sami Abdelsamea Elsherbini and Mr. Heng Wang for their support and help to accomplish my work.

Most importantly, none of this would have been possible without the love and patience of my family. I would like to express my love and gratitude to my parents for their moral support during this work. Unfortunately, my mother is not alive to watch me completing this work, but I am so confident that her soul continues to support me and enjoy this moment. May God Bless Her. My older brother Saeid has also passed away whose attention and consideration were always with me during my whole studying life. May God Bless Him.

Lastly, most of all for my loving, supportive, encouraging, and patient wife Mehrnaz Mohajer Jasbi and my son Rambod and my daughter Raya whose faithful support during all the stages of this research is so appreciated. Thank you so much.

Dedication

This thesis is dedicated:

To the Memory of my Mother

To the Memory of My Brother

To my lovely and supportive wife, Mehrnaz

To my lovely kids, Rambod and Raya

Contents

Nomenclature

$1,2,3$	Material Coordinate System (1: Fiber Direction, 2: Transverse Direction, 3: Thickness Direction)
$\sigma_{ij};i,j=1,2,3$	Triaxial Normal Stress Components
$\tau_{ij};i,j=1,2,3,i\neq j$	Triaxial Shear Stress Components
$\varepsilon_{ij};i,j=1,2,3$	Triaxial Strain State
$u_i;i=1,2,3$	Displacement Vector
$E_{ii};i=1,2,3$	Modulus of Elasticity
$G_{ij};i,j=1,2,3,i\neq j$	Shear Modulus
$\nu_{ij};i,j=1,2,3,i\neq j$	Poisson's Ratio
$\sigma^S_{iiJ},i=1,2,3,J=T,C$	Static Tensile an Compressive Strength
$\tau^S_{12},\tau^S_{13},\tau^S_{23}$	Static Shear Strength
$\sigma^F_{iiJ},i=1,2,3,J=T,C$	Residual Tensile and Compressive Strength
$\tau^F_{ij},i,j=1,2,3,i\neq j$	Residual Shear Strength
$\sigma^{\min}_{ij},i,j=1,2,3$	Minimum Cyclic Stress
$\sigma^{\max}_{ij},i,j=1,2,3$	Maximum Cyclic Stress
$R=\sigma^{\min}_{ij}/\sigma^{\max}_{ij}=0.1$	Stress Ratio (R is kept constant)
$\sigma_a=(\sigma^{\max}_{ij}-\sigma^{\min}_{ij})/2$	Alternating Stress
$\sigma_m=(\sigma^{\max}_{ij}+\sigma^{\min}_{ij})/2$	Mean Stress
N	Number of Cycles
N_f	Fatigue life at corresponding applied stress level
θ	Off-axis Angle
u_{ult}	Average Static Ultimate Flexural Displacement
$u_{\max}$	Maximum Flexural Displacement
$u_{\min}$	Minimum Flexural Displacement
FPDM	Fatigue Progressive Damage Modeling
LRR	Load Ratio Reduction
EDL	Endurance Deflection Level
DFM	Dominant Fatigue Failure Mechanism

List of Figures

List of Tables

Chapter 1. Introduction and Literature Survey

The aim of the present research is the investigation of fatigue failure initiation and propagation in bolted thick composite laminates. For the case of thin laminates, there are many different failure modeling techniques available in the literature which are mostly based on fatigue failure modeling of isotropic materials. Variety of failure mechanisms in thin composites however introduces limitations in their application. The main difference between fatigue failure mechanisms in orthotropic composites with that of isotropic materials is that in isotropic materials fatigue failure initiates from surface locations and some initiated cracks propagate to final failure. In composites, however, a kind of failure aggregation happens, meaning that the failure initiates at different locations and propagates in different paths. For this reason, various modeling techniques have been introduced for the case of fatigue failure of thin composite laminates. These techniques also consider only the material aspect of the fatigue failure. For the case of thick composite laminates, however, the structural aspects should also be taken into account.

In this chapter a combined material and structural approach is introduced to study the fatigue behavior of bolted thick composite laminates. For the material aspect, the available fatigue failure modeling techniques for thin composite laminates are investigated out of which fatigue life model based on quadratic failure equations is selected. To activate the failure equations the material is characterized in coupon level experiments. To take the structural aspect of thick composite laminates into account a 3D finite element model is developed which is used to identify both the locations of damage initiation and the damage mechanisms. The detail of 3D model will be explained in Chapter 2. Material properties obtained from characterization experiments are introduced in the 3D finite element model. The combination of material aspect and the structural aspect helps to understand the fatigue behavior of bolted thick composite laminates under flexural loading.

1.1. Fatigue Failure Modeling of Thin Composite Laminates

The primary reason for popularity of composite materials is their high specific stiffness and strength (stiffness and strength with respect to the density) enabling them to have large field of applications especially in aerospace, automobile and marine structures. In these applications, cyclic loadings which cause fatigue failure of structures need to be considered.

Fatigue is the main failure mechanism for structures under cyclic loading. Considerable research has been carried out for monolithic materials such as metals and progress has been made in devising fatigue-resistant materials as well as in developing methodologies for life prediction. Fatigue in metals occurs by initiation of single crack which propagates until catastrophic failure occurs. In contrast to metal, damage build up in composite is in global fashion rather than localized fashion.

Claude Bathias [1] summarized the fatigue behavior differences of composite materials versus metals. In the microscopic level, the fatigue damage in metals usually is created near surfaces because of slippage of layers and dislocations. Some of these surface cracks then propagate in a path perpendicular to the loading direction until final failure. However, the fatigue damage initiation and propagation in fiber reinforced composites is totally different. Generally, under cyclic loading some cracks are initiated in the matrix before fracture of fibers. These are microcracks with the initial thickness of one ply. The single cracks then coalesce to form the damage. After a certain crack density is reached, the delamination is developed leading to fiber fracture. Another main difference between fatigue of composites and metals is the difference of the endurance curve. The slope of endurance curve is less for composites than metals. Furthermore, the shape of endurance curve for metals is quasi-hyperbolic while the type of the endurance curve for composites is low-slope type, as shown in Figure 1-1.

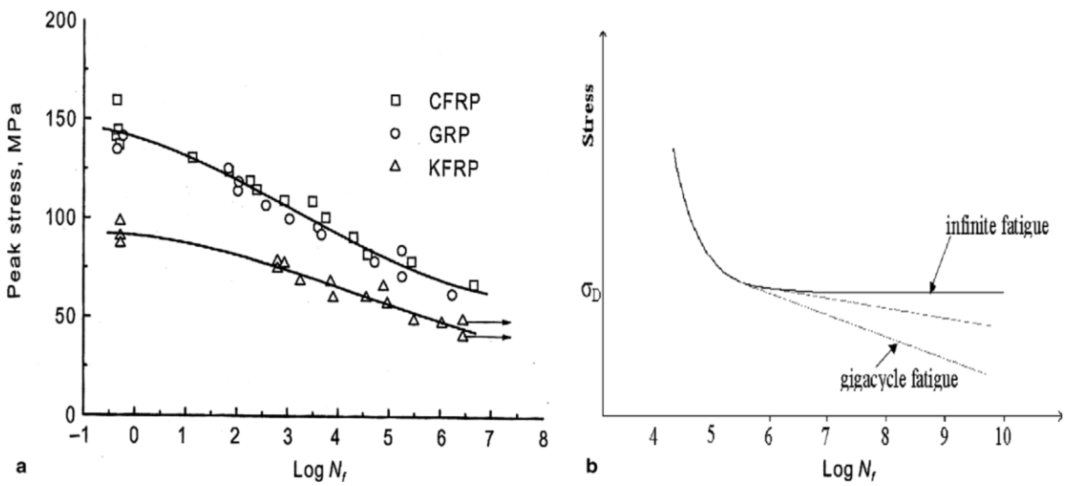

Figure 1-1 Comparison of the S–N curve shape for composites and metals: (a). stress/loglife curves for composite materials; and (b) stress/loglife curves for metals [1].

Metals and composites behave differently under different loading conditions as well. For example, metals are less sensitive to failure due to cyclic compressive loading because these loadings help to close the crack tips. However, for composites under cyclic compressive loading, damages initiate as fiber micro-buckling [2]. It is also well-known that metals under cyclic loading are notch sensitive while this phenomenon is practically un-known for composites.

For composite materials, fatigue analysis and consequent life prediction become difficult because the material properties of the constituents of the composite are quite different. The fatigue behavior of one constituent may be significantly affected by the presence of other constituents and the interfacial regions between the fibers and matrix. Fatigue properties of composites may vary significantly due to the large difference in the properties between the fibers and matrix and the composition of constituents [3].

In general, there are mainly two groups of internal and external parameters affecting the fatigue behavior of fiber reinforced composites. As the internal parameters one can refer to type of fibers, type of matrix and stacking sequence. At the other side the external parameters can be mentioned such as loading conditions and environmental parameters.

Fibers are the main load carrier constituents in the composites. Therefore, it is inherent that the type of fibers will affect the composite fatigue behavior. Regarding the type of matrix materials, there are many research-works stating that the fatigue strength of glass fiber reinforced composites is significantly dependent on the properties of the resin [4]. Fatigue damage initiation starts as cracks in the matrix material. Two common types of polymer matrices are thermosets and thermoplastics. From the fatigue strength point of view, thermoplastic resins have some advantages compared to thermosets in terms of ductility and toughness [5]-[7]. Thermoplastic resins provide longer fatigue life [7]. The other advantage of a tougher resin is its higher inter-laminar fracture toughness which will result in increased fatigue resistance against delamination [8]. The fracture toughness of fiber-reinforced composite is affected by the interface between matrix and fiber as well. Weaker interface tends to improve the fracture toughness by resisting the crack to propagate through the matrix, and reduces the effectiveness of the stress transfer [9].

Failure mechanisms of composite materials can be categorized in four major groups, fiber breakage, matrix cracking, fiber-matrix Interfacial debonding and delamination. Fiber failure happens under both tensile and compressive loading. The former is directly dependent on the fiber tensile strength. However, for the case of fiber breakage under compression, fiber's compressive strength is not playing a significant role. This failure mode depends mostly on fiber stability such as micro-buckling and kinking. Micro-buckling and kinking normally occur at free edges or areas at the vicinity of voids. This failure mode is mainly because of misalignment of fibers [10]. Matrix failure occurs under two failure modes. Inter-fiber (Intra-laminar) matrix fracture and inter-laminar fracture. Inter-fiber fracture initiates from the debonding of fibers and matrix and inter-laminar failure occurs between plies.

The interface between the fiber and matrix is critical for the function of the composite material. The interface may be considered as a third constituent of the material in addition to fibers and matrix. Failure of the interfacial bond occurs due to slipping between fibers and matrix which causes interfacial debonding [11]. Delamination on the other hand is caused by inter-laminar stress, which is a direct effect of micro-cracks in the resin [10].

The sequence of these failure modes depends on the type of composite laminate. As an example, one can refer to unidirectional composites. The fatigue behavior of these composites under tension-tension fatigue loading is mainly related to the strength of fibers and their alignment. In a perfectly aligned fiber reinforced unidirectional composites, in the early stage of fatigue loading the matrix cracks initiates along the fiber directions [12], [13]. Continuing cyclic loading causes cracks growing and accumulation which leads to stress concentration regions. After a certain number of cycles the stress state reaches the residual strength of the material and then final failure occurs.

For the case of multidirectional composites, two known features of cross- ply and angle-ply laminates can be referred. Harris [14] presented the damage progression in cross- ply laminates starting from matrix cracks in each ply ending in delamination and fiber breakage.

There are other types of composites in 3D format which can be referred as woven, stitched, z-pinned, braided and knitted composites. In comparison to 2D composites, 3D composites are known to have higher delamination toughness and impact damage resistant [15]-[17]. However, application of z-binders causes the resin rich areas to give rise to microstructural damages in the form of local in-plane distortion, fiber breakage and crimping [15].

The purpose of this section is to review existing fatigue modeling techniques and failure criteria of thin composite laminates in order to study the material aspect of fatigue failure initiation and propagation in thick composite laminates.

According to the literature [18], available fatigue failure models on thin composite laminates can be categorized in three major groups of *Fatigue Life Models*, *Phenomenological Models* and *Progressive Damage Models*, the fundamentals of which are mentioned and one reference article for each group is outlined in detail.

1.1.1. Fatigue Life Models

Fatigue life models do not consider the degradation mechanisms, but they use S-N curves or Goodman type diagrams to introduce some sort of failure criteria. The basic approach is similar to fatigue behavior investigation of metals [18]. One of the earliest fatigue life models for composites was introduced by Hashin and Rotem [3]. There are currently several fatigue life models available in the literature. Jen and Lee [19], [20] adopted Tsai-Hill failure criterion along with classical laminate theory (CLT) to investigate the fatigue response of AS4/PEEK APC-2 composites due to various stress ratios at room temperature and moisture. They observed good agreement between experimental results and proposed criterion. Philippidis and Vassilopoulos [21] modified Tsai–Hill criterion to develop a deterministic fatigue life model following the idea of developing available static failure criteria to cyclic loading. They validated proposed model through static and fatigue tests on glass/polyester off-axis specimens cut from multidirectional laminates. There was good correlation between experimental values and theoretical predictions. A fatigue life model based on the microstructural level was presented by Reifsnider and Gao [22]. The proposed model determines the failure of the composites by considering the interactions between the fibers and the matrix, as well as the interfacial bonding in the micromechanical analysis. Fawaz and Ellyin [23] developed a model that is able to predict the S-N curve of multi-directional (MD) laminate with arbitrary ply orientation based on S-N curve of a laminate with fibers aligned in one orientation (uni-directional, UD). Paramonov et al.[24] successfully developed a statistical fatigue life model which can predict the minimum and maximum number of cycles to failure of a composite structure. Jeon et al [25] evaluated the fatigue life and strength of a composite bogie frame for urban subway train. They performed fatigue test on bogie frame specimens to obtain S-N curves under tension-compression loading conditions and constructed Goodman type diagrams for predicting the failure. Park et al [26] developed a nonlinear constant life formulation to estimate more accurate S–N curves comparing previously developed linear constant life diagrams (CLD). Constant life diagrams can predict stress-life curves for various stress ratios under variable amplitude loading by using limited fatigue experimental data.

Having said that, the usefulness of the S-N curves to represent the resistance of a given material to the cyclic application of loads is questioned by R. Talreja and C. V. Singh [27-28]. The reason is mentioned as in application of S-N curves the role of constituent materials are not represented.

To resolve the issue, Talreja proposed a framework for conceptual interpretation of fatigue of composite materials emphasizing on the role of fibers and matrix as the constituent material of the composite.

1.1.1.1. Fatigue Life Based Model- Hashin Fatigue Failure Criteria

Regarding oscillatory state of combined plane stress loading the earliest criterion was proposed by Hashin and Rotem [3]. They presented a quadratic approximation theory. Their criterion was expressed in terms of three S-N curves, including variation of tensile off-axis fatigue failure stress for different off-axis angles, variation of transverse normal failure stress and the variation of shear failure stress versus number of cycles. The authors obtained the curves from fatigue testing of off-axis unidirectional specimens under uniaxial oscillatory load. They performed an extensive series of tests demonstrating good agreement of the failure criteria with experimental data.

Hashin continued to develop above mentioned quadratic approximation to unidirectional reinforced composites subjected to three-dimensional cyclic stress on the basis of transverse isotropy of the material [29]. He distinguished two different failure modes of fiber failure and matrix failure. In order to make this intersection between failure modes, he considered only the state of completely reversed cyclic loading.

Hashin Fatigue Failure Criteria (2D)

As mentioned above, Ref. [3] describes two different failure modes for lamina: Fiber Failure Mode and Matrix Failure Mode. Hashin failure criterion for cyclic loading is outlined as following. It should be noted that the notations have been changed due to have consistency in the whole thesis.

$$\sigma_{11} = \sigma_{11T}^{F} \tag{1-1}$$

$$\left(\frac{\sigma_{22}}{\sigma_{22T}^{F}}\right)^2 + \left(\frac{\sigma_{12}}{\tau_{12}^{F}}\right)^2 = 1 \tag{1-2}$$

where σ_{11} and σ_{22} are applied normal stress at axial and transverse on-axis directions and σ_{12} is the shear stress. σ_{11T}^{F}, σ_{22T}^{F} and τ_{12}^{F} are fatigue failure stresses which are functions of cyclic stress ratio, number of cycles and loading frequency.

Hashin Fatigue Failure Criteria (3D)

Hashin developed his criterion stated above for three-dimensional combined stress state for uni-directional composites in terms of quadratic stress polynomials considering transversely isotropy of the material [29]. The material behavior as S-N Curves for simple loadings is needed for combined stress state. Hashin distinguished the failure modes as Fiber Failure Mode and Matrix Failure Mode and presented the fatigue failure functions to be as following for the fiber failure mode:

$$F_f(\sigma_{11}, \sigma_{12}, \sigma_{13}, R, N) = 1 \tag{1-3}$$

And for the matrix failure mode:

$$F_m(\sigma_{22}, \sigma_{33}, \sigma_{12}, \sigma_{23}, \sigma_{13}, R, N) = 1 \tag{1-4}$$

Introducing these failure functions, Hashin failure criteria for reversed cycling is summarized below:

Failure criterion for fiber failure mode:

$$\left(\frac{\sigma_{11}}{\sigma_{11T}^{F}}\right)^2 + \frac{\sigma_{12}^2 + \sigma_{13}^2}{(\tau_{12}^{F})^2} = 1 \tag{1-5}$$

Failure criterion for matrix failure mode[2]:

$$\frac{(\sigma_{22} + \sigma_{33})^2}{(\sigma_{22T}^{F})^2} + \frac{\sigma_{12}^2 + \sigma_{13}^2}{(\tau_{12}^{F})^2} + \frac{\sigma_{23}^2 - \sigma_{22}\sigma_{33}}{(\tau_{23}^{F})^2} = 1 \tag{1-6}$$

Numerous studies conducted over the past decade indicate that the stress interactions proposed by Hashin do not always fit the experimental results, especially in the case of matrix or fiber in compression [30]. It is well known, for instance, that moderate transverse compression ($\sigma_{22} \prec$) increases the apparent shear strength of a ply, which is not well predicted by Hashin criteria. In addition, Hashin's fiber compression criterion does not account for the effects of in-plane shear, which reduces significantly the effective compressive strength of a ply. Several researchers have proposed modifications to Hashin's criteria to improve their predictive capabilities among which one can refer to modifications proposed by Sun [31] and Puck [32].

1.1.2. Phenomenological Models to Predict Residual Stiffness/Strength

Phenomenological models to predict the fatigue life of composites are based on degradation of a certain material property such as stiffness or strength. These consist of *Residual Strength Models* and *Residual Stiffness Models*.

1.1.2.1. Residual Strength Models

These models are based on strength observations from experiments. Two types of sudden-death and wear-out models can be classified. The former means that the strength of material is kept constant until a certain number of cycles where the strength is degraded drastically to zero. The latter is referring to the case that after reaching to the certain number of cycles, the strength decreases continuously. Some researchers have developed this model for glass reinforced composites. Epaarachchi JA and Clausen PD. [33] presented a model based on strength degradation of material considering the cyclic loading frequency "f" and stress ratio "R" to be independent variables. Sendeckyj [34] presented a function for monotonically decreasing of strength in terms of number of cycles. An attempt was made by Huston RJ. [35] to correlate the fatigue theory of Sendeckyj with the experimental results obtained from unidirectional carbon fiber reinforced epoxy.

1.1.2.2. Residual Stiffness Model

Similar to residual strength models, residual stiffness models deal with stiffness degradation of composite materials through experimental observations. The main difference between fatigue life models, residual strength models and residual stiffness models is that the first two models involve the destruction of test specimen under consideration, where there is no need to destroy the specimen to obtain residual stiffness [36]. In addition, residual stiffness is a well-defined engineering property and it can be easily measured. According to the literature, [37], there is a direct relation between damage developments in the composites with stiffness change. There are some notable stiffness degradation models in the literature among those one can refer to [35]-[38]. Zhang et al. [39] combined the strain failure criterion with Whitworth's stiffness degradation model [37] to introduce a phenomenological model for predicting failure in glass fiber reinforced composite laminates. This model is outlined in the next section.

1.1.2.3. Residual Stiffness Based Model- Zhang Model [39]

For a given specimen, the residual stiffness degradation is assumed to have the form [37]:

$$\frac{dE(n)}{dn} = -E(0)Q\upsilon n^{\upsilon-1} \tag{1-7}$$

where $E(0)$ is initial stiffness, n is the number of loading cycles, Q and υ are parameters dependent on the applied stress, stress ratio and frequency which can be approximated as $Q = a_1 + a_2\upsilon$ where a_1 and a_2 are material constants.

Integration of Equation (1-7) from 0 to N cycles and applying boundary conditions yields,

$$1 - \frac{E(N)}{E(0)} = \frac{a_1 + a_2\upsilon}{f^{\upsilon}}(N^{\upsilon} - 1) \tag{1-8}$$

Because failure stiffness $E(N)$ cannot be determined until the failure of specimen occurs, a strain failure criterion is introduced to substitute the failure stiffness, which assumes that failure occurs when the strain reaches the tensile ultimate strain. This failure criterion is based on the following assumptions: (i) For the case where the stress strain response remains linear to quasi-static failure, the stiffness of the undamaged specimen can be determined as $E(0) = \frac{\sigma_u}{\varepsilon_u}$, where σ_u is the ultimate strength and ε_u is the static ultimate strain. (ii) If the stress strain response remains linear during fatigue cycling, then the stiffness at failure can be defined as $E(N) = \frac{\sigma_{max}}{\varepsilon_f}$, where σ_{max} is the maximum applied stress and ε_f is the strain at fatigue failure. It is assumed that failure occurs when the strain at fatigue failure is equal to the ultimate strain ($\varepsilon_f = \varepsilon_u$), thus the relationship between the failure stiffness $E(N)$ and the applied stress $\sigma_{\max}$ is obtained and modified to account for nonlinear effects as [40]:

$$\frac{\sigma_{\max}}{\sigma_u} = b_1 \left[\frac{E(N)}{E(0)} \right]^{b_2} \tag{1-9}$$

where b_1 and b_2 are constants determined by experiments, $\sigma_{\max}$ is the maximum applied stress and σ_u is the ultimate stress.

After applying the strain failure criterion to Equation (1-8), the following stress-life relationship is obtained as,

$$1 - \left(\frac{\sigma_{\max}}{b_1 \sigma_u} \right)^{1/b_2} = \frac{a_1 + a_2 \upsilon}{f^{\upsilon}} (N^{\upsilon} - 1) \tag{1-10}$$

Equation (1-10) is applied to evaluate and predict the average fatigue life for fiber-reinforced composite materials, where the parameter υ is related to maximum applied stress $\sigma_{\max}$, stress ratio R and frequency f. The porosity and temperature are considered as constants. Consequently υ is defined as a function H as follows,

$$\upsilon = A_1 . H(R, \sigma_{\max}, \sigma_u) \tag{1-11}$$

where A_1 is assumed to be a constant.

The stress ratio R, stress σ_u and $\sigma_{\max}$ are the controlling parameters in fatigue failure mechanism of composites. Many researchers have shown that the effect of R and $\sigma_{\max}$ on the fatigue life of composites is non-linear and discontinuous. Following deterministic model developed by Sendeckyj and Hertzberg was used to postulate the following formulation [39]

$$H(R, \sigma_{\max}, \sigma_u) = \sigma_u^{1-\alpha} \sigma_{\max}^{\alpha} (1 - R)^{\alpha} \tag{1-12}$$

where α is a constant. To account for the fatigue life dependence on fiber angle, α is established as $\alpha = 1.6 - \psi \sin\theta$ where θ is the smallest angle between fiber and loading direction. In the absence of any $0°$ fibers, ψ is defined as: $\psi = R$ for $-\infty < R < 1$ (tension–tension and tension-compression loading), $\psi = \frac{1}{R}$ for $1 < R < \infty$ (compression–compression loading).

Substituting Equation (1-12) into Equation (1-11) yields

$$\upsilon = A_1 . \sigma_u \left(\frac{\sigma_{max}}{\sigma_u} (1 - R) \right)^{1.6 - \psi|sin\,\theta|} \tag{1-13}$$

For a specific composite material, ultimate stress σ_u, the smallest angle θ between the direction of fiber and loading, stress ratio R as well as ψ are all determined. As a result, υ is a function of maximum applied stress $\sigma_{\max}$. Using Equation (1-10), the expression of fatigue life could be written in the form of logarithm as,

$$LogN = \frac{1}{\upsilon} \log \left\{ \frac{1 - (\sigma_{\max} / b_1 \sigma_u)^{1/b_2}}{a_1 + a_2 \upsilon} . f^{\upsilon} + 1 \right\} \tag{1-14}$$

where

$$\upsilon = A_1 . \sigma_u \left(\frac{(1 - R)}{\sigma_u} \right)^{1.6 - \psi|\sin\theta|} . \left(\sigma_{\max} \right)^{1.6 - \psi|\sin\theta|} \tag{1-15}$$

There are five parameters a_1, a_2, b_1, b_2 and A_1 in this model which can be determined by experiment data. Furthermore, only a few straightforward fatigue tests are required at one stress ratio for several stress levels to calculate.

The authors tried to see the effect of different stress ratios and loading frequencies on the fatigue life of composites, as illustrated in Figure 1-2. In Figure 1-2 experimental data from open literature has been used to validate the proposed model. Figure 1-2 shows that the proposed model has good agreement with experimental data. Figure 1-2-a indicates the effect of increasing stress ratio in tension-tension fatigue life. According to the predicting model, it is found that for a given maximum stress the tension-tension fatigue life of glass fiber reinforced polymer composite increases with the increasing stress ratio R.

Figure 1-2-b indicates that the fatigue life of GFRP composite increases when the frequency f is higher, providing the temperature of specimen is controlled inside an environmental chamber to remain unchanged. The model adequately addresses the non-linear effect of frequency on the fatigue life of the composites at isothermal conditions.

Due to the viscoelastic property of matrix materials, it has been found that most of the polymer composites show increased fatigue life when the load frequency increases at a constant room temperature. However, in case of temperature increase of the composite specimen, the fatigue life shows a significant decrease [41].

The behavior of composites under compression-compression fatigue loading is totally different with respect to different stress ratios. Figure 1-3 shows that in a compression-compression fatigue loading, increasing the stress ratio R reduces the fatigue life of composite.

The first deficiency of this modeling method is that, this stiffness-based model is validated for specific type of loading conditions and is not evaluated in a wide range of loading levels. Furthermore, all experimental data for model validation are related to thin laminates and the possible application of the model for thick laminates is not investigated.

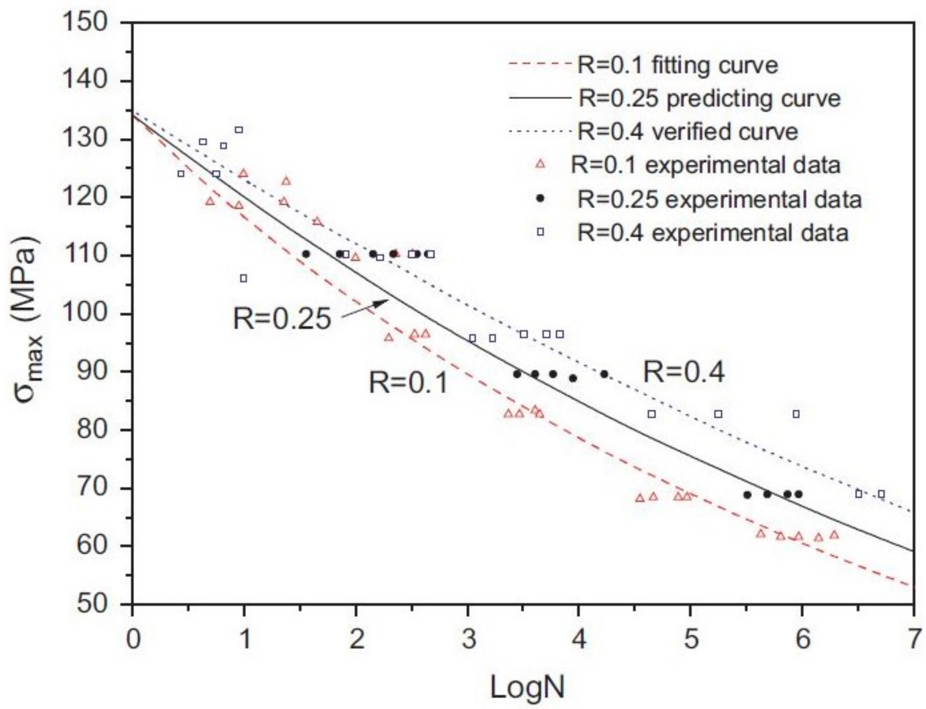

a)

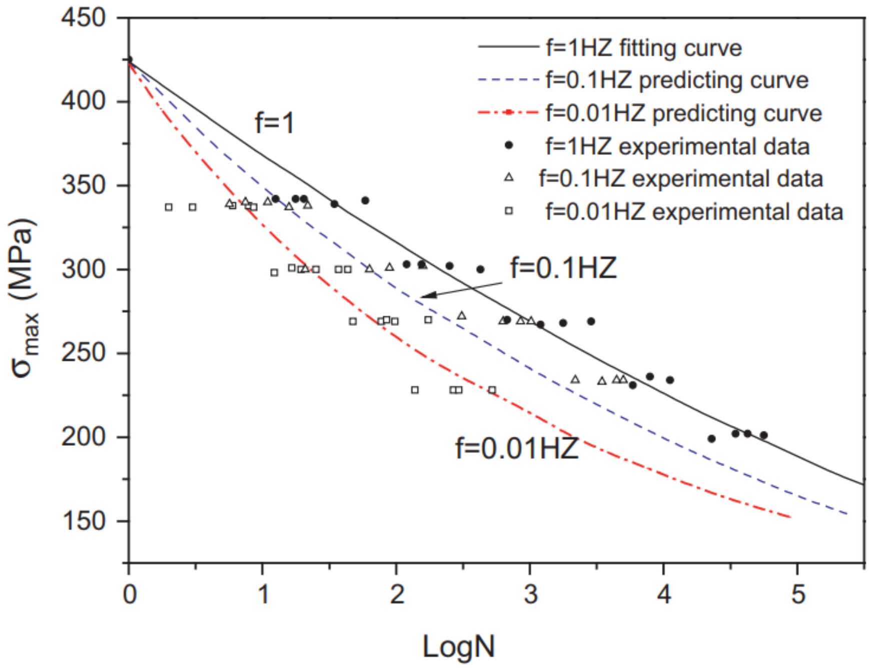

b)

Figure 1-2 a) Fatigue behavior of (±45°) E-Glass–Epoxy composite specimens under tension-tension fatigue experiments, b) Fatigue behavior of E-Glass/Epoxy (0°/90°) composite specimens under different frequencies [39]

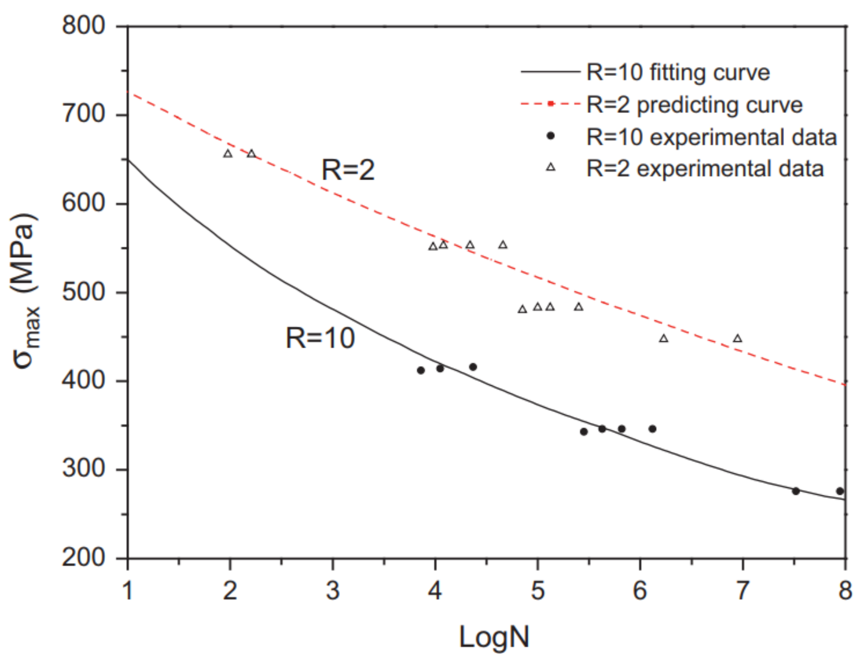

Figure 1-3 Fatigue behavior of Glass/Polyester $(0°)_2$ composite specimen under compression fatigue experiments [39].

1.1.3. Progressive Damage Models

Progressive damage modeling is the most advanced modeling technique compared to the earlier mentioned fatigue damage modeling of composites. The main advantage of these models is that they are capable of not only determining the number of cycles to failure of the composite materials but also, they provide the mechanical property degradation such as stiffness and strength degradation. Joris Degrieck and Wim Van Paepegem [18] classified this model into two major groups: model predicting damage growth and model predicting residual mechanical properties.

1.1.3.1. Model Predicting Damage Growth

Some models have been proposed to simulate damage accumulation for specific damage types, such as matrix cracks and delaminations. Schon [42] proposed a simplified method to describe delamination growth in fiber-reinforced composites. The delamination growth rate under fatigue loading is assumed to be described by the Paris Law. Bergmann [43] developed an empirical delamination propagation model which combines all fracture modes (mode I tension, mode II shear and mode III shear) in one equation. The governing equation of Bergmann model is:

$$\frac{dA}{dN} = c_1(f(G_t))^n = c_2 \varepsilon^n A^m \qquad (1\text{-}16)$$

where G_t is the total of mode I, II and III energy release rates, A is the delaminated area, N is the respective number of cycle and ε is the induced strain. The parameters c_1, c_2, n and m are determined from experiments.

Dahlen and Springer [44] have successfully built an empirical delamination propagation model that includes the effect of shear reversal in mode II delamination growth. Shear reversal takes place when the surfaces bounding the delamination are moving in both positive and negative directions.

1.1.3.2. Model Predicting Residual Mechanical Properties

This model requires the relationships of the residual mechanical properties of composites with their damage variables. Shokrieh [45]-[48] has constructed a model which is able to predict the fatigue damage progression of complicated composite structures provided the properties of the composite materials are fully characterized using modified Hashin failure criterion. To characterize a composite material, experimental results based on the three loading conditions of tension, compression and shear on fibers and resin are required. For each combination of load and fiber or matrix testing, two different sets of tests are performed [45]:

- Fatigue test of specimen until a certain number of cycle followed by a static test until failure. This is to determine the residual stiffness and strength.
- Fatigue test to failure to form the S-N curve.

1.1.3.3. Progressive Damage Based Model- Hallett Model [49]-[52]

One of the most common failure modes in composites is delamination. From the viewpoint of linear elastic fracture mechanics, this failure mode occurs through three well known fracture modes of Mode I, Mode II and Mode III. There has been a lot of research done for characterizing and predicting delamination based on Linear Elastic Fracture Mechanic (LEFM) out of which one can refer to stress intensity factor (SIF), J Integral and virtual crack closure technique (VCCT). The disadvantage of all these methods is necessity to pre-define an existing crack such that they are not capable to predict crack initiation. To overcome the limitation associated with VCCT, interface element analysis has been successfully applied to numerical simulation of inter-laminar fracture in composite structures. The interface elements have the properties of prepreg material. This requires the material to be experimentally characterized to obtain required material properties. In the finite element model, interface elements are then located between adjacent laminae to simulate both initiation of delamination and following growth without specifying a pre-defined crack.

Quasi Static Modeling- Interface Element's Constitutive Law [49]

According to Wen-Guang Jiang et al [49] and considering the low thickness of the intermediate matrix material between plies in a composite, it is appropriate to determine the response in terms of the traction versus separation relationship.

The bilinear interface formulation adopted in this work for the mixed-mode softening law can be illustrated in a single three-dimensional map by representing the normal opening mode (mode I) on the $0-\sigma_I-\delta_{normal}$ plane, and the transverse shear mode (mode II) on the $0-\sigma_{II}-\delta_{shear}$ plane, as shown in Figure 1-4. The triangles $0-\sigma_I^{\max}-\delta_I^f$ and $0-\sigma_{II}^{\max}-\delta_{II}^f$ are the bilinear responses in pure opening mode and in pure shear mode, respectively. Any triangle between these two triangles (for example blue triangle as shown in the Figure 1-4) shows the bilinear mixed mode response.

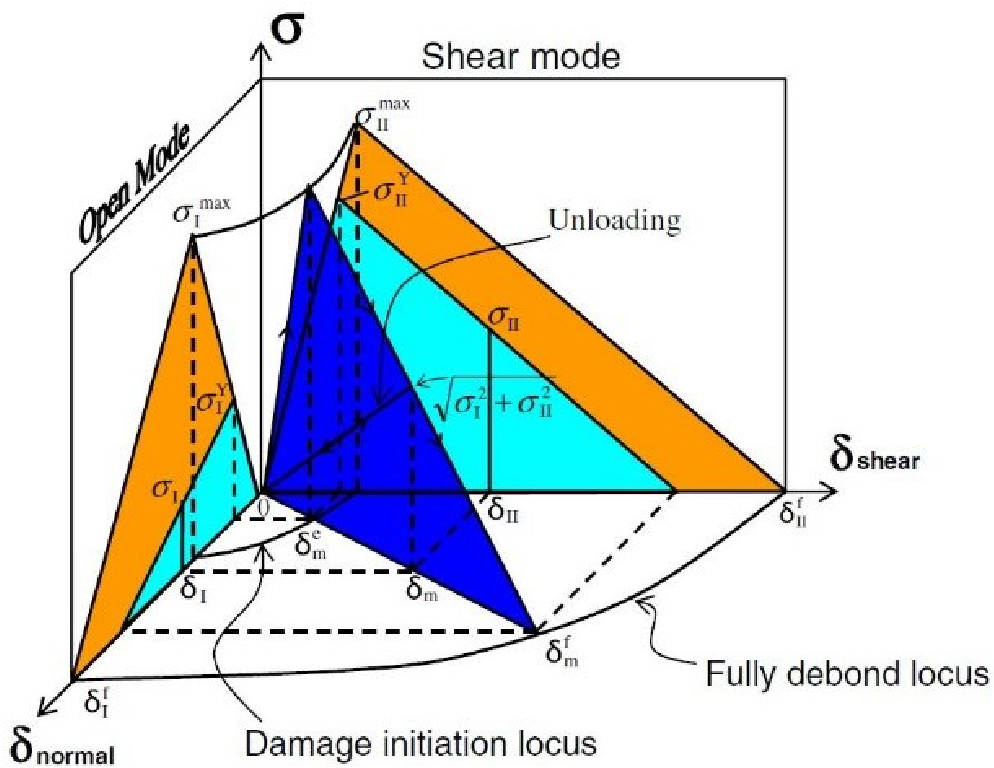

Figure 1-4 Interfacial bilinear mixed-mode softening law [49]

The following quadratic damage initiation criterion under a multi-axial stress state has been successfully used to predict the onset of delamination in previous investigations [49], and is adopted here:

$$\sqrt{\left(\frac{\max(\sigma_I,0)}{\sigma_I^{\max}}\right)^2+\left(\frac{\sigma_{II}}{\sigma_{II}^{\max}}\right)^2}=1 \qquad (1\text{-}17)$$

where σ_I is the normal inter-laminar tensile stress, σ_{II} is the shear stress resultant of the interface, $\sigma_I^{\max}$ is the inter-laminar tensile strength, and $\sigma_{II}^{\max}$ is the inter-laminar shear strength. Furthermore $\max(\sigma_I,0)$ equals to:

$$\max(\sigma_I,0)=\begin{cases}\sigma_I & , \quad \sigma_I \succ \\ 0 & , \quad \sigma_I \le 0\end{cases} \qquad (1\text{-}18)$$

For a given mode ratio the relative displacement corresponding to softening onset (or damage initiation), δ_m^e, can be calculated using Equation (1-17) as,

$$\delta_m^e=1/\sqrt{\left(E_I\cos I/\sigma_I^{\max}\right)^2+\left(E_{II}\cos II/\sigma_{II}^{\max}\right)^2} \qquad (1\text{-}19)$$

where E_I and E_{II} are the initial tensile and shear stiffnesses of the interface, which are high since the interface is assumed to be thin. The direction cosines are defined as,

$$\cos I=\delta_I/\delta_m \quad , \quad \cos II=\delta_{II}/\delta_m=\sqrt{1-(\cos I)^2} \qquad (1\text{-}20)$$

Experimental results indicate that interface failures under mixed-mode conditions can be covered by the power law. The following failure criterion is thus adopted [53], [54]:

$$\left(\frac{G_I}{G_{IC}}\right)^\alpha+\left(\frac{G_{II}}{G_{IIC}}\right)^\alpha=1 \qquad (1\text{-}21)$$

where $\alpha \in (1.0-2.0)$ is an empirical parameter derived from mixed-mode tests, G_{IC} and G_{IIC} are critical energy release rates for pure mode I (opening) and pure mode II (shear), respectively. The relative displacement corresponding to the interface failure under mixed-mode can be obtained as,

$$\delta_m^f=\left(\left(\frac{\sigma_I^Y\cos I}{2G_{IC}}\right)^\alpha+\left(\frac{\sigma_{II}^Y\cos I\,I}{2G_{IIC}}\right)^\alpha\right)^{-\frac{1}{\alpha}} \qquad (1\text{-}22)$$

Under quasi-static loading, a static damage parameter, d_s, is used to track the accumulation of irreversible damage, where:

$$d_s = \frac{\delta_m - \delta_m^e}{\delta_m^f - \delta_m^e} \tag{1-23}$$

Element failure occurs when d_s reaches a value of unity.

Fatigue Modeling- Combined Crack Initiation and Propagation [52]

May and Hallett [51] used cohesive interface elements for modelling initiation and propagation of damage in composites under fatigue loading in a single, coherent analysis. For this purpose, damage initiation laws based on S-N curves for initiation are applied to all interface elements within a zone of characteristic length which is called initiation zone. Once a macroscopic crack has been initiated, crack propagation model is activated to follow damage accumulation based on Paris law.

Crack Initiation Phase [50]

Semi-logarithmic S-N curves for initiation are commonly used to describe the relationship between applied stress and fatigue life. These S-N curves are assumed to behave linearly on a semi-logarithmic plot as they are described as follows,

$$\frac{\sigma}{\sigma_{stat}} = 1 - s.log(N) \tag{1-24}$$

where σ is the applied cyclic stress, σ_{stat} is the static failure stress, resulting in the ratio, σ / σ_{stat} which is the severity, s is a constant called shape parameter and N is the number of cycles.

Equation (1-24) can be rearranged to calculate the number of cycles until initiation for a known severity σ / σ_{stat} and shape parameter s,

$$N_{ini} = 10^{\frac{1-\sigma/\sigma_{stat}}{s}} \tag{1-25}$$

Using the definition of the cycle frequency, $\partial N / \partial t$, it is now possible to calculate the ‘‘pseudo time”, t_{ini}, until initiation,

$$t_{ini} = \frac{N_{ini}}{\partial N / \partial t} \tag{1-26}$$

The initiation damage parameter, d_{fi}, is initially zero and increases to one at the time of damage initiation in the element. The damage accumulation rate, $\partial d_{fi} / \partial t$, can be expressed as,

$$\frac{\partial d_{fi}}{\partial t} = \frac{1}{t_{ini}} \tag{1-27}$$

The damage d_{fi} is updated after every time step, δt, in the explicit analysis,

$$d_{fi}(t) = d_{fi}(t - \delta t) + \frac{\partial d_{fi}}{\partial t} \delta t \tag{1-28}$$

Fatigue initiation damage is accumulated as a function of cycles and progresses from 0, no damage, to 1 at damage initiation.

The problem of fatigue failure initiation prediction using above mentioned procedure is that semi-logarithmic S-N curves are normally obtained during testing of specimens up to final failure. The authors did not state that the S-N curves for failure initiation, not final failure, should be obtained as the model input. It seems that during experiments a failure initiation mechanism such as either dropping of load bearing capacity up to a certain percentage or reaching a certain final strain should be added to prepare the initiation S-N curves.

Crack Propagation Phase [50]

Following presented interface element formulation Harper and Hallett [50] proceeded to analyze delamination crack propagation under cyclic loading using cohesive zone interface element degradation law. Development of the law is based on a detailed study of the numerical cohesive zone and the extraction of strain energy release rate from this zone, enabling a direct link with experimental Paris Law data.

Paris Law model is used to calculate the required rate of crack propagation, $\partial a / \partial N$. In the reference paper a model developed by Blanco et al. [55] has been implemented. Using Blanco's model, the rate of crack propagation is expressed in the form of,

$$\frac{\partial a}{\partial N} = C(\Delta G)^m \tag{1-29}$$

where C and m are experimental coefficients and

$$\Delta G = G_{\max}(1 - R^2) \tag{1-30}$$

where G_{max} is the maximum strain energy release rate in each fatigue cycle and ΔG is the change in strain energy release rate during each fatigue cycle. R is the ratio between the minimum and maximum load within each fatigue cycle. Assuming tension–tension fatigue loading, this allows the maximum strain energy release rate in each fatigue cycle, G_{max} , to be converted to the change in strain energy release rate during each fatigue cycle, ΔG, using Equation (1-30). The conversion of $G_{\max}$ to ΔG is a requirement of the Paris Law model.

Now we need to define the fatigue damage propagation parameter d_f. The traction–displacement response extracted from a single element in a typical DCB (Double Cantilever Beam) test deviates significantly from the bi-linear quasi-static response as shown in Figure 1-5. Because of this fact it is required to define an 'unwanted fatigue damage' parameter $d_{f,u}$ as indicated in Figure 1-6. Following this definition, fatigue damage parameter of d_f is defined using following equation:

$$\frac{\partial d_f}{\partial N} = \frac{1 - d_s - d_{f,u}}{0.5\left(\frac{G_T}{G_C}\right) L_{CZ,f}} \frac{\partial a}{\partial N} \tag{1-31}$$

where G_T is integrated strain energy release rate, G_C is the instantaneous critical fracture energy and L_{CZ} is the length of cohesive zone.

Fatigue damage is added to the interface element's static damage parameter, d_s, giving a value for total damage accumulated, D_{tot}:

$$D_{tot} = d_s + d_f \tag{1-32}$$

D_{tot} is used to calculate the interface element stress, σ_m , after each model time-step, with element failure occurring when the total damage (D_{tot}) reaches unity:

$$\sigma_m = \sigma_{m,\max}(1 - D_{tot}) \tag{1-33}$$

Presented cohesive interface model can be summarized as following:

1- Crack Initiation Phase: For this phase the interface elements should be introduced to the areas of interest to make the possibility of initiation modeling based on prescribed S-N curve.

2- Crack Propagation Phase: After damage initiation in the first phase and reaching to a certain size of crack, the crack propagation is activated to find the rate of crack growth based and Paris Law type equations.

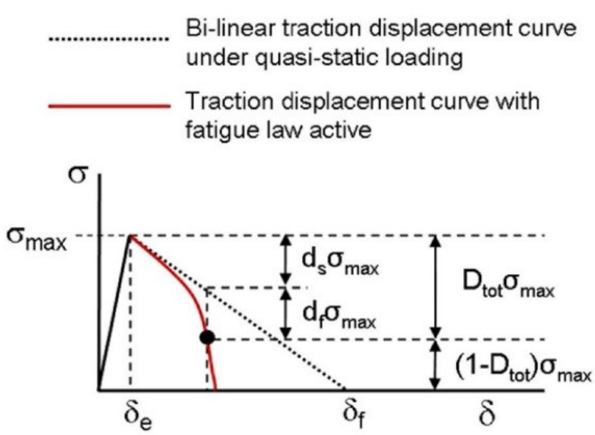

Figure 1-5 Definition of the static and fatigue damage parameters [50]

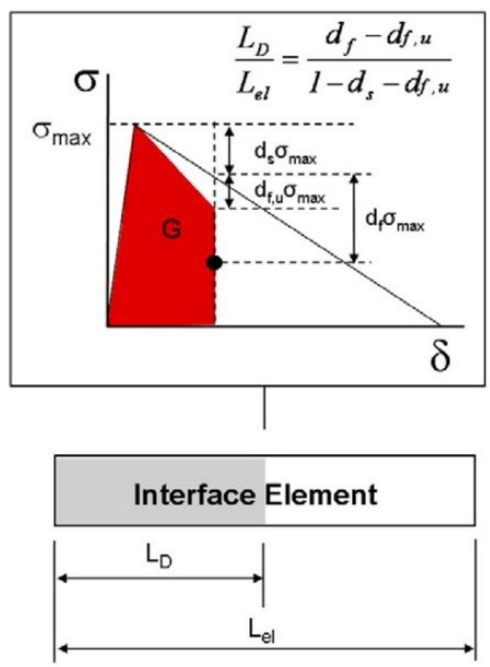

Figure 1-6 Definition of interface element crack length, accounting for unwanted fatigue damage [50]

The idea of this modeling technique is mainly based on progressive damage models in metals. As mentioned in the introduction, there is a fundamental difference between damage mechanisms of metals with those of composites. In metals, crack initiates in a critical location, normally near to the edges, and propagates up to final failure. However, in composites, at the early stages of cyclic loading, cracks are initiated in the matrix material at different locations. At a certain density of initiated cracks, we can say that damage initiates. For the propagation phase, a kind of damage aggregation happens which leads to final fracture. Hence, for the case of laminated composites, one can say that “damage occurrence” and “damage aggregation” take place which is totally different than that of “crack initiation” and “crack propagation", which is related to metals.

1.2. Problem Statement- Yoke of Helicopter

A specific application of thick Glass/Epoxy composite laminates is the Yoke of Helicopter which is investigated in this research. The yoke is the component which connects the main blades to the rotor shaft. High flappability and low weight requirement of the yoke, make composite materials an appropriate choice for designers.

Once a helicopter leaves the ground, it is acted upon by three aerodynamic forces; Thrust, Drag, Lift in addition to the weight. Understanding how these forces work and knowing how to control them with the use of power and flight controls are essential to flight. As shown in Figure 1-7, main forces acting on a helicopter are defined as follows:

- Thrust- the forward force produced by the power plant/propeller or rotor. It opposes or overcomes the force of drag. Generally, it acts parallel to the longitudinal axis.
- Drag- a rearward, retarding force caused by disruption of airflow by the wing, rotor, fuselage, and other protruding objects. Drag opposes thrust and acts rearward parallel to the relative wind.
- Lift- opposes the downward force of weight, is produced by the dynamic effect of the air acting on the airfoil. Lift acts perpendicular to the flightpath through the center of lift.
- Weight- the combined load of the aircraft itself, the crew, the fuel, and the cargo or baggage. Weight pulls the aircraft downward because of the force of gravity. It opposes lift and acts vertically downward through the aircraft’s center of gravity (CG).

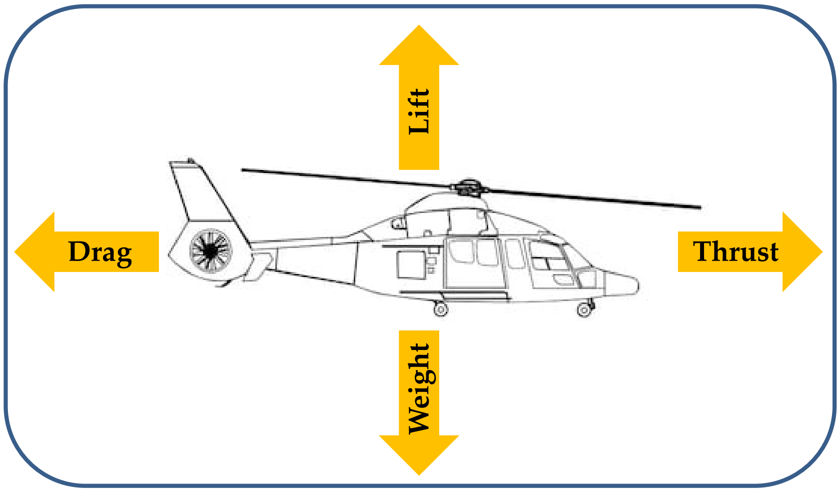

Figure 1-7 Main forces acting on a helicopter in forward motion

Main forces which are applied on the yoke are transferred from the helicopter blades. Hence, before consideration of the yoke itself, one needs to understand the type of forces that are acting on the blades. As shown in Figure 1-8 there are three main forces acting on a blade; Lift force, Drag force and Centrifugal force. Lift is the upward force caused by the interaction between the air flow and the airfoil. Drag is the force of the air resisting the movement of the airfoil. The centrifugal force represents the tendency of the rotor blade to fly away from the center.

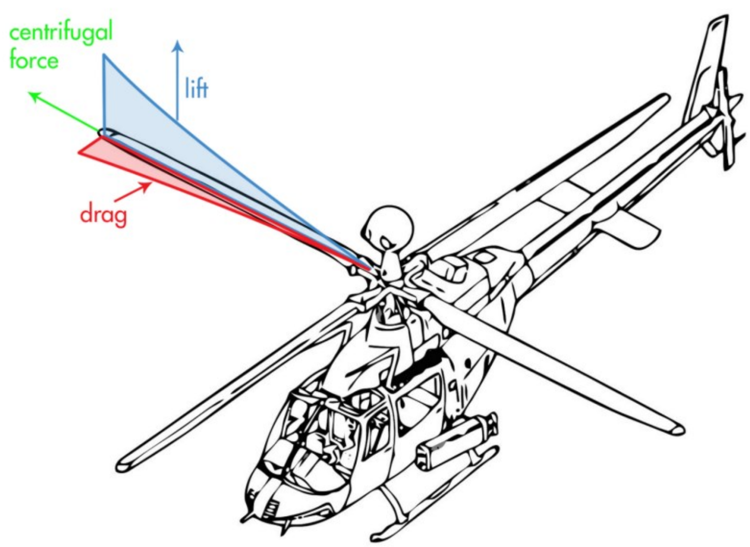

Figure 1-8 Main forces acting on a helicopter blade [56]

Because of the forces on the rotor blades, the blades tend to cone. This means they tend to tilt upward during flight. This is caused by the combination of lift and the centrifugal forces. The centrifugal force tries to make the blade as horizontal as possible, while the lift force tries to move the blade up. The combination of these forces makes the helicopter blade rotate slightly upwards. When the pitch of the blade is changed, the lift generated by that blade changes too, this means that there's a relation between the angle of attack and the coning angle. The coning is shown in Figure 1-9.

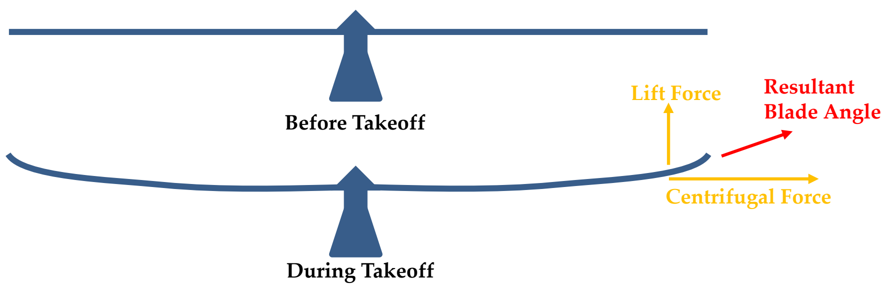

Figure 1-9 Blade coning in vertical flight

The change in the angle of attack during the rotation of the blades makes changes in the amount of the lift force. Therefore, the resultant force of lift and centrifugal forces changes too, although the amount of the centrifugal force could be constant in the constant speed of rotation. This makes the blades have flexural motion in vertical direction. The same motion is transferred to the yoke. It means that the yoke experiences a flexural motion.

The main forces that act on the blade, as shown in Figure 1-8, are transferred to the yoke through the bolted joint. The resultant of lift and drag forces on the blade are vertical and lateral bending moments on the yoke. This means that the yoke experiences cyclic bending moments in vertical and lateral planes plus the constant centrifugal force in constant rotational speed, as shown in Figure 1-10. The yoke is also loaded by bolted clamping joint.

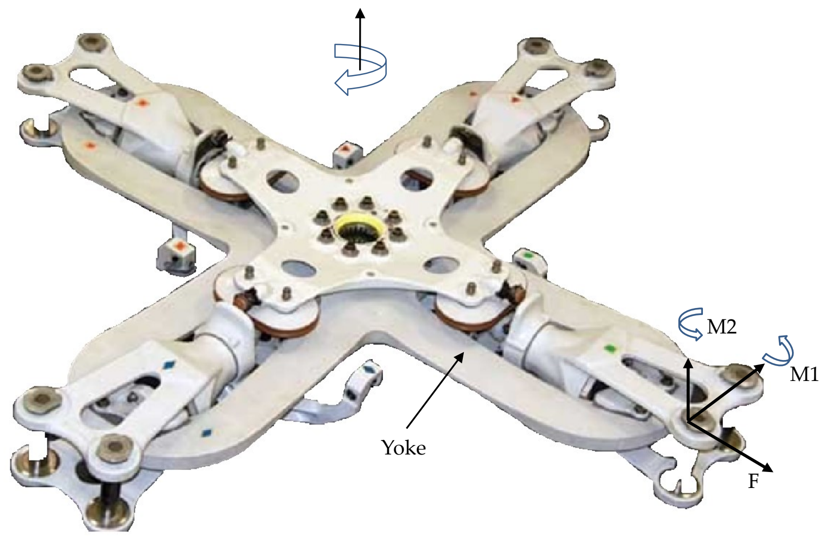

M1: Resultant Moment on the Yoke from the Lift Force on the Blade
M2: Resultant Moment on the Yoke from the Drag Force on the Blade
F: Centrifugal Force

Figure 1-10 Forces acting on the yoke of helicopter

As shown in Figure 1-10, the yoke of helicopter has a complex tapered structure. To simulate its dynamic motion experimentally, one needs a complicated test equipment capable of applying simultaneous resultant dynamic moments (M1 and M2 in Figure 1-10) and static centrifugal force (Force F in Figure 1-10). In this research, however, the structure has been reduced to a simplified case of bolted cantilever beam. The main reason is the availability of the test equipment for such experiments. Furthermore, the idea is to develop a numerical model which could capture the experimental results. If the results of the developed model could correspond with the experimental results of simplified structure, the model could be developed for the case of real structure without requiring further experimental results for such a complicated structure. As shown in Figure 1-11, flexural fatigue behavior of a simplified structure as the bolted composite laminate is investigated in the present research. In this simplified structure the actuator force is applied vertically which simulates the resultant bending moment from the lift force on the blade. This is in addition to bolted clamping joint force.

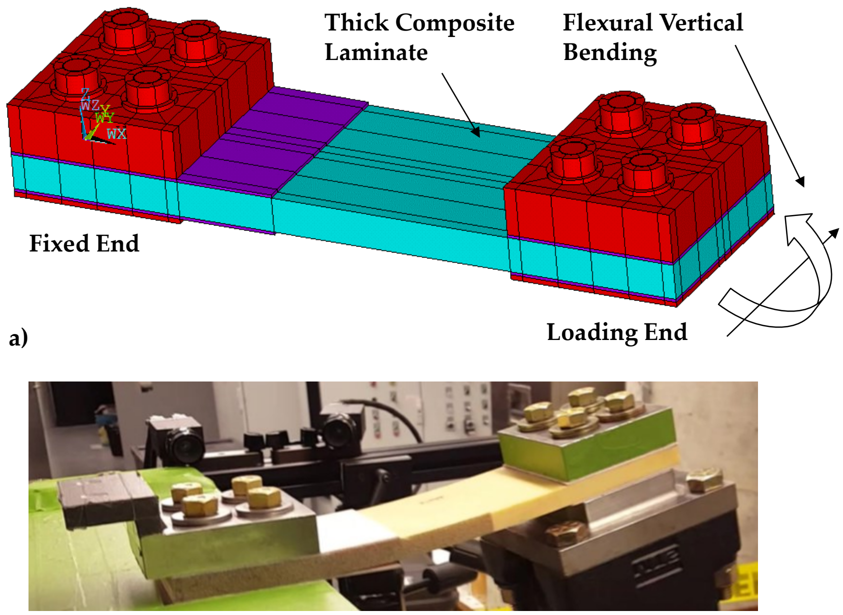

b)

Figure 1-11 The yoke of helicopter a) Simplified numerical model, b) Simplified test specimen on the flexural loading equipment

1.3. Applicability of Presented Fatigue Models on Behavior of Thick Composite Laminate Representing the Yoke of Helicopter

As mentioned at the beginning of this chapter, available fatigue modeling techniques of composite materials are classified in three major groups; Fatigue Life Models, Phenomenological Models and Progressive Damage Models using cohesive elements. These models have been mainly developed and validated for thin laminates. In thin composite laminates the material aspect dominates the laminates' behavior. In a thick laminate, however, the structural aspect takes more concern. In this section the applicability of these modeling techniques for the case of fatigue behavior of thick composite laminate representing the yoke of helicopter is discussed.

1.3.1. Applicability of Fatigue Life Models

Considering the developed fatigue life models available in the literature, one common point can be highlighted. All criteria are speaking about and validated upon using certain constituent materials, laminate stacking sequences and loading conditions. Even for the simple case of homogenous and isotropic materials there is variety of failure theories (i.e. those theories are applicable for ductile materials are different than those are applicable for brittle materials). Therefore, considering the specific state of the problem a suitable criterion should be selected, and if needed, be developed. Furthermore, the effect of thickness change is not accurately considered, as long as most of existing fatigue life models are based on in-plane stress assumption. For the case of thick laminates, the stress state is tri-axial. Furthermore, thick laminate is more a structure than a material. This means that the structural aspect should be taken into account. By stand-alone application of fatigue life models on the thick composite laminates, the material aspect is activated while the structural aspect is scanned over. This would result in deviation of the modeling results with that of practical experiments. Therefore, further investigation regarding applicability of fatigue life models for thick composite laminates by taking both material and structural aspects into account is necessary.

1.3.2. Applicability of Phenomenological Models

Phenomenological models deal with the strength and stiffness degradation of the material. These models are based on the material properties obtained from coupon level experiments related to the thin laminates. Similar to the fatigue life models, the stand-alone application of phenomenological models is not enough to study the fatigue behavior of the thick laminates because it does not deal with the structural aspect. Further investigation needs to be considered in order to verify the applicability of the phenomenological models on the fatigue behavior of thick laminates.

1.3.3. Applicability of Cohesive Zone Model

The model based on cohesive interface elements seemed to be applicable for a combined modeling of failure initiation and propagation in a thick laminate. However, there are limitations associated with cohesive zone model (CZM). The first drawback is that for predicting the fatigue failure initiation, interface elements should be located in the areas of critical stress. It means that a pre-performed stress analysis is necessary to find these critical points to insert interface elements and then activate the fatigue initiation model. For the case of thick laminate with different thicknesses, the comprehensive experimental and finite element results, which will be presented in Chapter 5, show that the maximum out-of-plane shear stress which is the most contributing stress component for the delamination is extremely localized. In this section as an example the profile of out-of-plane shear strain on the side surface of a 70-layer laminate is represented in Figure 1-12 to show the location of the maximum shear strain (which is directly related to shear stress). By this in hand one could conclude that the interface elements could be inserted in the area of maximum shear stress to activate the initiation model. However, the results of the laminates with different thicknesses show that this area of maximum out-of-plane shear strain changes from one thickness to another and also from one deflection level to another. The deflection level is the ratio of applied maximum displacement at the time of fatigue loading to the ultimate quasi static flexural displacement. This means that it is impossible to develop a single coherent model using interface elements that could be applicable for different test conditions and different laminate thicknesses.

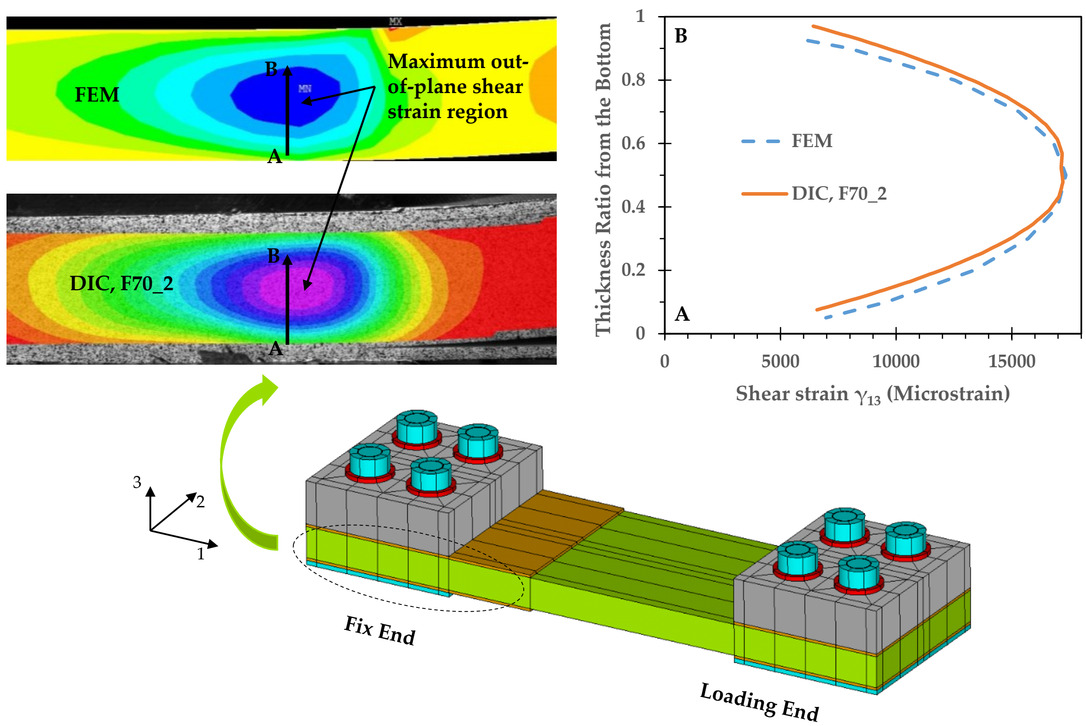

Figure 1-12 FEM and DIC results for distribution of shear strain on the side surface. 70-Layer Laminate at 1.57 (in) of actuator displacement

Furthermore, in a thick laminate, cracks do not always follow the intuitive in-plane path; rather, they may flow between layers as well as re-initiate in new layers. It is impractical to model crack initiation in thick laminates entirely by interface elements because of run-time issues. Therefore, an algorithm is required to predict the most probable location of interface elements in a thick laminate to activate the initiation modeling. The second concern is that S-N curves for failure initiation, rather than final failure, should be obtained which needs further experimental considerations. Finally, the proposed model based on interface elements has been validated for simple test cases [49]-[52]. Test cases include short beam shear test (SBS), double notched shear test (DNS) and double cantilever beam test (DCB) where critical points can be easily predicted.

1.4. Differences between material and structure

Main differences between material and structure could be outlined as following:

1. The material properties do not depend on the geometry. Structure properties do depend on geometry of the sample.
2. For material properties, there are no loading conditions, no boundary conditions. Structure properties depend on boundary and loading conditions.
3. Material properties do not depend on the spatial variation in the sample. Structure properties depend on the spatial variation in the sample.

A piece of thick composite may be considered as a material. However, in order to obtain its properties, one has to subject the sample to some tests. It is difficult to grap onto the sample and provide a uniform state of stress across the thickness. This is because the grapping can only occur on the surface layers. There is no guarantee that the same grapping shear force is applied equally across the thickness. If the whole thickness is not subjected to a uniform state of stress, then one can not obtain one single strength value for the whole sample. As such, a piece of thick laminate may not be qualified as a material.

1.5. A Combined Material and Structural Approach for Fatigue Failure Modeling of Bolted Thick Composite Laminates Representing the Yoke of Helicopter

In this study a combined material and structural approach is introduced to study the fatigue behavior of thick composite laminates subjected to bolt loads. The first part of the approach comprises the selection of the fatigue life model, presented by Hashin and Rotem [3] and developed by Hashin [29], to study the material aspect of fatigue behavior of bolted thick laminate representing the yoke of helicopter. The reason for selection of Hashin type failure criterion is that it is mode dependent which enables us to distinguish between different failure modes. Furthermore, only three S-N curves are needed to characterize the material to be able to apply the criterion to complex state of stress.

The second part of the approach comprises a 3D finite element model which takes the structural aspect of fatigue behavior into account. The structural aspect is related to the locations of damage initiation and the damage mechanisms which are identified by the 3D finite element model. The fatigue material properties obtained from coupon level experiments are introduced in 3D finite element model. Then the failure equations are activated. The combination of fatigue material properties, failure equations and the 3D finite element model enable the entire model to include both material and structural aspects in one single fatigue model.

The chart in Figure 1-13 shows the main steps pertaining to the combined material and structural approach. The process comprises two major sections; 1- Experimental Work, 2- Developping the Fatigue Progressive Damage Model (FPDM). The experimental section contains two sub-sections. In the first sub-section the raw material is characterized to obtain the quasi static and fatigue material properties which are required for material property degradation schemes. The second sub-section is manufacturing and testing of thick laminates with different thicknesses under different deflection levels. The deflection level is the ratio of maximum flexural actuator displacement to the ultimate flexural actuator displacement coming from quasi static experiments. The results of material characterization and thick laminate tests are presented in Chapter 2 and Chapter 4, respectively.

The second section of the process is related to the fatigue progressive damage modeling of thick composite laminates subjected to bolt loads. This section comprises three sub-sections.

Firstly, the 3D model is constructed in the finite element analysis environment to perform stress analysis. The initial orthotropic material properties obtained from coupon level quasi static experiments are introduced into the model. After first solution of the model, the locations of high stress regions are identified, and the tri-axial stress vectors are obtained. Secondly, the resultant stress components are introduced in the failure criteria equations to obtain the failure status of each element. Finally, based on the failure status of the elements, the material property of elements is reduced following the material property degradation scheme. The procedure continues step by step until the final failure occurs.

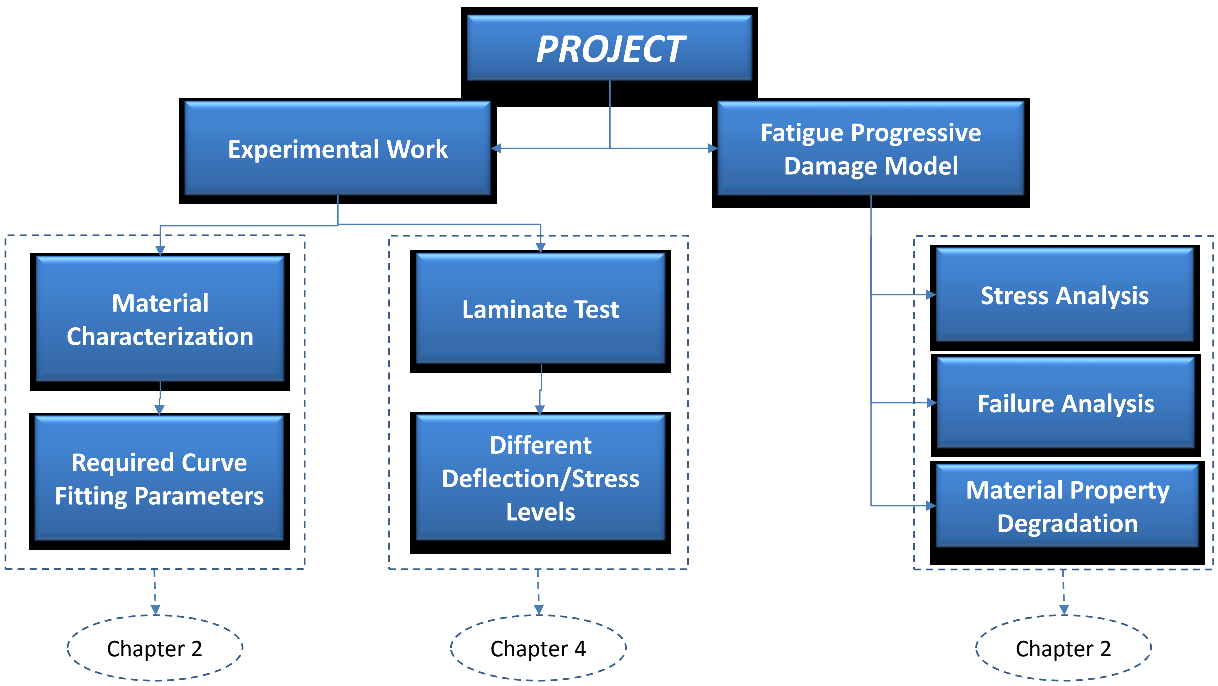

Figure 1-13 Main Steps of the Project

One can summarize the main steps of combined material and structural model as follows:

1. The combined material and structural model performs 3D finite element analysis on the bolted thick laminate subjected to bending load, using material properties obtained from fatigue tests on thin coupons.
2. For each cycle of loading, it identifies regions of high stresses.
3. It goes through many cycles of loading, modifying the material properties after each cycle.

4. When a certain location of the structure has stress combinations that exceed a certain value based on Hashin failure criterion, it degrades the material properties in that location.
5. It keeps on performing the analysis with some regions that are degraded.
6. It continues doing the above procedure until some crack initiation occurs.
7. It monitors the change in stiffness of the sample as it moves along. It then compares the change in stiffness with the change in the actuator force in the experiments.
8. The comparison results show that the calculation agrees with the experimental stiffness reduction. This is to validate the model.

The details of fatigue progressive damage modeling are presented in Chapter 2. Flowchart in Figure 2-1 shows the main steps of FPDM.

1.6. Summary

Available fatigue failure models on thin composite laminates were categorized in three major groups; *Fatigue Life Models*, *Phenomenological Models* and *Progressive Damage Models*.

The purpose of proposed research is to develop a method to investigate the fatigue failure initiation and propagation in thick composite laminates subjected to bolt holes in a single coherent model. Most of available modeling techniques are based on fracture mechanics formulation which are able to model the problems having pre-defined cracks, but they cannot predict the fatigue failure initiation.

The model based on cohesive interface elements seemed to be applicable for a combined modeling of failure initiation and propagation. However, there are limitations associated with cohesive zone model (CZM). The main drawback is that for predicting the fatigue failure initiation, interface elements should be located in the areas of critical stress. In laminates with different thicknesses, however, the area of critical stress varies from one thickness to another and also from one deflection level to another. Furthermore, it is impractical to model the thick laminate entirely by interface elements. Therefore, there is uncertainty in applicability of cohesive zone model to study the fatigue behavior of thick laminates.

For the case of helicopter yoke three major loading mechanisms are; *Flexural Aerodynamic Lift and Drag Loads, Axial Tension due to Centrifugal Forces and Bolted Joints Clamping Loads*. These forces make a complicated tri-axial stress state. This leads to have limitation in application of phenomenological models. However, application of fatigue life models based on Hashin type failure equations is applicable for such structure to predict the location of damage initiation. After initiation happens the material is degraded following a prescribed material degradation scheme to simulate the fatigue behavior of the laminate. It means that both initiation and propagation are simulated in one single coherent model. Material degradation procedure is performed based on obtained information from material characterization experiments for the same material used for manufacturing of thick laminates. This model enables us to consider both material aspect which is related to material properties obtained from characterization tests and structural aspect which is considered with developed 3D finite element model.

To sum-up, in this study a combined material and structural approach is introduced to study the fatigue behavior of thick composite laminates. The first part of the approach comprises the selection of the fatigue life models to study the material aspect of fatigue behavior of thick laminate. The second part of the approach comprises a 3D finite element model which takes the structural aspect of fatigue behavior into account by identifying the locations of the damage initiation and the damage mechanisms. The combination of fatigue material properties, failure equations and the 3D finite element model enable the entire model to include both material and structural aspects in one single fatigue model.

1.7. Thesis Organization

Available fatigue models to apply on thin composite laminates are presented in Chapter 1. Out of three major categories, fatigue life models are employed to model the material aspect of the fatigue failure initiation and propagation in a bolted thick-laminated structure.

For the structural aspect, a 3D finite element model is developed which is combined with the material failure stresses to consider both material and structural aspects of behavior of thick composite laminates under cyclic loading. The 3D finite element model is used to identify the locations of the damage initiation and the damage mechanisms. Development of a fatigue progressive damage model (FPDM) based on Hashin type failure criteria equations is explained in Chapter 2. The model is to study the behavior of thick glass/epoxy composite laminates numerically under cyclic flexural loading. This finite element package is capable of a quick and accurate parametric study of fatigue failure of thick composite laminates. In the third section of Chapter 2 the results of material characterization experiments are presented. These experiments were performed to obtain material properties for material degradation schemes.

Chapter 3 provides the procedure for manufacturing of glass epoxy laminates. Both test coupons and thick composite laminates were manufactured using hand lay-up and autoclave process. However, different bagging processes were employed for thin and thick laminates to avoid resin loss at the time of curing. Physical test results showed acceptable quality of the laminates as regards of resin content and fiber volume fraction.

In Chapter 4 the results of series of quasi static and fatigue flexural loading experiments which were designed and conducted on different thickness unidirectional laminates are presented. These laminates were constrained by bolts to investigate the fatigue behavior from both structural and material points of view. The experiments revealed that damage initiation and propagation in thick laminates take place in a localized fashion rather than global fashion which could happen for thin composite laminates under fatigue loading. Based on the experiments, the dominant failure mode was delamination in certain locations of the laminates. Furthermore, the experimental results showed that the fatigue lives of thick laminated depend on the level of the prescribed deflection at the time of flexural loading. The higher is the applied deflection, the faster is the reduction in fatigue life.

The results of experiments and finite element analysis are summarized and compared in Chapter 5. As shown in the results, by the evolution of load cycles under constant displacement loading, the load bearing capacity of the laminate decreases. The reduction in load bearing capacity is faster for higher deflection levels. This phenomenon is captured by the FPDM. The numerical results of FPDM show that the dominant failure mode is delamination with a localized fashion, corresponding with the results of experiments. The delamination failure also leads to a major drop in the load bearing capacity of the laminates. The correspondence between two phenomena, i.e. decreasing of load bearing capacity and decreasing of number of un-damaged elements, shows that the number of un-damaged elements could be taken as an indication of fatigue damage progression in the laminate. This phenomenon is directly related to the stiffness degradation of the whole laminate.

Chapter 6 summarizes the main contributions and publications of this research along with the path to continue the work.

Chapter 2. Fatigue Progressive Damage Modeling (FPDM)

Manufacturing and testing of composites are very costly and time consuming. Because of the nature of the composites, existence of large scattering in the test results is also unavoidable. Analytical or numerical models are required to overcome these difficulties in order to have a good understanding of the behavior of the composite materials. These models are also capable of parametric study of the composite structures without necessity to perform comprehensive experiments. In this chapter a parametric finite element fatigue progressive damage modeling (FPDM) is developed using ANSYS Parametric Design Language (APDL). The model is capable of parametric study of the structure. The present chapter comprises two parts. In the first part the development of the FPDM based on Hashin-Type failure equations is explained. In the second part the model is validated against the experimental results for both test coupons and thick laminates. Both material and structural aspects of fatigue behavior of bolted thick composite laminates are considered in the FPDM. For the material aspect the S-N Curves as the material properties under cyclic loading are obtained. For the structural aspect, the 3D finite element model is developed which can take material aspect into account with prescription of fatigue material properties into the finite element structural model.

2.1. Fatigue Progressive Damage Modeling (FPDM)

The flowchart of the process to perform FPDM is shown in Figure 2-1. Referring back to Figure 1-13, the main steps are: stress analysis, failure analysis and material property degradation. These steps are explained in the following sections. The model can capture the fatigue damage progression based on failure equations. In each load step, the failure status of the elements is examined. In case that failure happens, the material of the element is degraded, and the next loading step is applied.

2.1.1. Stress Analysis- Structural Aspect

Structural aspect concerns with location of failures and damage mechanisms. Stress analysis was performed using ANSYS parametric design language (APDL) to identify the damage locations and mechanisms, and hence, to consider the structural aspect. Figure 2-2 shows the 3D model of the thick laminate. The model comprises of steel plates, steel bolts and washers, glass/epoxy buffer pads, rigid plates and the thick glass/epoxy composite laminate. Model constructing components are shown in Figure 2-3. The total number of elements of the model without thick glass/epoxy composite laminate is 67872. For the thick glass/epoxy composite laminate four different stack-ups of $[0]_{50}$, $[0]_{60}$, $[0]_{70}$ and $[0]_{80}$ have been considered. To reduce the run time of the model, 10 elements are considered in the thickness direction for all stack-ups. This means that each element contains 5, 6, 7 and 8 layers for $[0]_{50}$, $[0]_{60}$, $[0]_{70}$ and $[0]_{80}$ laminates, respectively. By this assumption the total number of elements for all stack-ups is 21880. 20-Node Solid 186 element was selected for all solid volumes. Frictional contact elements were considered between the surfaces of following components in the 3D model: thick composite laminate and steel bolts, buffer pads and steel plates, buffer pads and rigid plates. All other contacts are considered as glued and bonded contacts without any relative motion, separation or collapsing. The details of static finite element model can be found in reference [57].

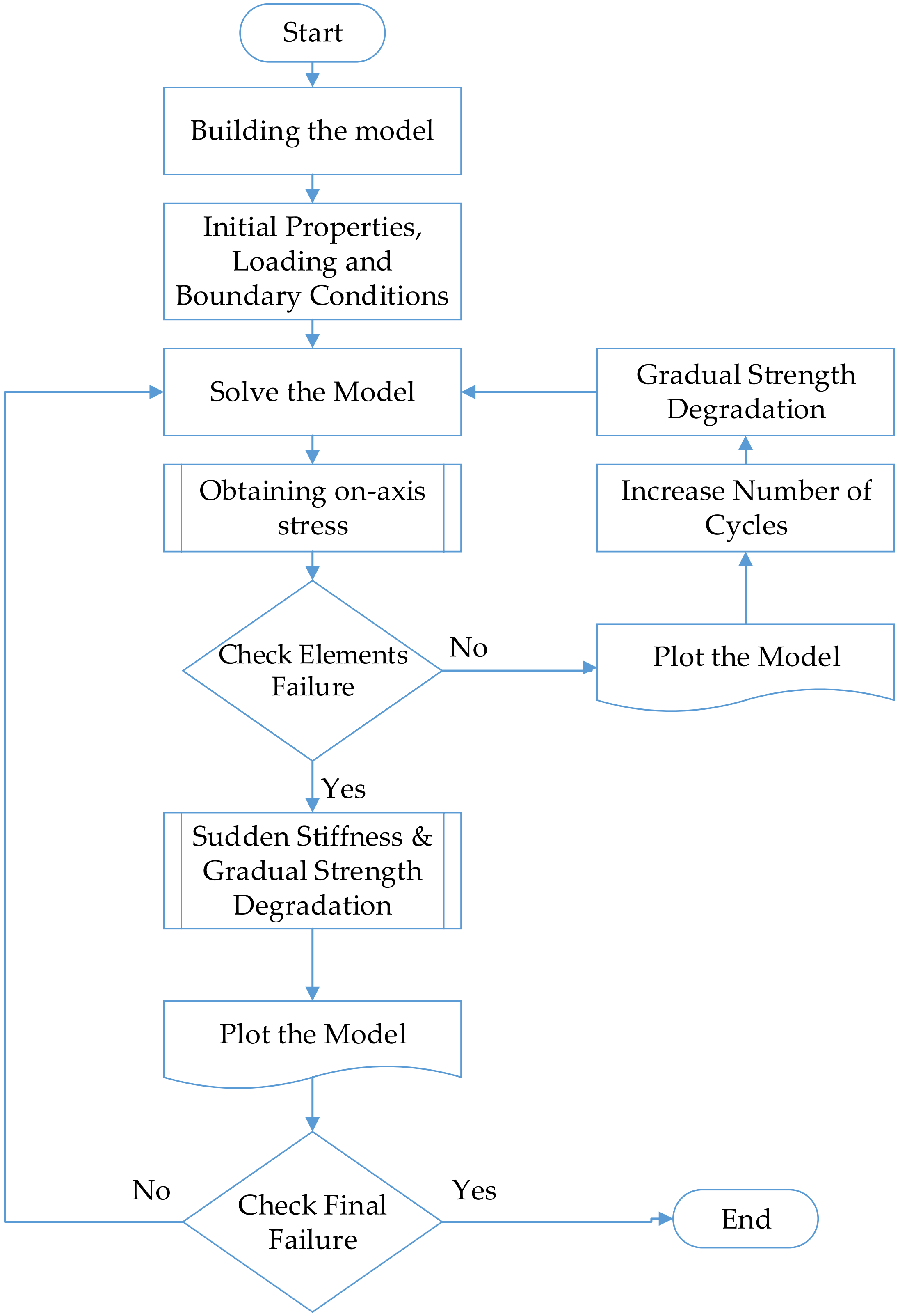

Figure 2-1 Flowchart of Fatigue Progressive Damage Modeling (FPDM)

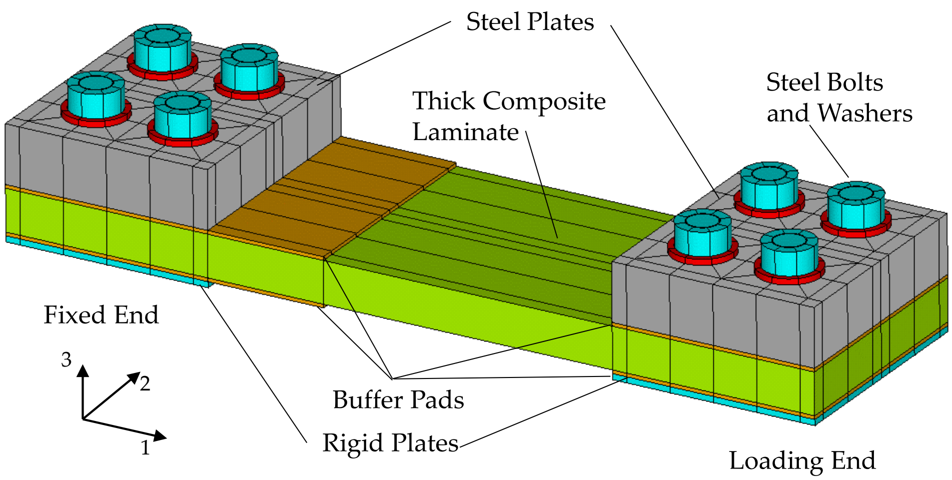

Figure 2-2 Three-dimensional model of thick composite laminate showing different components

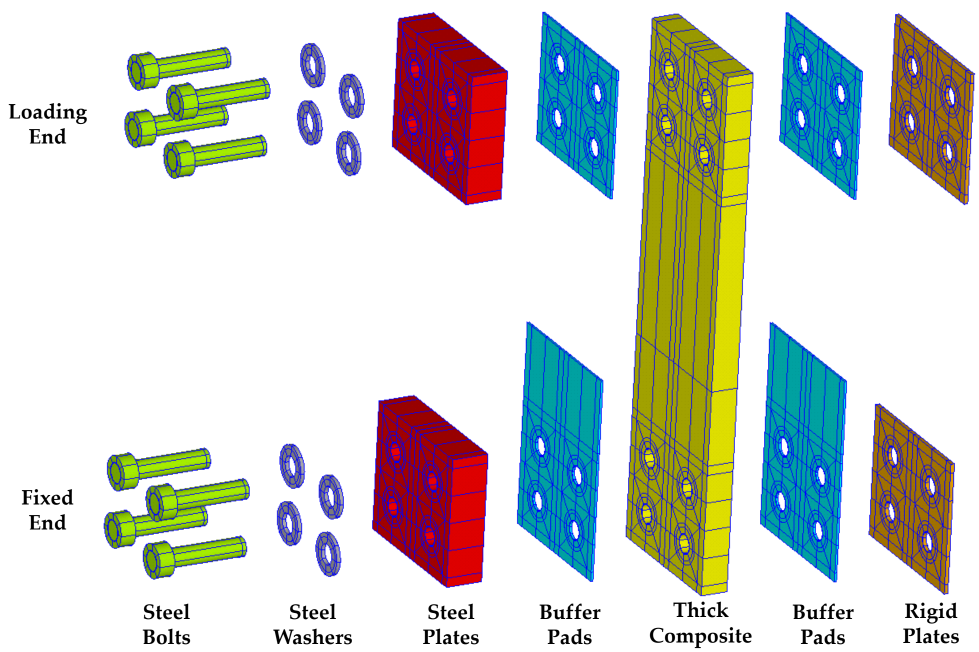

Figure 2-3 Finite Element Constructing Components

2.1.2. Failure Analysis- Material + Structural Aspect

There are many failure criteria that have been presented for the static failure analysis of composite laminates such as maximum stress criterion, Tsai-Wu criterion, Tsai-Hill criterion and Hashin failure criterion. Almost all these criteria have been developed for failure analysis of composites under fatigue loading by replacing the ultimate static strength of materials with that of residual strength of materials. In this study a combination of maximum stress criterion and Hashin fatigue failure criteria [58] are selected for the failure analysis because firstly, these criteria are mode- dependent and secondly, they are easy to apply in the progressive damage modeling. The failure criteria equations are outlined below:

Tensile fiber failure:

The Hashin failure equation for fiber failure in tension is as follows:

$$\left(\frac{\sigma_{11}}{\sigma_{11T}^{F}}\right)^2+\left(\frac{\tau_{12}}{\tau_{12}^{F}}\right)^2+\left(\frac{\tau_{13}}{\tau_{13}^{F}}\right)^2=1, \sigma_{11}>0 \tag{2-1}$$

In this equation the shear stresses are contributing to the fiber failure. However it has been shown experimentally that considering the contribution of shear stresses makes the criterion to be over conservative [59], [60]. For this reason, instead of Hashin criterion for fiber failure in tension, maximum stress criterion is applied for fiber failure in tension as follows:

$$\frac{\sigma_{11}}{\sigma_{11T}^{F}}=1 \ , \ \sigma_{11}>0 \tag{2-2}$$

Compressive fiber failure:

$$\frac{\sigma_{11}}{\sigma_{11C}^{F}}=1 \ , \ \sigma_{11}<0 \tag{2-3}$$

Tensile matrix failure:

$$\left(\frac{\sigma_{22}}{\sigma_{22T}^{F}}\right)^2+\left(\frac{\tau_{12}}{\tau_{12}^{F}}\right)^2+\left(\frac{\tau_{23}}{\tau_{23}^{F}}\right)^2=1, \sigma_{22}>0 \tag{2-4}$$

Compressive matrix failure:

$$\left(\frac{\sigma_{22}}{\sigma_{22C}^{F}}\right)^2+\left(\frac{\tau_{12}}{\tau_{12}^{F}}\right)^2+\left(\frac{\tau_{23}}{\tau_{23}^{F}}\right)^2=1 \ , \ \sigma_{22}<0 \tag{2-5}$$

Fiber/Matrix shear-out:

$$\left(\frac{\sigma_{11}}{\sigma_{11T}^{F}}\right)^2+\left(\frac{\tau_{12}}{\tau_{12}^{F}}\right)^2+\left(\frac{\tau_{13}}{\tau_{13}^{F}}\right)^2=1 \ , \ \sigma_{11}<0 \tag{2-6}$$

Delamination in tension:

$$\left(\frac{\sigma_{33}}{\sigma_{33T}^F}\right)^2+\left(\frac{\tau_{13}}{\tau_{13}^F}\right)^2+\left(\frac{\tau_{23}}{\tau_{23}^F}\right)^2=1\text{ , }\sigma_{33}>0 \qquad (2\text{-}7)$$

Delamination in compression:

$$\left(\frac{\sigma_{33}}{\sigma_{33C}^F}\right)^2+\left(\frac{\tau_{13}}{\tau_{13}^F}\right)^2+\left(\frac{\tau_{23}}{\tau_{23}^F}\right)^2=1\text{ , }\sigma_{33}<0 \qquad (2\text{-}8)$$

In the failure criteria equations as outlined above, the numerators are three-dimensional stress state which would reasonably be considered as critical stress state after a certain number of cycles. The denominators are material failure strengths which are summarized below:

$\sigma_{iiJ}^F, i=1,2,3, J=T,C$ Residual Tensile and Compressive Strength

$\tau_{ij}^F, i,j=1,2,3, i\neq j$ Residual Shear Strength (2-9)

To obtain material failure strengths, S-N curves are obtained prior to implementing the criteria equations. Failure strengths depend on the stress ratio of applied cyclic load, R, and the number of cycles, N.

2.1.2.1. Material Failure Strengths (S-N Curves) - Material Aspect

A) S-N Curve for Strength in the Fiber Directions

Unidirectional specimens were manufactured with fibers along the axial direction to obtain S-N Curve of $\sigma_{11T}^F=\sigma_{11T}^F(R,N)$. The specimen geometry and the number of required specimens are summarized in Section 2.3, Material Characterization Experiments.

B) S-N Curve for Shear Strength in 12 Directions

To obtain axial shear failure strength, $\tau_{12}^F=\tau_{12}^F(R,N)$, the direct method is applying torsional moment on a Thin-Walled tube as depicted in Figure 2-4, but manufacturing of these types of test specimens is difficult and expensive. In addition, applying torsional moment is a challenging endeavor.

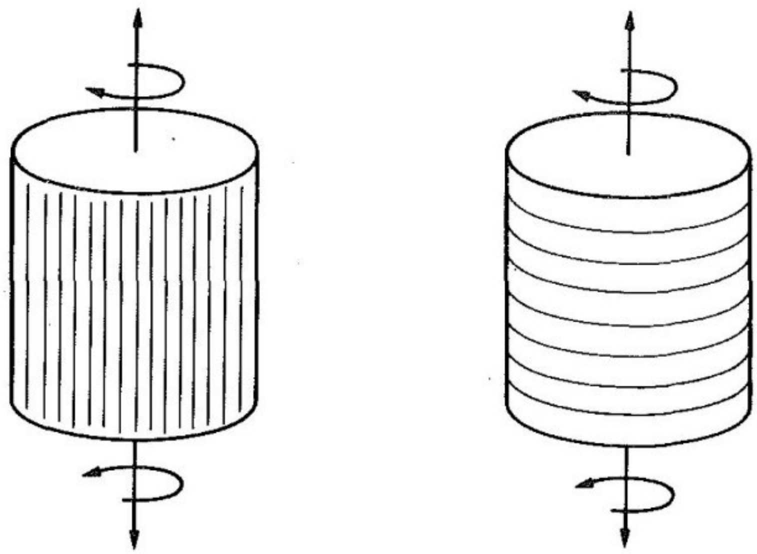

Figure 2-4 Thin-Walled tube Specimens

For solving this problem there is an alternative method (off-axis specimens) which is explained in Section **E**, below.

C) S-N Curve for Strength in Transverse Directions

The direct method to obtain this failure strength in normal transverse direction, $\sigma_{22T}^{F} = \sigma_{22T}^{F}(R,N)$, is loading flat plate specimens with fibers perpendicular to the loading direction. But according to the literature huge test data scattering has been observed in this method. Therefore, similar to the case of axial shear failure strength, the alternative method of off-axis specimens will be applied as discussed in Section **E**.

D) S-N Curve for Shear Strength in 23 directions

To obtain S-N Curve for shear strength in the transverse direction, $\tau_{23}^{F} = \tau_{23}^{F}(R,N)$, specimens must be made with fibers normal to their plane, it means that specimens should be made by transverse cuts through unidirectional laminates therefore the specimens will be small. However, as an alternative assumption it is reasonable to assume that τ_{23}^{F} is the same as the matrix shear failure strength.

E) Alternative Method of S-N Curves for in-Plane Transverse and Shear Strength

As mentioned in Sections **B** and **C**, in order to find normal transverse strength $\sigma_{22T}^F = \sigma_{22T}^F(R,N)$ and shear strength $\tau_{12}^F = \tau_{12}^F(R,N)$, the direct method would be applying transverse normal stress and in-plane shear stress, respectively. But for the former test data scattering happens and for the latter there is difficulty for specimen manufacturing and load application. For this reason, the alternative method of using the specimens in two different off-axis angles is used. The procedure consists of loading the specimens in two different angles until matrix failure happens. Then the Hashin criterion equation for matrix failure is used to calculate two failure strengths. To explain the process, assume that axial stress of σ is applied with angle θ between load and fiber directions as depicted in Figure 2-5.

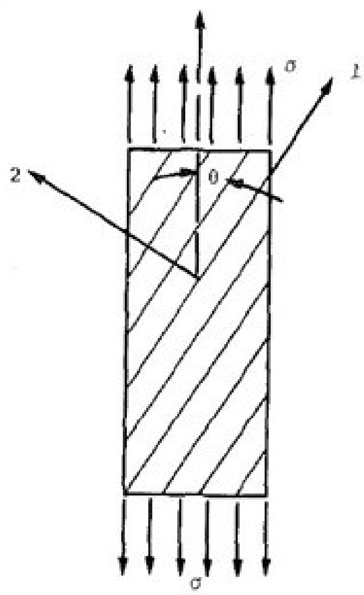

Figure 2-5 Off-axis loading of uni-directional fiber reinforced composite

The resultant stresses in the principal coordinate system will be;

$$
\begin{aligned}
\sigma_{11} &= \sigma \cos^2 \theta \\
\sigma_{22} &= \sigma \sin^2 \theta \\
\sigma_{12} &= \sigma \cos\theta \sin\theta
\end{aligned}
\tag{2-10}
$$

If it is assumed that the specimen fails in the matrix mode, so the Hashin failure equation for matrix failure in the plane stress state which is:

$$\left(\frac{\sigma_{22}}{\sigma_{22T}^{F}}\right)^2+\left(\frac{\sigma_{12}}{\tau_{12}^{F}}\right)^2=1 \tag{2-11}$$

will stand. Substituting from Equation (2-10) into Equation (2-11) yields Equation (2-12),

$$\frac{\sin^4\theta}{\left(\sigma_{22T}^{F}\right)^2}+\frac{\cos^2\theta\sin^2\theta}{\left(\tau_{12}^{F}\right)^2}=\frac{1}{\sigma^2} \tag{2-12}$$

If the test is done for two different angles of θ_1 and θ_2 up to matrix failure, then:

$$\begin{cases}\dfrac{\sin^4\theta_1}{\left(\sigma_{22T}^{F}(R,N)\right)^2}+\dfrac{\cos^2\theta_1\sin^2\theta_1}{\left(\tau_{12}^{F}(R,N)\right)^2}=\dfrac{1}{\sigma_1^{\,2}}\\[2ex] \dfrac{\sin^4\theta_2}{\left(\sigma_{22T}^{F}(R,N)\right)^2}+\dfrac{\cos^2\theta_2\sin^2\theta_2}{\left(\tau_{12}^{F}(R,N)\right)^2}=\dfrac{1}{\sigma_2^{\,2}}\end{cases} \tag{2-13}$$

Equation (2-13) can be solved for normal strength of $\sigma_{22T}^{F}=\sigma_{22T}^{F}(R,N)$ and shear strength of $\tau_{12}^{F}=\tau_{12}^{F}(R,N)$.

2.1.3. Material Property Degradation

The main difference between quasi-static and fatigue modeling is that in static modeling when the load increases, the stress in the element increases. At a certain point the stress in the element reaches the static strength which results in element failure. During this period the material properties of the elements remain unchanged. After failure the material properties are degraded. This process is called sudden degradation of material properties. However, for the fatigue modeling case, the material property is degraded gradually because of the intrinsic material property degradation under cyclic loading. This process is called gradual degradation of material properties.

2.1.3.1. Sudden Material Property Degradation

In this study, based on different failure modes which were explained in the previous sections, the stiffness properties of elements in the finite element model are suddenly degraded as described in the following [61]:

$$
\begin{aligned}
&\textit{Fiber Failure}: \\
&\quad [E_{11},E_{22},E_{33},\upsilon_{12},\upsilon_{23},\upsilon_{13},G_{12},G_{23},G_{13}] \rightarrow [0,0,0,0,0,0,0,0,0] \\
&\textit{Matrix Failure}: \\
&\quad [E_{11},E_{22},E_{33},\upsilon_{12},\upsilon_{23},\upsilon_{13},G_{12},G_{23},G_{13}] \rightarrow [E_{11},0,E_{33},0,\upsilon_{23},\upsilon_{13},G_{12},G_{23},G_{13}] \\
&\textit{Fiber / Matrix shear} - \textit{out Failure}: \\
&\quad [E_{11},E_{22},E_{33},\upsilon_{12},\upsilon_{23},\upsilon_{13},G_{12},G_{23},G_{13}] \rightarrow [E_{11},E_{22},E_{33},0,\upsilon_{23},\upsilon_{13},0,G_{23},G_{13}] \\
&\textit{Dela}\min\textit{ation Failure}: \\
&\quad [E_{11},E_{22},E_{33},\upsilon_{12},\upsilon_{23},\upsilon_{13},G_{12},G_{23},G_{13}] \rightarrow [E_{11},E_{22},0,\upsilon_{12},0,0,G_{12},0,0]
\end{aligned}
\tag{2-14}
$$

It should be mentioned that in the numerical solution, stiffness values which should be degraded to zero, are degraded to small numeric values.

2.1.3.2. Gradual Material Property Degradation

In fatigue modeling, even if the element is not failed, the material property of element should be degraded gradually between cycle intervals. A generalized material property degradation procedure which is developed by Adam et al. [62], [63] and modified by Shokrieh [45]-[48] is used to degrade the strength of elements during fatigue loading. Residual strength of a unidirectional ply under arbitrary stress state and stress ratio is presented by the following equation (Note: the material degradation equations in this section are to obtain material failure stresses other than those explained in Section 2.1.2.1):

$$
\begin{aligned}
&\sigma_{iiJ}^{F}(N,\sigma_{ij},R) = \left[1 - \left(\frac{\log(N) - \log(0.25)}{\log(N_f - \log(0.25)}\right)^{\beta}\right]^{1/\alpha} (\sigma_{iiJ}^{S} - \sigma_{ij}) + \sigma_{ij}, i = 1,2,3, J = T,C \\
&\tau_{ij}^{F}(N,\tau_{ij},R) = \left[1 - \left(\frac{\log(N) - \log(0.25)}{\log(N_f - \log(0.25)}\right)^{\beta}\right]^{1/\alpha} (\tau_{ij}^{S} - \tau_{ij}) + \tau_{ij}, i,j = 1,2,3, i \neq j \\
&\alpha \textit{ and } \beta = \exp\textit{erimental curve fitting parameters}
\end{aligned}
\tag{2-15}
$$

Required curve fitting parameters for Equation (2-15) for different fatigue loading conditions are shown in Table 2-1 [48].

Table 2-1 Fitting parameters used in strength and stiffness degradation models [48]

Fatigue Loading Condition	Constants for Equation (2-15)	
	α	β
Longitudinal tension	10.03	0.47
Longitudinal compression	49.06	0.03
Transverse tension	9.63	0.13
Transverse compression	67.4	0.001
In-plane shear	0.16	9.11
Out-of-plane shear	0.2	12

In Equation (2-15), parameter N_f as the fatigue life under prescribed stress, is required to be obtained for each stress level and stress ratio. This parameter is obtained using following equation developed by Adam et al. [64]:

$$\begin{aligned} &u = \frac{\ln(a/f)}{\ln[(1-q)(c+q)]} = A + B\log(N_f) \\ &f \; and \; u = curve\ fiting\ parameters \\ &q = \sigma_m / \sigma_{iiT}^F \\ &a = \sigma_a / \sigma_{iiT}^F \\ &c = \sigma_{iiC}^F / \sigma_{iiT}^F \end{aligned} \tag{2-16}$$

For shear loading conditions, Equation (2-16) is then modified as following with the parameter $c = 1$ because the positive and negative shear stresses act similarly and there is one single shear strength. $\log_{10}$ is added to Equation (2-16) for better fitting of experimental values:

$$u' = \log_{10}\left(\frac{\ln(a/f)}{\ln[(1-q)(c+q)]}\right) = A' + B'\log(N_f) \tag{2-17}$$

All parameters are defined in Nomenclature section at the beginning of this thesis. Required curve fitting parameters for Equation (2-16) for different fatigue loading conditions are shown in Table 2-2 [48].

Table 2-2 Fitting parameters used in the fatigue life model [48]

Fatigue Loading Condition	Constants for Equation (2-16)	
	A	B
Longitudinal tension	1.06	0.07
Longitudinal compression	1.06	0.07
Transverse tension	0.99	0.96
Transverse compression	0.99	0.96
In-plane shear	0.1	0.2
Out-of-plane shear	0.3	0.1

2.2. Connection between Material Characterization and Analysis of Thick Laminates

In this study the fatigue analysis of thick laminates has been considered from both material and structural points of view.

To take material analysis aspect into account, the raw material was characterized through quasi static and fatigue characterization tests. The results of the characterization tests are presented in the next section.

For the structural point of view, the 3D finite element model was prepared to identify the locations of failures and damage mechanisms. This is performed by providing the stress components of the whole elements of the laminate. At each loading step, the model is reconstructed using the newly degraded material properties. The model is solved to obtain new stress field of the elements. The stiffness of the failed elements is also degraded suddenly following the procedure that was explained in the previous section. The main steps which show the clear connection between the material characterization phase and the finite element analysis of the thick laminate are shown in Figure 2-6.

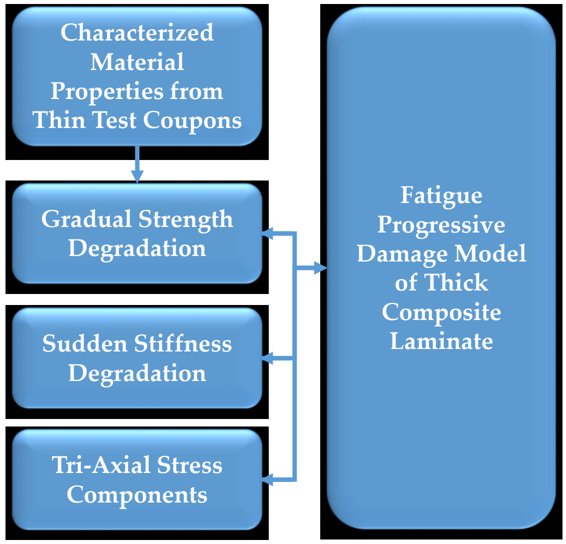

Figure 2-6 Application of characterized thin laminates' material properties in fatigue analysis of thick laminates

2.3. Material Characterization Experiments

Following the presented approach in Section 1.5 the raw material should be characterized to obtain required quasi static and fatigue material properties. In this section the results of characterization tests are presented, and the key material properties are summarized.

2.3.1. Orthotropic Material Properties

Static material properties were obtained through quasi-static tests based on corresponding ASTM Standards. The aim was to obtain orthotropic material properties of Glass Epoxy PrepReg CYCOM S2/E773 material. All panels were manufactured using hand lay-up and autoclave process. Panels were cured per industry prescribed cure cycle. Glass epoxy tabs were attached after curing. The manufacturing procedure is explained in detail in Chapter 3. Test matrix for material characterization tests is shown in Table 2-3. Figure 2-7 shows all the manufactured samples for 0° tension and compression and ±45 inter-laminar shear tests.

Table 2-3 Test Matrix for Material Characterization to obtain Orthotropic Material Properties
Material: Glass Epoxy Prepreg CYCOM S2/E773

Mechanical Property	Panel	Ply Orientation	# of Plies	# of Samples	Sample Dimension (LxWxT)(in)	Nominal Thickness (in)	Panel Size (L x W) L = 0° fiber direction (in)	Test Method	Tab (LxT)
Quasi Static Loading									
0° Tension (Quasi Static) $\sigma_{11T}^{S}, E_{11T}, \upsilon_{12}$	A1	$[0]_5$	5	7(1)	10x0.5x0.040	0.045	12x8	ASTM D3039	2.25x0.062
90° Tension (Quasi Static) $\sigma_{22T}^{S} = \sigma_{33T}^{S}, E_{22T}, \upsilon_{21}$	A2	$[90]_{10}$	10	11(1)	9x1x0.080	0.090	12x12	ASTM D3039	2x0.062
0° Compression (Quasi Static) σ_{11C}^{S}	A3	$[0]_{14}$	14	6(1)	5.5x0.5x0.120	0.126	8x8	ASTM D3410	2.5x0.06
90° Compression (Quasi Static) $\sigma_{22C}^{S} = \sigma_{33C}^{S}$	A4	$[90]_8$	8	8(1)	5.5x1x0.058	0.072	8x12	ASTM D3410	2.5x0.06
In-Plane Shear (Quasi Static) $\tau_{12}^{S} = \tau_{13}^{S}, G_{12}$	A5	$[\pm 45]_{16}$	16	7(1)	10x1x0.144	0.144	10x12	ASTM D3518	No need

Note (1): Minimum required samples are 5 based on reference ASTM Standard.

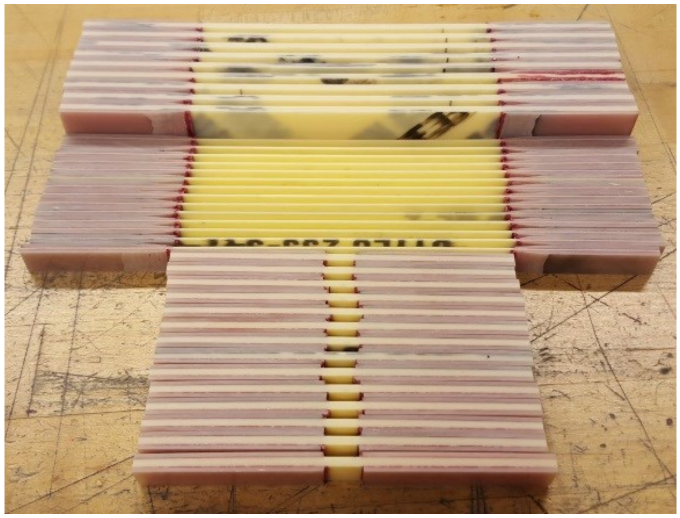

Figure 2-7- Manufactured Test Coupons for Quasi Static Characterization

2.3.1.1. 0° Tension Test

The reference standard is ASTM D3039. To meet the thickness requirements of mentioned standard, 5-ply laminates were manufactured to have the nominal thickness of 0.045 (in). Seven samples were tested. To monitor the strains and to obtain the Poisson Ratio, Tee-Rosette strain gages were attached on the samples. The strain gauges were the product of Vishay Precision Group and the product number was C2A-06-125LT-350. Figure 2-8 shows the picture of samples after final failure. It should be noted that for 0° test coupons, the failure mechanism is in such a way that the samples explode completely without any pre-indication of failure nor a kind of progressive failure. For this reason, the failure is named as “final” failure when the applied load drops suddenly to zero.

Figure 2-8- 0° Samples after final failure

The results of all 0° tension tests are summarized at Table 2-4. Three material properties of $\boldsymbol{\sigma}^{S}_{\boldsymbol{11T}}$, $\boldsymbol{E_{11T}}$**and** $\boldsymbol{v_{12}}$ were obtained. All coefficient of variations are well below 10 which are acceptable.

Table 2-4- 0° Tension Test Results

NO	Specimen	Thickness (in)	Width (in)	Area (in^2)	Max Force (lb)	Tensile Strength $\boldsymbol{\sigma}^{S}_{\boldsymbol{11T}}$ (Msi)	Modulus E_{11T} (Msi)	Poisson Ratio v_{12}
1	ST11-01	0.04133	0.49638	0.021	5610.56	273.46	7436.19	0.28
2	ST11-02	0.04497	0.49653	0.022	5387.25	241.28	6708.85	0.28
3	ST11-03	0.04522	0.49980	0.023	5496.47	243.21	7036.99	0.28
4	ST11-04	0.04478	0.49693	0.022	5201.77	233.74	6949.95	0.28
5	ST11-06	0.04515	0.49818	0.022	5515.38	245.20	6837.91	0.28
6	ST11-07	0.04503	0.49475	0.022	5456.82	244.92	6945.18	0.28
7	ST11-10	0.04520	0.49335	0.022	5617.48	251.91	6748.17	0.28
Mean Value					5469.4	247.68	6951.89	0.28
Standard Deviation					132.7	11.66	225.32	0.00
Coefficient of Variation					2.4	4.71	3.24	0.81

2.3.1.2. 90° Tension Test

For the 90° tension test, 10-layer laminates were manufactured to meet the minimum requirement of ASTM D3039. 11 samples were tested. To monitor the strains and to obtain the Poisson Ratio, Tee-Rosette strain gages were attached on the samples. Figure 2-9 shows the pictures of samples after failure. All failures took place in the gage length and were accepted based on reference standard.

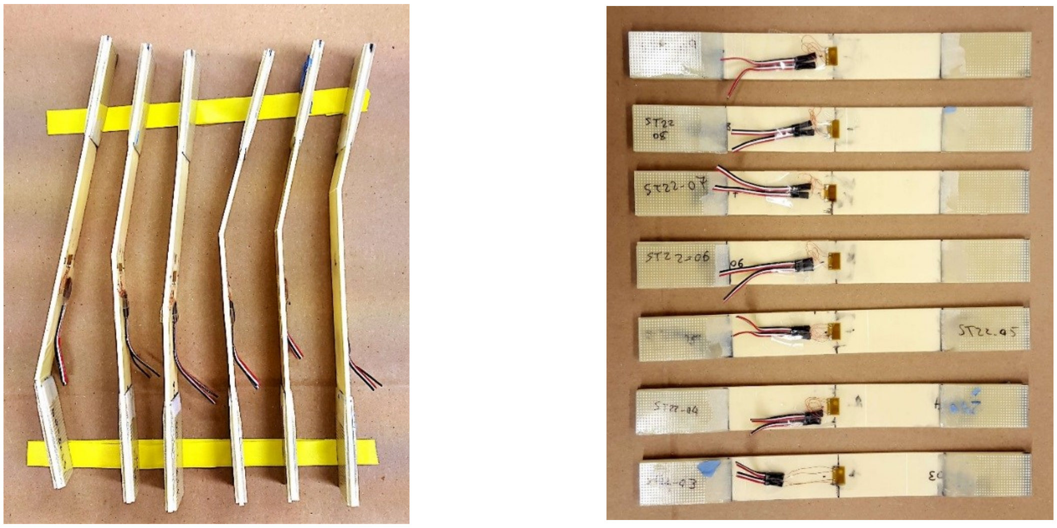

Figure 2-9- 90° Tensile Samples after Failure

The results of 90° Tension tests are summarized in Table 2-5. Eleven samples were tested in this section. However, the strain recording equipment was disconnected for samples ST22-02 up to ST22-10. For this reason, the stiffness properties are missing for samples ST22-02 up to ST22-10 in Table 2-5. Tensile strength values are calculated for all samples.

Table 2-5- 90° Tension Test Results

NO	Specimen	Thickness (in)	Width (in)	Area (in^2)	Max Force (lb)	Tensile Strength σ_{22T}^{S} (Msi)	Chord Modulus E_{22T} (Msi)	Poisson Ratio υ_{21}
1	ST22-01	0.09080	0.99323	0.090	784.90	8.70	1728.31	0.06
2	ST22-02	0.08800	0.98533	0.087	741.35	8.55	-	-
3	ST22-03	0.08898	0.99112	0.088	806.57	9.15	-	-
4	ST22-04	0.09052	0.98990	0.090	822.84	9.18	-	-
5	ST22-05	0.09127	0.99442	0.091	833.07	9.18	-	-
6	ST22-06	0.09152	0.99433	0.091	866.63	9.52	-	-
7	ST22-07	0.09088	0.99145	0.090	812.13	9.01	-	-
8	ST22-08	0.08893	0.99507	0.088	849.34	9.60	-	-
9	ST22-09	0.08742	0.99445	0.087	702.43	8.08	-	-
10	ST22-10	0.08632	0.99638	0.086	770.37	8.96	-	-
11	ST22-11	0.08917	0.99450	0.089	686.33	7.74	1737.85	0.06
		Mean Value			788.7	8.88	1733.08	0.06
		Standard Deviation			55.8	0.55	NA	NA
		Coefficient of Variation			7.1	6.15	NA	NA

2.3.1.3. 0° Compression Test

The reference standard for compression test is ASTM D3410. To meet the thickness requirements of mentioned standard, 14-ply laminates were manufactured to have the nominal thickness of 0.126 (in). Six samples were tested. For these samples, small size Tee-Rosette strain gages were attached because of small gage length. The strain gage product number was CEA-06-062UT-350. Figure 2-10 shows the picture of samples after failure.

Figure 2-10- 0° Compression Samples after failure

Table 2-6 summarizes the compression test results of 0° samples. The results are acceptable based on low coefficient of variations.

Table 2-6- 0° Compression Test Results

NO	Specimen	Thickness (in)	Width (in)	Area (in^2)	Max Force (lb)	Compressive Strength σ_{11C}^{S} (Msi)	Modulus E_{11C} (Msi)
1	SC11-04	0.12465	0.49800	0.062	-8448.99	136.11	-
2	SC11-05	0.12215	0.50180	0.061	-9007.89	146.96	7108.07
3	SC11-07	0.11995	0.49785	0.060	-8392.52	140.54	7588.36
4	SC11-09	0.12510	0.49840	0.062	-8487.67	136.13	7887.76
5	SC11-10	0.12540	0.49870	0.063	-8379.26	133.99	7482.31
6	SC11-12	0.11915	0.49835	0.059	-8315.64	140.05	-
Mean Value					-8505.3	138.96	7516.62
Standard Deviation					231.2	4.25	278.83
Coefficient of Variation					-2.7	3.06	3.71

2.3.1.4. 90° Compression Test

For 90° compression test, 8-layer laminates were manufactured to meet the minimum requirement of ASTM D3410. Eight samples were tested. To monitor the strains, Tee-Rosette strain gages were attached on the samples. Smaller strain gages of C2A-06-125LT-350 were selected again for small gage length. Figure 2-11 shows the picture of samples after failure. All failures took place in the gage length and are acceptable based on reference standard.

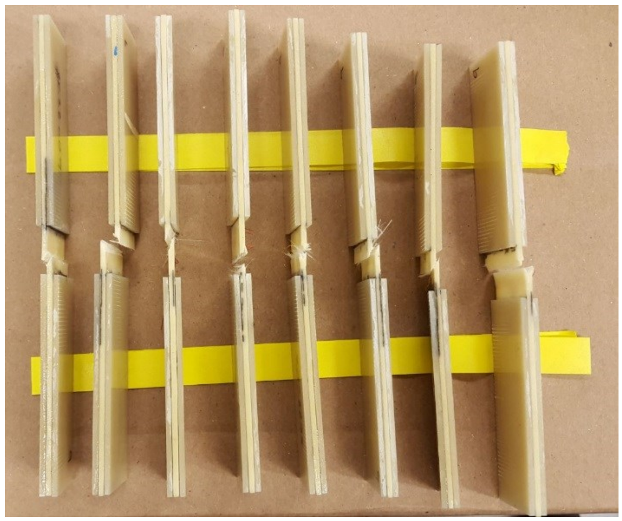

Figure 2-11- 90° Compression Samples after Failure

The results of 90° Compression tests are summarized in Table 2-7.

Table 2-7- 90° Compression Test Results

NO	Specimen	Thickness (in)	Width (in)	Area (in^2)	Max Force (lb)	Compressive Strength σ^{S}_{22C} (Msi)	Modulus E_{22C} (Msi)
1	SC22-01	0.06435	0.99340	0.064	-1405.65	21.99	2387.41
2	SC22-02	0.06535	0.99615	0.065	-1209.90	18.59	2351.73
3	SC22-05	0.07930	0.99605	0.079	-1349.43	17.08	2142.32
4	SC22-06	0.07935	1.00010	0.079	-1594.97	20.10	1620.85
5	SC22-07	0.07470	0.99725	0.074	-1368.30	18.37	1761.30
6	SC22-08	0.07075	0.99500	0.070	-1408.79	20.01	1748.75
7	SC22-09	0.06700	0.99785	0.067	-1396.29	20.89	1878.77
8	SC22-11	0.05865	1.00375	0.059	-1417.36	24.08	2209.71
Mean Value					-1393.8	20.14	2012.60
Standard Deviation					98.6	2.07	277.33
Coefficient of Variation					-7.1	10.29	13.78

2.3.1.5. ±45 Inter-laminar Shear Test:

The reference standard for inter-laminar shear test is ASTM D3518. To meet the thickness requirements of mentioned standard, 16-ply laminates were manufactured to have the nominal thickness of 0.144 in. 7 samples were tested. To monitor the strains, Tee-Rosette strain gages were attached on the samples. The strain gages were product of Vishay Precision Group and the product number was C2A-06-125LT-350. Figure 2-12 shows the pictures of samples after failure.

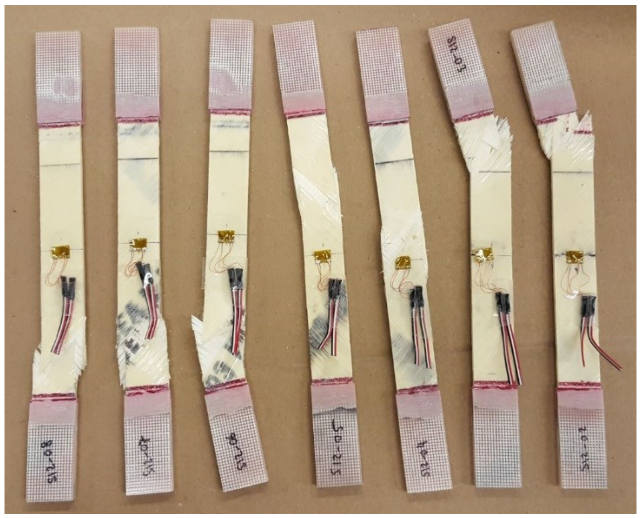

Figure 2-12- ±45 Inter-laminar Shear Samples after Failure

The results of ±45 Inter-laminar Shear Test are summarized in Table 2-8. Based on coefficient of variation, the results of all samples are acceptable.

Table 2-8- ±45 Inter-laminar Shear Test Results

NO	Specimen	Thickness (in)	Width (in)	Area (in^2)	Max Force (lb)	Shear Strength τ_{12}^{S} (Msi)	Modulus G_{12} (Msi)
1	S12-02	0.14358	0.99993	0.144	4466.12	15.55	610.75
2	S12-03	0.14683	0.99937	0.147	4607.56	15.70	617.55
3	S12-04	0.13615	1.00275	0.137	4372.72	16.01	641.55
4	S12-05	0.14243	0.99835	0.142	4471.50	15.72	629.23
5	S12-06	0.14598	0.99855	0.146	4556.81	15.63	608.38
6	S12-07	0.14355	0.99955	0.143	4504.46	15.70	616.81
7	S12-08	0.14727	1.00042	0.147	4640.63	15.75	606.45
Mean Value					4517.1	15.72	618.67
Standard Deviation					85.1	0.13	11.70
Coefficient of Variation					1.9	0.85	1.89

2.3.1.6. Summarized Orthotropic Material Properties:

Orthotropic material properties of CYCOM S2/E773 are summarized in Table 2-9.

Table 2-9 Orthotropic Material Properties for S2/E773 Prepreg

No	Parameter	Unit	Mean Value	Standard Deviation	Coefficient of Variation
1	E_{11T}	Msi	6951.67	225.32	3.24
2	E_{22T}	Msi	1733.20	4.77	0.28
3	E_{11C}	Msi	7517.32	278.83	3.71
4	E_{22C}	Msi	2013.13	277.33	13.78
5	G_{12}	Msi	619.31	11.7	1.89
6	υ_{12}	-	0.28	0.00	0.81
7	υ_{21}	-	0.06	0.00	0.74
8	σ_{11T}^{S}	Msi	247.68	11.66	4.71
9	σ_{22T}^{S}	Msi	8.88	0.55	6.15
10	σ_{11C}^{S}	Msi	138.96	4.25	3.06
11	σ_{22C}^{S}	Msi	20.14	2.07	10.29
12	τ_{12}^{S}	Msi	15.72	0.13	0.85

2.3.2. Material Properties for Degradation Scheme

In this section the results of material failure stresses as S-N Curves as required for Hashin failure equations in the material degradation scheme are presented. The required material properties are explained in Section 2.1.2.1. The aim was to characterize the material for cyclic loading. However quasi static tests were performed on required on-axis and off-axis test coupons to obtain the ultimate quasi static strength of test coupons. The cyclic loading was performed for each test coupon category to obtain fatigue failure stresses. The schematic drawing of test coupons for both quasi static and cyclic loading is shown in Figure 2-13.

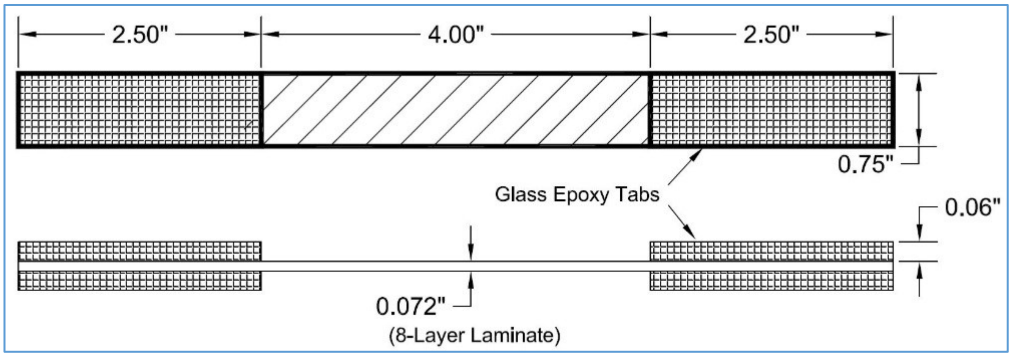

Figure 2-13 Characterization test coupons' schematic drawing

To meet the thickness requirement of test coupons, 8-layer laminates were manufactured for 0°, 30° and 45° off-axis samples using hand lay-up and autoclave process. The manufacturing process is explained in Chapter 3.

2.3.2.1. Quantity of Test Coupons for Fatigue Material Characterization

For each angle, four specimens were tested under quasi static loading to obtain ultimate strength of the specimens. This is followed by cyclic loading at three different stress levels. Stress level is the ratio of applied stress at the time of fatigue loading to the ultimate quasi static strength. For each stress level, four replica samples were tested.

Table 2-10 shows the number of specimens required to obtain each failure stress along with off-axis angles.

Table 2-10 Required Quantity of Specimens for Material Characterization to Obtain Material Failure Stresses (S-N Curves) for Implementing Hashin Failure Criteria

Mechanical Property	Panel	Ply Orientation	# of Plies	# of Samples	# of Stress Levels	Nominal Thickness (in)	Panel Size (L x W) L = 0° fiber direction (in)	Test Method	Remark
Quasi Static Loading									
0° Tension (Quasi Static) $\sigma_{11T}^{S}, E_{11T}, \nu_{12}$ (T-gage)	A1	$[0]_8$	8	4	NA	0.06	15.25x10.00	ASTM D3039	
30° Tension (Quasi Static) $\sigma_{22T}^{S}, \tau_{12}^{S}$ (T-gage)	A2	$[30]_8$	8	4	NA	0.06	15.25x10.00	ASTM D3039	Note (3)
45° Tension (Quasi Static) $\sigma_{22T}^{S}, \tau_{12}^{S}$ (T-gage)	A3	$[45]_8$	8	4	NA	0.06	15.25x10.00	ASTM D3039	Note (3)
Cyclic Loading									
0° Tension-Tension (Fatigue) σ_{11T}^{F} (Linear Pattern, High Endurance-gage)	A1	$[0]_8$	8	12	3	0.06	15.25x10.00	ASTM D3479	
30° Tension-Tension (Fatigue) $\sigma_{22T}^{F}, \tau_{12}^{F}$ (Linear Pattern, High Endurance-gage)	A2	$[30]_8$	8	12	3	0.06	15.25x10.00	ASTM D3479	Note (4)
45° Tension-Tension (Fatigue) $\sigma_{22T}^{F}, \tau_{12}^{F}$ (Linear Pattern, High Endurance-gage)	A3	$[45]_8$	8	12	3	0.06	15.25x10.00	ASTM D3479	Note (4)

Table 2-8 Continued

Notes:

Note (1): All Samples have 0.06" nominal thickness. (8-layer laminate)

Note (2): Load cycling frequency was 3 Hz.

Note (3): To obtain transverse normal strength σ_{22T}^{S} *and shear strength* τ_{12}^{S} *, the procedure is the same as the case of fatigue failure stresses* $\sigma_{22T}^{F}(R,N)$ *and* $\tau_{12}^{F}(R,N)$ *which was illustrated in Section 2.1.2.1 (E). It means that testing of off axis specimens at two different angles will reach to following equations to obtain* σ_{22T}^{S} *and* τ_{12}^{S}*:*

$$\begin{cases} \dfrac{\sin^4\theta_1}{\left(\sigma_{22T}^{S}\right)^2} + \dfrac{\cos^2\theta_1 \sin^2\theta_1}{\left(\tau_{12}^{S}\right)^2} = \dfrac{1}{\sigma_1{}^2} \\ \dfrac{\sin^4\theta_2}{\left(\sigma_{22T}^{S}\right)^2} + \dfrac{\cos^2\theta_2 \sin^2\theta_2}{\left(\tau_{12}^{S}\right)^2} = \dfrac{1}{\sigma_2{}^2} \end{cases} \tag{2-18}$$

Note (4): Fatigue failure stresses of σ_{22T}^{F} *and* τ_{12}^{F} *are obtained from Equation (2-13).*

2.3.2.2. Quasi Static, 0° Test Coupons

To set up fatigue tests, firstly the ultimate static strength of test coupons was obtained. For this reason, four 0° samples were tested uni-directionally up to failure. Figure 2-14 shows the force-displacements diagram of those test coupons. The figures show the average displacement and actuator force of about 0.364 (in) and 13124 (lbs), respectively.

Table 2-11 summarizes the static tensile strength of 0° specimens. As shown in Table 2-11, the average tensile strength of 272.40 Ksi was obtained which is in good agreement with the UTS of 0° samples coming from reference data sheet of prepreg material (CYCOM E773-S2) to be in the range of 240-260 Ksi.

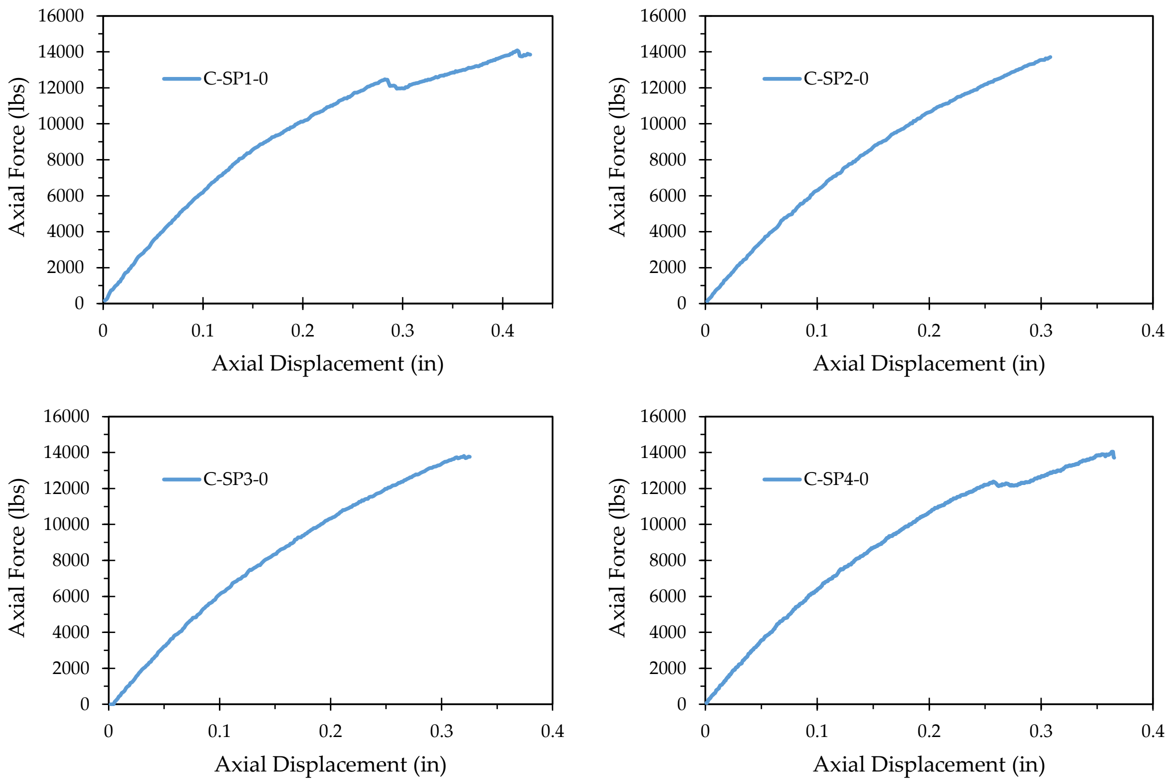

Figure 2-14 Force vs Displacement Diagram of four 0° samples

Table 2-11 Values of Tensile Force and Ultimate Tensile Strength for 0° Samples

Item	Specimen Number	Average[(a)] Width(in)	Average[(a)] Thickness(in)	Section Area(in^2)	Static Tensile Force (lbs)	Static Tensile Strength (Ksi)
1	C-SP1-0	0.7362	0.0665	0.0490	12480.04	254.95
2	C-SP2-0	0.7389	0.0667	0.0493	13831.15	280.44
3	C-SP3-0	0.7315	0.0638	0.0467	13812.49	296.04
4	C-SP4-0	0.7377	0.0650	0.0479	12373.03	258.18
Mean Value					13124.18	272.40
Standard Deviation					698.70	16.80
Coefficient of Variation					5.32	6.17

[(a)] Average value is the average of width and thickness obtained at three different points in the gauge length of each test coupon.

2.3.2.3. Quasi Static, 30° Test Coupons

Similar to 0° samples, the ultimate static strength of 30° test coupons was obtained. Four 30° test coupons were tested up to failure. Figure 2-15 shows the force- displacement diagram for those samples. The figures show the average displacement and actuator force of about 0.046 (in) and 934 (lbs), respectively.

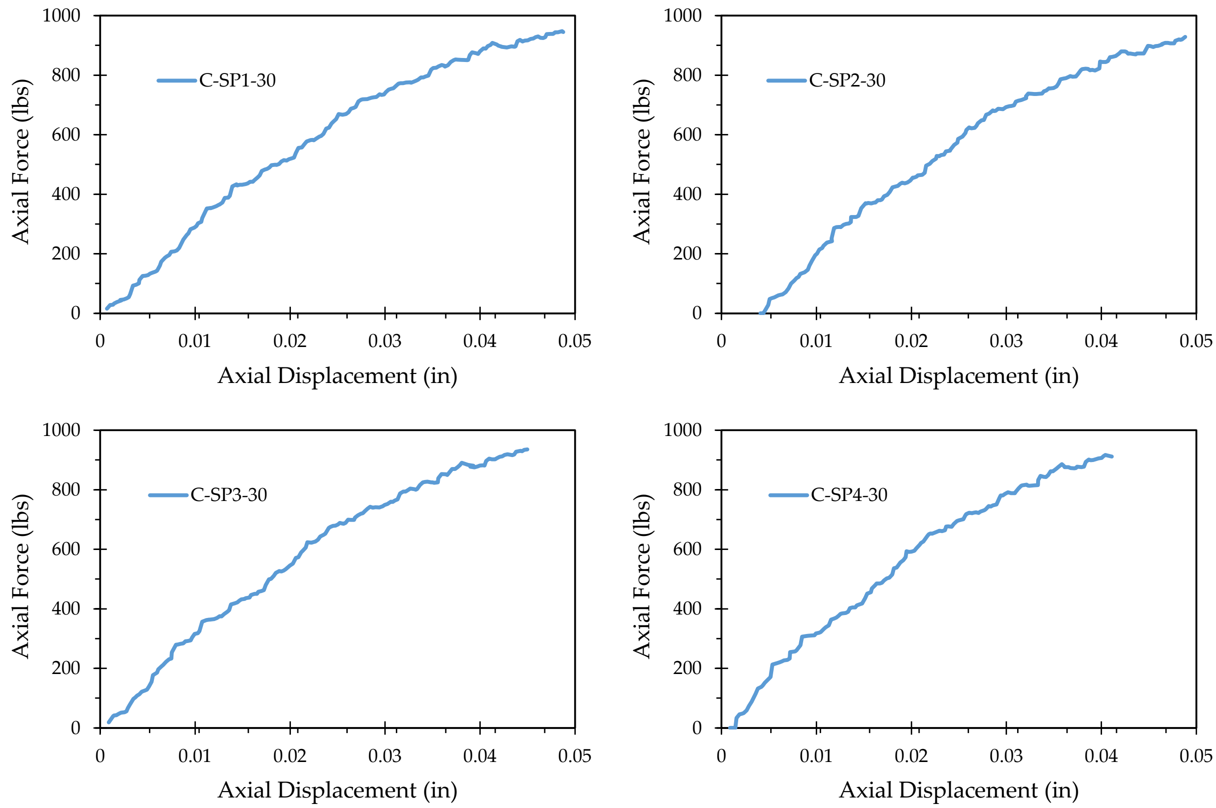

Figure 2-15 Force vs Displacement Diagram of four 30° samples

Table 2-12 shows the static tensile strength of 30° samples.

Table 2-12 Values of Tensile Force and Ultimate Tensile Strength for 30° Samples

Item	Specimen Number	Average[(a)] Width(in)	Average[(a)] Thickness(in)	Section Area(in^2)	Static Tensile Force (lbs)	Static Tensile Strength (Ksi)
1	C-SP1-30	0.7408	0.0728	0.0540	944.42	17.50
2	C-SP2-30	0.7346	0.0723	0.0531	926.44	17.45
3	C-SP3-30	0.7404	0.0728	0.0539	935.65	17.35
4	C-SP4-30	0.7369	0.0729	0.0538	929.36	17.29
Mean Value					933.97	17.40
Standard Deviation					6.89	0.08
Coefficient of Variation					0.74	0.47

(a) Average value is the average of width and thickness obtained at three different points in the gauge length of each test coupon.

2.3.2.4. Quasi Static, 45° Test Coupons

Similar to 0° and 30° samples, Figure 2-16 shows the diagrams of force versus displacements of four 45° samples. The figures show the average displacement and actuator force of about 0.037 (in) and 636 (lbs), respectively.

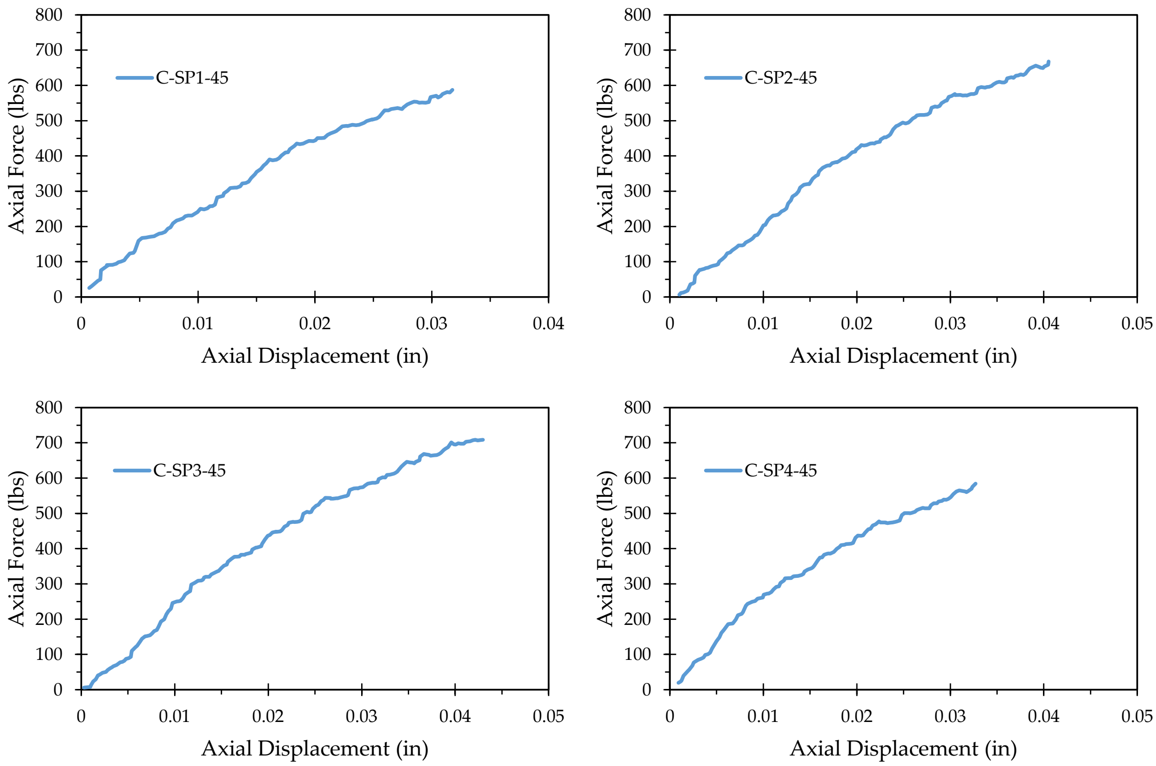

Figure 2-16 Force vs Displacement Diagram of four 45° samples

Table 2-13 shows the static tensile strength of 45° specimens.

Table 2-13 Values of Tensile Force and Ultimate Tensile Strength for 45° Samples

Item	Specimen Number	Average[(a)] Width(in)	Average[(a)] Thickness(in)	Section Area(in^2)	Static Tensile Force (lbs)	Static Tensile Strength (Ksi)
1	C-SP1-45	0.7285	0.0602	0.0438	587.43	13.40
2	C-SP2-45	0.7244	0.0689	0.0499	667.68	13.38
3	C-SP3-45	0.7317	0.0742	0.0543	708.60	13.05
4	C-SP4-45	0.7364	0.0602	0.0443	582.26	13.13
Mean Value					636.49	13.24
Standard Deviation					53.67	0.15
Coefficient of Variation					8.43	1.15

[(a)] Average value is the average of width and thickness obtained at three different points in the gauge length of each test coupon.

2.3.2.5. Cyclic Loading, 0° Samples

The average static ultimate tensile strength (UTS) for 0° samples which is shown in Table 2-11 is 272.4 Ksi. Considering this ultimate strength, cyclic loading was applied on replica samples, for 5 different stress levels of 85%, 70%, 60%, 50% and 40% of UTS. Figure 2-17 shows the S-N curve which corresponds to stress in the fiber direction $\sigma_{11T}^{F} = \sigma_{11T}^{F}(R,N)$.

S-N curve was prepared in semi-logarithmic scale. According to the literature the trend in this scale is expected to be linear which is reasonably matching with obtained number of cycles for different stress levels.

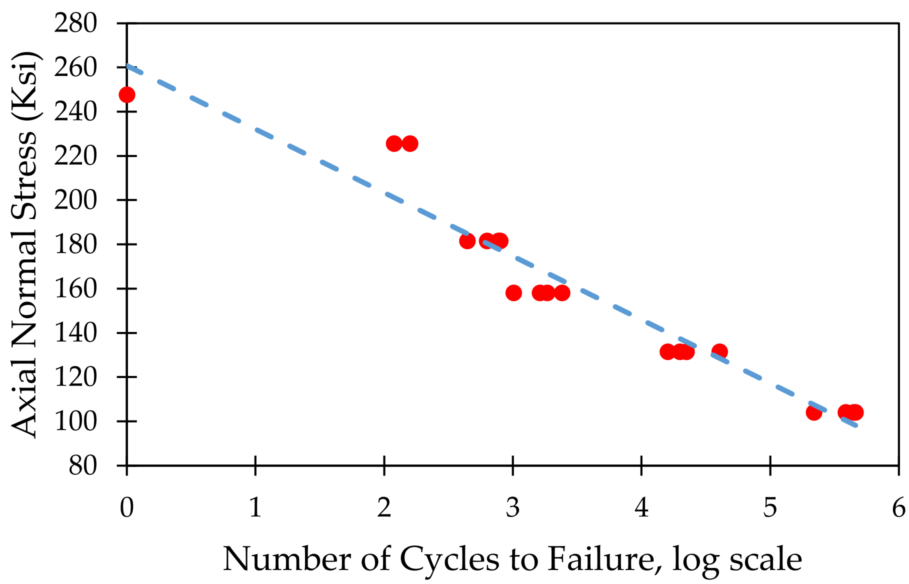

Figure 2-17 Number of cycles to failure of 0° samples under different stress levels

As shown in Figure 2-17, the number of cycles for the highest stress level of 85% of UTS is almost 150 which seems to be too low. The reason for this could be the large amount of displacement which was required to apply this amount of stress level, almost 0.218 (in). It means that the specimen was not able to withstand this large displacement under cyclic loading.

2.3.2.6. Cyclic Loading, 30° and 45° Samples

The results of cyclic loading for 30 and 45 degree off-axis samples are shown in Figure 2-18. The figure of transverse normal strength and transverse shear strength versus number of cycles is shown in Figure 2-19.

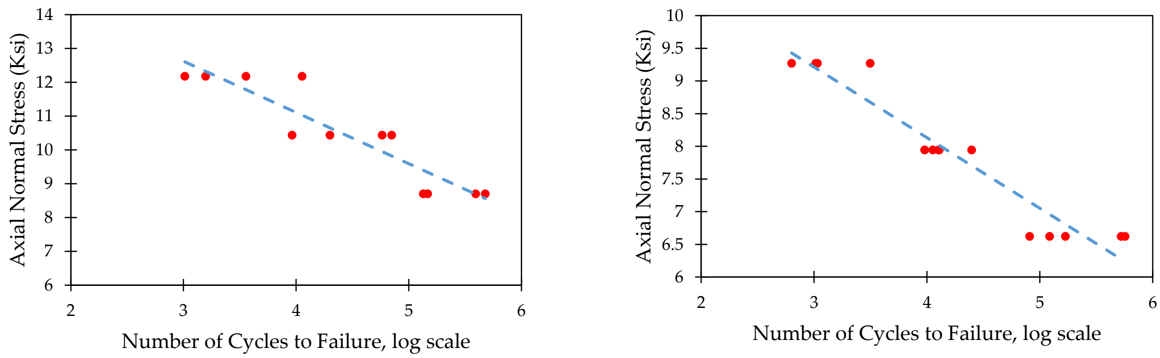

a) *b)*

Figure 2-18 S-N Curves for a) 30 and b) 45 degrees samples at different stress levels

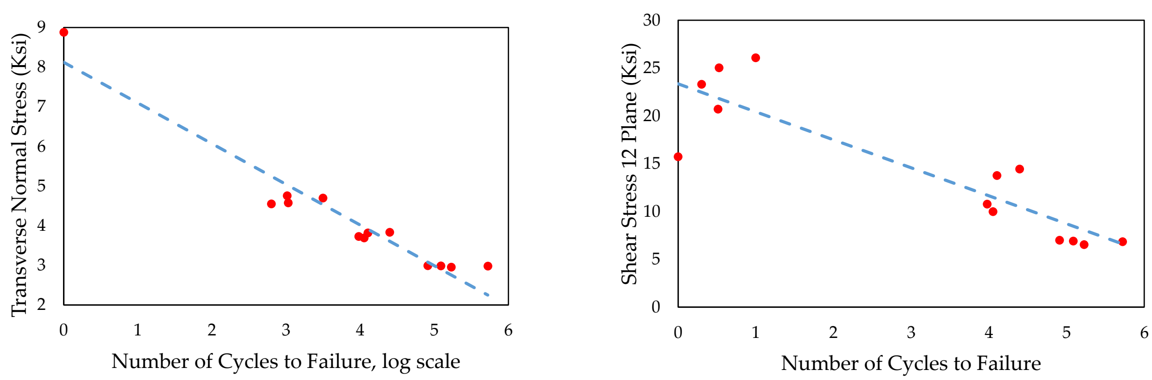

Figure 2-19 Material failure stresses for transverse normal and shear stress

2.4. Model Validation

The results of FPDM is validated against the results of experiments corresponding to both coupon level characterization tests and laminate tests.

2.4.1. Validation against Test Coupon Results

Fatigue tests were conducted on test coupons. Some results were shown in Figure 2-17 and Figure 2-18. To validate the results of fatigue progressive damage modeling, the test coupons were modeled within the FPDM. Although the stress state in these coupons seemed to be equal for all elements, there are stress gradients as the result of boundary conditions. Therefore, there will be stress gradients in the model and we need to apply finite element analysis to check the failure state of the test coupons. Figure 2-20 shows the progression of fatigue failure for the case of 0-degree samples under uni-axial fatigue tests to obtain σ_{11T}^{F}. For this specimen, applied fatigue loading was 50% of the average static strength. As shown in figure at the early stage of fatigue loading some elements fail under matrix tension failure mode (Yellow Elements). The number of failed elements increases until number of cycles reaches to 15,000, when some elements fail under fiber tension failure mode (Red Elements). Accumulation of failed elements under fiber failure mode results in failure of the whole specimen. The indication for the final failure of these samples is the failure of all elements in the width of the specimen under fiber failure mode. The number of cycles at failure is 17,000 which is corresponding with the experimental number of cycles for the specimens under 50% of deflection level in Figure 2-21-a (Axial normal strength of 123 Ksi).

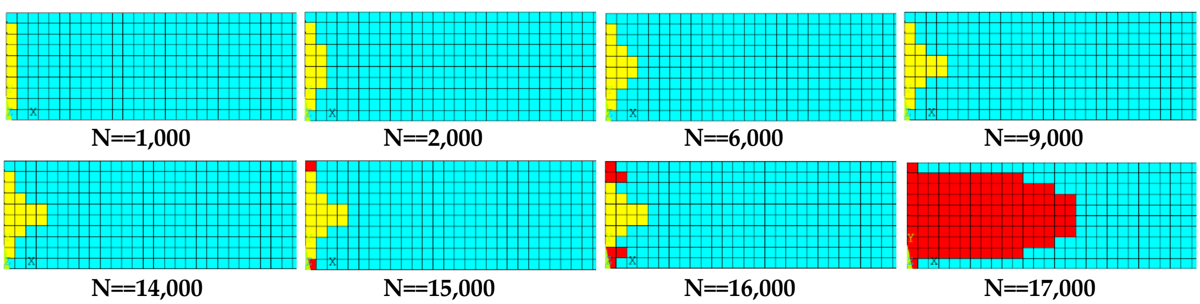

Figure 2-20 Progression of fatigue damage in 0 degree test coupons where applied maximum load is 50% of maximum static load

FPDM has been applied for the 30 and 45 degrees off-axis samples as well. Results of FPDM as number of cycles at failure for each case are combined with the test results of corresponding experiments in Figure 2-21. As shown in the figure, there is good correspondences between the results of experiments and those of FPDM for the coupon level tests.

2.4.2. Validation against Thick Laminates' Test Results

After validation of the finite element model for the simple coupon test samples as discussed in the previous section, preliminary 3D model of laminate was prepared in the ANSYS environment, as shown in Figure 2-22. The element type for all solid element is SOLID 186. The total number of elements of the model is 163777, and the number of elements for the thick composite laminate is 39021.

a)

b)

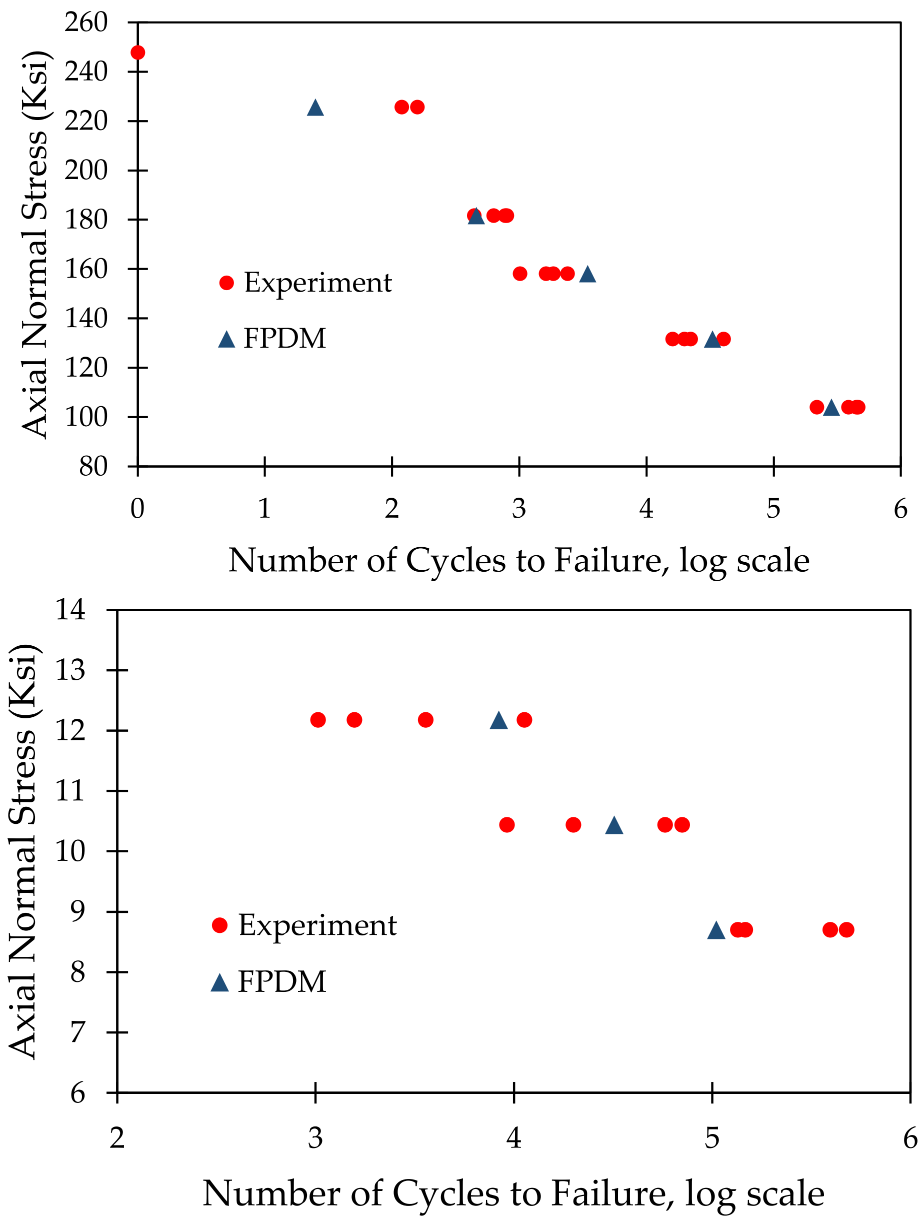

c)

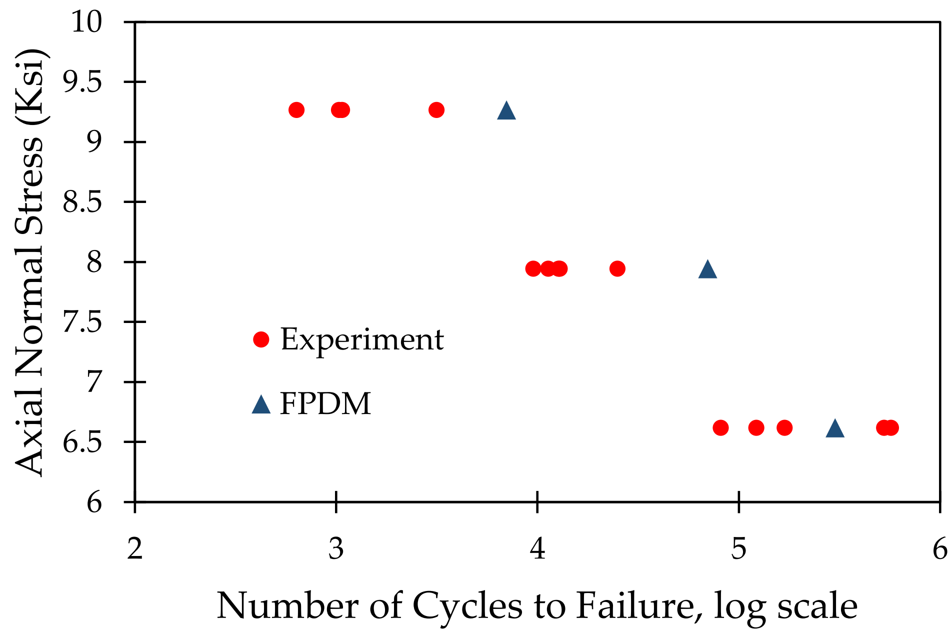

Figure 2-21 Comparison of experimental results with FPDM for a) 0-degree b) 30-degrees c) 45-degrees test coupons

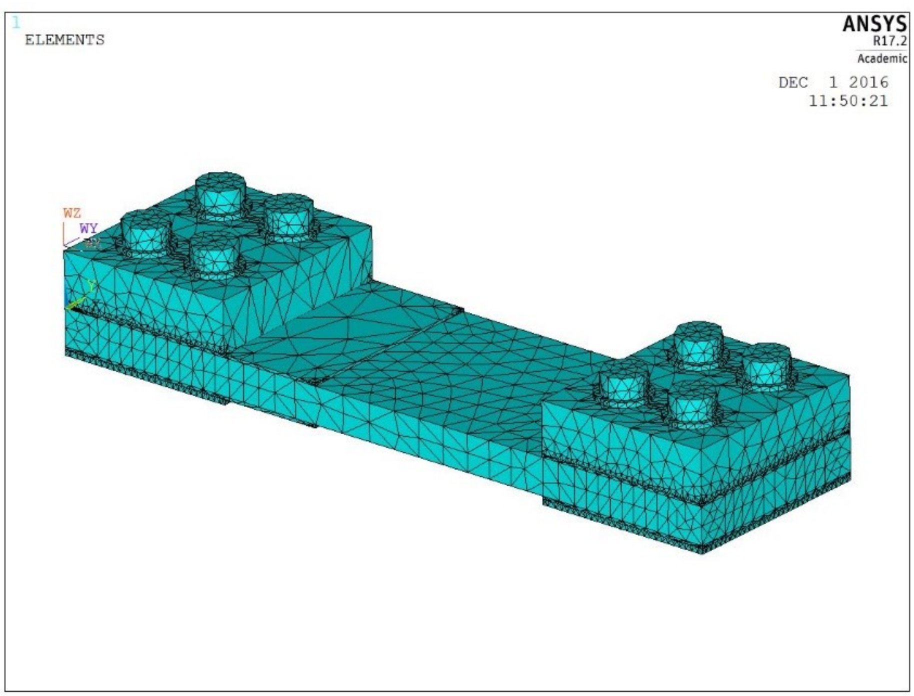

Figure 2-22 Finite Element model of thick composite laminate

2.4.2.1. Validation against available in-house test results

Wendy Xiong [65] performed fatigue tests on 80-layer unidirectional laminates with the stacking sequence of $[0]_{80}$. She performed experiments under four deflection levels. She obtained the final fatigue life for 75% of deflection level as 110,000 cycles. Based on this value the finite element model was solved up to 120,000 cycles with the load step increment of 6,000 cycles. The load step increment was selected since each run was taking almost an hour to get solved. Therefore, the whole model was solved twenty times. The progression of damage in twenty steps is shown in Figure 2-23. The yellow elements are those failed under matrix failure mode and the red elements are those failed under fiber failure mode based on Hashin-Type failure equations.

Based on the experiments reported by Wendy Xiong [65], the first delamination happened at almost 25,000 cycles. As shown in the Figure 2-23 the elements start to fail under matrix failure mode from the beginning. At 24,000 cycles there are almost 2,000 failed elements. One can consider delamination as the matrix failure. In this case the result of finite element model is fairly matching with that of experiment.

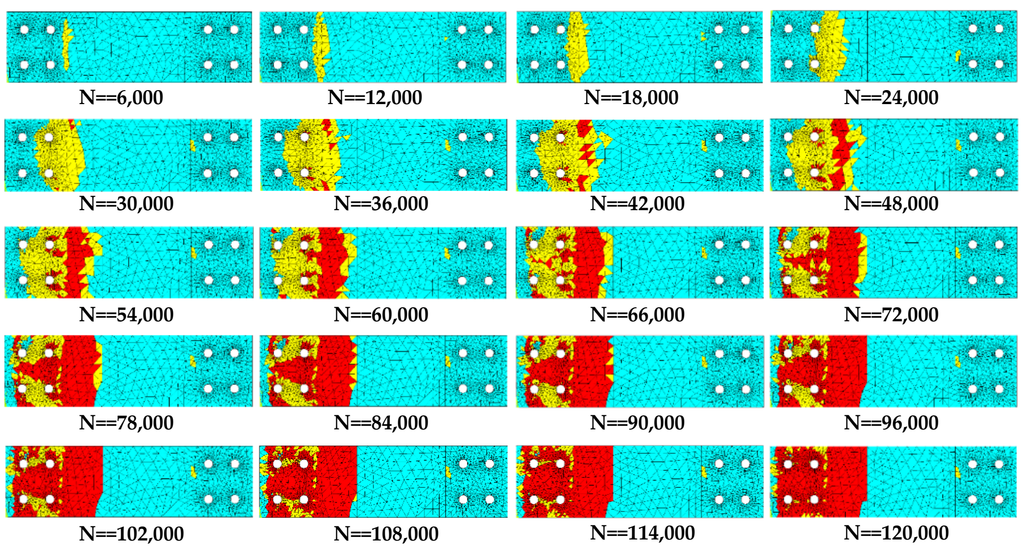

Figure 2-23 Progression of fatigue failure in the laminate for 75% of deflection level

2.5. Summary

In this chapter, a fatigue progressive damage modeling (FPDM) was developed to numerically study the behavior of thick glass/epoxy composite laminates under cyclic flexural loading. This finite element model is capable of a quick and accurate parametric study of fatigue failure of thick composite laminates.

In fatigue failure analysis of bolted thick composite laminates, the structural aspect should be taken into account, in addition to material aspect which is more applicable for thin laminates. In the developed model, the material aspect is taken into consideration using the fatigue material properties obtained from characterization experiments as S-N Curves. The structural aspect is also taken into consideration by the 3D model which identifies the location of failures and damage mechanisms by providing the tri-axial stress state of the laminate in different load cycles. At each cycle interval the material property is degraded, and the new stress state is obtained. The new stress state is processed using the failure equations which leads to track the failure propagation in the laminate. This is to state that the developed fatigue progressive damage model can consider both material and structural aspects of the thick laminate under cyclic flexural loadings.

At the end of the chapter, the results of the FPDM is validated against coupon level test results and available in-house fatigue test results and a good agreement is observed.

Chapter 3. Manufacturing of Composite Laminates

Application of advanced long-fiber composite materials especially in aerospace industry is continuously increasing. This is because of their numerous advantages including high stiffness, high strength, light weight, durability and flexibility in design. From the emergence of composite materials, many different manufacturing techniques have been introduced. In the last decade more focus has been on the manufacturing of composites using automated methods such as Automated Fiber Placement (AFP). The reason is that automated methods are more suitable for mass productions. However, manual techniques still have their place in manufacturing because of their capability in producing composites which have more desirable mechanical and physical properties. Traditional hand lay-up combined with advanced autoclave curing technique is used to produce large composite parts such as aircraft wings. The most important advantage of hand lay-up using autoclave manufacturing technique is to produce higher fiber volume fraction composites. In this study the composite laminates were manufactured using hand lay-up and autoclave technique which is described in this Chapter.

3.1. Manufacturing of Composite Laminates

In present research the laminates were manufactured using hand lay-up and autoclave manufacturing process. Raw material was provided by the industrial partner. The material was Glass/Epoxy prepreg CYCOM E773/S2. The manufacturing process mainly included five steps; Hand Lay-up and Bagging, Curing, Trimming and Drilling of Thick Laminate without Buffer Pads, Buffer Pad Bonding and Machining to the Final Size. Strain gauges and speckle patterns required for DIC measuring system were applied on the surfaces of thick laminates.

3.1.1. Hand Lay-up and Bagging

3.1.1.1. Thin Laminates

The material was characterized to obtain the fundamental material properties. The characterization tests were performed according to corresponding ASTM standard and the test results were provided in Chapter 2. In this section the manufacturing of test coupons as thin laminates is outlined.

The prepreg roll was taken off the freezer and left at room temperature for one hour in the moisture barrier bagging until it reached room temperature (thawed). This allows the temperature of the roll to increase to the room temperature. Then the prepreg was cut in required dimensions and number of layers for each test according to the test panel. The layers were left at room temperature for another 24 hours in order to make prepregs be more sticky at the time of stacking up. Then the hand lay-up procedure was followed to prepare the assembly to cure. At the time of laying up, each three layers were stacked up using roller to squeeze out the air bubbles between layers. After stacking the first three-layer, the laminate was placed under breather and inside the vacuum chamber to do debulking for 5 minutes under 27in Hg vacuum pressure. Debulking was performed to obtain better consolidation of the layers. The process of debulking was repeated until the whole required layers were stacked up. Then the laminate was ready to do bagging. The bagging procedure was performed following industrial partner prescriptions.

In contrast to wet layup, prepregs are manufactured to provide specific resin content. The bagging procedure was in such a way to avoid resin loss during curing.

3.1.1.2. Thick Laminates

Laminates with three different thickness were manufactured using hand lay-up and autoclave process. The number of layers were selected as 50, 60 and 70 layers. The nominal thickness of the laminates is 0.45, 0.54 and 0.63 (in), respectively. All laminates were made in the lay-up sequence of $[0]_n$, where "n" is the number of layers. It means that all laminates were uni-directional.
The prepreg material was stored inside the freezer. The roll of the prepreg was taken out of freezer about one hour before cutting and left at room temperature in the moisture barrier bagging. The prepreg sheets were cut in required dimensions and number of layers. The sheets were left at room temperature for 24 hours in order to make the prepreg more sticky to have good consolidation. Each three layers were stacked at each interval to do debulking. Debulking was performed under 27 (inHg) vacuum pressure for five minutes for each three-layer stack up. The process was repeated until all layers were stacked up. Backing papers of layers were counted at the time of stack up in order to prevent leaving a backing paper inside the laminate. After stacking of the whole layers, the laminate was left under vacuum for about 15 minutes in order to improve consolidation. Then the stack up was ready to do bagging.

In manufacturing of thick laminates good care was taken in order to control the resin loss at the time of curing. In this project a special bagging procedure was proposed by industrial partner and employed to prevent the amount of the resin loss inside the Autoclave.

3.1.2. Curing

ASC system (Autoclave Systems for Aerospace Composites) available at Concordia Center for Composites (CONCOM) was used to cure the composite laminates. The capacity of the equipment is 800°F temperature and 300 Psig pressure. The system is capable of real-time control of pressure, temperature and the vacuum at the time of curing.

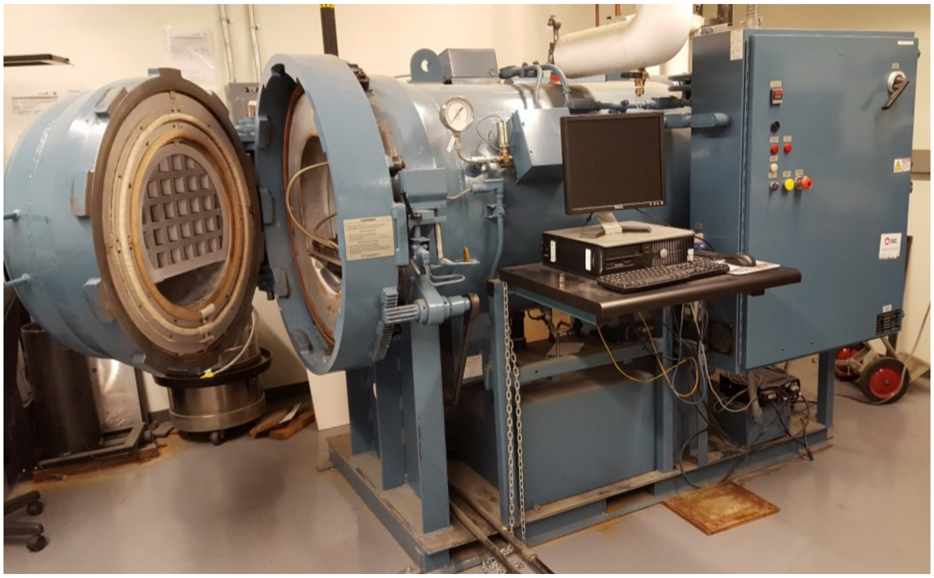

Figure 3-1 ASC Autoclave used to cure composite laminates

Selected material for this study was CYCOM S2/E773 Glass/Thermoset Epoxy prepreg (Pre-Impregnated). Laminates were cured according to industry prescribed curing cycle whose main steps are outlined as below:

a. Minimum 27 in Hg vacuum to initiate cure cycle
b. Pressurize to 10 psig
c. Ramp to 170 °F @ 2 °F/min
d. Hold for 60 min
e. Pressurize to 90 psig
f. Turn off vacuum
g. Ramp to 275 °F @ 2 °F/min
h. Hold for 60 min
i. Cool down @ 3 °F/min
j. Controlled using lagging thermocouple

Figure 3-2 shows the prescribed curing cycle. The curing cycle has been tailored through experience to result in better physical and mechanical properties of the laminates. After bagging the laminates were positioned inside the autoclave. The vacuum valves were installed and the 27 in Hg vacuum pressure was applied. The vacuum leak test was performed for one minute. The criterion for maximum vacuum pressure loss during this period was less than 3.7 percent. Once the vacuum leak test was successful, the autoclave was closed, and the curing recipe was loaded. As shown in the Figure 3-2 the temperature is increased from room temperature to 170°F by 2°F/min. 10 Psig pressure is applied during this period. Then the system is held for 60 minutes when the pressure is increased to 90 Psig and the temperature is increased to 275°F by 2°F/min. To control the resin content of the laminates at the beginning of this time segment, the vacuum pressure is vented after pressurizing to 90 Psig. The aim is to reduce the resin loss when the resin is totally liquid. Once the temperature reaches to 275°F the system is dwelled for 60 minutes. After this time segment the pressure is kept constant while the temperature is dropped to room temperature by the rate of 3°F/min.

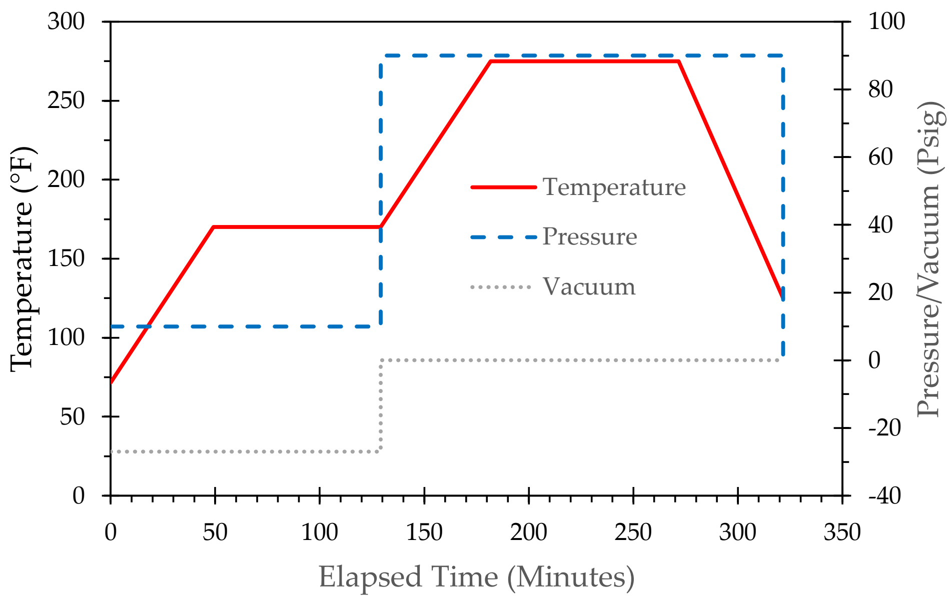

Figure 3-2 Curing cycle of S2/E773 Glass/Epoxy prepreg

Physical tests were performed to check the quality of laminates after curing. Table 3-1 summarizes the average values of quality test results.

Table 3-1 Quality Test Results

Item	Description	Reference Code	Unit	Amount
1	Fiber Volume Fraction	ASTM D2584-11	%	52
2	Void Content	ASTM D2734-09	%	1
3	Density	ASTM D792	g/ cm^3	1.89
4	Resin Weight Content	ASTM D3171-15	%	32

3.1.3. Trimming and Drilling- Laminate without Buffer Pads

At the time of hand lay-up, the cuboid of 16 (in) x 6(in) x t (in) were made where "t" is the laminate thickness and depends on the number of layers. After curing, the laminates were trimmed to the final cuboid of 14 (in) x 4(in) x t (in). This means that one inch extra dimension was considered all around in order to make specimens to have more uniform edges and minimize edge effects. After curing, the laminates were trimmed and machined to the final size and the holes were drilled in the machining shop. Figure 3-3 shows the schematic drawing of the laminates. The coordinate system is positioned at the left corner as shown. Two side surfaces which are parallel to 13 plane are defined as "Side A" and "Side B", at y=0 (in) and y=4 (in), respectively.

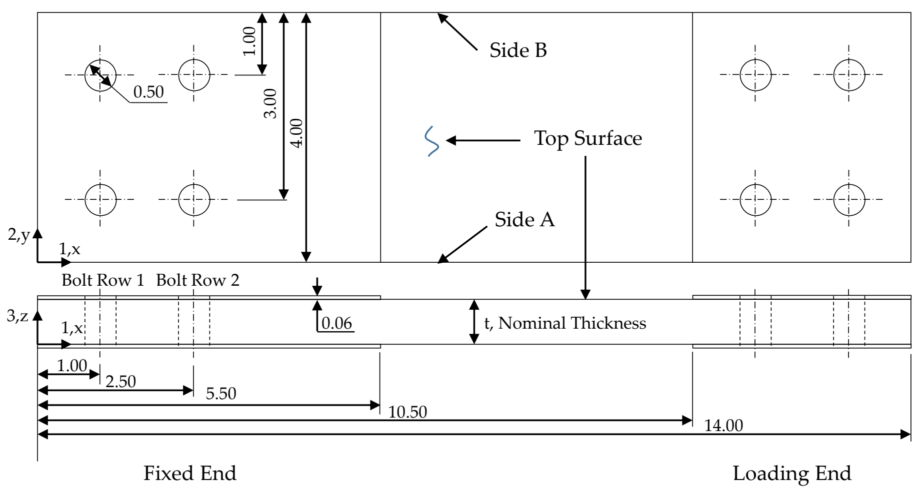

Figure 3-3 Schematic drawing of thick composite laminates

Figure 3-4 shows the picture of the laminate after machining to the final size.

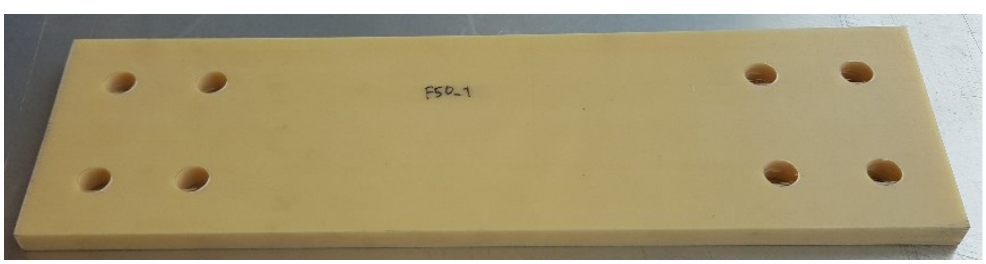

Figure 3-4 Laminate after trimming the edges and drilling the holes

3.1.4. Buffer Pad Bonding

After trimming and drilling of the laminate without buffer pads, the tabs were glued to the laminates in desired locations. The tab's material was Glass/Epoxy Ultra High Temperature Garolite (G-7) as a product of McMASTER-CARR company. The tabs are supplied in 12”x12” square laminates. The thickness was 1/16”. Thermosetting modified epoxy structural adhesive film was used to glue the tabs to the laminates. The commercial specification of the adhesive was 3M™ Scotch-Weld™ Structural Adhesive Film AF 163-2 as a product of TM manufacturer.

To bond the buffer pads, the area of the laminates which should be bonded to the tabs as well as the surfaces of tab materials were sanded using 220 grit sanding paper and electric sanding equipment as shown in Figure 3-5.

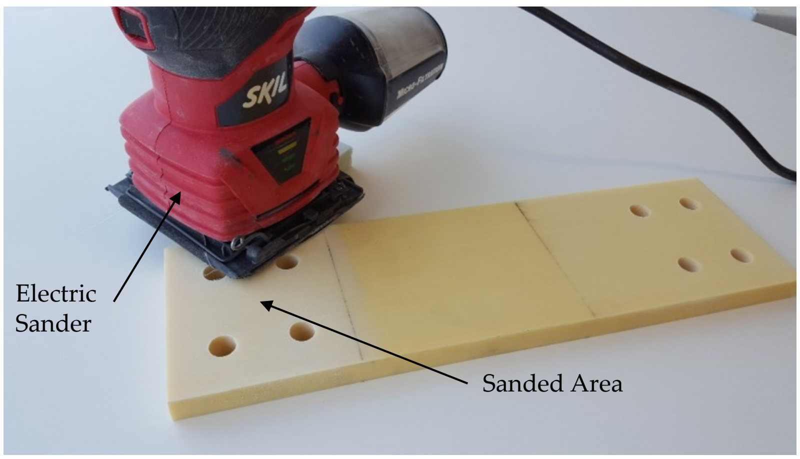

Figure 3-5 Sanding of areas to be bonded using adhesive film

The adhesive film was supplied having backing papers on both sides. After the adhesive film was cut to required size, the backing paper of one side was peeled off and attached to the laminate. Using heating gun, the attached adhesive film was heated up to around 250°F to make sure that the first adhesive surface is bonded to the laminate. The backing paper of the other side of the adhesive film was peeled off and the tab was placed on top of that.

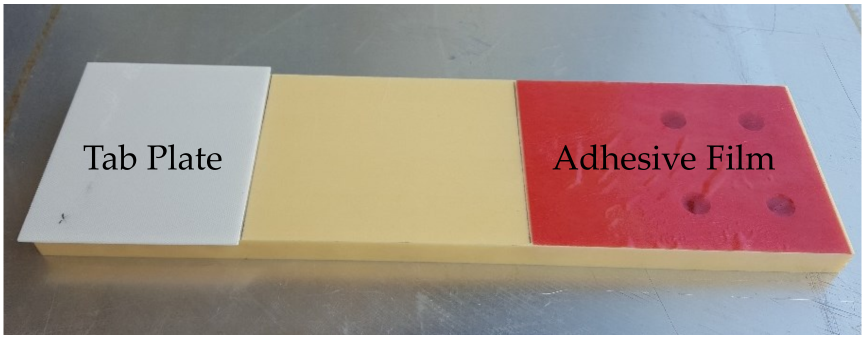

Figure 3-6 Application of adhesive film to bond the tabs

After attaching all the tabs, the assembly was bagged. The schematic of bagging for buffer pad bonding is shown in Figure 3-7

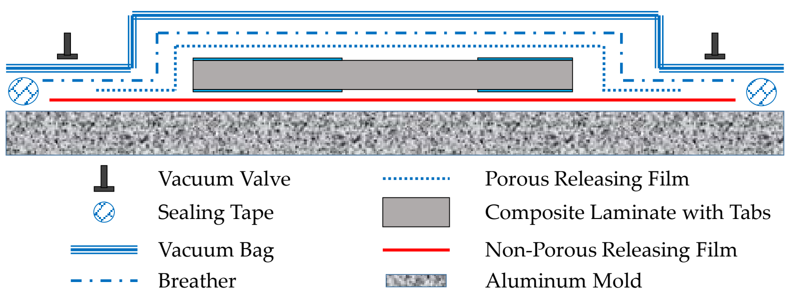

Figure 3-7 Bagging procedure for the tabs

The assembly was placed in the autoclave to cure. The curing cycle which was proposed by adhesive film' supplier is shown in Figure 3-8. As shown in the Figure 3-8, the temperature is increased from room temperature to 100°F. Then temperature is kept constant for 35 minutes. At the end of this time interval, the autoclave pressure is applied by 40 Psig and the temperature increases sharply to 230°F. Then the temperature is kept constant for 90 minutes and decreases from 230°F to 100°F in almost 30 minutes. At the end of this segment the temperature is kept constant for 20 minutes. The autoclave pressure is released at the end of this segment.

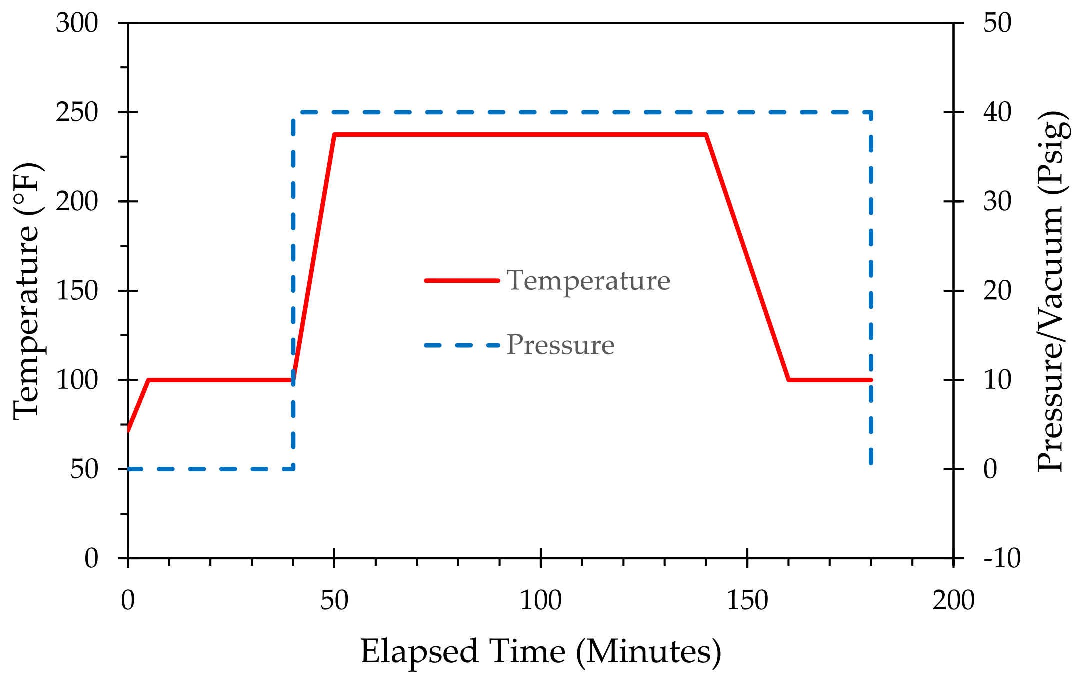

Figure 3-8 Curing cycle for installation of tabs

3.1.5. Trimming and Drilling to the final Size

After taking the whole assembly out of autoclave, the specimens were trimmed to the final required dimensions. The holes were drilled in the buffer pads. Final manufactured thick laminate is shown in Figure 3-9.

Figure 3-9 Manufactured Thick Laminates

3.2. Preparation of Thick Laminates for Flexural Testing

The experiment setup for quasi static and fatigue testing of thick laminates is outlined in Chapter 4. Strain gauges and digital image correlation (DIC) system were used to record the strain field of the laminates for quasi static testing. Therefore, it was required to install strain gauges and prepare the surfaces for DIC system. The advantage of the DIC system is providing the whole field strain distribution without contacting the specimen. The strain gauges are also used because they are more accurate. The strain gauges were used to compare and correlate the results with the results of DIC system. For quasi static specimens there were five strain gauges installed in the positions that are shown in Figure 3-10.

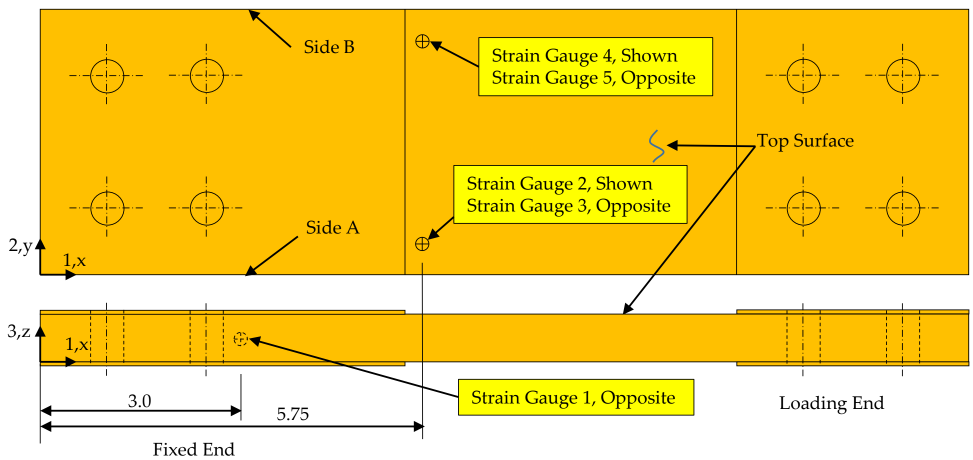

Figure 3-10 Position of installed strain gauges on the laminate

For the DIC system the top surface and "Side A" surface of the laminates were provided with speckle pattern to be able to have required contrast for DIC cameras. The prepared specimen is shown in Figure 3-11.

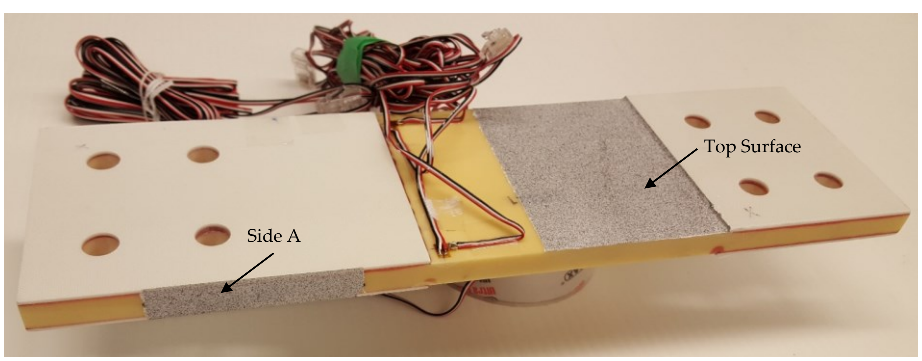

Figure 3-11 Speckle Pattern on the Top Surface and "Side A" Surface of the Laminate

3.3. Summary

The procedure for manufacturing of glass epoxy laminates was explained in this chapter. Both test coupons and thick composite laminates were manufactured using hand lay-up and autoclave process. Specific bagging procedure was proposed by industrial partner and was employed to avoid resin loss at the time of curing.

Chapter 4. Quasi Static and Fatigue Testing of Thick Laminates

In this study raw material was furnished by industrial partner as the glass-epoxy prepreg (Pre-impregnated) rolls to study the fatigue behavior of bolted thick composite laminates. At the first step, it was required to characterize the material to obtain orthotropic material properties. This was achieved by performing quasi-static experiments based on corresponding ASTM standards. At the second step, fatigue material properties as S-N curves were also obtained following corresponding ASTM standards. The results of material characterization experiments were presented in Chapter 2. Thick glass-epoxy laminates of different thickness having 50, 60 and 70 layers were manufactured and tested under quasi static and fatigue loading. To take the available test setup' capacity into consideration, all characterization tests and thick laminates' tests were performed under 3 Hz of the loading frequency. Furthermore, the loading setup was not able to apply cyclic loading on thinner than 50-layer laminates, since they required larger displacement. This means that in this study, the thickness threshold between thin and thick laminates was not determined. Instead, the comparison of the behavior of thick laminates with different thicknesses was examined.

Through the fatigue experiments the load bearing capacity of the laminates were recorded which are compared against laminates with different thicknesses to discover the thickness effect on failure mechanisms and final fatigue life of laminates. A new parameter called "Endurance Deflection Level (EDL)" is defined. "EDL" is the deflection level below which no damage would initiate inside the laminate. The relation between the "EDL" and the thickness is explained. This chapter summarizes the results of experiments on thick composite laminates.

4.1. Quasi Static Loading Experiments of Thick Laminates

Quasi static tests were performed using test setup as shown in Figure 4-1. The test equipment has been designed and manufactured at Concordia Center for Composites (CONCOM). A MTS controller is attached to the actuator to control the actuator force and displacement. A swivel joint is used between the actuator and the laminate to be able to minimize the tensile force in comparison to the bending moment, so that to have closely pure bending. The same idea has also been applied in the finite element model to simulate well the experiments, hence the tensile force has been considered as negligible.

Digital image correlation (DIC) system was used to read the strains of top and "Side A" surface as defined at Section 3.1.3. For each specimen, 5 strain gauges were installed to measure the strains of certain points as explained in Section 3.2. All quasi static tests were performed under displacement control by 0.2 in/min of actuator displacement. For the DIC system the reference images were taken before fastening of end bolts. After fastening both ends and starting the test, at each 0.2 (in) displacement the actuator was stopped to take the DIC pictures. For each thickness the results of DIC and strain gauge systems are shown in Chapter 5 and are compared with the results of finite element modeling.

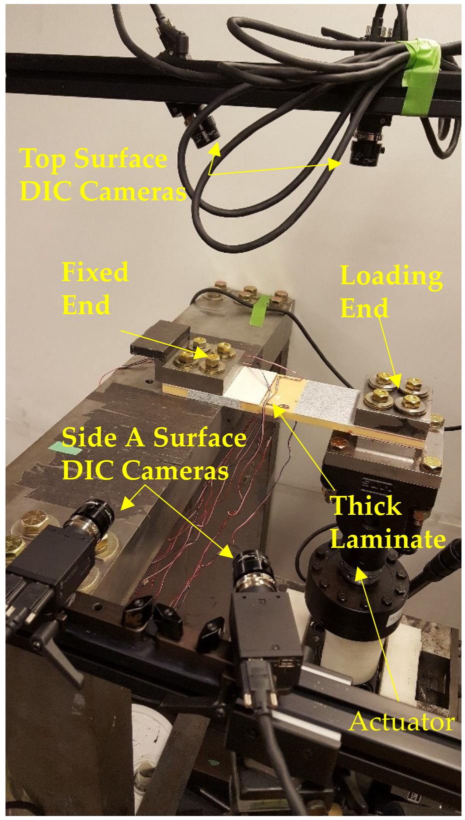

Figure 4-1 Test setup for quasi static tests

Table 4-1 shows the actuator displacement and actuator force of three laminates with different thicknesses at quasi static flexural experiments.

Table 4-1 Ultimate Force and Displacement of Three Laminates with Different Thickness under Quasi Static Test

Specimen No.	Laminate Stack-up	Nominal Thickness (in)	Actuator displacement at failure (in)	Actuator force at failure (lb)
F50_1	$[0]_{50}$	0.45	2.50	1332.9
F60_4	$[0]_{60}$	0.54	2.24	1963.7
F70_2	$[0]_{70}$	0.63	1.60	2326.0

Actuator force versus displacement for samples under quasi static tests is shown in Figure 4-2. For all laminates, there is a drop in force- displacement diagram at the beginning of the displacement which is marked in Figure 4-2. This load drop is because of debonding of the buffer pads from the laminates which took place at the early stage of the experiment.

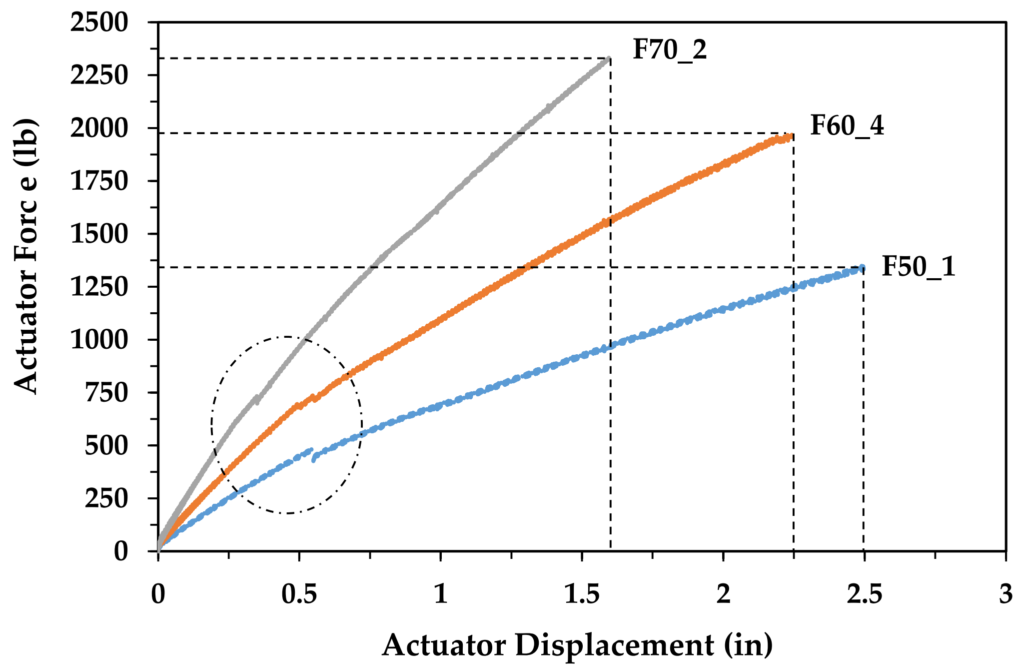

Figure 4-2 Force- displacement diagram of 50, 60 and 70-layer zero-degree unidirectional laminates under quasi static tests until final failure

After finishing quasi static tests, the specimens were cut in transverse directions to observe the failure status inside the laminates. Figure 4-3 shows the delamination and shear-out cracks in F50_1 specimen which failed at 1332.9 (lb) of actuator force. In this figure the “x” coordinate is along the length of the specimen. The “y” and “z” coordinates are in the width and thickness direction of the specimen, respectively. The whole width and thickness of the specimen corresponding to each transverse cut is shown in the figure.

The failures as shown in Figure 4-3 could be categorized in two groups based on the transverse location. From the second row of the bolt holes, which is designated as “Section E-E” in Figure 4-3, towards the fixed end of the laminate, there are shear-out cracks. Shear-out cracks are those which are produced because of existence of the bolt holes. From “Section E-E” towards the loading end, a horizontal delamination is observed which propagates until “Section G-G”.

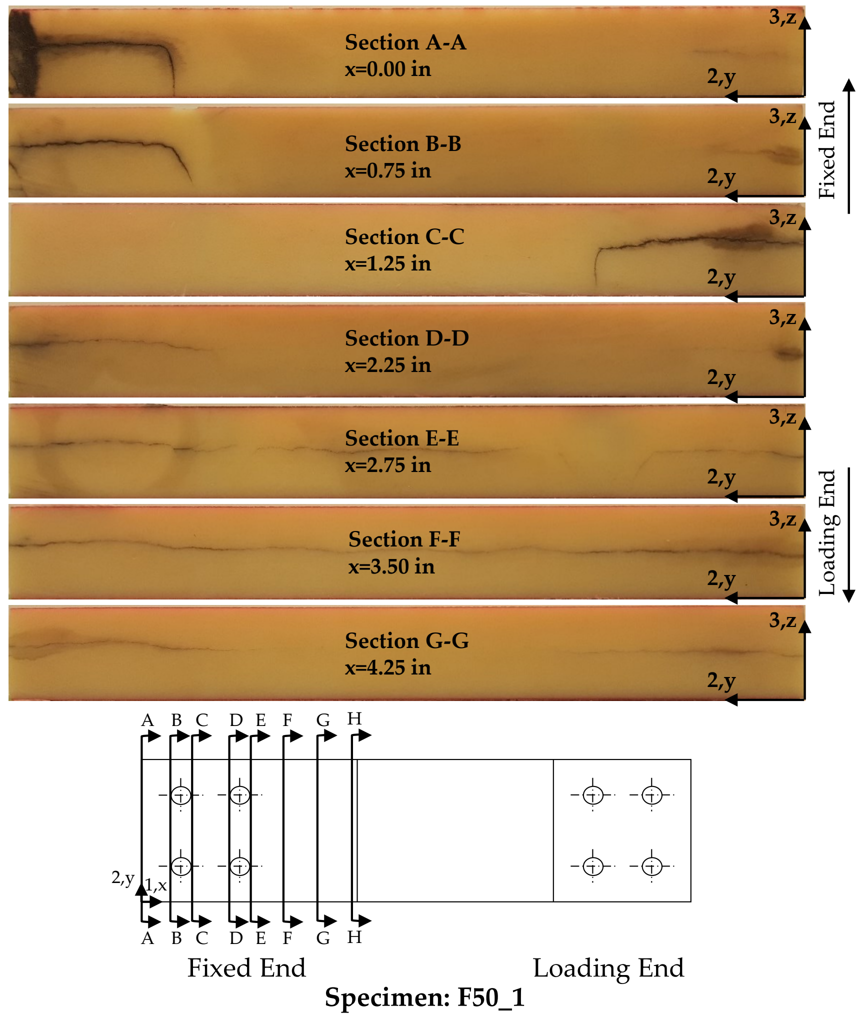

Figure 4-3 Transverse sections representing failure damages of specimen F50_1 under quasi static loading, failed at 1332.9 (lb) of actuator force

Similar damage mechanisms, but not with the same damage intensity status, is observed for F60_4 specimen which failed at 1963.7 (lb) of the actuator force, as shown in Figure 4-4. Referring to Figure 4-3 and Figure 4-4, the failure status of thick laminates under quasi static failure is a combination of shear-out cracks and delamination. The case is different for the behavior of thick laminates under cyclic loading as will be discussed in following section.

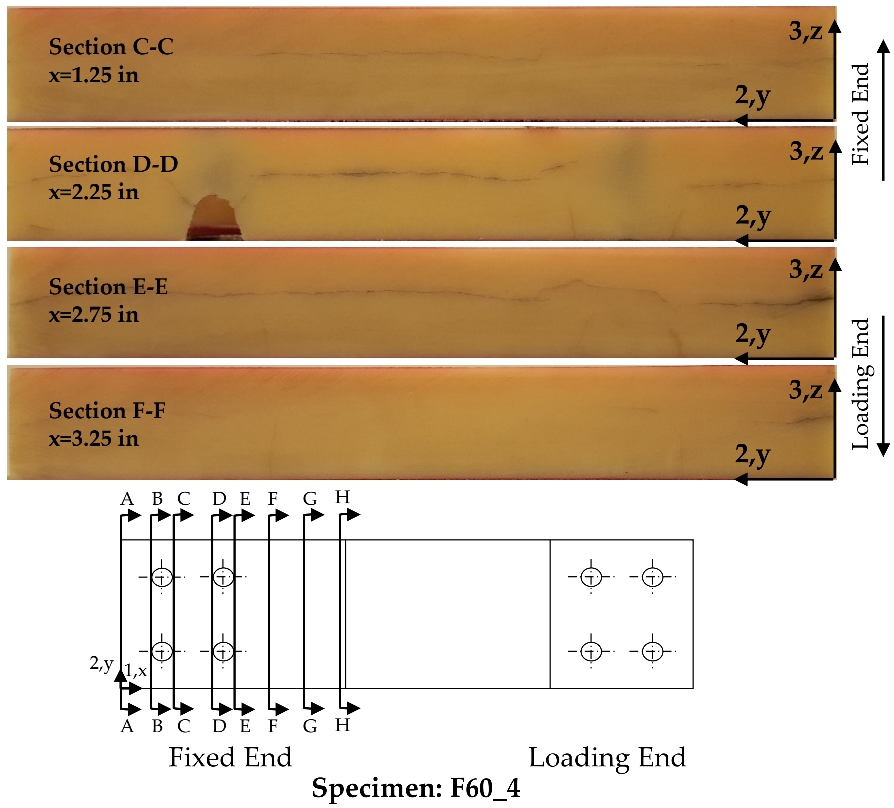

Figure 4-4 Transverse sections representing failure damages of specimen F60_4 under quasi static loading, failed at 1963.7 (lb) of the actuator force

4.2. Cyclic Loading Experiments of Thick Laminates

Fatigue tests were performed using the same test machine which was used for quasi static tests. However, the test setup was different. For the DIC system for fatigue tests, four cameras were used to focus on two side surfaces as shown in Figure 4-5, instead of top surface which was inspected by DIC in quasi static tests. Furthermore, a thermal camera was used to record the temperature of "Side A" surface.

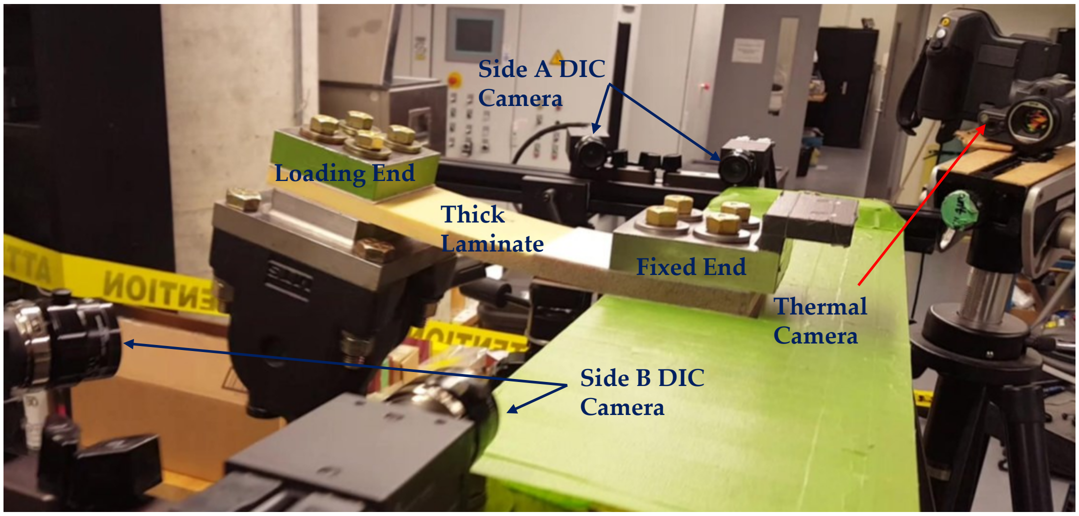

Figure 4-5 Test setup for fatigue tests

All fatigue experiments were performed under displacement control test. Test frequency was 3 (Hz) which was selected as the same frequency for material characterization phase. The specimens were loaded between minimum and maximum actuator displacement by the frequency selected. The ratio between minimum and maximum displacements is named as "Deflection Level". The maximum value for the actuator displacement is determined based on the ultimate displacement at quasi static failure of the same thickness laminate as listed in Table 4-1. For each thickness three samples were tested under three different deflection levels. The status of tested samples under fatigue loading is summarized in Table 4-2.

Table 4-2 Actuator Displacements for Three Laminates with Different Thicknesses under Different Deflection Levels of Fatigue Tests

Specimen No.	Number of layers	Nominal Thickness (in)	Deflection Level (%)	Maximum Actuator displacement (in)	Minimum Actuator displacement (in)
F50_5	50	0.45	60	1.4	0.14
F50_3	50	0.45	65	1.5	0.15
F50_4	50	0.45	70	1.6	0.16
F60_2	60	0.54	60	1.3	0.13
F60_1	60	0.54	65	1.4	0.14
F60_3	60	0.54	70	1.5	0.15
F70_4	70	0.63	60	0.9	0.09
F70_5	70	0.63	70	1.1	0.11
F70_1	70	0.63	75	1.2	0.12

After aligning the specimen in the test setup, the reference DIC image was taken with the bolts not tightened. Then the actuator was loaded to position the specimen at the maximum displacement. During this period, the actuator was stopped every 0.2 (in) of actuator displacement to take DIC images. After running the fatigue test, the actuator was programmed to stop every 1,002 cycles to take DIC images. This system could capture the delamination appearance and growth on the side surfaces. For the thermal images the same procedure was followed.

4.2.1. 50-Layer Laminates

4.2.1.1. Specimen No. F50_5, 60% Deflection Level

F50_5 was tested under 60% of deflection level. The maximum actuator displacement at fatigue loading was 1.4 (in). Figure 4-6 shows the load ratio reduction (LRR) and “Side A” surface temperature. For this specimen delamination appeared on “Side A” at around 596,000 cycles. This is the point that the load ratio starts to decrease drastically as indicated in Figure 4-6. Having said that, the load ratio did not decrease by more than 14% after one million cycles.

“Side A” surface temperature increased by 8.3°C during one million cycles. However, most of the temperature increase is related to the period between 10,000 and 50,000 number of cycles. One can say that after reaching of the side surface temperature to around 31°C at 50,000 cycles, heat transfer through convection equalizes the generated heat inside the specimen with that of transferred to the environment, due to larger temperature gradient. Furthermore, the drastic temperature rise starting from 10,000 cycles could correspond to the first initiated delamination inside the laminate.

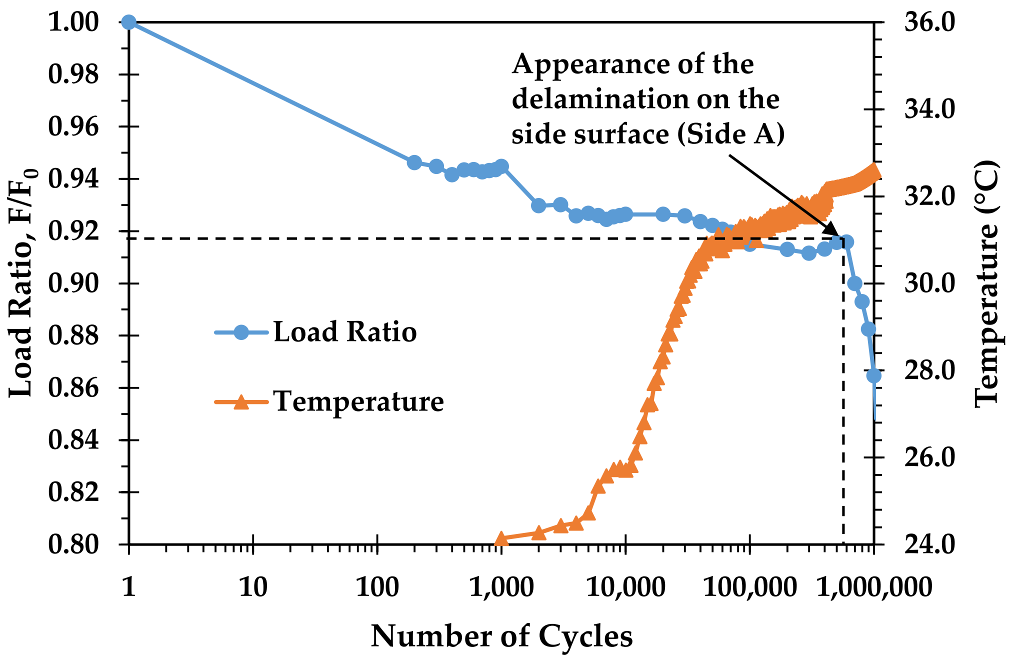

Figure 4-6 Load ratio reduction (LRR) and "Side A" maximum surface temperature for sample F50_5 under 60% deflection level

DIC out-of-plane shear strain contour of "Side A" is shown in Figure 4-7 at two different number of cycles. From the starting point of fatigue cycles up to N1=520,038 the contour of shear strain shows the maximum region well centered at around mid-thickness. By approaching the number of cycles corresponding to the appearance of the delamination on the side surface, the maximum value region moves upward to the upper half of the thickness. This could be because upper half of the specimen is under compressive longitudinal stress which helps to occurrence of delamination under compression.

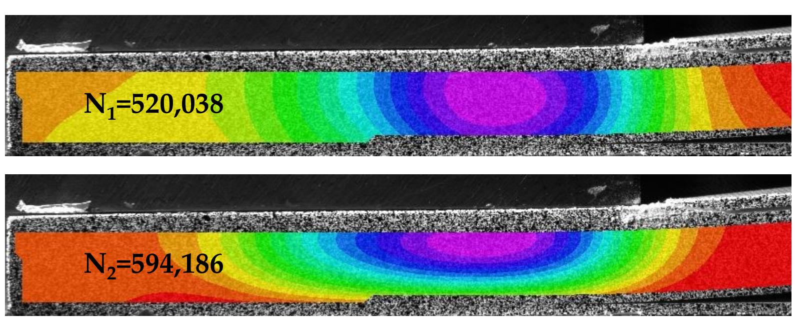

Figure 4-7 Out-of-plane shear strain γ_{13} distribution on the "Side A" surface of specimen F50_5 at two different number of cycles

The numerical values of out-of-plane shear strain were extracted from DIC system using the system software. The relocation of the out-of-plane shear strain profile is shown in Figure 4-8. This figure shows that with increasing of number of cycles the region for maximum value for out-of-plane shear strain moves upward in the thickness direction. The reason for this could be the existence of the compressive stresses on the upper half of the specimen. Observing this behavior, there is an expectation to see the appeared delamination in the upper half- thickness of the laminate. The profile also shows that the out-of-plane shear strain increases sharply at the last 12% of the whole fatigue life of the specimen before appearance of the delamination on the "Side A" surface. This fact is to support the idea that there is a correlation between the sharp increase of out-of-plane shear strain and that of occurrence of delamination.

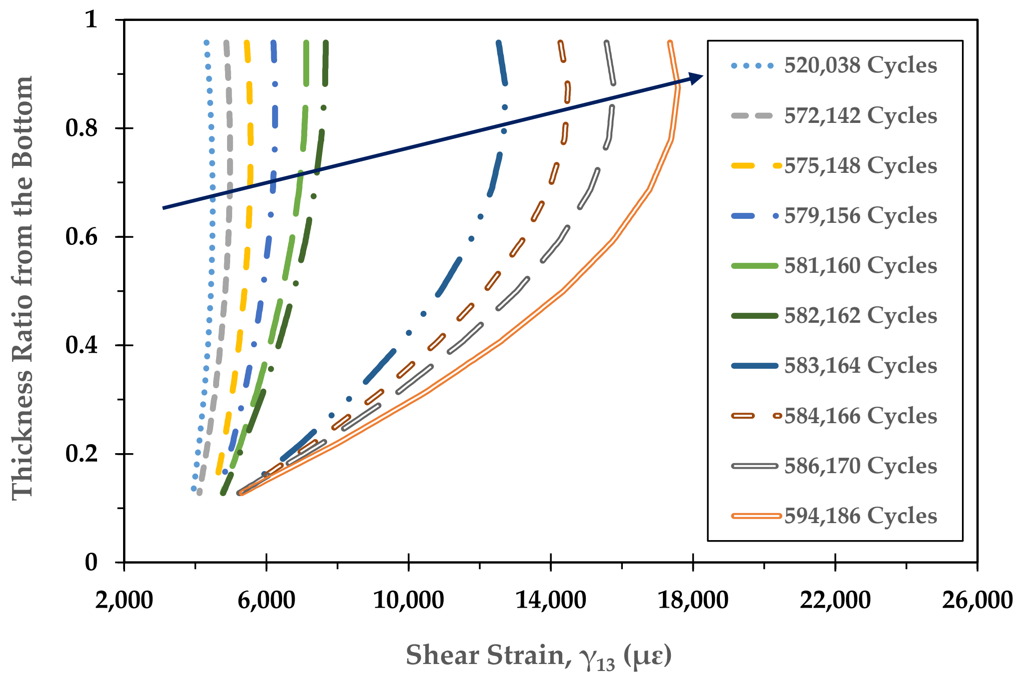

Figure 4-8 Profile of out-of-plane shear strain γ_{13} on the side surface of specimen F50_5 at different number of cycles

Figure 4-9 shows the amounts of maximum out-of-plane shear strain on the "Side A" surface of F50_5 specimen. From the beginning of the fatigue loading, the shear strain is almost constant until N=524,038 cycles as indicated as "Region 1". The slight decrease of shear strain in "Region 1" could be because of the relaxation of the specimen under constant amplitude displacement loading. At N=524,038 cycles the shear strain starts to increase sharply which relates to "Region

2”. One cycle interval before appearance of the delamination on the “Side A” surface, the shear strain sees its maximum value.

One can say that the “Region 1” in Figure 4-9 is the part of the fatigue life of the specimen where damage has not yet initiated inside the specimen. At N=520.038 cycles, the damage initiates so that the sharp increase in out-of-plane shear strain on the “Side A” surface starts to happen. “Region 2” is then related to the propagation of the internal crack inside of the laminate until it appears on the “Side A” surface at 596,000 cycles.

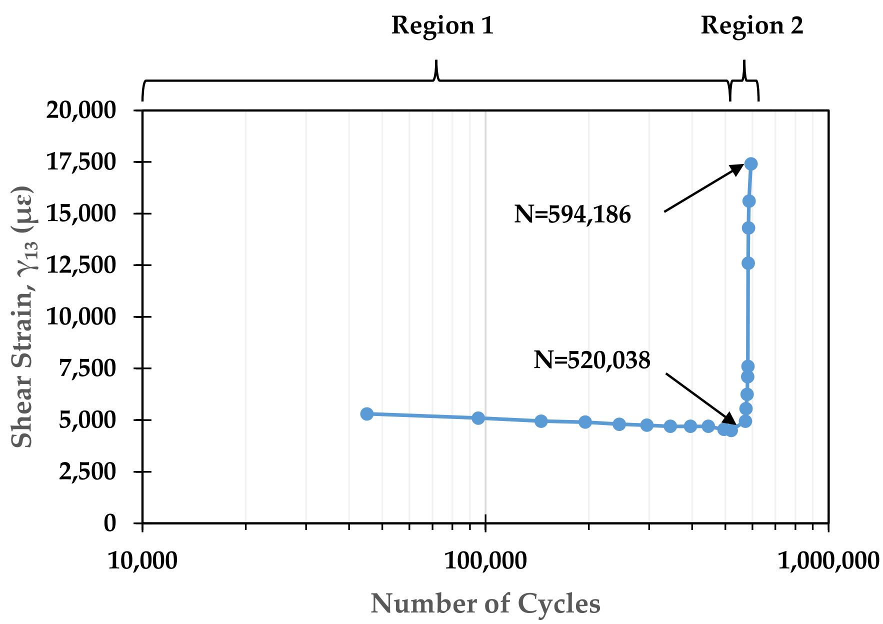

Figure 4-9 Maximum out-of-plane shear strain γ_{13} on the “Side A” surface of specimen F50_5 versus number of cycles

The final state of the specimen F50_5 is shown in Figure 4-10. There is a delamination on “Side A” which has propagated to the end of the specimen. There is no delamination observed on the “Side B” surface.

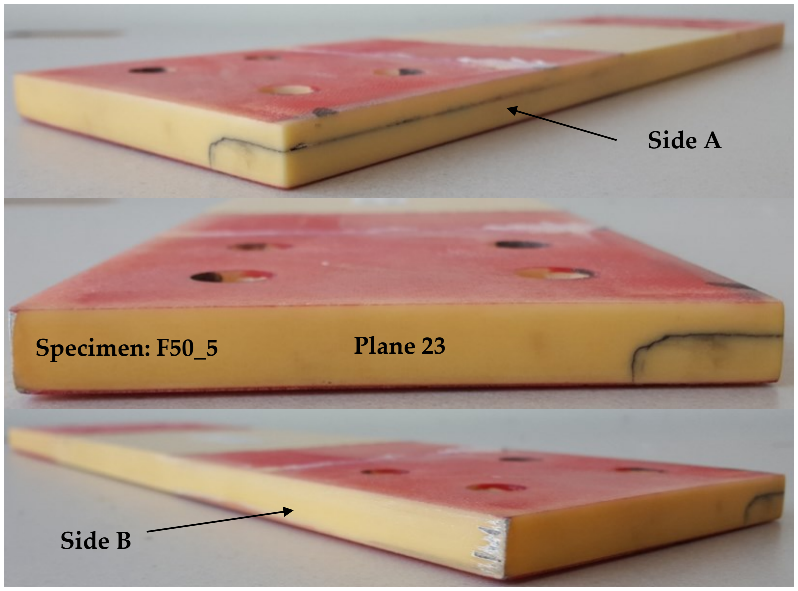

Figure 4-10 Delamination and shear-out cracks of specimen F50_5 after final failure

After finishing the test, the specimen was cut in transverse directions at different locations. Two sections are shown in Figure 4-11. The upper picture shows the shear-out crack starting from the zero point in x axis. At x=2.75 in, which is the transverse cut right after the second row of the bolt holes, another shear-out crack is observed as shown in the lower picture.

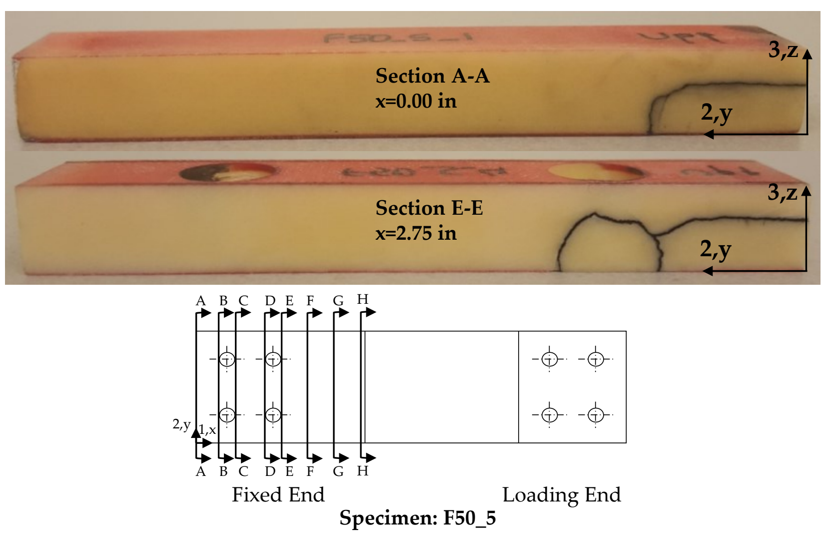

Figure 4-11 Delamination and shear-out cracks of specimen F50_5 on the transverse planes at different locations

4.2.1.2. Specimen No.: F50_3, 65% Deflection Level

This specimen was tested with 1.5 (in) of maximum actuator displacement which corresponds to 65% of deflection level. The load ratio reduction (LRR) and "Side A" surface temperature are plotted in Figure 4-12. The discontinuity in the temperature profile is because of the technical interruption that happened during the test and the experiment was restarted the day after. Load ratio profile shows a mild decrease at the beginning part until about N=40,000 cycles where load ratio starts to decrease dramatically. At this point there was no damage appeared on the surfaces of the laminate based on the DIC images and observation of the test specimen under fatigue loading. Therefore, this point is assumed to correspond to the initiation of damage inside the laminate which is indicated as "1st Internal Delamination" in Figure 4-12. Based on the load ratio figure, this specimen failed at around N=488,000 cycles as it lost more than 20% of load bearing capacity.

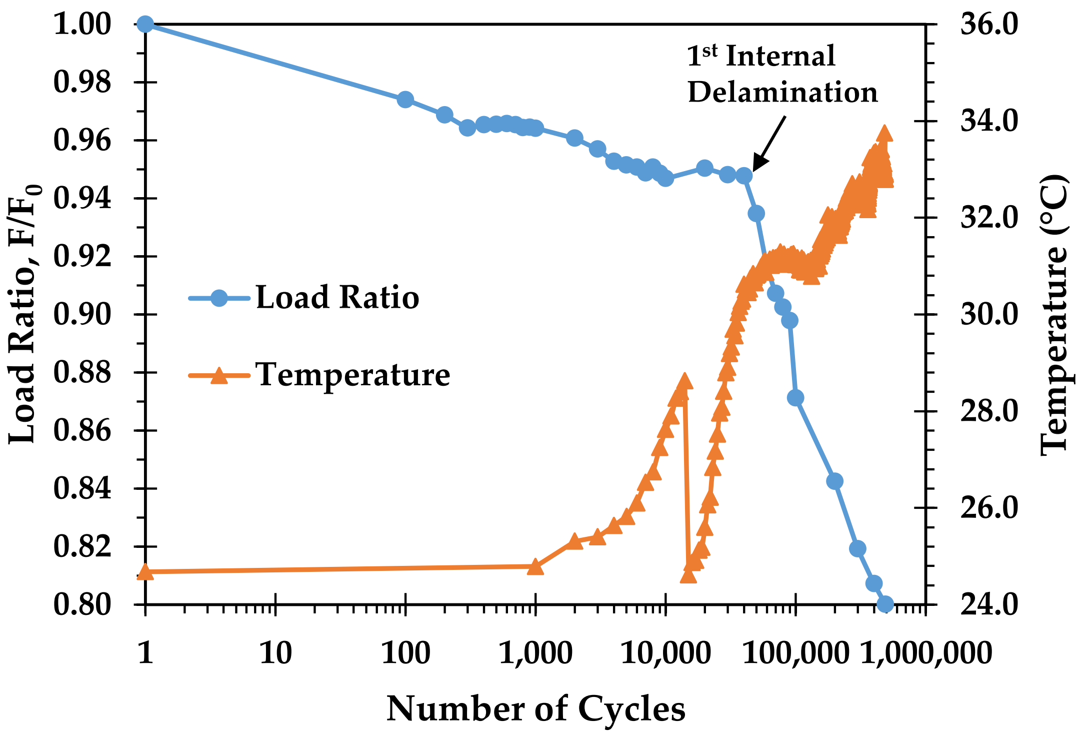

Figure 4-12 Load ratio reduction (LRR) and "Side A" surface temperature for specimen F50_3 under 65% deflection level

From the DIC images that were being taken every 1,002 cycles, delamination damages appeared on the side surfaces before the final failure. Figure 4-13 shows the DIC images of the side surfaces at two different cycle intervals. The first interval as N_1=1,002 cycles is almost the beginning of the cyclic loading. N_2 is related to the cycle interval right before the appearance of the delamination on that side surface. As shown in the figure, the delamination appears on "Side B" earlier at N=97,194 (One cycle interval after N2=96,192 for this side surface). Later, the delamination appears on "Side A" at N=219,438 (One cycle interval after N2=218,436 for this side surface). Furthermore, the contour of the shear strain shows that for both side surfaces, at N=1,002 cycles, the contour of the maximum out-of-plane shear strain region is well centered at the mid thickness. However, for the contours corresponding to the cycle interval before appearance of delamination on each side, the maximum region moves to the upper half-thickness for the "Side A" and lower half-thickness for the "Side B". This could be because of the un-symmetry arises from either manufacturing of the test specimen or the test setup as will be discussed in Section 4.3. Henceforth it is expected to see the delamination on "Side A" and "Side B" on the upper and lower half-thickness of the laminate, respectively.

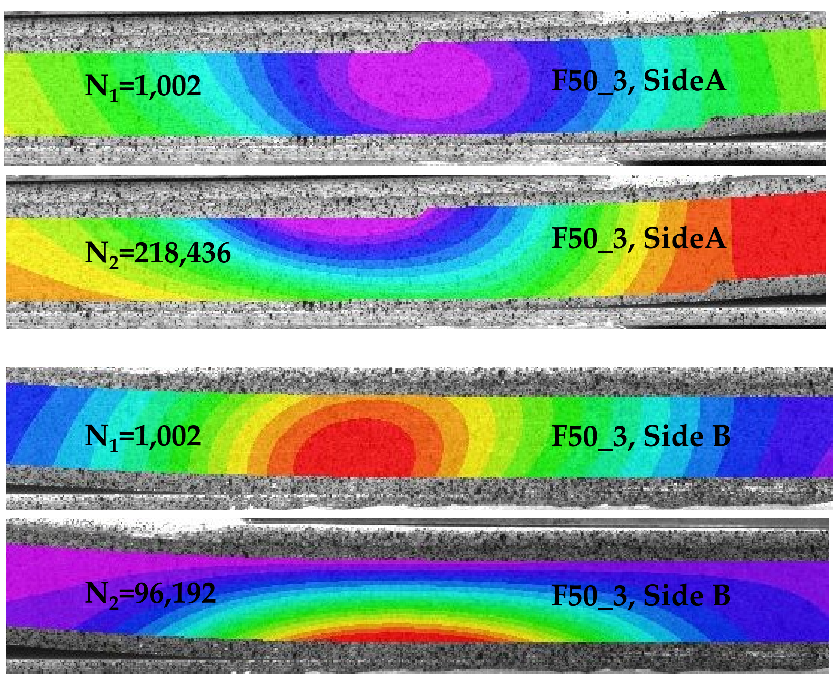

Figure 4-13 DIC images of two side surfaces at two different cycle intervals: N_1 the first cycle interval, N_2 one cycle interval before appearance of delamination on the side surface for specimen F50_3 under 65% deflection level

“Side A” of the specimen F50_3 was scanned by thermal camera and the temperature profile is shown in Figure 4-12. Furthermore, as explained above delamination appeared on “Side A” at N=219,438. Figure 4-12 shows that the temperature of “Side A” surface starts to increase sharply after mentioned number of cycles. The reason is the generated heat because of the friction of two surfaces generated by delamination. This shows that there is a correspondence between the appearance of the delamination on the side surface and that of sharp temperature increase.

The profile of maximum out-of-plane shear strain on two side surfaces of the laminate versus number of cycles is shown in Figure 4-14. The profile on both surfaces shows a sharp increase of shear strain before appearance of the damage on each side surface. The plateau region of both curves is related to the part of fatigue life before crack initiation inside the laminate. The figure shows that the jump in shear strain happens on “Side B” earlier in time which is another indication for earlier appearance of the delamination on “Side B”. Similar to previously discussed specimens, the reason for difference in the behavior of two side surfaces as regards of delamination appearance and maximum out-of-plane shear strain is existence of un-symmetry coming from either manufacturing of the thick laminates or the test setup.

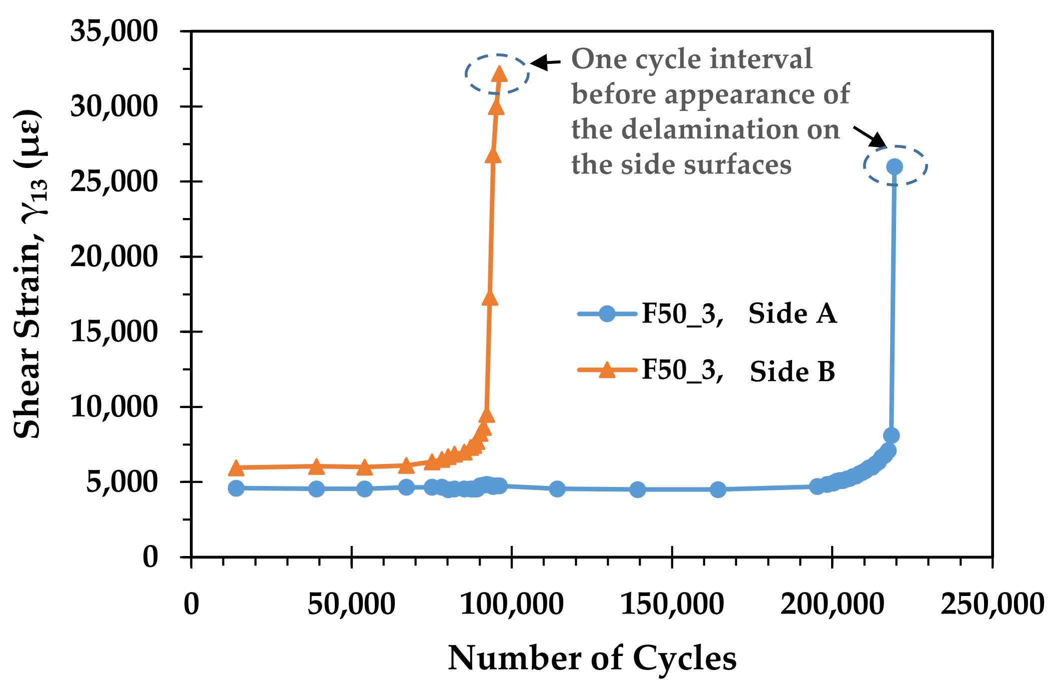

Figure 4-14 Maximum out-of-plane shear strain on the two side surfaces of specimen F50_3 versus number of cycles

4.2.1.3. Specimen No.: F50_4, 70% Deflection Level

This sample was tested under 70% deflection level. Required actuator force to maintain the displacement level decreases as shown in Figure 4-15. The figure shows that load ratio is decreasing continuously until Point A which corresponds to the occurrence of the first delamination inside the laminate, since load ratio of the sample decreases sharply after this point. This is considered as internal damage because at this point there was no damage appeared on the side surfaces of the laminate. For this reason, this point is indicated as "1st Internal Delamination" in Figure 4-15. The corresponding number of cycles to this point is about 11,000. The sample failed at around 47,000 cycles which is shown as point B in Figure 4-15. 20% of reduction in load bearing was considered as final failure.

Temperature profile in Figure 4-15 shows that "Side A" surface temperature starts to increase sharply after N=11,000 cycles which shows the correlation between initiation of delamination and sharp increase of the side surface temperature. The total temperature increase of the laminate during the whole fatigue life is about 10°C.

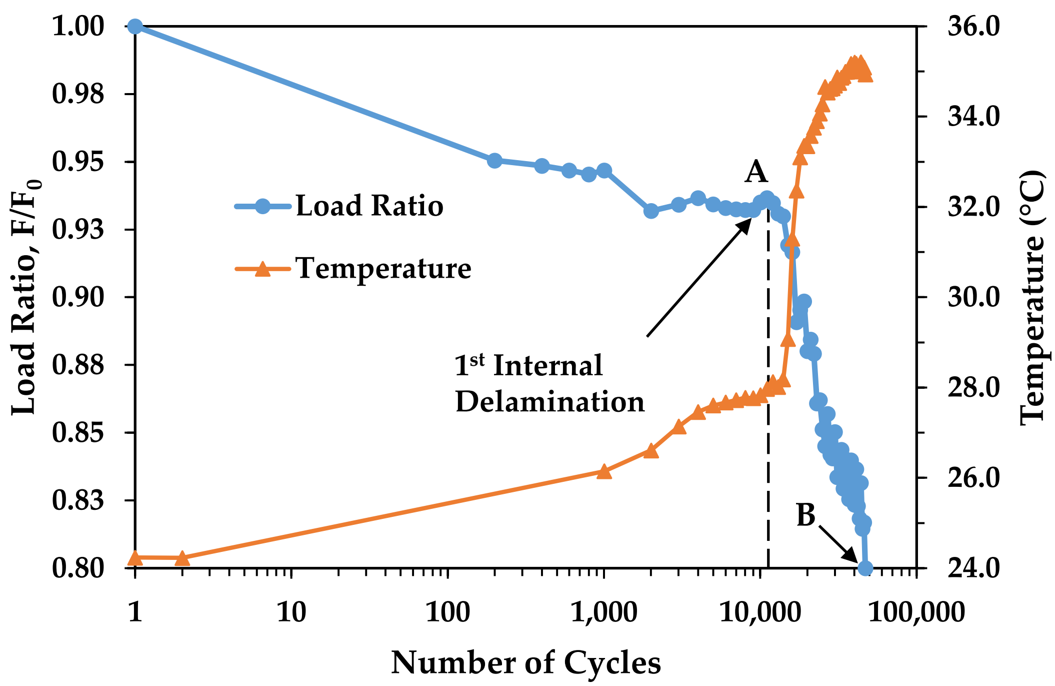

Figure 4-15 Load ratio reduction and "Side A" maximum surface temperature for specimen F50_4 under 70% deflection level

Figure 4-16 shows the contour of out-of-plane shear strain distribution on the side surfaces of the laminate at the time of cyclic loading. In this figure N is the interval number of cycles and N_f is the final fatigue life of the specimen. N_f corresponds to the point that delamination on “Side B” grew to the end point of the fixed end which happened at N_f =47,094 cycles based on corresponding DIC image. This is corresponding with the failure point B of Figure 4-15. As can be seen from the pictures in Figure 4-16, first delamination appeared on “Side A” at N/N_f=0.34. For this side the DIC picture for the previous step of N/N_f=0.32 shows the contour of out-of-plane shear strain. These consecutive DIC images at different fatigue steps show that the delamination appears in the area of the side surface where maximum out-of-plane shear strain occurs.

Comparing different N/N_f related to two side surfaces show that the first delamination appears on “Side A” at N/N_f=0.34 while it appears at N/N_f=0.49 on “Side B”. Although the delamination on “Side A” appears earlier in time, the one which appears on “Side B” propagates entirely to the edge of the fixed end at final failure. This means that the propagation rate of crack on “Side B” is more than that of “Side A”.

In a completely symmetric laminate and test setup, two side surfaces are expected to behave exactly as the same. However, because of the manufacturing discrepancies such as thickness variation and off-centered bolt holes, as well as un-symmetry of the test setup, initiated damages inside the laminate and those appeared on the side surfaces behave differently. This is seemed to be intrinsic behavior of the manufacturing and the test setup and it is impossible to some extent to control manufacturing and testing parameters to have completely symmetric test setup.

DIC images show the delamination crack. Crack lengths are extracted from DIC images at different cycle intervals. Figure 4-17 shows the crack growth on two side surfaces of laminate. As shown in Figure 4-17 delamination appears on “Side A” at around 16,000 cycles while it appears at around 23,000 cycles on “Side B”. The first appeared delamination on “Side B” is longer than that of “Side A”. Furthermore, the delamination growth rate is more for the crack on “Side B” as well. At the final failure which happens at 47,094 cycles, the crack on “Side B” reaches the end of the fixed end as shown in the lowest picture in Figure 4-16. Again, the difference in behavior of two side surfaces of the laminate under fatigue loading, is because of the un-symmetry coming from either manufacturing of the laminate or the test setup as will be explained in Section 4.3.

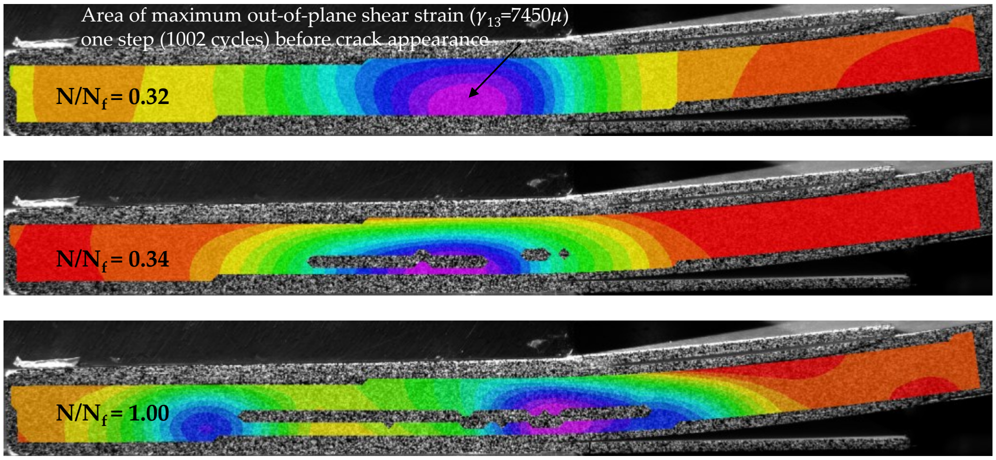

"Side A"

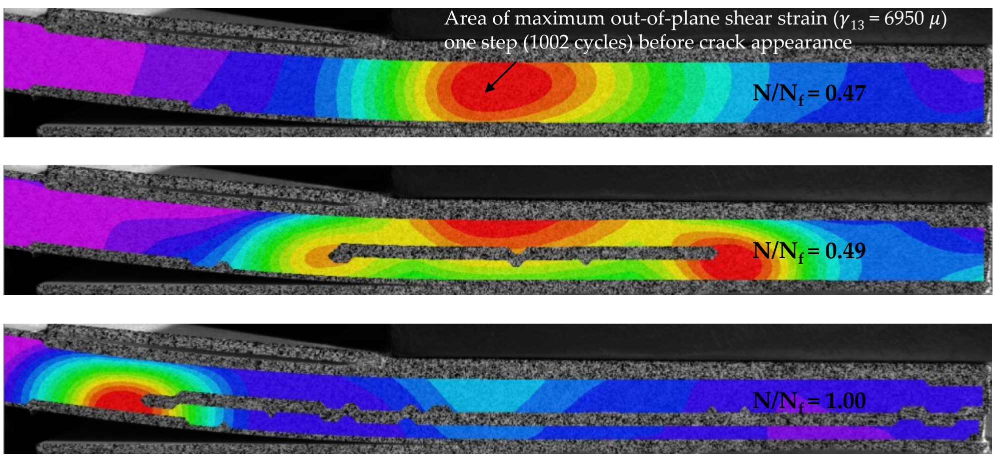

"Side B"

Figure 4-16 Out-of-plane shear strain γ_{13} distribution on the side surfaces for specimen F50_4 under 70% deflection level

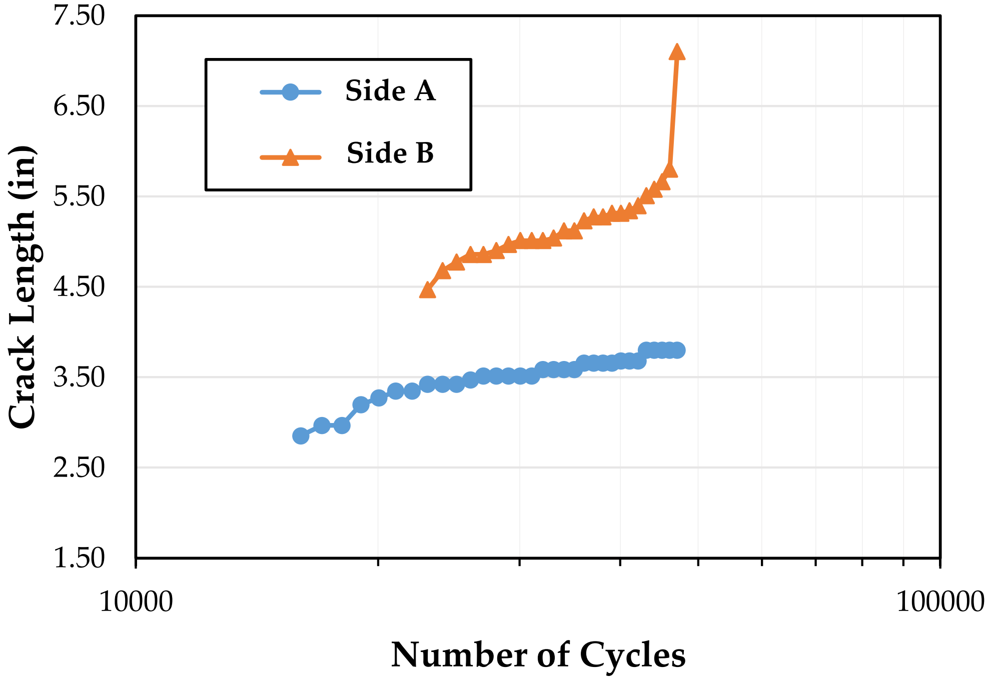

Figure 4-17 Delamination crack length growth on the side surfaces vs number of cycles for specimen F50_4 under 70% deflection level

The important stress element seems to be out-of-plane shear stress. As shown above the delamination occurs in the area of maximum out-of-plane shear strain. The increase of maximum out-of-plane shear strain is shown in Figure 4-18. The values are related to the strains in the cycle intervals until the first appearance of the crack on the side surfaces. It is seen that for both side surfaces, there is a sharp increase in the amount of maximum out-of-plane shear strain at one cycle interval before appearance of delamination on the side surfaces. The difference between the two curves in Figure 4-18 is because of un-symmetry of the laminates or the test setup. The mild increase of out-of-plane shear strain at the "Region 1" of the Figure 4-18 is related to the part of fatigue life before damage initiation. After initiation, the propagation takes place in shorter time. One can say that because of the material degradation under fatigue loading, the side surface strains increase gradually until the point that material can not sustain more shear strain. This is the point that delamination appears on the side surfaces.

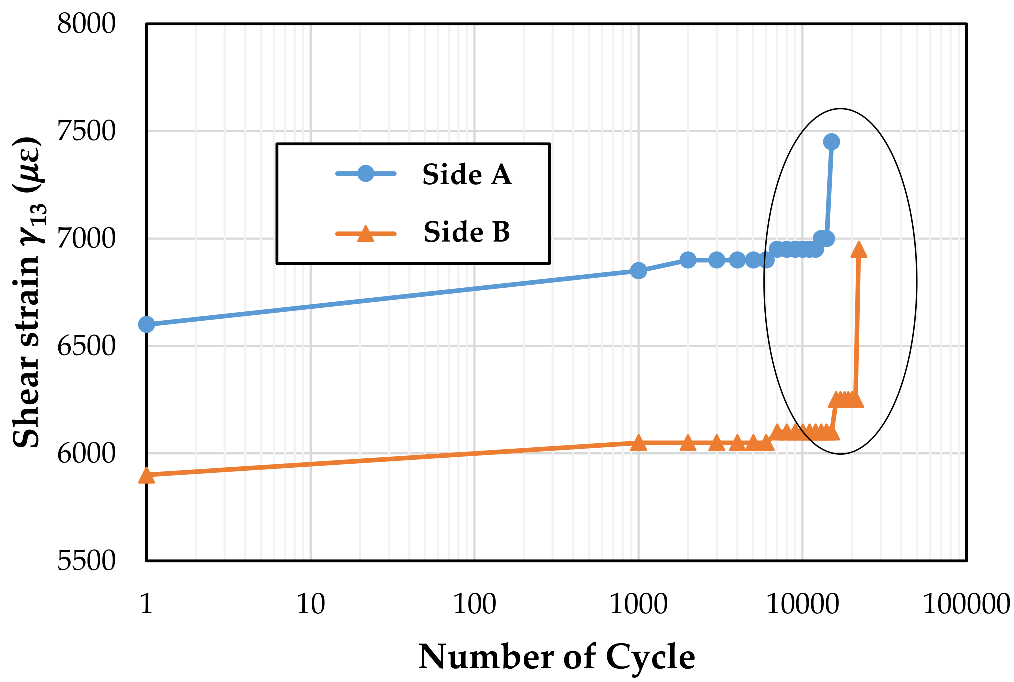

Figure 4-18 Maximum out-of-plane shear strain γ_{13} on the side surfaces vs number of cycles for specimen F50_4 under 70% deflection level

Figure 4-19 shows the picture of the laminate after final failure. As shown in the figure the final crack length of the delamination on “Side A” is much less than that of corresponding crack for “Side B”. However, the former appeared earlier in time. Furthermore, this picture shows that the delamination on “Side B” propagated towards the fixed end and appeared on the plane 23 as a shear-out crack.

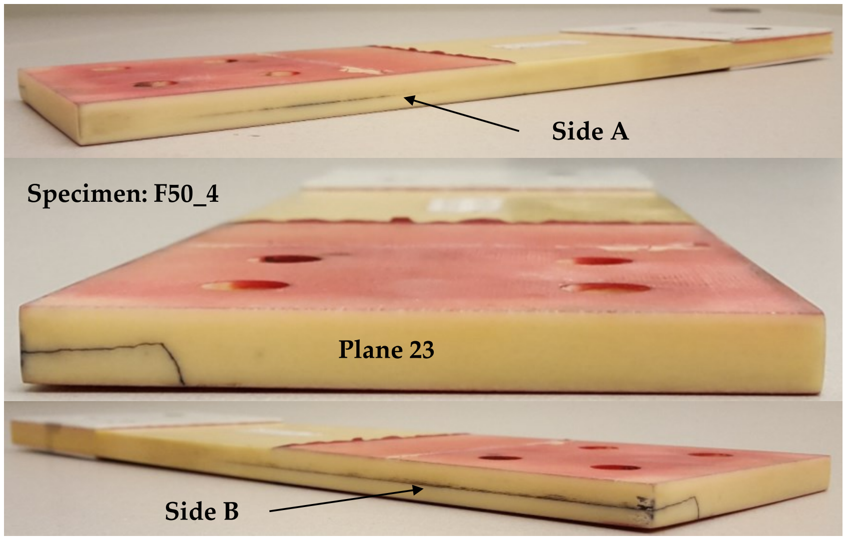

Figure 4-19 Delamination and shear-out cracks of specimen F50_4 under 70% deflection level after final failure

4.2.2. 60-Layer Laminates

4.2.2.1. Specimen No.: F60_2, 60% Deflection Level

F60_2 was tested under 60% of deflection level. The maximum actuator displacement was 1.3 (in). At this loading level, load ratio did not decrease by more than 7.7% after one million cycles as shown in Figure 4-20. Furthermore, there was no damage observed on the side surfaces of the laminate. The temperature of the "Side A" surface did not increase by more than 2.6°C.

Out-of-plane shear strain profile on the two side surfaces of specimen F60_2 is plotted in Figure 4-21. The shear strain amount is less than 5% different on the two surfaces at the beginning of the cyclic test. This is to say that the specimen is in a good condition as regards of symmetry. Furthermore, the figure shows that after one million cycles the shear strain has increased by around 10%. This is to support the fact that there is no damage appeared on the side surfaces, unless the out-of-plane shear strain increases sharply.

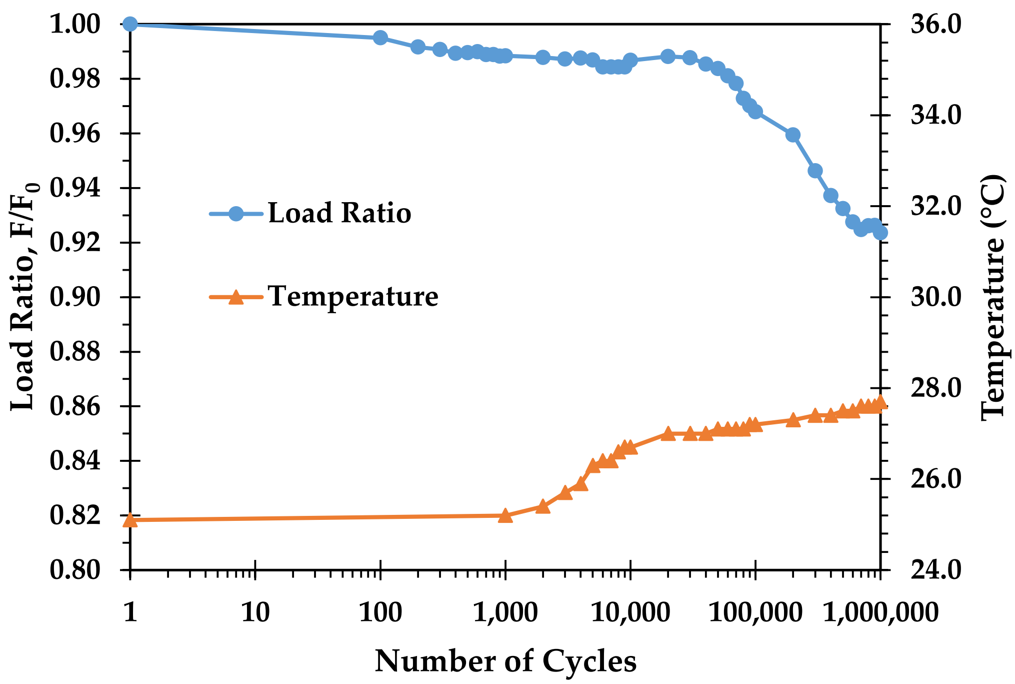

Figure 4-20 Load ratio reduction for sample 60_2 under 60% deflection level

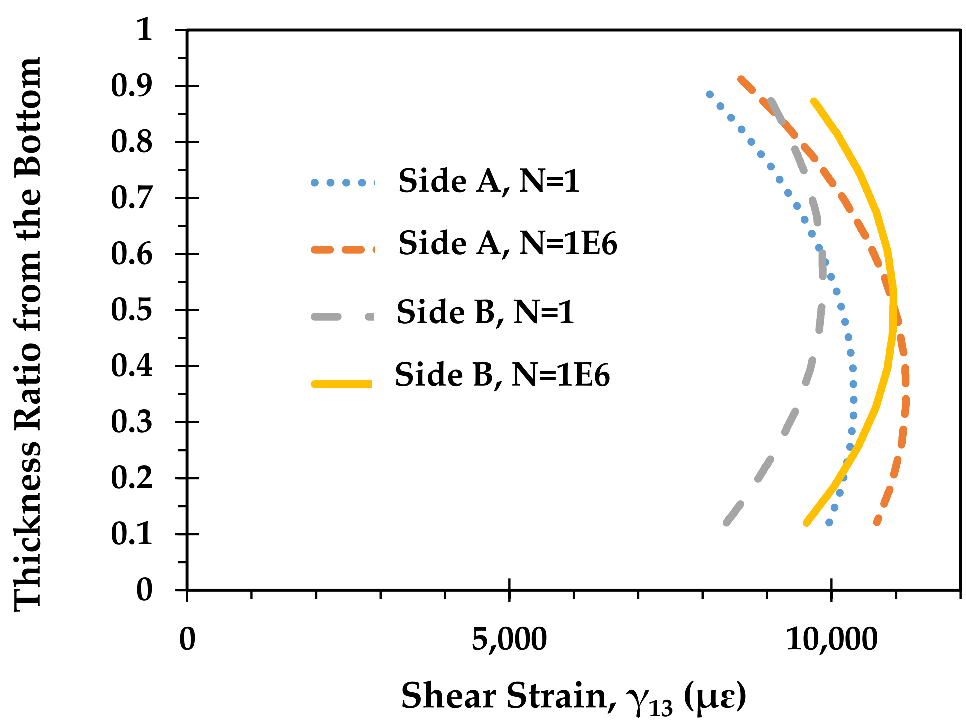

Figure 4-21 Profile of out-of-plane shear strain on the two side surfaces of specimen F60_2 at different number of cycles

Figure 4-22 is a quantitative representation of out-of-plane shear strain increase on the side surfaces. Based on this figure the increase of shear strain on the side surfaces are by 7.8% and 11.0% for “Side A” and “Side B”, respectively. Based on the experimental result of specimens with appeared cracks on the side surfaces, more that 15% increase in shear strain is observed for appearance of delamination on the side surfaces.

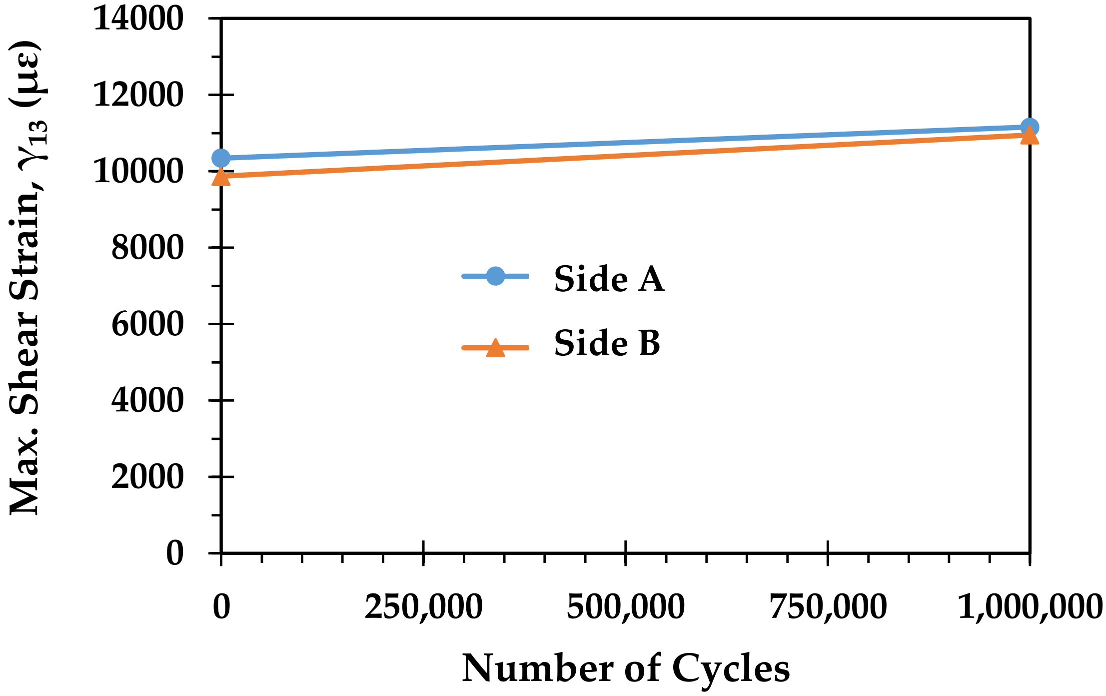

Figure 4-22 Maximum out-of-plane shear strain on the two side surfaces of specimen F60_2 versus number of cycles

Another fact that is seen at all experiments is that the central part of maximum out-of-plane shear strain region relocates towards the fixed end of the laminate on both side surfaces. This is shown in Figure 4-23. In this figure the edge of the steel plate as a fix point is indicated. Two contours at the beginning and the end of cyclic loading show a relocation of maximum shear strain region by almost 0.15 (in) on both side surfaces.

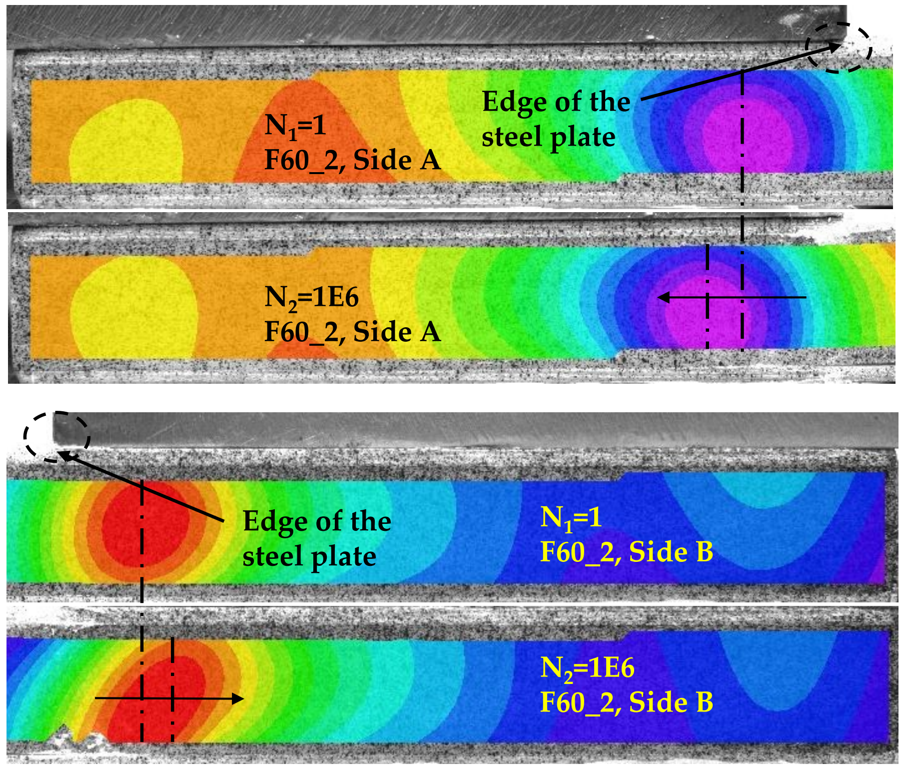

Figure 4-23 DIC images of two side surfaces of specimen F60_2 at the beginning and the end of cyclic loading

As shown in Figure 4-20, the actuator force pertaining to F60_2 specimen under 60% of deflection level decreased by 7.7% after one million cycles, less than 20% of decrease which is taken as an indication of laminate failure. Furthermore, there was not any delamination appeared on the side surfaces. Based on these indications one can say that this specimen did not fail structurally. However, cross section cuts applied on different transverse locations as shown in Figure 4-24 shows the internal cracks initiated inside the specimen. From the pictures shown in Figure 4-24 one can conclude that the delamination and shear-out cracks initiate from “Section E-E” which is the cross section right after the second row of the bolt holes in the fixed end of the laminate. It is seen from other section cuts of “Section D-D” and “Section F-F” that the initiated damages propagate towards the fixed and loading end of the laminate. From these observations it is concluded that for the laminate structure under fatigue loading, the initiation area is always located at “Section E-E”.

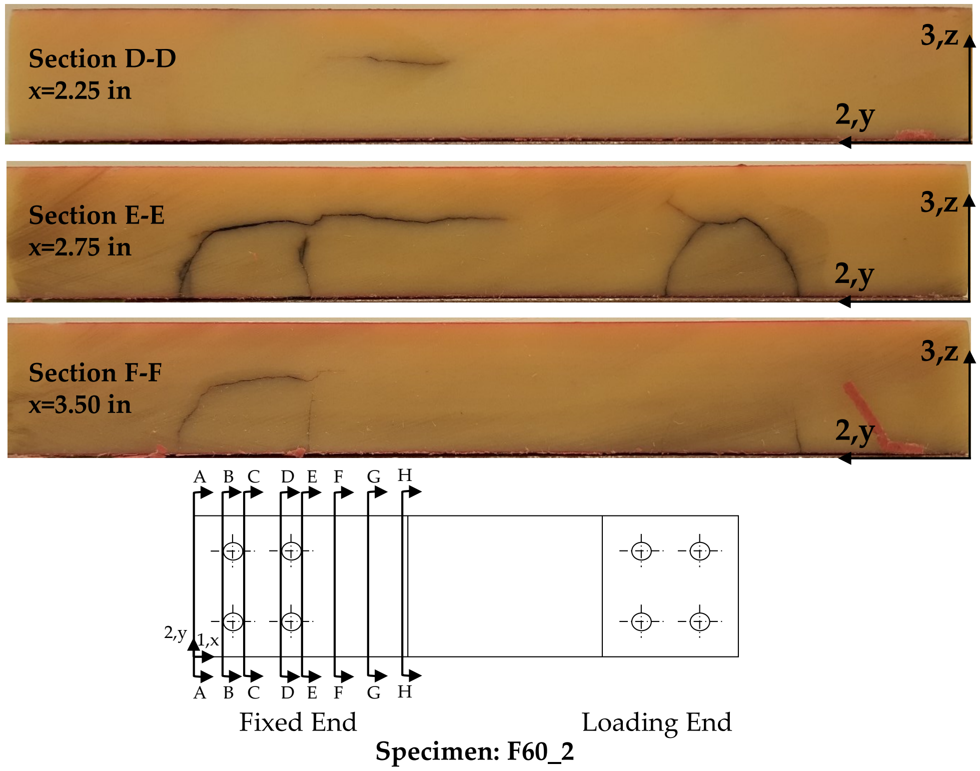

Figure 4-24 Delamination and shear-out cracks of specimen F60_2 on the transverse planes at different locations

4.2.2.2. Specimen No.: F60_1, 65% Deflection Level

Maximum actuator displacement of 1.4 (in), as the 65% of corresponding maximum displacement of static loading, was applied to specimen F60_1. The load ratio reduction and "Side A" maximum temperature of this specimen is plotted in Figure 4-25. During experiment a crack was heard around 7,300 cycles without appearance of the crack on the side surfaces. This is taken as an indication for the initiation of the crack inside the laminate. This point is indicated in the load ratio curve and it is corresponding with the point that the load ratio starts to decrease dramatically. The final fatigue life of the specimen was determined as 34,000 cycles as the load bearing capacity of the laminate decreased by more than 20% at that time. Maximum temperature diagram shows a sharp increase of around 16°C during the fatigue loading. This temperature increase is because of the heat generation as the result of friction between the two surfaces of the delamination.

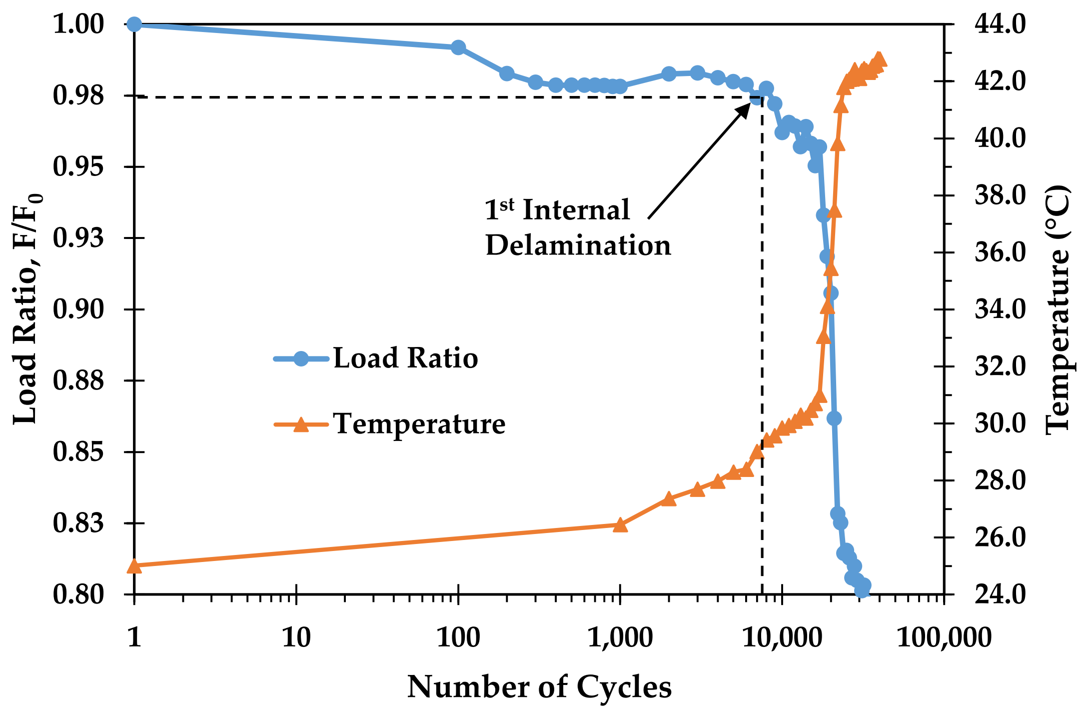

Figure 4-25 Load ratio reduction for sample 60_1 under 65% deflection level

The delamination appeared on "Side A" at around 17,000 cycles. Although at N=34,000 cycles the actuator force to maintain required displacement decreased by more than 20%, the specimen was left intentionally under cyclic loading. Another delamination appeared on "Side B" at around 37,000 cycles. Figure 4-26 shows the DIC contours for out-of-plane shear strain on "Side B" surface of the specimen at the beginning of fatigue loading and one cycle interval before appearance of delamination on "Side B" surface. It is shown in Figure 4-26 that the center of maximum out-of-plane shear strain relocates from point " O ", located at mid-thickness, to point " O' ", located at upper half-thickness of the laminate, close to the fixed end. Appearance of the delamination on upper half-thickness of "Side B" surface proves the correspondence between delamination appearance and the maximum out-of-plane shear strain.

Figure 4-27 shows the maximum out-of-plane shear strain profile on two side surfaces for F60_1 specimen under 65% of deflection level. The figure shows dramatic increase of shear strain before appearance of delamination on both side surfaces. This trend supports the idea that out-of-plane shear strain has a plateau trend until the delamination crack gets close to the side surfaces and it takes its maximum value at the cycle interval before appearance of the crack on the side surfaces.

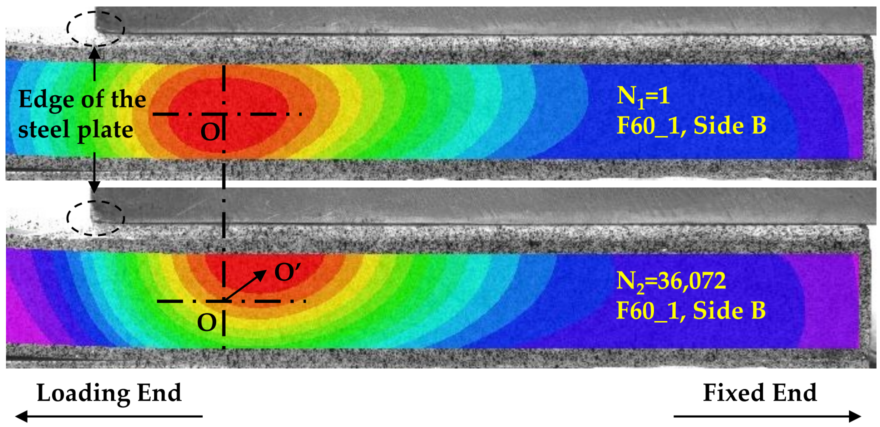

Figure 4-26 DIC images of "Side B" surface of specimen F60_1 at the first and one cycle interval before appearance of delamination

Figure 4-27 also shows that there is a considerable difference between both occurrence time and the value of out-of-plane shear strain pertaining to two side surfaces. The crack appears earlier for "Side A' than "Side B". Furthermore, the maximum value for shear strain is about 15,500 and 19,500 micro-strain for "Side A" and "Side B" respectively. These differences are related to un-symmetry of either the laminate itself or the test setup as explained for previous specimens.

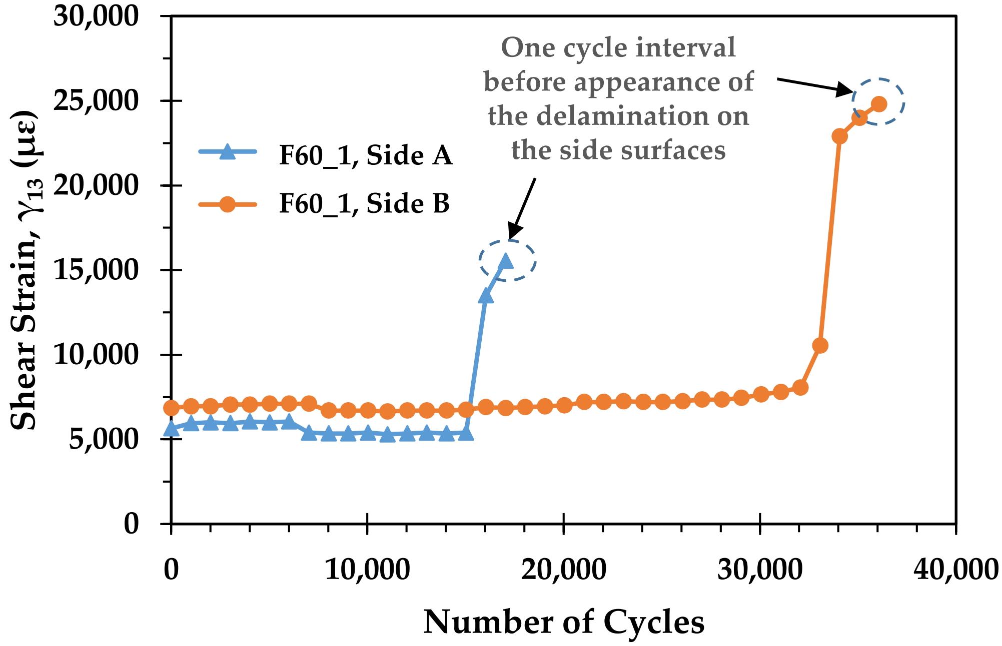

Figure 4-27 Maximum out-of-plane shear strain on the two side surfaces of specimen F60_1 versus number of cycles

Out-of-plane shear strain profile on the "Side B" surface of F60_1 specimen is plotted in Figure 4-28 for different stages of cyclic loading. Figure 4-28 shows that in further to increase of shear strain, the maximum region relocates to the upper half of the thickness. Therefore, it is expected to observe the delamination on the upper half of the thickness as well.

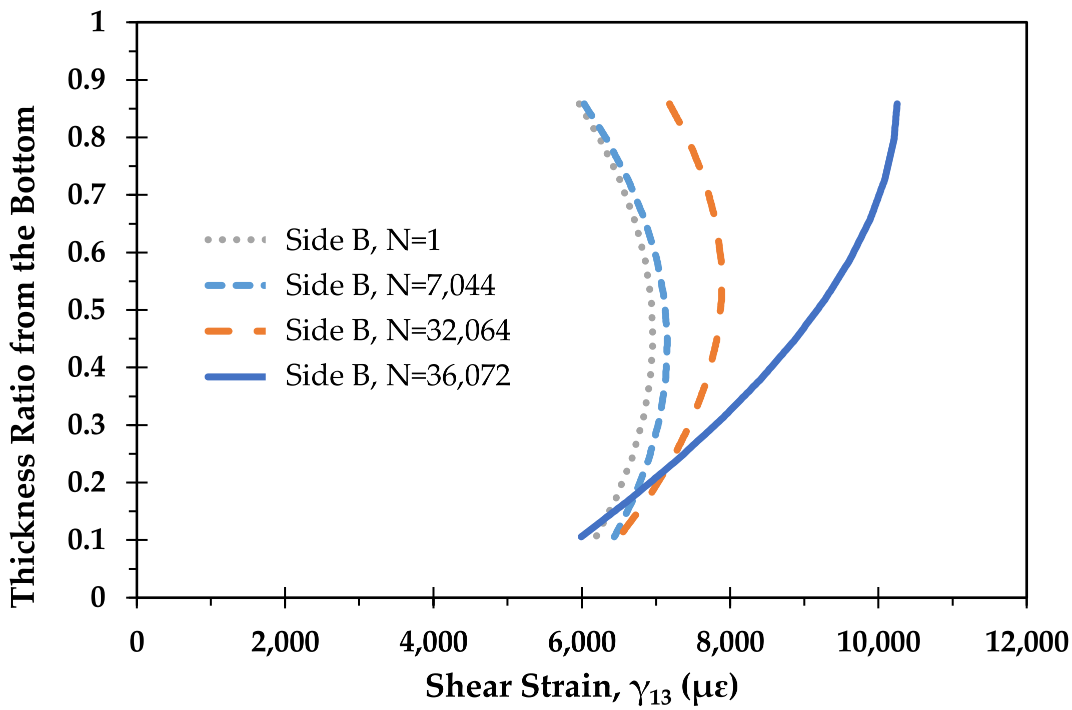

Figure 4-28 Profile of out-of-plane shear strain on the "Side B" surface of specimen F60_1 at different number of cycle

Figure 4-29 shows the transverse section cuts of specimen F60_1 at different locations. Similar to other specimens, the most critical section is "Section E-E" which corresponds to the section right after the second row of the bolt holes. As shown for the specimen F60_2 in previous section as well, all damages initiate from this location and propagate towards both ends of the laminate. However, the cracks which propagate towards the fixed end, as shown in "Section A-A' of Figure 4-29, are more critical than the others propagate towards the loading end. The reason is that in the bolted area of the fixed end, the clamping compressive stresses contribute more in the failure of the test specimen.

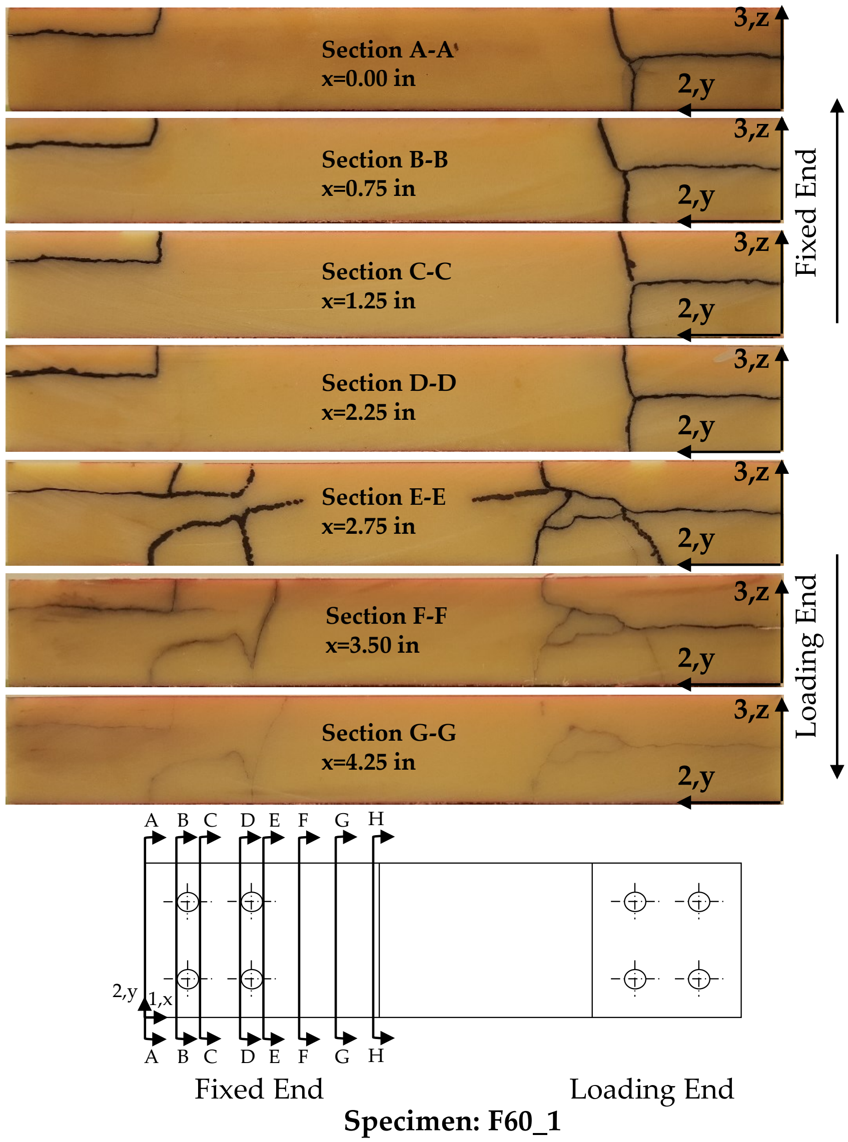

Figure 4-29 Delamination and shear-out cracks of specimen F60_1 on the transverse planes at different locations

4.2.2.3. Specimen No.: F60_3, 70% Deflection Level

Specimen F60_3 was tested under 70% of deflection level requiring 1.5 (in) of actuator displacement to maintain the level. During the test the clear sounds of two cracks were heard at around 4,000 and 7,000 cycles. The first audible sound is corresponding with the point in the load ratio reduction curve as indicated as "Point A" in Figure 4-30. After "Point A" the load ratio starts to decrease dramatically. The final fatigue life of this specimen is about 24,000 cycles when the load bearing capacity decreased by more than 20% (Point B in Figure 4-30). Because of the appearance of the delamination on "Side A" surface which happened at around 7,000 cycles, the maximum temperature of this side surface increased by more than 26°C during the whole fatigue life.

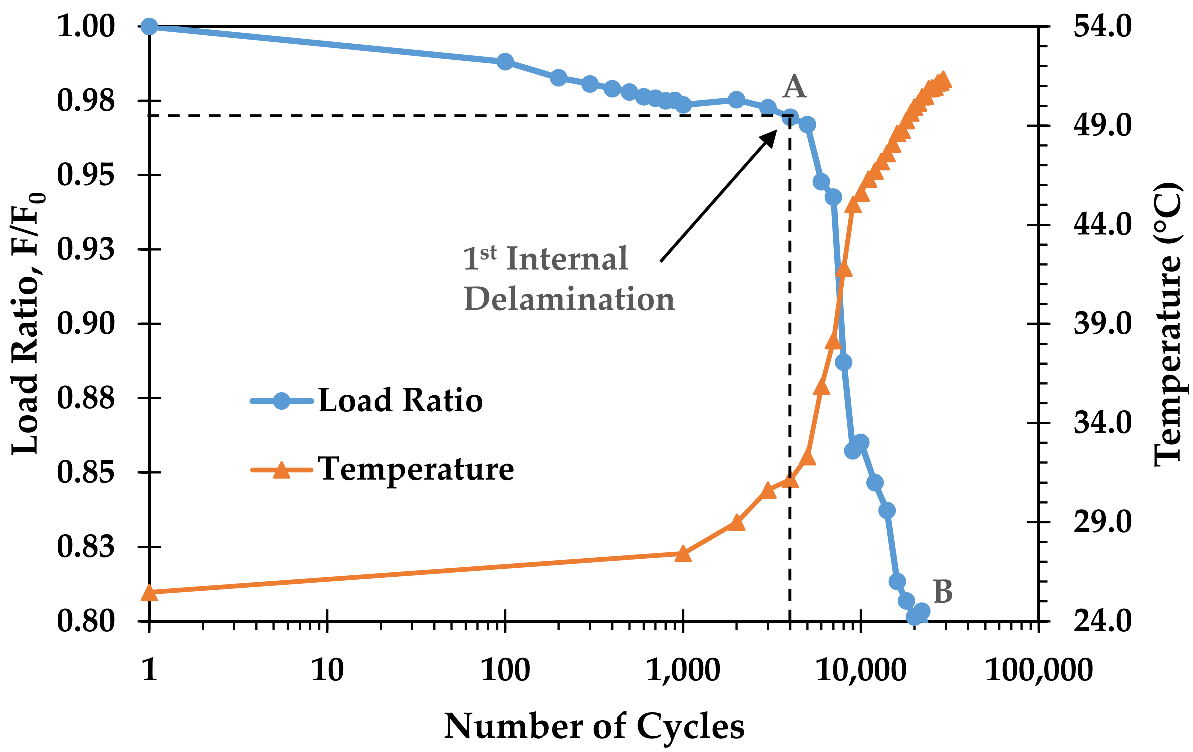

Figure 4-30 Load ratio reduction and "Side A" maximum surface temperature for sample F60_3 under 70% deflection level

Out-of-plane shear strain profile on "Side A" of specimen F60_3 is shown in Figure 4-31. The figure shows a dramatic increase of the shear strain corresponding to one cycle interval preceding the appearance of the delamination on "Side A" surface. Furthermore, the maximum shear strain region relocates from mid-thickness to the lower half-thickness of the "Side A" surface. For this reason, it is expected to observe the appeared delamination in lower half-thickness of the laminate.

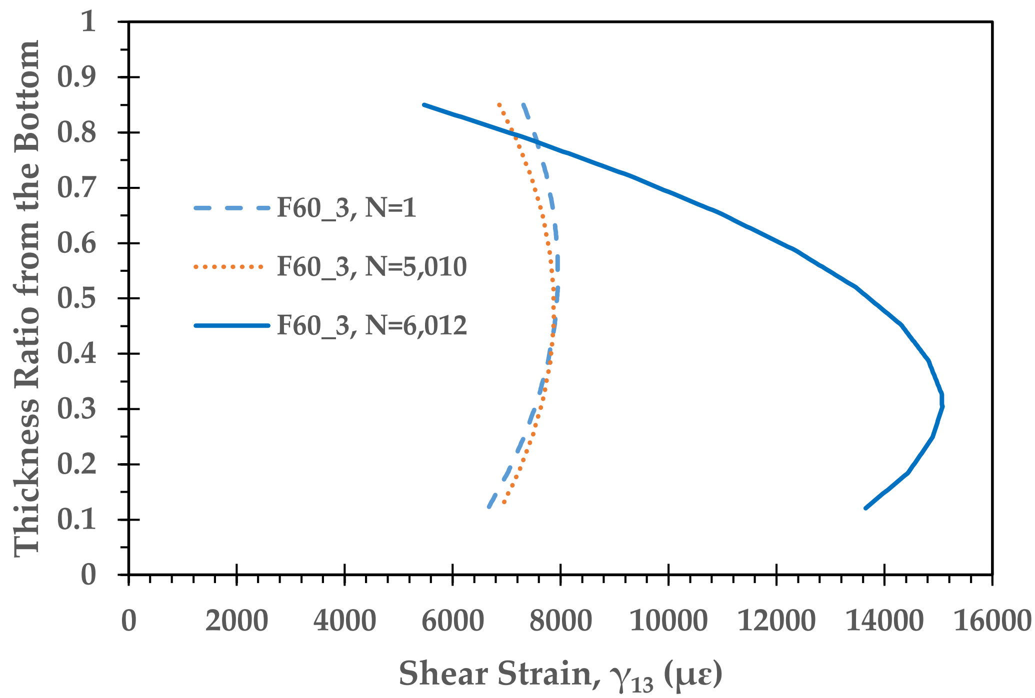

Figure 4-31 Profile of out-of-plane shear strain on the "Side A" surface of specimen F60_3 at different number of cycles

DIC contours for strain distribution on the "Side A" surface are shown in Figure 4-32. At the first cycle the maximum region of the shear strain is well centered around mid-thickness. However, as it was shown in Figure 4-31, the region of maximum shear strain relocates to the lower half-thickness of the laminate. The appearance of the delamination on the lower half-thickness proves the importance of out-of-plane shear strain relating to the delamination crack.

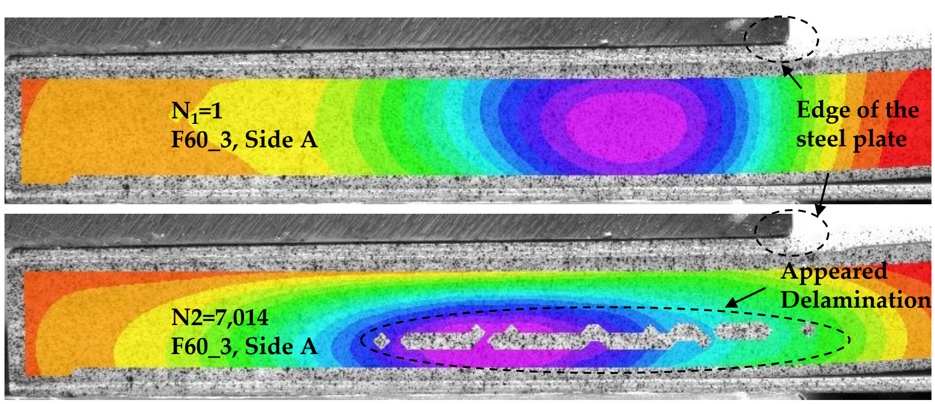

Figure 4-32 DIC images of "Side A" surface of specimen F60_3 at the first cycle and the first appearance of delamination

Specimen’s picture after failure and section cuts at two different locations for F60_3 are shown in Figure 4-33. Delamination and shear-out cracks were appeared on “Side A” surface only. However, the picture for Section E-E shows that internal cracks have been occurred close to the “Side B” surface as well. Furthermore, Section E-E shows the cracks are almost symmetric, although those close to the “Side A” surface seemed more dense and were appeared on the side surface. From these pictures one can conclude that the initiated cracks propagate downward because of existence of bolt holes in the laminate. The reason could be related to the compressive stresses because of conical bolt clamping pressure’ profile which changes the direction of delamination propagation towards the bottom of the laminate.

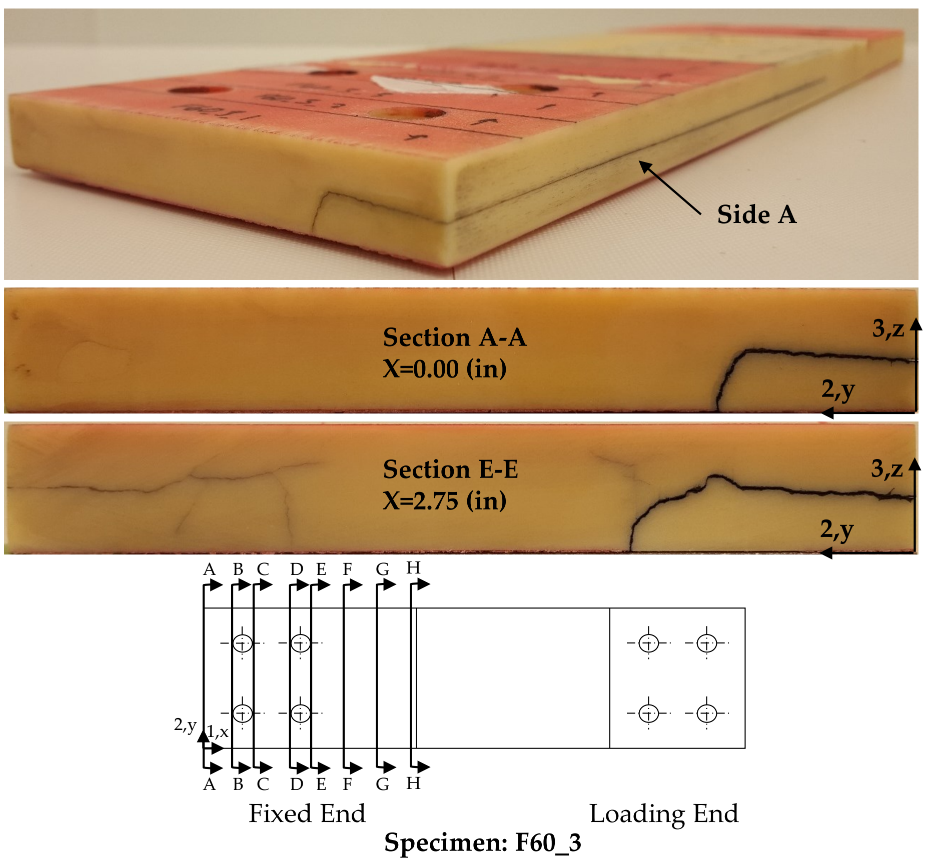

Figure 4-33 Delamination and shear-out cracks of specimen F60_3

4.2.3. 70-Layer Laminates

4.2.3.1. Specimen No.: F70_4, 60% Deflection Level

F70_4 was tested under fatigue loading with 0.9 (in) of maximum actuator displacement. Up to one million cycles, there was not reduction in the load ratio by more than 6%. There was not any damage appeared on the side surfaces. Therefore, it is not expected to see the sharp increase in the maximum side surface temperature as is shown in Figure 4-34.

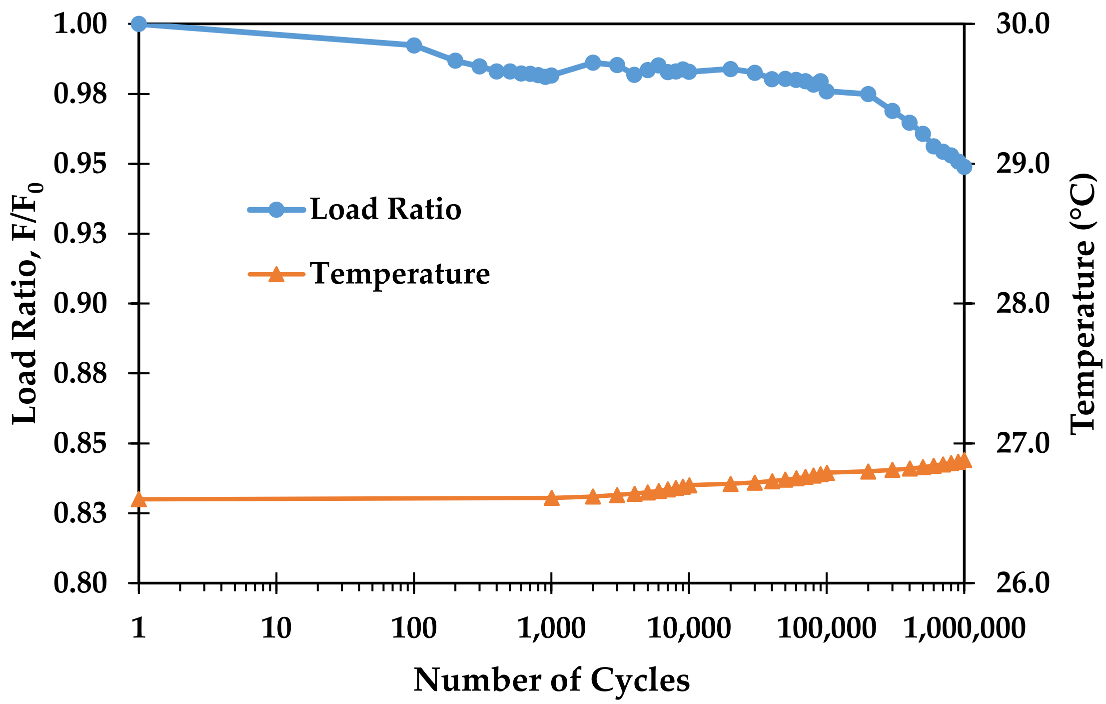

Figure 4-34 Load ratio reduction for sample 70_4 under 60% deflection level

Figure 4-35 shows the DIC images for the out-of-plane shear strains of two side surfaces at the beginning and the end of cyclic loading. For each side there is not any considerable change in the profile, but the relocation of the central maximum shear strain region towards the fixed end which was measured to be around 0.12 (in).

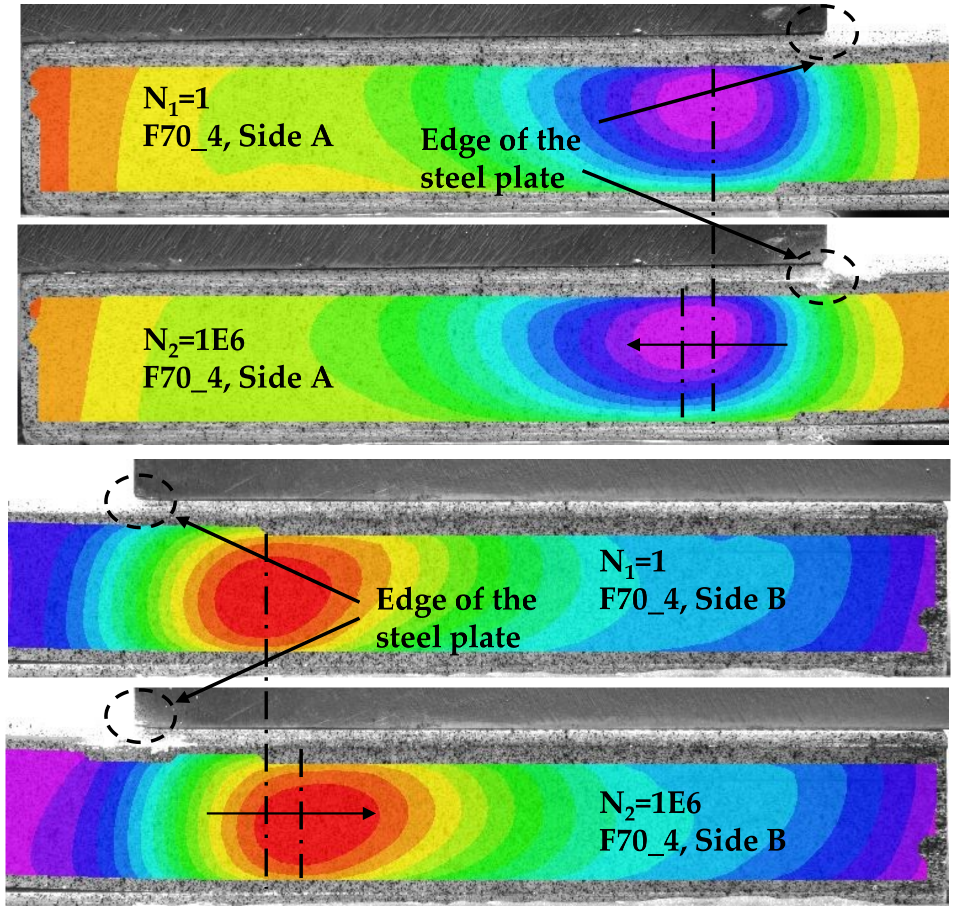

Figure 4-35 DIC images of two side surfaces of specimen F70_4 at the beginning and the end of cyclic loading

The profile of out-of-plane shear strain is shown in Figure 4-36. The figure shows that the shear strains on the two side surfaces remained constant after one million cycles, although the profiles show the difference in the magnitude between two side surfaces. This difference is mostly because of un-symmetry arises from either manufacturing of the test specimen or the test setup as will be discussed in Section 4.3.

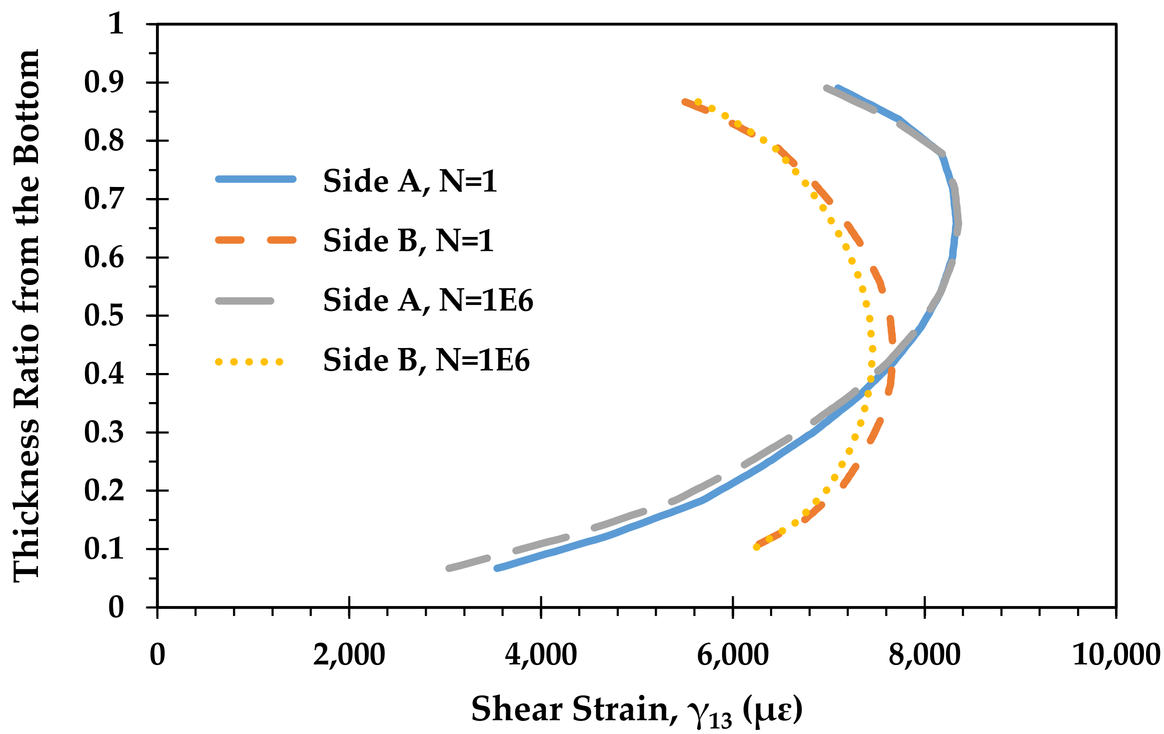

Figure 4-36 Profile of out-of-plane shear strain on the two side surfaces of specimen F70_4 at different number of cycles

Based on experiments performed under lower deflection levels, i.e. 60% of deflection level for 60 and 70-layer laminates, the delamination does not grow to appear on the side surface. These tests are suitable to observe the damage initiation region. Furthermore, it was noticed that the critical region of this specific laminate is the transverse section cut right after the second row of the bolt holes, Section E-E. Figure 4-37 shows the section cut as Section E-E which has been made after cyclic loading of F70_4 specimen. The circled areas show the initiated cracks. For This specimen the initiated cracks seem to be symmetric. It is expected that by continuing cyclic loading beyond one million cycles, these cracks could propagate towards fixed and loading end of the laminate.

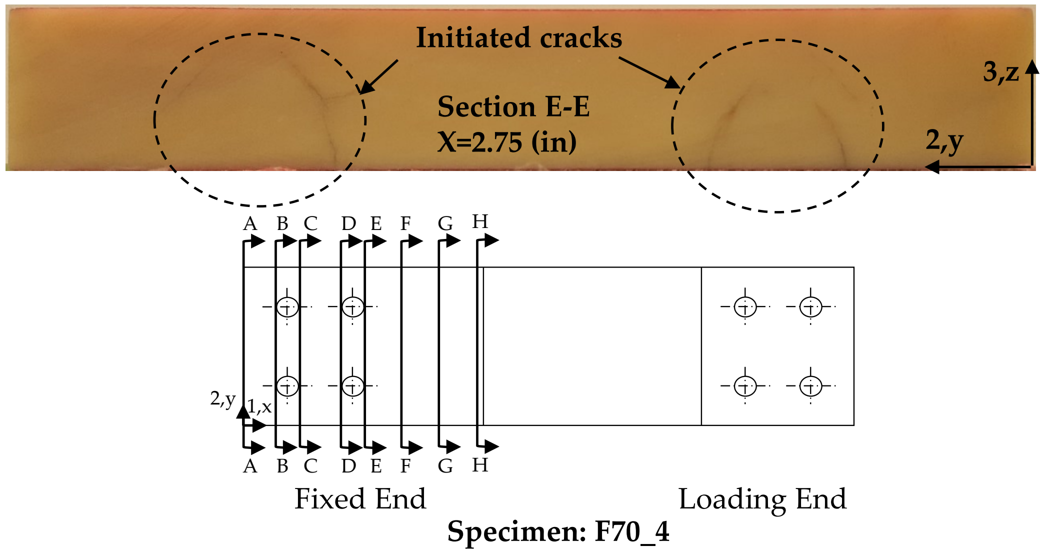

Figure 4-37 Initiated cracks at Section E-E of F70_4 specimen under 60% of deflection level

4.2.3.2. Specimen No.: F70_5, 70% Deflection Level

Actuator displacement of 1.1 (in) was applied to specimen F70_5 as the 70% of deflection level. Almost 15% of the loading capacity decreased under displacement control test until one million cycles as shown in Figure 4-38. The "Side A" surface temperature increased by 7°C.

In Figure 4-39, DIC contours for out-of-plane shear strain shows no significant change between N=1 and N=1E6 number of cycles. The area of the maximum shear strain, however, relocates towards the fixed end by almost 0.22 (in) as shown in the middle picture. The specimen was left under fatigue loading for 90,000 more cycles where the maximum shear strain region appeared to narrow down as shown in the bottom picture.

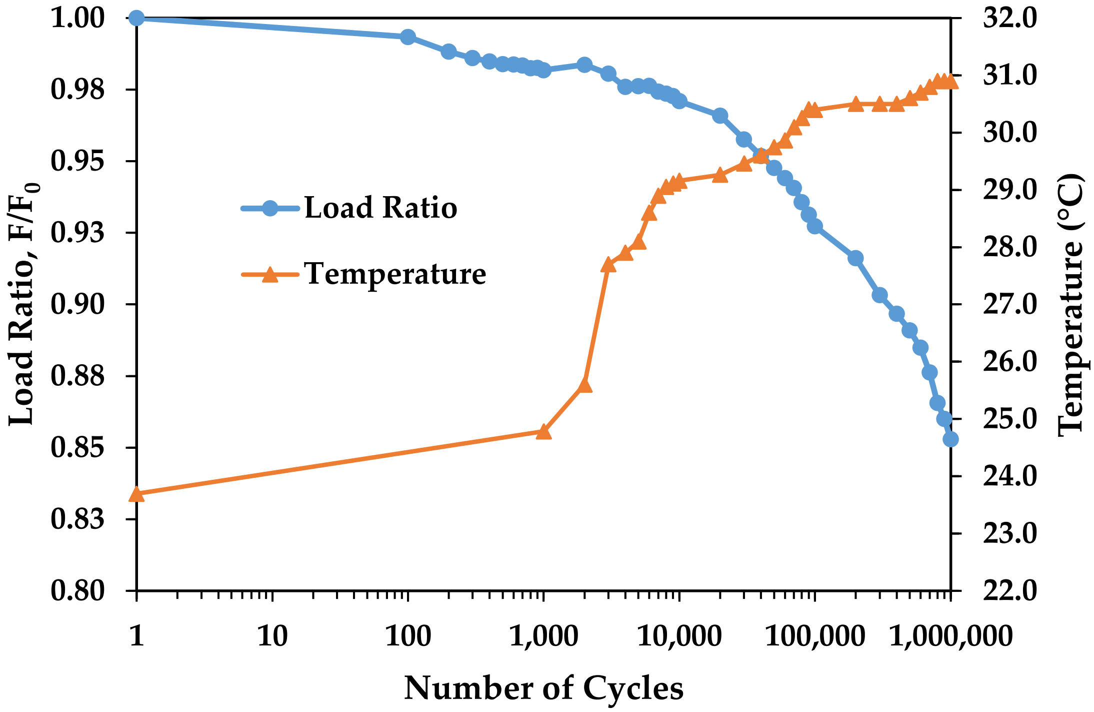

Figure 4-38 Load ratio reduction for sample 70_5 under 70% deflection level

For all specimens discussed earlier it is observed that with progression of cyclic loadings, the region of maximum out-of-plane shear strain relocates towards the fixed end. For the laminates under higher deflection levels, the delamination starts to appear on the side surfaces from mentioned region. For the laminates without appearance of the delamination on the side surfaces, the maximum out-of-plane shear strain region narrows down and relocates, but remains around mid-thickness. This could be taken as a general behavior of thick laminates under cyclic loading.

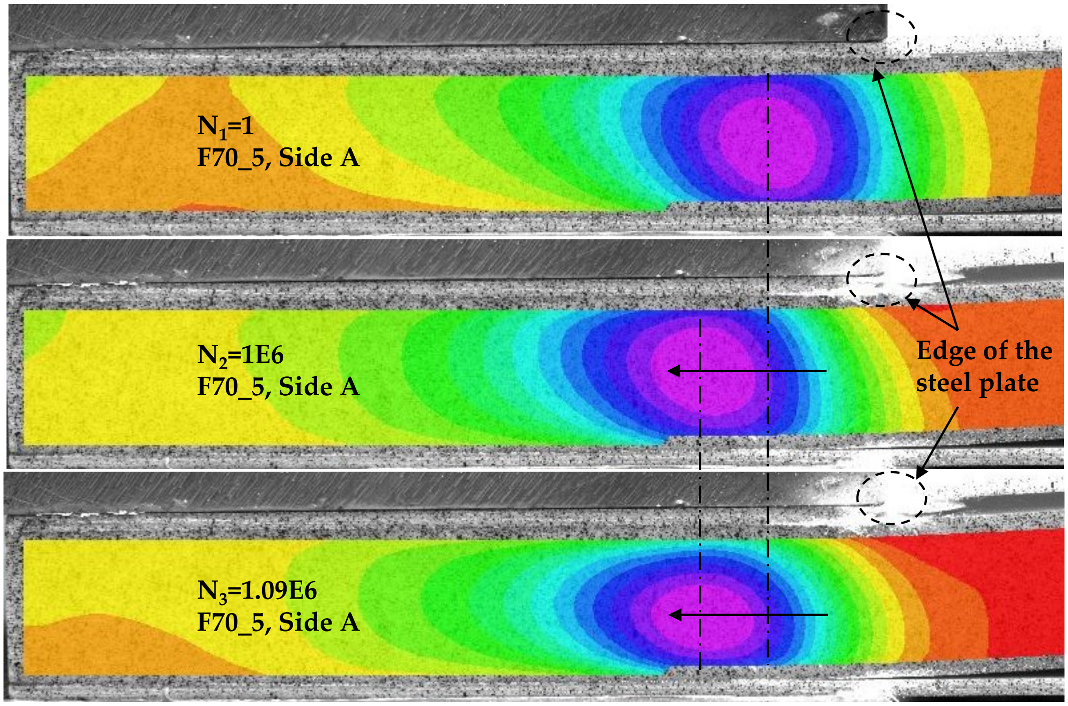

Figure 4-39 DIC images of "Side A" surface of specimen F70_5 at three stages of cyclic loading

Figure 4-40 shows the profile of the out-of-plane shear strain on the "Side A" surface of F70_5 specimen at three different number of cycles. As expected based on the DIC contours shown in Figure 4-39, there is not a significant change in the shear strain profile related to N=1 and N=1E6 cycles. At N=1.09E6 however the profile changes drastically and the maximum value of the shear strain increases by 41%. The maximum shear strain region also relocates to the bottom half-thickness of the laminate This is the point that by further progression of fatigue loading, the appearance of delamination on the "Side A" surface is expected to happen, however the experiment was stopped at 1.09E6 number of cycles.

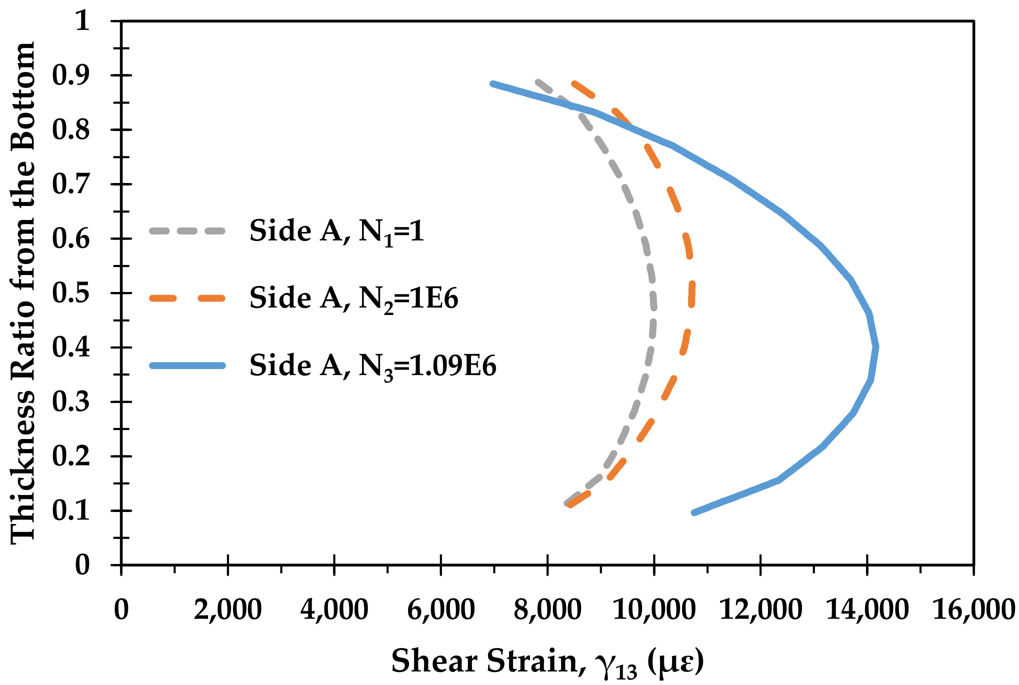

Figure 4-40 Profile of out-of-plane shear strain on the "Side A" surface of specimen F70_5 at different number of cycles

Although the DIC cameras did not capture any damage on the side surfaces of F70_5 specimen, the transverse section cuts of the specimen at different locations show internal delamination and shear-out cracks as shown in Figure 4-41. Similar to other specimens, the critical section as regards to crack density is "Section E-E". The internal cracks of this specimens show that the loading condition and the laminate itself have been symmetric, since the initiated cracks are symmetric. Shear-out cracks are created because of the existence of the bolt holes. The horizontal delamination at "Section E-E" which has partially propagated to the "Section D-D" has occurred almost at the mid-thickness location. This could happen because of out-of-plane normal and shear stresses, since the bending longitudinal normal stresses are expected to be negligible at the mid-thickness. Another observation from the section cuts of F70_5 specimen is that the shear-out cracks propagate towards the loading end of the specimen while delamination propagates towards the fixed end. The crack representation of this specimen seems to be ideal case as it corresponds well with the results of the finite element analysis.

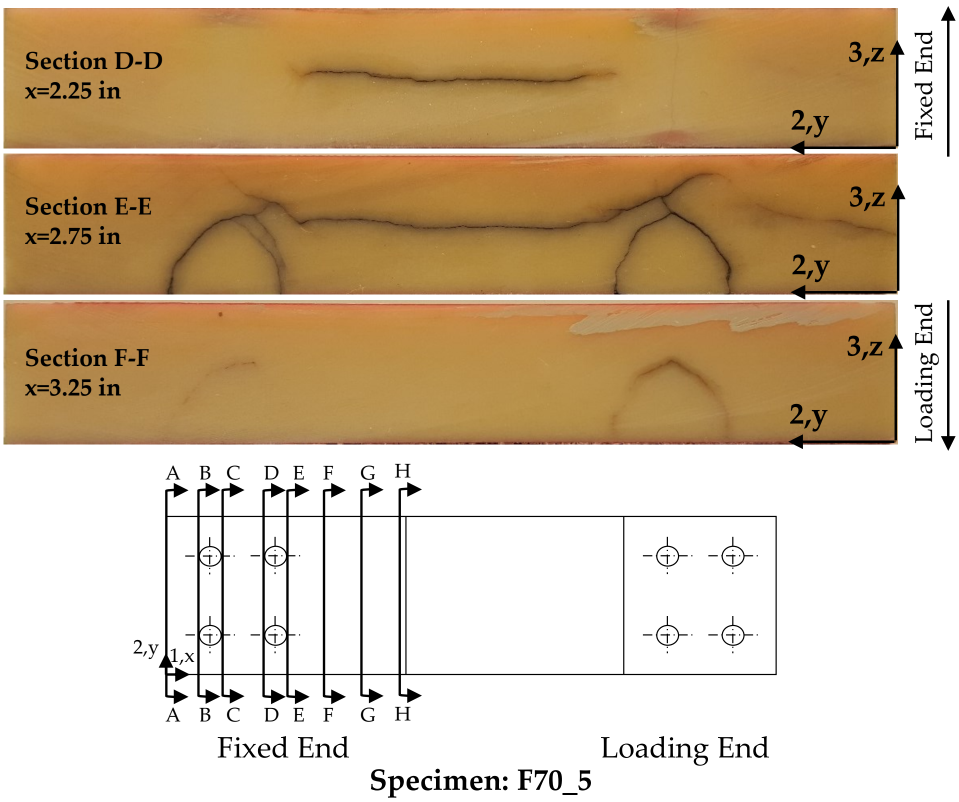

Figure 4-41 Delamination and shear-out cracks of specimen F70_5

4.2.3.3. Specimen No.: F70_1, 75% Deflection Level

F70_1 specimen experienced 1.16 (in) of maximum actuator displacement during cyclic loading. At around 500,000 cycles, the specimen lost its load bearing capacity by more than 20% under displacement control test which is considered as final failure of the laminate. The load ratio and "Side A" maximum temperature of this specimen versus number of cycles is plotted in Figure 4-42. During the whole fatigue life, the "Side A" maximum surface temperature increased by about 6°C. The reason for small temperature increase is that delamination did not appear on "Side A" surface during the entire period of fatigue loading. Instead at around N=277,000 cycles delamination appeared on "Side B".

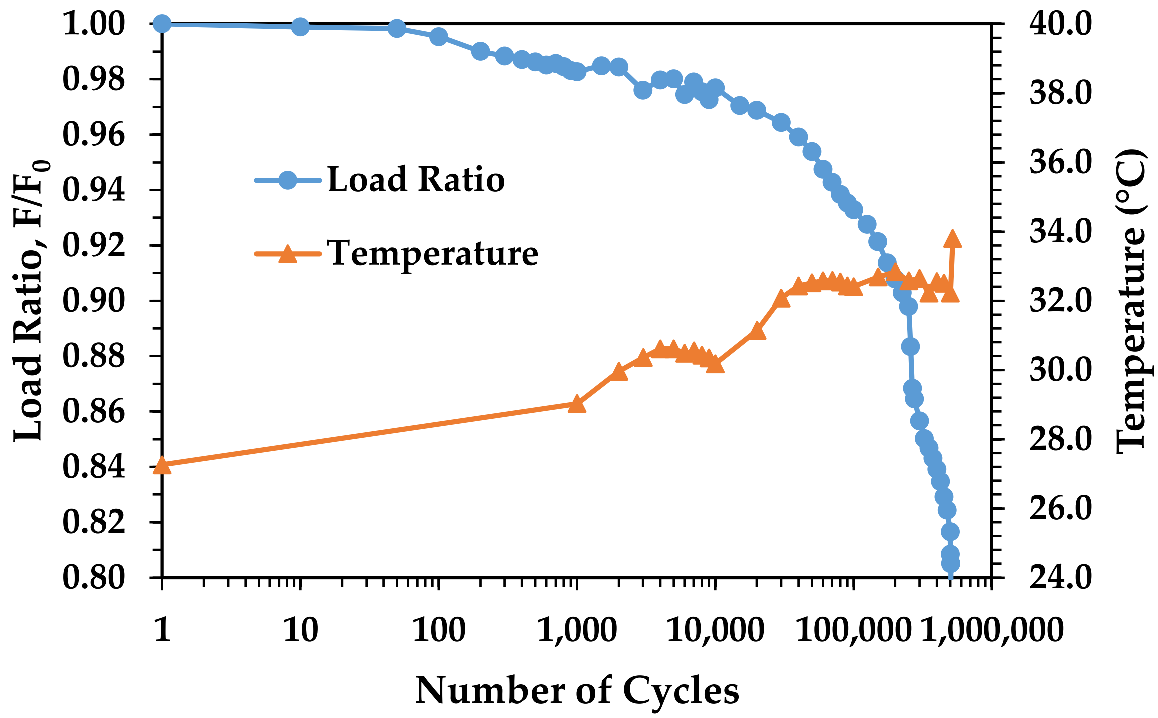

Figure 4-42 Load ratio reduction for sample 70_1 under 75% deflection level

Figure 4-43 shows the DIC contours of out-of-plane shear strain on the two side surfaces of F70_1 specimen at two different stages of the cyclic loading; First cycle and one cycle interval before appearance of the delamination on the “Side B” surface. The damage appeared on “Side B” surface at around 277,554 cycles. For each side the bottom picture shows the relocation of the maximum shear strain region towards the fixed end of the laminate. The amount of the relocation is about 0.15 (in) and 0.29 (in) for “Side A” and “Side B”, respectively. The larger relocation of the region for “Side B” is an indication of probable appearance of the delamination on this side surface in the following cycles which was seen during the experiment at 277,554 cycles.

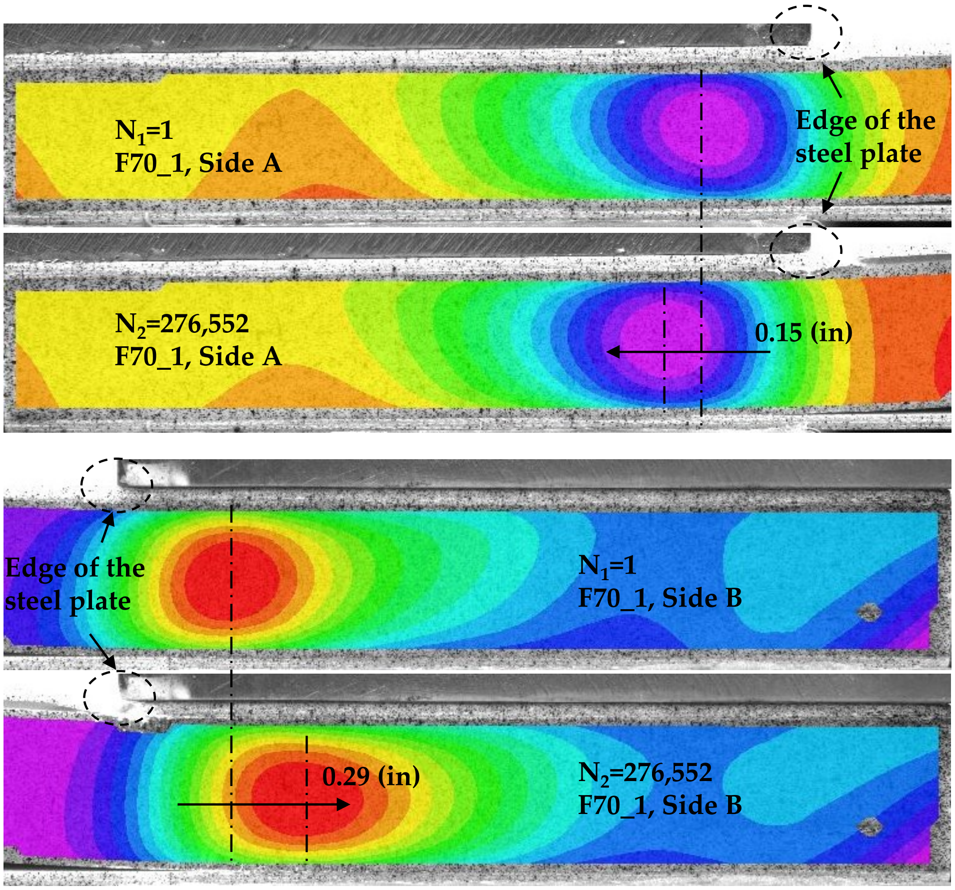

Figure 4-43 DIC images of two side surfaces of specimen F70_1 at two different stages of cyclic loading

At the same number of cycles corresponding to the DIC images of Figure 4-43, the profiles of maximum shear strain for both side surfaces are plotted in Figure 4-44. As shown in Figure 4-44 the increase of maximum shear strain related to the two cycle intervals are 4.3% and 21.2% for “Side A” and “Side B” respectively. This could be taken as another indication for probability of appearance of the delamination on “Side B”, since the increase in the shear strain is larger.

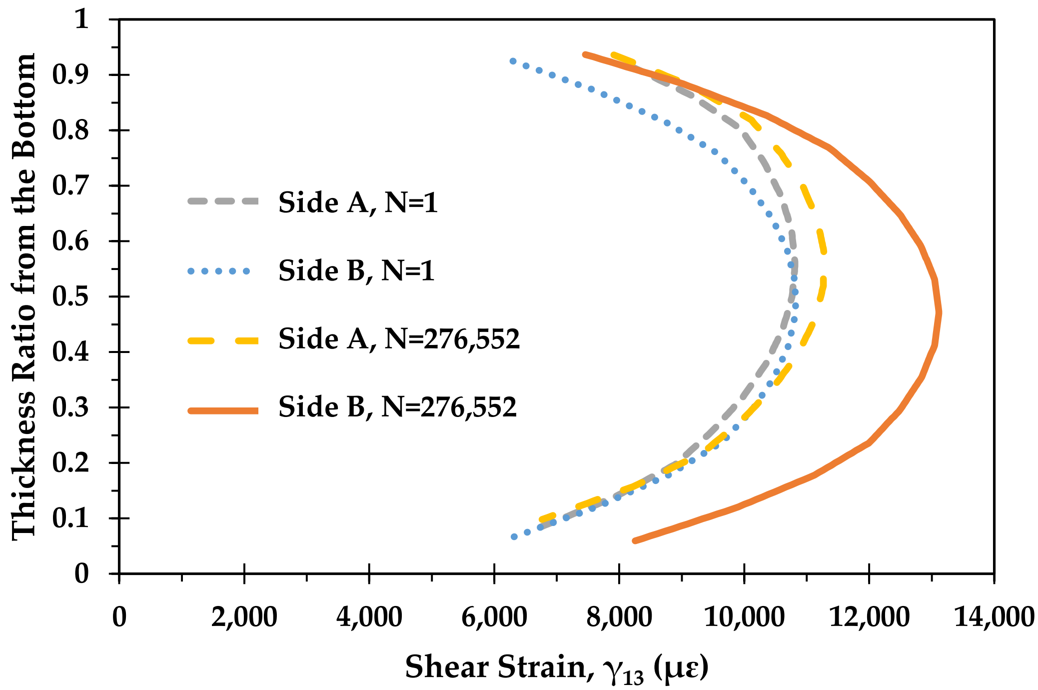

Figure 4-44 Profile of out-of-plane shear strain on the two side surfaces of specimen F70_1 at different number of cycles

Figure 4-45 shows the delamination and shear-out cracks occurred in the F70_1 specimen. The section cuts prove the progression of the delamination towards the "Side B" surface. Furthermore, the crack density is the largest for "Section E-E", similar to other tested specimens. The same observation is seen as the occurrence of shear-out cracks because of the second row of the bolt holes and propagation towards the loading end of the laminate. Occurred cracks also seem to be in-symmetric. However, the behavior of F70_1 totally resembles the case of other tested specimens.

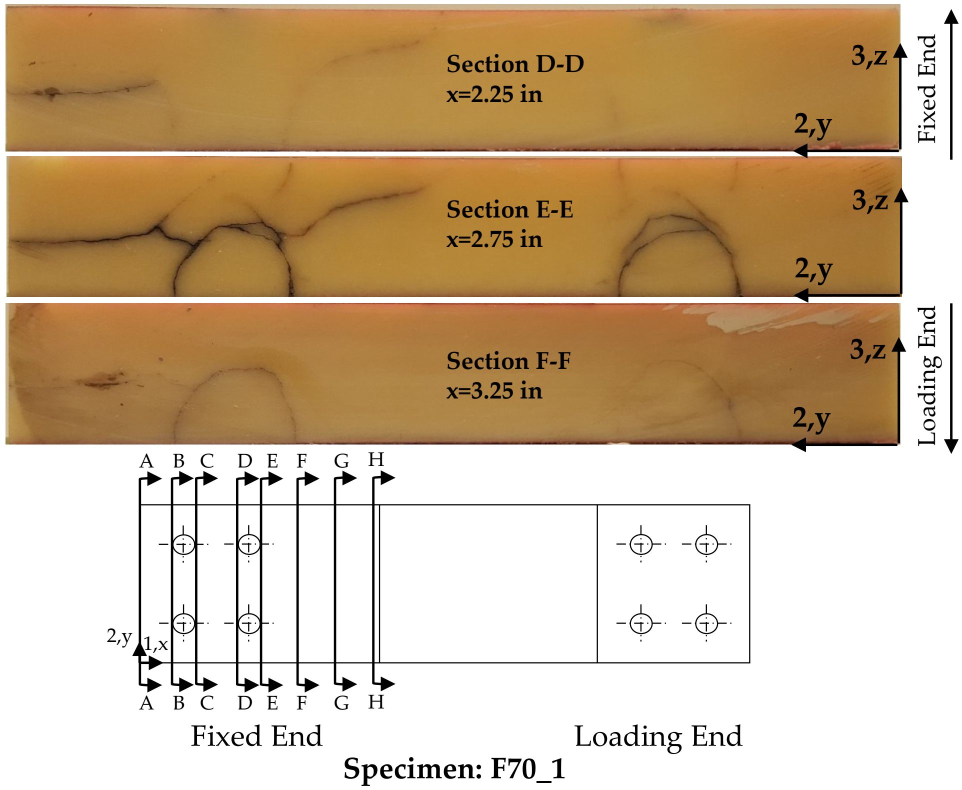

Figure 4-45 Delamination and shear-out cracks of specimen F70_1 under 75% of deflection level

4.2.4. Thickness effect on fatigue behavior of thick laminates

In this section, the behavior of the laminates with different thicknesses are compared with respect to the thickness effect. As shown in Table 4-2, for each thickness and deflection level, one specimen was tested.

4.2.4.1. 50-Layer Laminates under Cyclic Loading

Figure 4-46 shows the Load Ratio Reduction (LRR) curve for 50-Layer laminates. The required actuator displacements to maintain different deflection levels are summarized in Table 4-2. As shown in Table 4-2, the difference between required maximum displacements for three different deflection levels was 0.1 (in). This shows that by a small change in actuator displacement, the fatigue behavior of the laminate changes drastically. The LRR curve for each deflection level has two distinguished regions. The first region, indicated as “Region 1” in Figure 4-46, is the time that the LRR reduces mildly. This region is considered as gradual stiffness and strength degradation under cyclic loading. Based on the experiments, there was not any considerable damage observed during this period for the laminates. Over “Region 1”, the maximum decrease in LRR is about 8% which is related to 60% of deflection level. However, this reduction in LRR happened in the most time domain of the fatigue life.

The end point of “Region 1”, is related to the time that interior damages initiate. After initiation, the LRR decreases drastically for all deflection levels. The most focus of this research has been on the damage initiation phase which corresponds to the “Region 1” in Figure 4-46. For 50-Layer laminate the ratio of the time corresponding to initiation phase to the total fatigue life is 23% for 70% of deflection level. The same ratio is almost 60% for 60% of deflection levels. This means that for the larger deflection level, the interior damages start to appear earlier in time in comparison to the total fatigue life. It is expected that a threshold deflection level as “Endurance Deflection Level (EDL)” should exist for the same thickness group. “Endurance Deflection Level (EDL)” is defined as the deflection level below which no damage would initiate inside the laminate. Refer to the experiments on 50-Layer laminates under different deflection levels, one can assume that for 50-Layer laminates the “Endurance Deflection Level (EDL)” could be around 45%.

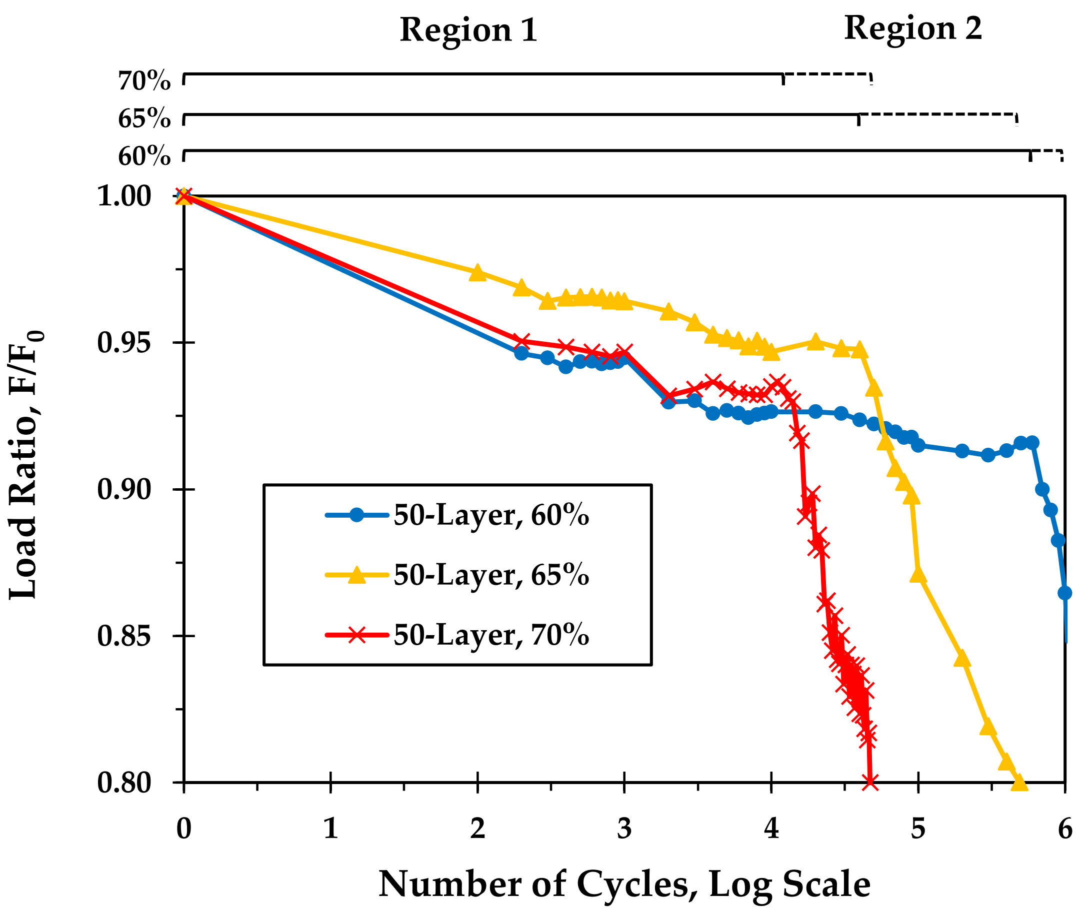

Figure 4-46 Load Ratio Reduction (LRR) versus Number of Cycles for 50-Layer Laminates under Three Deflection Levels

4.2.4.2. 60-Layer Laminates under Cyclic Loading

The behavior of 60-Layer laminates is almost similar but different in comparison with 50-Layer laminates as shown in Figure 4-47. For 60-Layer thickness group, the LRR decreases slightly in “Region 1” as the initiation phase for all deflection levels. However, there is a drastic decrease of LRR for two higher deflection levels of 65% and 70% in the “Region 2”. For the 60% deflection level LRR decreases by 7.5% after one million cycles which is less than 14% of LRR decrease for corresponding 50-Layer laminate. One can say that for 60-Layer laminates under 60% of deflection level, the “Endurance Deflection Level (EDL)” could be higher, assumed to be 50%.

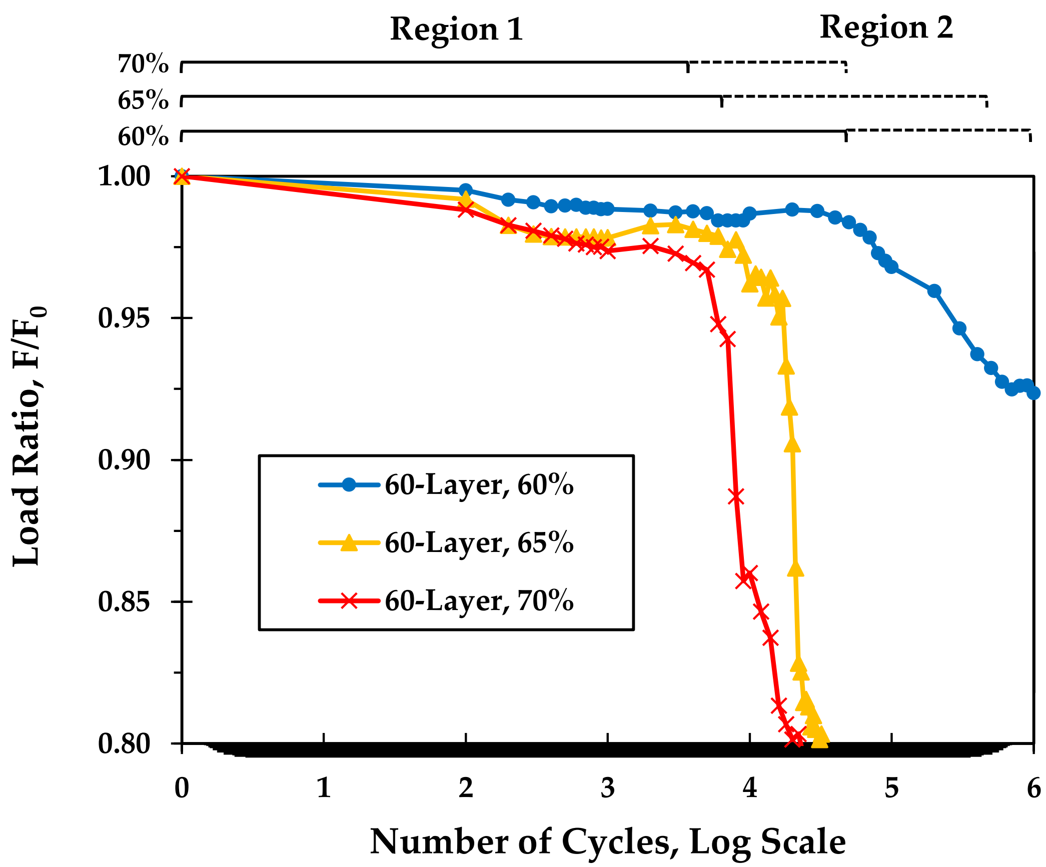

Figure 4-47 Load Ratio Reduction (LRR) versus Number of Cycles for 60-Layer Laminates under Three Different Deflection Levels

4.2.4.3. 70-Layer Laminates under Cyclic Loading

Similar to 60-Layer laminates, there is a slight decrease in LRR for the group of 70-Layer laminates as seen in "Region 1" of Figure 4-48. For the 70-Layer laminate under 60% of deflection level, there is almost 5% decrease in LRR under fatigue loading during one million cycles. This is the lowest decrease in LRR in comparison to 60 and 50-Layer laminates where the decrease in LRR for the same deflection level was 7.5% and 14%, respectively. This concludes that the thicker the laminate is, the less is the decrease in LRR for the same deflection level. For the case of "Endurance Deflection Level (EDL)" it can be concluded that EDL for 70-Layer laminates should be around 55% which is higher than that is corresponding to 50 and 60-Layer Laminates.

Furthermore from Figure 4-48 it is seen that the laminate under 70% deflection level did not fail until one million cycles. For this reason, the third 70-Layer laminate was tested under 75% deflection level which failed at around 504,000 cycles. From these behaviors one can conclude that the thicker laminates can sustain higher deflection levels without initiation of any failure.

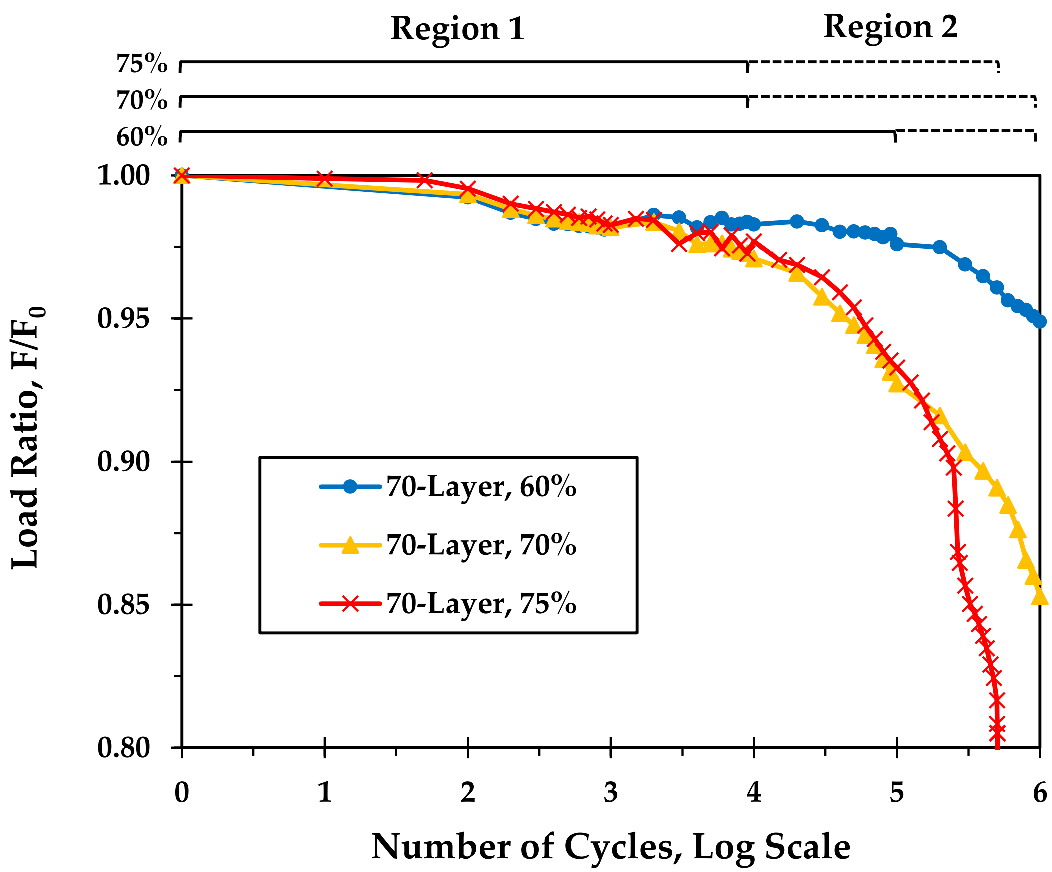

Figure 4-48 Load Ratio Reduction (LRR) versus Number of Cycles for 70-Layer Laminates under Three Different Deflection Levels

4.2.4.4. Thickness Effect on the LRR of Laminates with Different Thicknesses under Cyclic Loading

Comparing the behavior of the three thickness group of 50, 60 and 70-Layer laminates, following main conclusions can be made:

- The thicker the laminate is, the less decrease in LRR is observed for similar deflection levels. This means that thicker laminates are less susceptible to degrade under higher deflection levels.
- The “Endurance Deflection Level (EDL)” is higher for thicker laminates.

4.3. Probable reasons of un-symmetric damage style

For most of the test specimens presented in this chapter, the damage style which was shown on the transverse section cuts, was un-symmetric. The un-symmetric damage style in the transverse cuts could be because of variabilities that arise in the experiment from both manufacturing and the test setup which makes the failure style to be un-symmetric.

The two important variations coming from manufacturing could be first the variation in the thickness of the specimens which could happen because of either non-uniform autoclave pressure on the caul plate at the time of curing or the thickness variation of the each ply. The second variation could arise from the fact that the drilled holes could be a little off-centered which could lead to have non-uniform bolt-clamping forces.

With regards to the test setup, the actuator could be a little off-centered with respect to the longitudinal center line of the specimens. Otherwise the appeared delamination damages shall be completely symmetric. The unsymmetrity of the laminate or the loading setup leads to release the energy at one side of the laminate by creating new surfaces. The energy release at one side results in not to create new failure surfaces at the other side of the laminate as shown in the section cuts of tested specimens.

4.4. Summary

In this chapter, series of quasi static and fatigue flexural loading experiments were designed and conducted on unidirectional laminates with different thicknesses. These laminates were constrained by bolts to investigate thick laminates’ behavior from both material and structural points of view. To take material property into account, test coupons were characterized to obtain orthotropic material properties and material failure stresses required for application of failure equations. The results of coupon level experiments were presented in Chapter 2.

Based on the experiments on thick laminates, the dominant failure modes were delamination and shear-out cracks in certain locations of the laminates. This means that damage initiation and propagation in thick laminates take place in a localized fashion rather than global fashion which could happen for thin composite laminates. For the specific laminate structure which was tested in this study, the two dominant failures were observed to initiate from a specific location. The repetition of the same damage style for laminates with different thicknesses proved that for the laminates of the same thickness range, the damage style should be the same. The threshold for the thickness range as regards of the convention point from thin to thick laminates was not investigated in this research for the specific structure of the laminates. The reason is that the loading setup was not able to retain required higher displacement at 3 (Hz) of frequency for thinner than 50-layer laminates.

The experimental results showed that the fatigue lives of thick laminates depend on the level of the prescribed deflection at the time of flexural loading. The higher is the applied deflection, the faster is the reduction in fatigue life. This fact is however the intrinsic behavior of all materials under cyclic loading.

The main observations from both quasi static and cyclic loading experiments can be summarized as below:

- Based on experimental results, the damage mechanisms of laminates under quasi static loading were somewhat different than that of cyclic loadings. For all specimens under quasi static loading, horizontal delamination was observed to initiate from the critical section and propagate towards the loading end of the laminate. However, for the laminates under cyclic loading, in addition to delamination, shear-out cracks also propagated in the same direction. For the failures which were propagated towards the fixed end, the failure mechanisms seemed to be similar, as a combination of delamination and shear-out cracks, for laminates under both quasi static and cyclic loadings.

- All Fatigue experiments were performed under displacement control mode. The actuator force versus number of cycles were plotted for all laminates which was called as “load ratio reduction (LRR)” curve. From the load ratio reduction curve, it was observed that the load bearing capacity of the laminates decreased smoothly until a damage initiated inside the laminate. From this point the figures showed that the load bearing capacity of the laminates started to decrease drastically until the final failure of the laminates.
- 20% or more decrease in actuator force was taken as indication of laminates’ failure. When the load bearing capacity did not decrease by 20%, the laminate was left until one million cycles under fatigue loading. Two other damage initiation indications were first audible sounds during the experiments and second sudden drop in the actuator force.
- “Side A” surface of the laminates under cyclic loading was scanned with thermal camera to obtain the temperature change. There was a drastic temperature increase, i.e. more than 15°C, when the delamination was appeared on the side surface. For the temperature changes less than15°C the delamination was not appeared on the “Side A” surface. This concludes that 15°C could be taken as a threshold for the temperature increase above which delamination could appear on the side surface.
- Side surfaces of the laminates were scanned by digital image correlation (DIC) setup. The setup is able to provide all six components of whole field side surface strains. After analyzing the DIC results, among all six available strain components, i.e. three normal and three shear strain components, out-of-plane shear strain τ_{13} seemed to provide useful information about the strain field of the side surfaces.
- It was observed from all fatigue experiments that the maximum out-of-plane shear strain of the side surfaces takes an almost constant trend at the beginning of the cyclic loading and it starts to increase drastically when the delamination reaches to the side surface.
- The whole field out-of-plane shear strain contours showed that the maximum region of the shear strain relocates towards the fixed end of the laminate. The delamination then starts to appear on the side surface from those maximum shear strain regions.

- In most of the experiments the maximum region of the shear strain was well centered on the mid-thickness. However, in some specimens the maximum region of the shear strain relocated to either upper or lower half-thickness of the laminates where the delamination appeared at the same upper or lower half-thickness region. The reason is seemed to be the un-symmetry of the experiment as regards of either manufactured laminates or the test setup, or both together.
- In some fatigue experiments the damage style in transverse section cuts seemed to be un-symmetric. This fact is because of variabilities that arise in the experiment from both manufacturing and the test setup which makes the failure style to be un-symmetric. The two important variations coming from manufacturing could be first the variation in the thickness of the specimens which could happen because of either non-uniform autoclave pressure on the caul plate at the time of curing or the thickness variation of each ply. The second variation could arise from the fact that the drilled holes would be a little off-centered which could lead to have non-uniform bolt-clamping forces. With regards to the test setup, the actuator could be a little off-centered with respect to the longitudinal center line of the specimens. Otherwise the appeared delamination and shear-out damages shall be completely symmetric.
- The thicker the laminate is, the less decrease in load ratio reduction (LRR) is observed for corresponding deflection levels. This means that thicker laminates are less susceptible to degrade under higher deflection levels.
- The "Endurance Deflection Level (EDL)" is the deflection level below which no damage would initiate inside the laminate. The "EDL" is higher for thicker laminates.

Chapter 5. Comparison between experimental and numerical results

Quasi static and cyclic experiments were performed on laminates with different thicknesses and the results were summarized in Chapter 4. In this chapter the results are analyzed in order to investigate the thickness effect on the behavior of bolted thick Glass/Epoxy laminates under both quasi static and fatigue loading. The experimental results of 50, 60 and 70-Layer laminates are compared with the results of developed fatigue progressive damage model (FPDM). Furthermore, the FPDM is applied for the case of available in-house fatigue experimental results of 80-Layer laminates. The agreement between the results of experiments with those of developed fatigue progressive damage model shows that the introduced approach as the application of coupon level material properties along with the 3D finite element model is suitable to study the fatigue behavior of thick composite laminates.

5.1. Quasi Static Loading

The dominant failure modes of all tested samples were seen to be delamination and shear-out cracks. Horizontal delamination was initiated from critical section after the second row of the bolt holes and propagated towards the loading end of the laminates under quasi static loading. A combination of delamination and shear-out cracks also propagated towards the fixed end of the laminates. The most contributing stress component for delamination is out-of-plane shear stress τ_{13}. For the quasi static testing of thick laminates, "Side A" surface of the laminates was monitored by measurement system of digital image correlation (DIC) in order to obtain the whole field strain of the side surface. In addition to DIC, one strain gauge was installed on "Side B". The location of this strain gauge was estimated from finite element analysis which was able to provide the point of maximum shear strain. Four strain gauges were installed on the top and bottom surface of the laminates. For the definition of side surfaces and location of the strain gauges refer to Chapter 3. In the following sections the numerical results are compared with the results of strain gages and DIC system for laminates with different thicknesses under quasi static loading.

5.1.1. 50-Layer Laminate under Quasi Static Loading

For specimen F50_1 the profile of the shear strain corresponding to 2.36 (in) of upward actuator displacement is shown in Figure 5-1. In this figure the results of FEM, DIC and strain gauge are integrated and show good correspondence. The maximum shear strain is around 19,000 $\mu\varepsilon$. There was only one strain gauge attached on the "Side B" Surface of the laminate as shown as "Strain Gauge 1" in Figure 3-10.

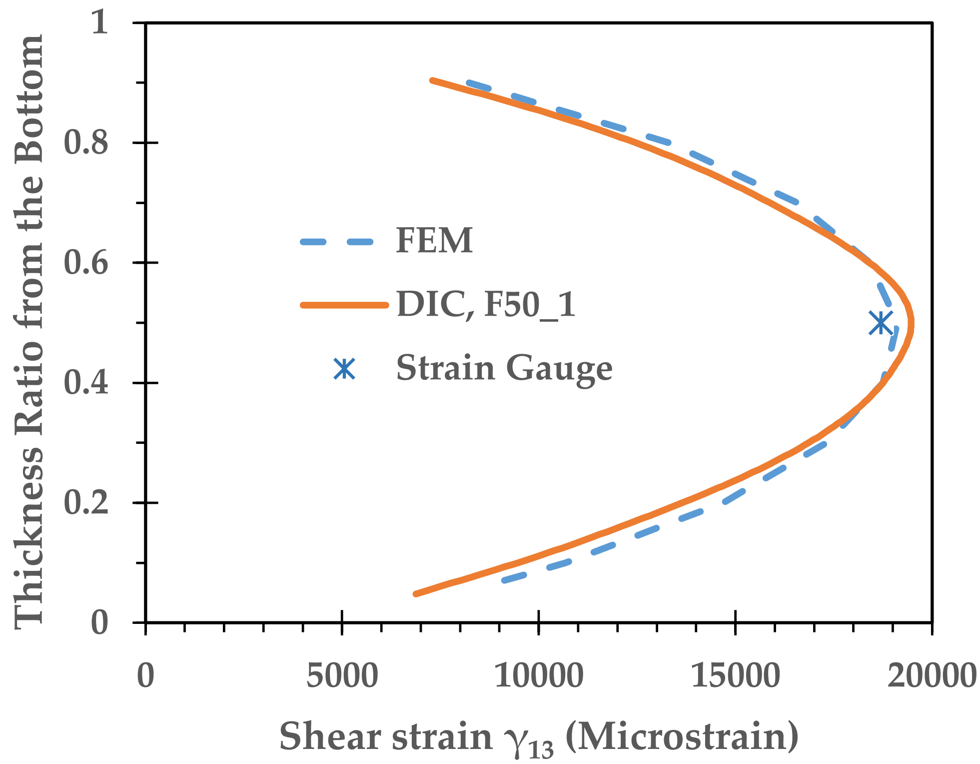

Figure 5-1 Profile of shear strain on the side surface. Sample F50_1 at 2.36 (in) of actuator displacement

The distributions of out-of-plane shear strain γ_{13} of FEM and DIC are shown in Figure 5-2. Two contours show good correspondence between the contour results of finite element and the experiment.

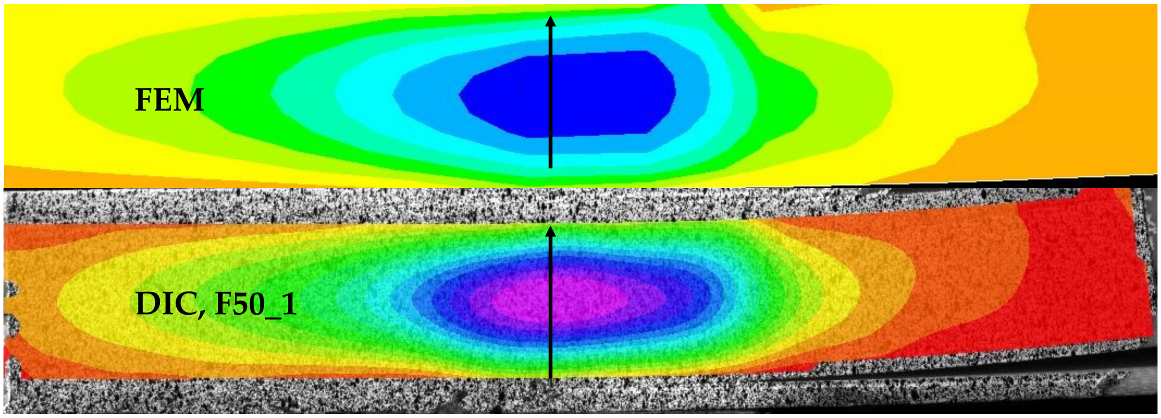

Figure 5-2 FEM and DIC contour results for distribution of out-of-plane shear strain on the side surface. Specimen F50_1 at 2.36 (in) of upward actuator displacement

5.1.2. 60-Layer Laminate under Quasi Static Loading

Similar to the 50-layer laminate, the FEM and experimental results of out-of-plane shear strain are compared in Figure 5-3 for the 60-layer laminate under 2.16 (in) of actuator displacement. The maximum shear strain is around 20,100 με.

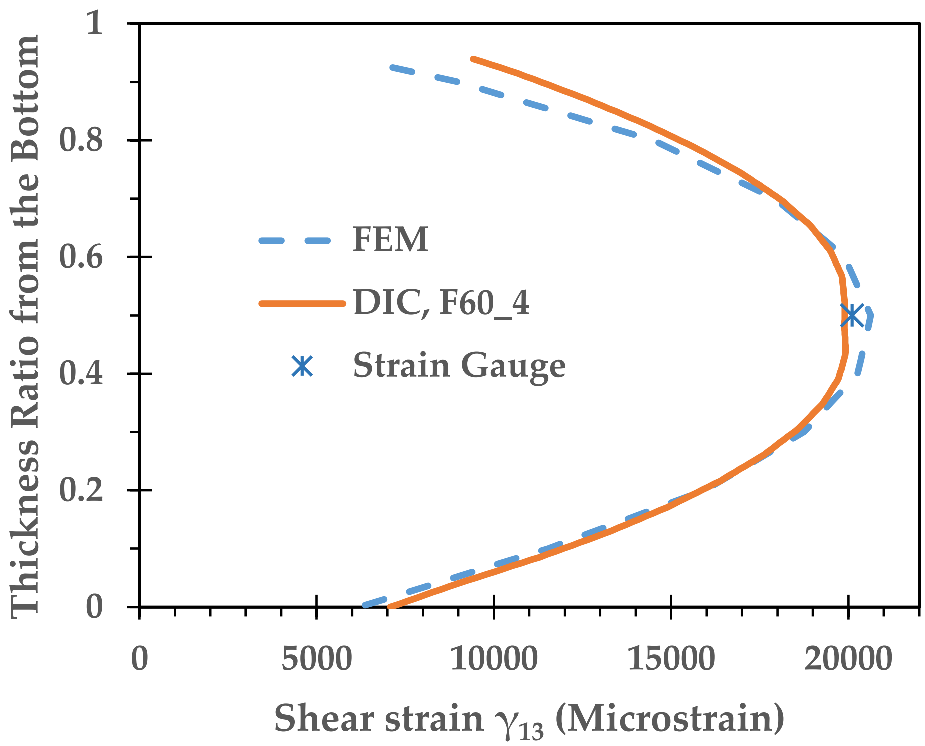

Figure 5-3 Profile of out-of-plane shear strain on the side surface. Sample F60_4 at 2.16 (in) of actuator displacement

Figure 5-4 shows the FEM and DIC contours of shear strain for the same laminate. The contours show the correspondence between the two contour results.

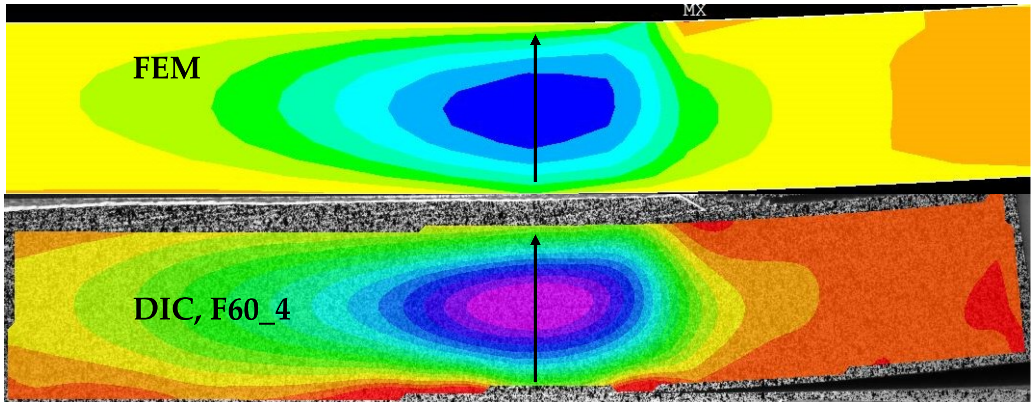

Figure 5-4 FEM and DIC results for distribution of out-of-plane shear strain on the side surface. Sample F60_5 at 2.16 (in) of upward actuator displacement

5.1.3. 70-Layer Laminate under Quasi Static Loading

For the 70-layer laminate under 1.57 (in) of upward actuator displacement, the FEM, DIC and strain gauge results are combined in Figure 5-5. The maximum shear strain for this case is around 17,000 με. There is a good correspondence between the results of FEM and the experiment.

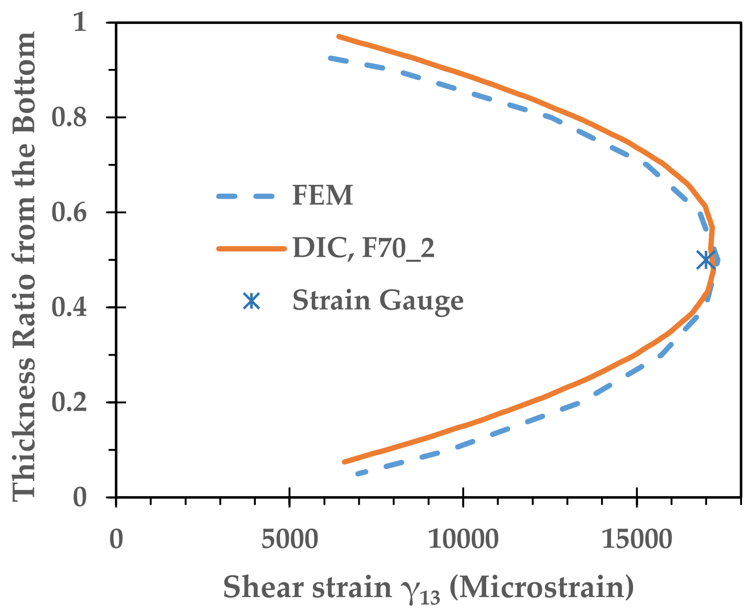

Figure 5-5 Profile of out-of-plane shear strain on the side surface. Sample F70_2 at 1.57 (in) of upward actuator displacement

Figure 5-6 shows the FEM and DIC distributions of shear strain on the side surface for the 70-layer laminate.

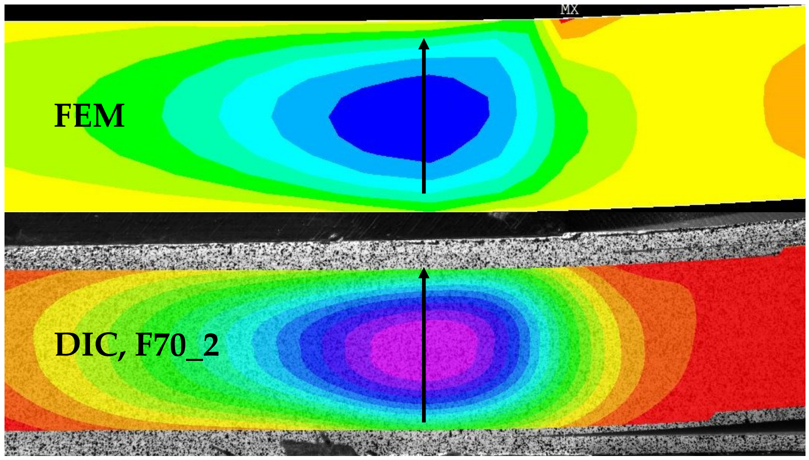

Figure 5-6 FEM and DIC results for distribution of out-of-plane shear strain on the side surface. Sample F70_2 at 1.57 (in) of upward actuator displacement

5.1.4. Comparison of Behavior of Laminates with Different Thicknesses under Quasi Static Loading

As mentioned at the beginning of this chapter, the out-of-plane shear stress is the most contributing stress component for delamination damage mechanism. To understand the behavior of laminates under flexural loading, different-thickness laminates were solved using finite element analysis model with prescribing the same actuator displacement of 1.57 (in) for all thicknesses. Figure 5-7 shows the results of the shear strain on the side surface for three laminates with different thicknesses. The graph shows that the shear strain increases by increasing of the thickness of the laminates for the same actuator displacement.

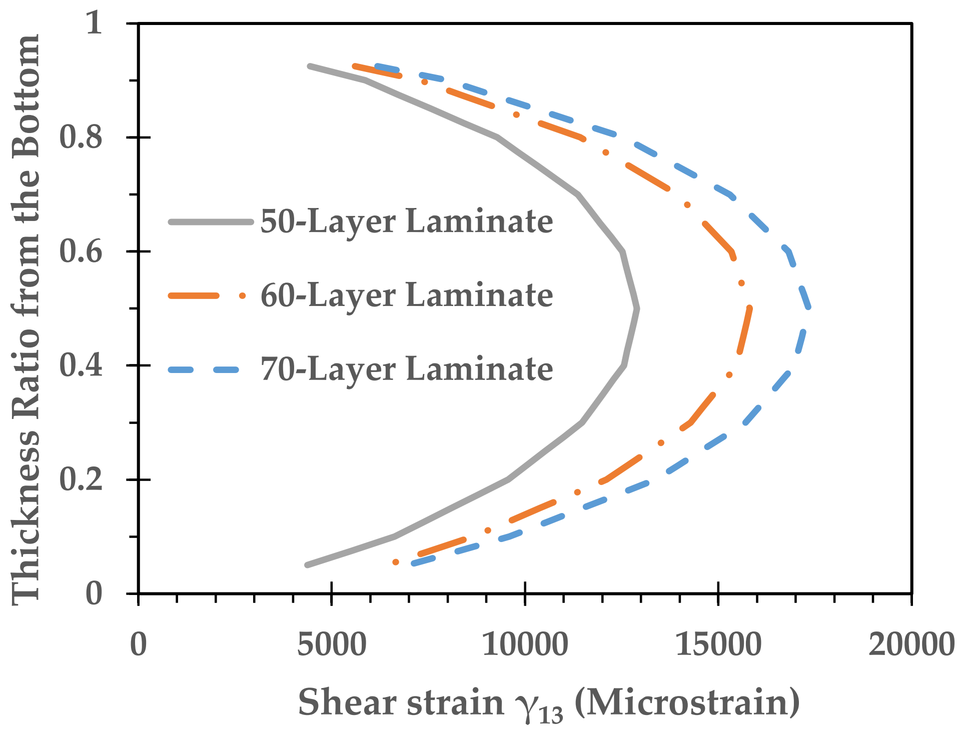

Figure 5-7 FEM results for out-of-plane shear strain on the side surface at 1.57 (in) of upward actuator displacement for 50, 60 and 70-layer unidirectional laminates

The main contributing stress elements for occurrence of delamination are out-of-plane normal and shear stress elements. When the out-of-plane stresses reach a certain value, the delamination occurs in the laminate. Out-of-plane shear stress is directly related to the out-of-plane shear strain which was measured during the experiments. Figure 5-8-a shows the DIC contour of the shear strain on the "Side A" Surface of 70-Layer laminate around the fixed end area. The profile of the shear strain distribution along the line in the thickness direction is shown in the Figure 5-8-b. As shown in Figure 5-8-b the maximum shear strain occurs at almost the mid thickness. Based on the shear strain profile in the Figure 5-8-b, the difference between the maximum shear strain and the shear strains at the 1/3 of the thickness from the top and the bottom is about 10%. It means that the maximum values of the shear strain occur in a region between 1/3 and 2/3 of elevation from the bottom. This is to explain the reason for the occurrence of delamination between these elevations which was observed in the experiments.

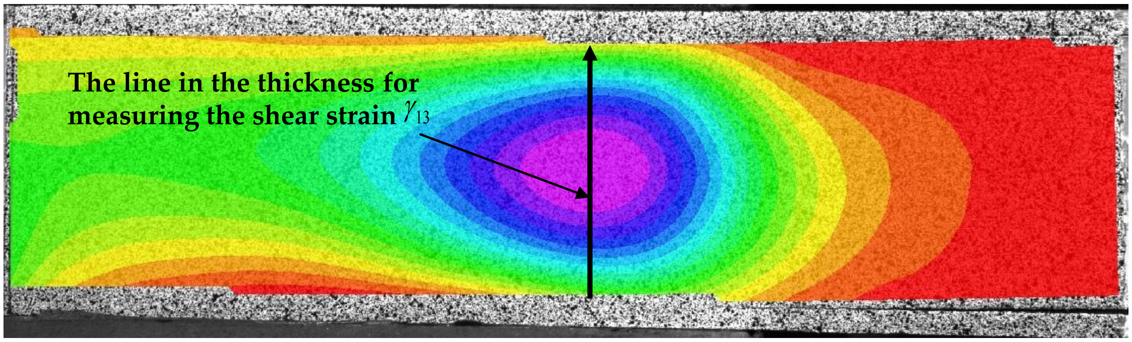

DIC contour of γ_{13} shear strain on the Side A Surface

a)

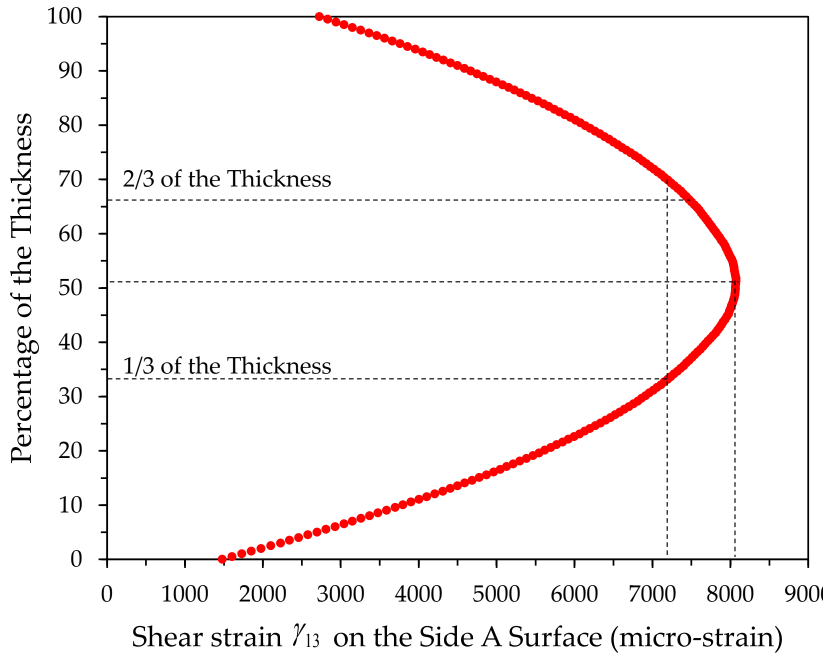

b)

Figure 5-8 a) DIC contour of out-of-plane shear strain on the "Side A" Surface, b) Shear strain on the "Side A" Surface, for 70-Layer laminate

Figure 5-9-a shows the DIC contour of the in-plane shear strain on the Top Surface of 70-Layer laminate between the two bolted regions. The profile of the shear strain along the line in the width direction (Line AB) is shown in Figure 5-9-b. The profile shows that in-plane shear strain is almost symmetric and it changes between -800 and +750 micro strain.

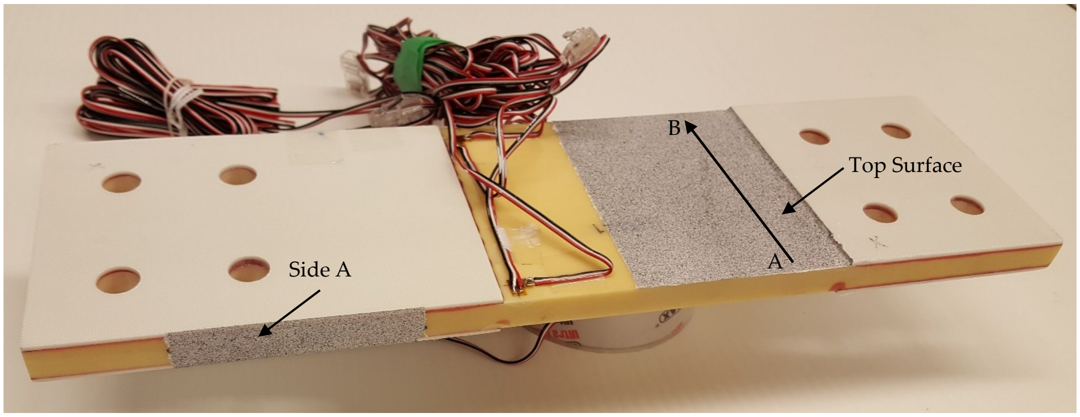

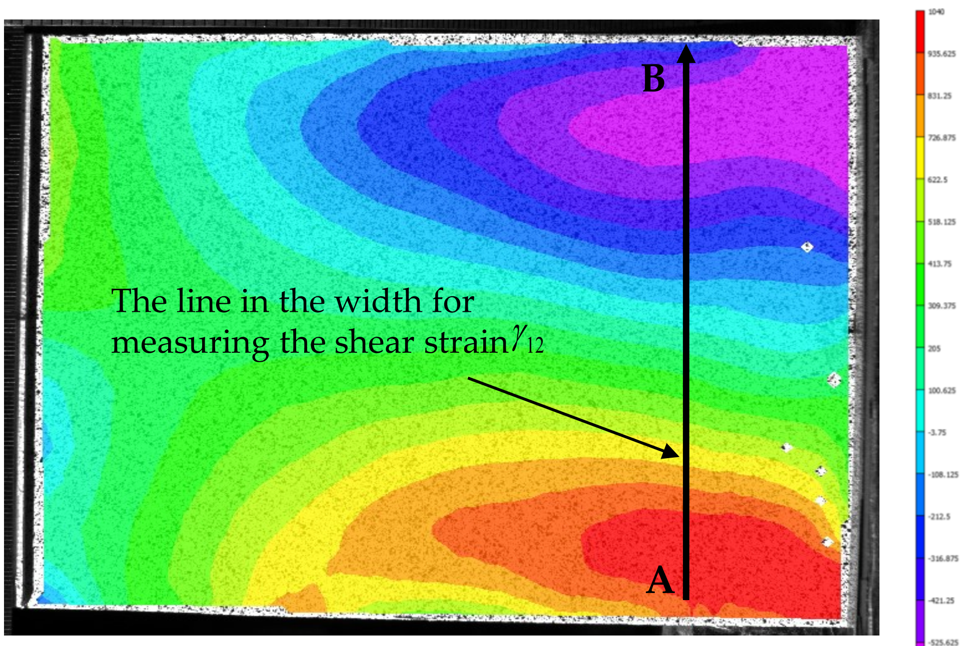

DIC contour of γ_{12} shear strain on the Top Surface

a)

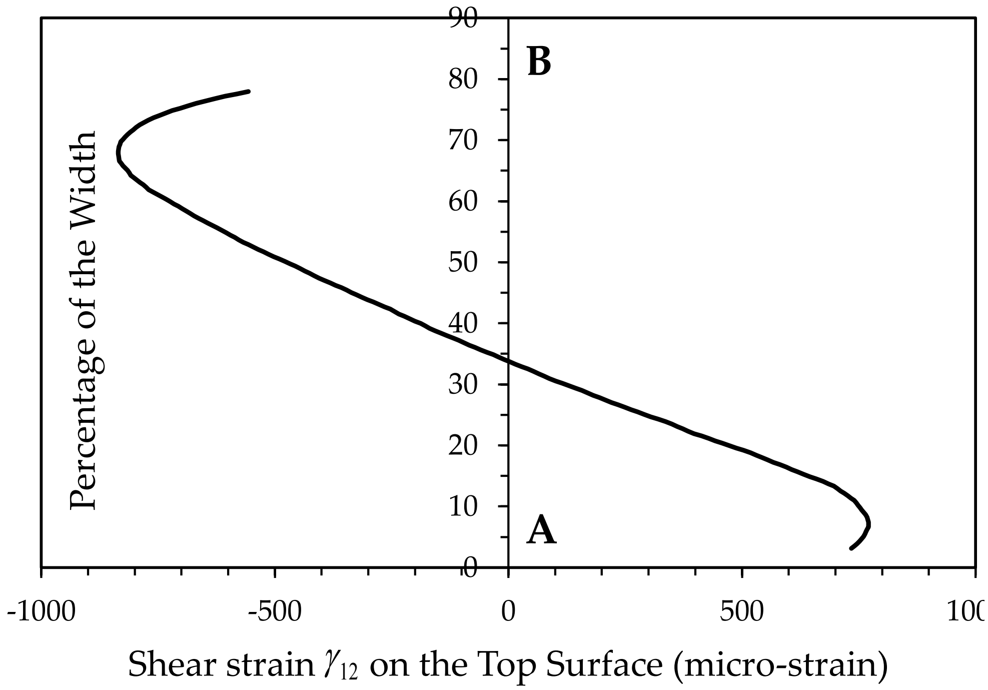

b)

Figure 5-9 a) DIC contour of shear strain on the Top Surface, b) Shear strain on the Top Surface, for 70-Layer Laminate

The results of finite element analysis for the distributions of out-of-plane normal and shear stresses of the fixed end of the laminate are shown in Figure 5-10. This figure is related to the static analysis of 80-Layer laminate with 0.9 (in) of actuator displacement. Figure 5-10 shows that maximum absolute shear stress in the laminate and maximum out-of-plane normal stress occur around the second row of the bolt holes. Therefore, this area is expected to be the most probable area of failure initiation.

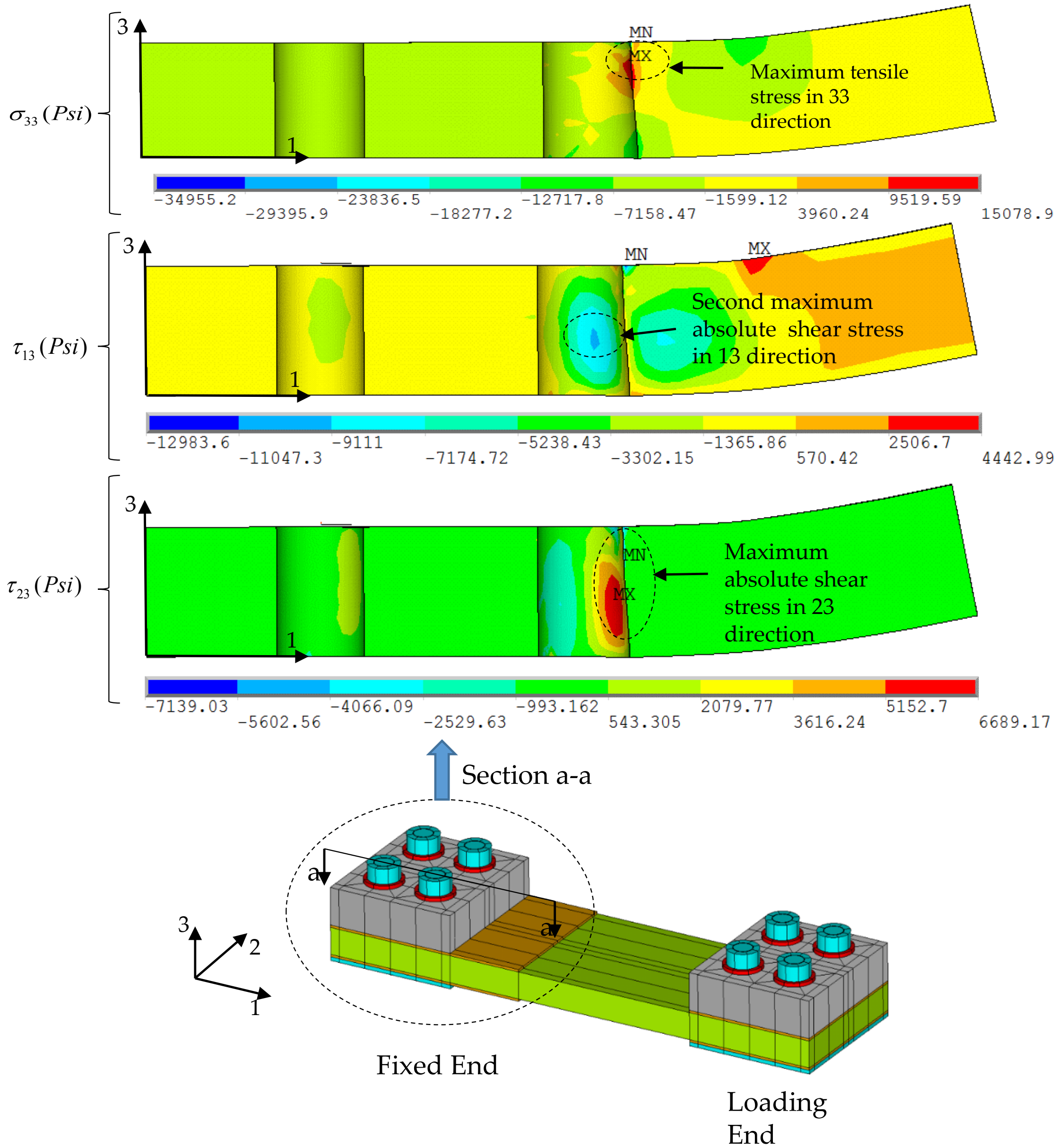

Figure 5-10 Distributions of out-of-plane normal and shear stresses at the fixed end

5.2. Cyclic Loading

Three different thickness group of unidirectional 50, 60 and 70-layer laminates were studied in this research to investigate the thickness effect on the fatigue behavior. Testing of thinner than 50-layer laminates was not practical because of limitation in loading capacity of the test setup, since thinner laminates required larger displacement at the time of fatigue loading. The loading machine was not able to retain those large displacements with respect to 3 Hz as the test frequency. This means that the thickness threshold as the transition point from thin to thick laminates was not obtained. Instead, the comparison of the behavior of thick laminates with different thicknesses was examined.

The behavior of 50, 60 and 70-layer laminates were observed to follow the same style as regards of the initiation location and damage style. The summary of the fatigue experimental results of these laminates were explained in Chapter 4. In this section the results of FPDM are compared with the results of experiments to validate the calculations.

5.3. FPDM Results Verification for Laminates under Cyclic Loading

In this section, the developed fatigue progressive damage model (FPDM) is examined against the experimental results of thick laminates with different thicknesses as regards of both Load Ratio Reduction (LRR) curves and Dominant Fatigue Failure Mechanism (DFM).

5.3.1. Load Ratio Reduction (LRR) Curves

5.3.1.1. LRR for 50-Layer Laminates

Four 50-Layer laminates were tested in this research. One under quasi static and the other three under three different deflection levels. The deflection level is the ratio of the maximum applied actuator displacement at the time of fatigue loading to the ultimate quasi static displacement at the failure under quasi static loading. The 50-Layer laminate under quasi static loading failed at 2.50 (in) of actuator displacement. Based on this ultimate displacement, three deflection levels of 60%, 65% and 70% were tested which required 0.14 (in), 0.15 (in) and 0.16 (in) of actuator displacement at the time of fatigue loading. The actuator displacement required to run these deflection levels are summarized in Table 5-1.

Table 5-1 Three Deflection Levels of $[0]_{50}$ Laminates			
Deflection Level	*60%*	*65%*	*70%*
R-ratio	*0.1*	*0.1*	*0.1*
U_{ult} (in)	*2.50*	*2.50*	*2.50*
U_{min} (in)	*0.14*	*0.15*	*0.16*
U_{max} (in)	*1.40*	*1.50*	*1.60*

To verify the accuracy of the developed fatigue progressive damage model (FPDM), all deflection levels listed in Table 5-1 were solved for to obtain the load ratio reduction from the model and compare the finite element results with the experimental ones for 50-Layer laminates.

Figure 5-11 shows the comparison of the results for 60% of deflection level. As discussed in Chapter 4, the 50-Layer laminate under 60% of deflection level did not fail until 1M cycles. The indication for failure was taken as the actuator force reduced by more than 20% of initial value. Based on the LRR behavior of this laminate, the finite element model was solved for by 20,000 iterations for the first 100,000 cycles and continued until 1M cycles by 100,000 cycle-iteration. The results of FPDM are integrated in the LRR curve extracted from experiment as shown in Figure 5-11. The figure shows a good agreement. However, the results of FPDM under-estimate the experimental results for the case of 60% of deflection level.

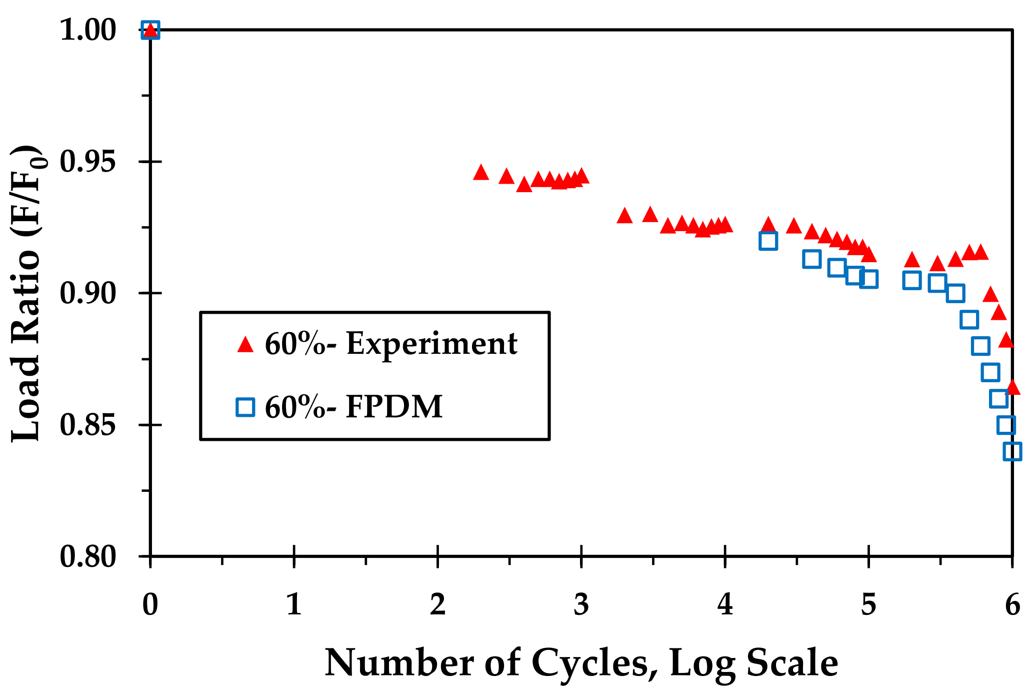

Figure 5-11 Comparison of load ratio reduction curves of experiments and FPDM for 60% of deflection level- 50-Layer Laminates

For 50-Layer laminate under 65% of deflection level, the results of experiment and FPDM are integrated in Figure 5-12. Tested laminate failed at about 488,000 cycles as shown in Chapter 4. Based on the experimental result, the FPDM was solved for by 10,000 iterations until 100,000 cycles and then 100,000 iteration until 500,000 cycles. The integrated results show that the FPDM could capture the results of experiment. Similar to the 60% of deflection level an under-estimation is observed for FPDM results.

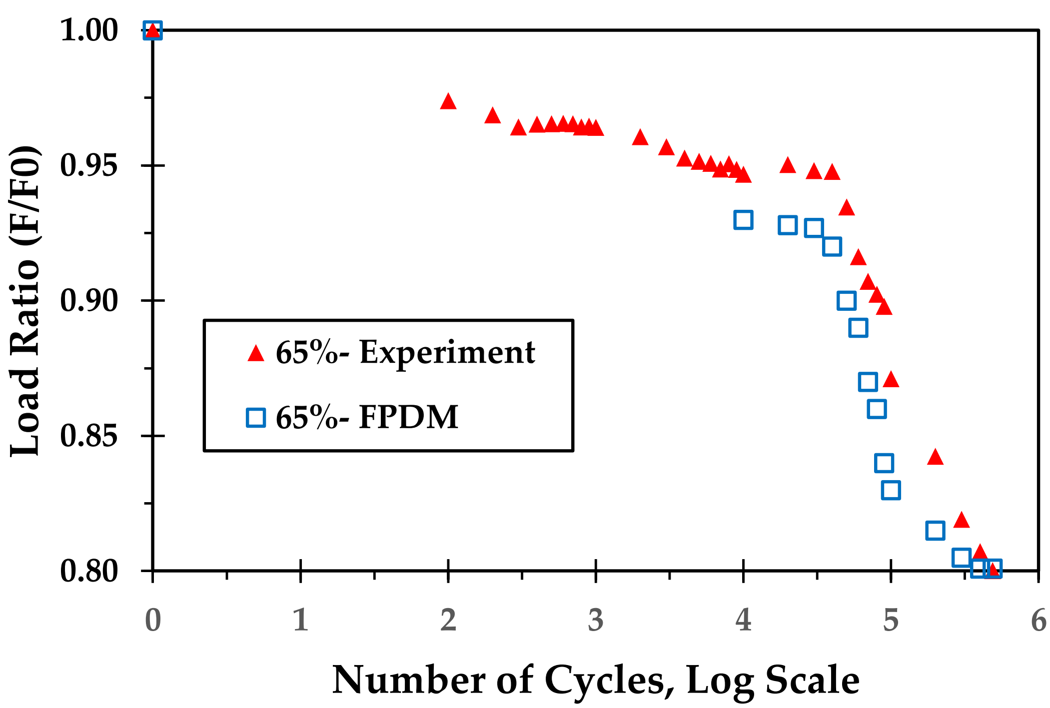

Figure 5-12 Comparison of load ratio reduction curves of experiments and FPDM for 65% of deflection level- 50-Layer Laminates

Figure 5-13 shows the comparison of experimental and FPDM results for 50-layer laminate under 70% of deflection level. The specimen failed at around 47,000 cycles. The finite element model was solved for by 1,000 cycle intervals until 10,000 cycles and 10,000 until 50,000 cycles. The trend of FPDM results resembles the experimental results showing however a bit of under estimation.

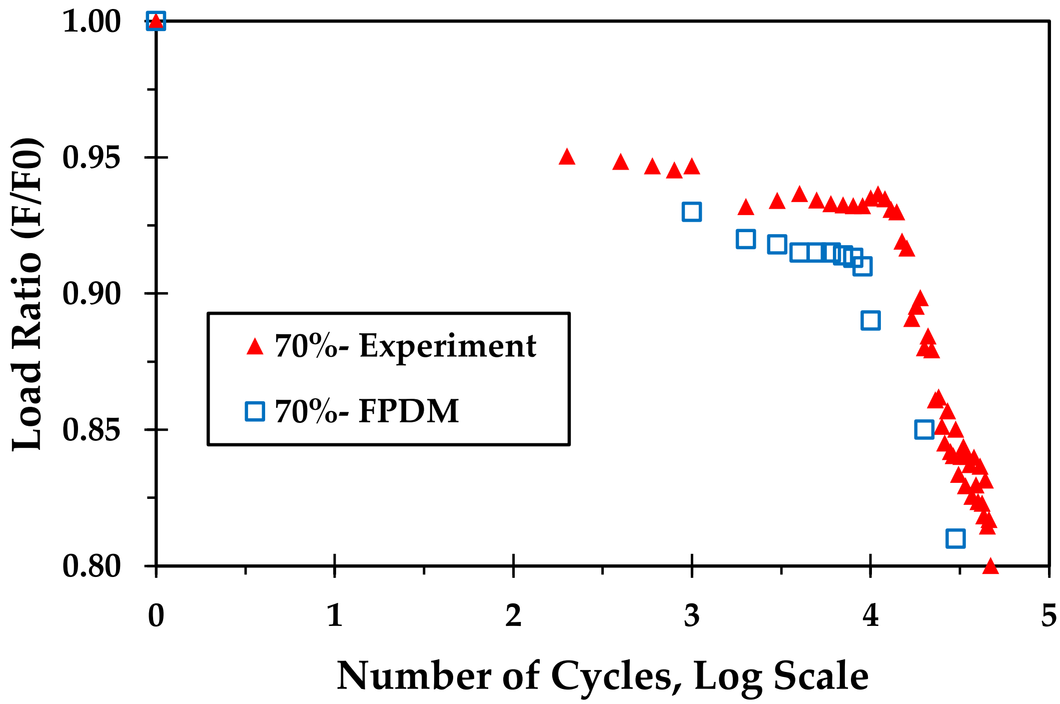

Figure 5-13 Comparison of load ratio reduction curves of experiments and FPDM for 70% of deflection level- 50-Layer Laminates

5.3.1.2. LRR for 60-Layer Laminates

Four 60-Layer laminates were manufactured and tested in this research. One of the specimens was tested under quasi static experiment. This specimen failed at 2.24 (in) of upward actuator displacement. Based on this ultimate value, three deflection levels were planned to perform the cyclic experiments. The maximum actuator displacement was adjusted at 0.13 (in), 0.14(in) and 0.15 (in) for 60%, 65% and 70% of deflection levels, respectively. The ultimate actuator displacement and minimum and maximum cyclic displacements for 60-Layer laminates are summarized in Table 5-2.

Table 5-2 Three Deflection Levels of $[0]_{60}$ Laminates

Deflection Level	*60%*	*65%*	*70%*
R-ratio	*0.1*	*0.1*	*0.1*
U_{ult} (in)	*2.24*	*2.24*	*2.24*
U_{min} (in)	*0.13*	*0.14*	*0.15*
U_{max} (in)	*1.30*	*1.40*	*1.50*

60-Layer laminate under 60% of deflection level did not fail until 1M cycles. Following the experimental results, the FPDM was solved for by 1,000 cycle intervals until 10,000 cycles. This was followed by 10,000 cycle intervals until 100,000 cycles and continued by 100,000 cycle intervals until 1M cycles. The integrated results of experiment and FPDM as shown in Figure 5-14 show good agreement between the two sets of results. However similar to all other comparison results until now, the FPDM under-estimates the results of experiments.

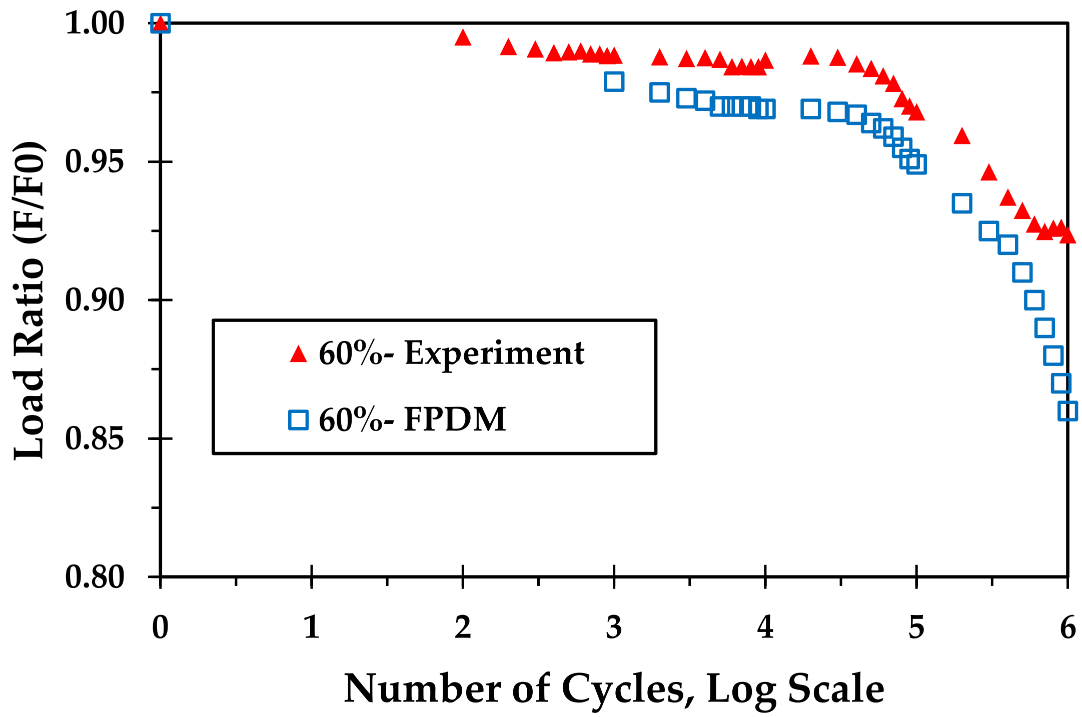

Figure 5-14 Comparison of load ratio reduction curves of experiments and FPDM for 60% of deflection level- 60-Layer Laminates

Figure 5-15 shows the comparison between experimental and FPDM results for 60-Layer laminate under 65% of deflection level. The final fatigue life was determined as 34,000 cycles from the experiment. Based on this value the FPDM was solved for until 40,000 cycles by 1,000 cycle intervals. The FPDM results also under-estimate the results of experiment for this laminate.

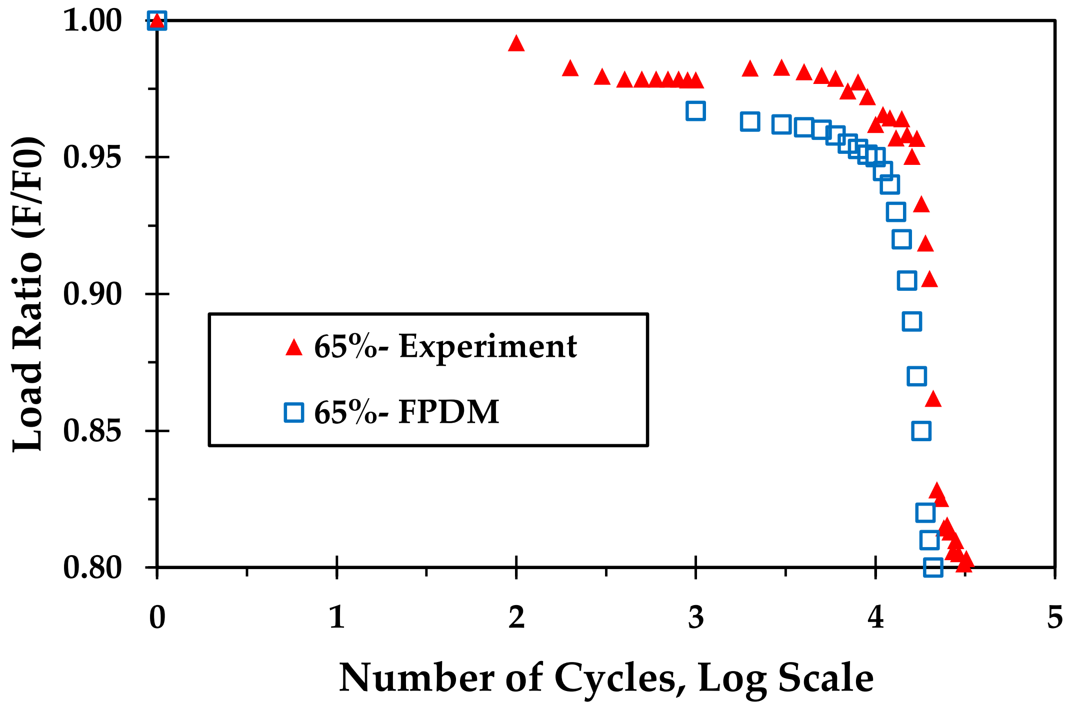

Figure 5-15 Comparison of load ratio reduction curves of experiments and FPDM for 65% of deflection level- 60-Layer Laminates

The comparison between results of FPDM and experiment for 60-Layer laminate under 70% of deflection level is shown in Figure 5-16. The specimen under this deflection level failed at 29,000 cycles. The FPDM was solved for until 30,000 cycles by 1.000 cycle intervals. The FPDM results are capturing the experimental results.

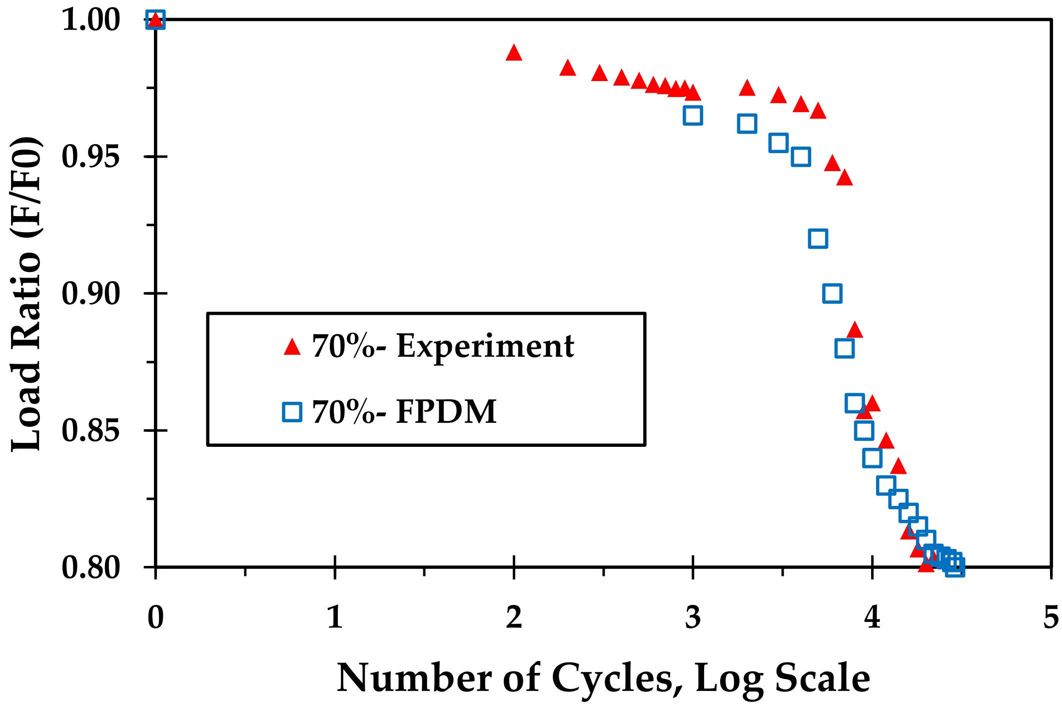

Figure 5-16 Comparison of load ratio reduction curves of experiments and FPDM for 70% of deflection level- 60-Layer Laminates

5.3.1.3. LRR for 70-Layer Laminates

Similar to 50-Layer and 60-Layer laminates, four 70-Layer laminates were manufactured and tested. The 70-Layer specimen under quasi static experiment failed at 1.60 (in) of upward actuator displacement. Based on this ultimate actuator displacement, three deflection levels were planned. Table 5-3 summarizes the deflection levels and required maximum and minimum actuator displacement for 70-Layer laminates.

Table 5-3 Three Deflection Levels of $[0]_{70}$ Laminates

Deflection Level	*60%*	*70%*	*75%*
R-ratio	*0.1*	*0.1*	*0.1*
U_{ult} (in)	*1.60*	*1.60*	*1.60*
U_{min} (in)	*0.09*	*0.11*	*0.12*
U_{max} (in)	*0.90*	*1.10*	*1.20*

The first 70-Layer laminate was tested under 60% of deflection level. This specimen did not fail until 1M cycles. The load bearing capacity of the specimen did not decrease by more than 5%. The results of experiment and FPDM are integrated in Figure 5-17. The results of FPDM capture the experimental results with a margin of under estimation which was seen for other thick laminates.

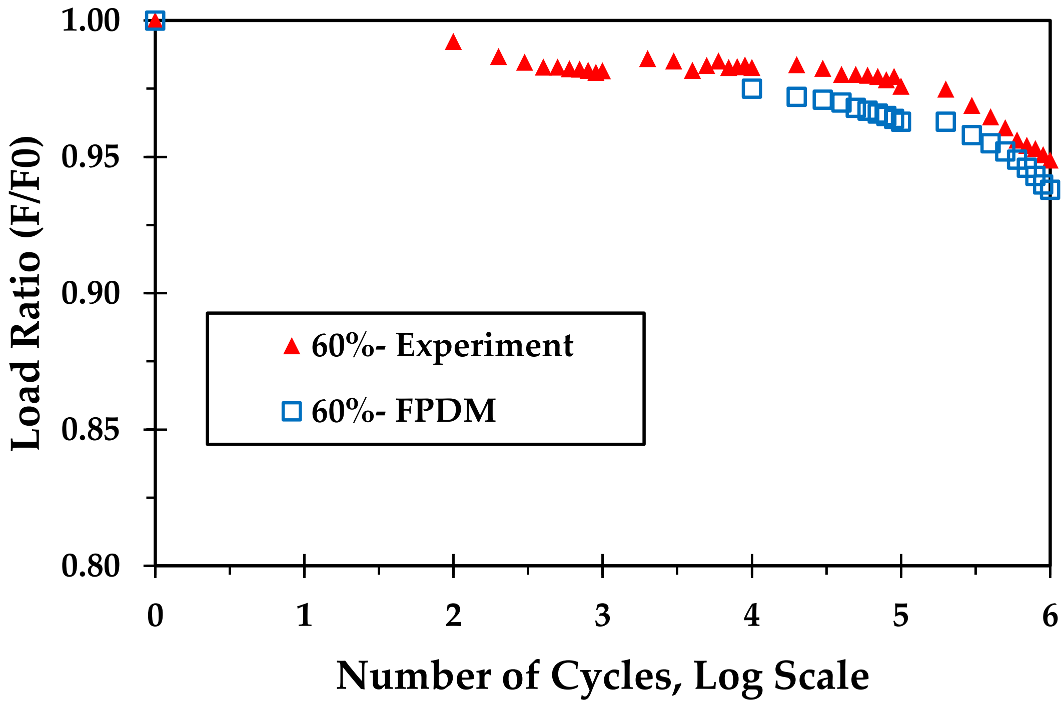

Figure 5-17 Comparison of load ratio reduction curves of experiments and FPDM for 60% of deflection level- 70-Layer Laminates

The next 70-Layer laminate was tested under 70% of deflection level, not under 65%, because the load bearing capacity of the specimen under 60% of deflection level did not fall down by more than 5% and it was predicted there could not be any failure for the laminate under 65% of deflection level. The specimen under 70% of deflection level did not fail because the load bearing capacity did not decrease by more than 20%. This laminate was also solved for by FPDM and the results are intergraded in Figure 5-18. There is an agreement between the results of experiments and that of FPDM with a margin of under estimation for the results of FPDM.

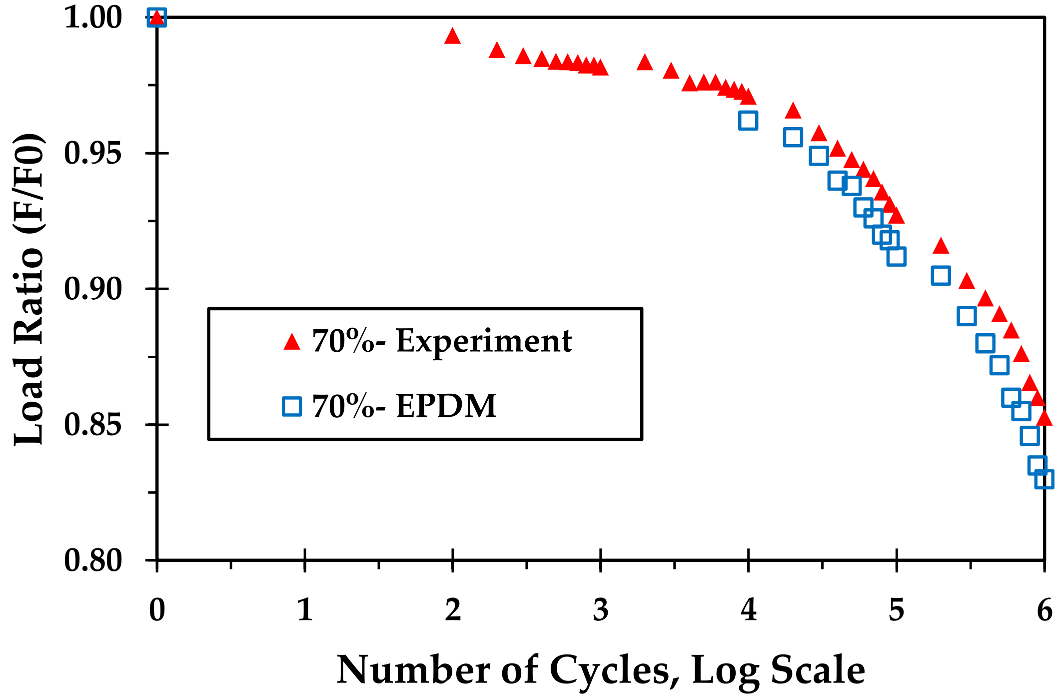

Figure 5-18 Comparison of load ratio reduction curves of experiments and FPDM for 70% of deflection level- 70-Layer Laminates

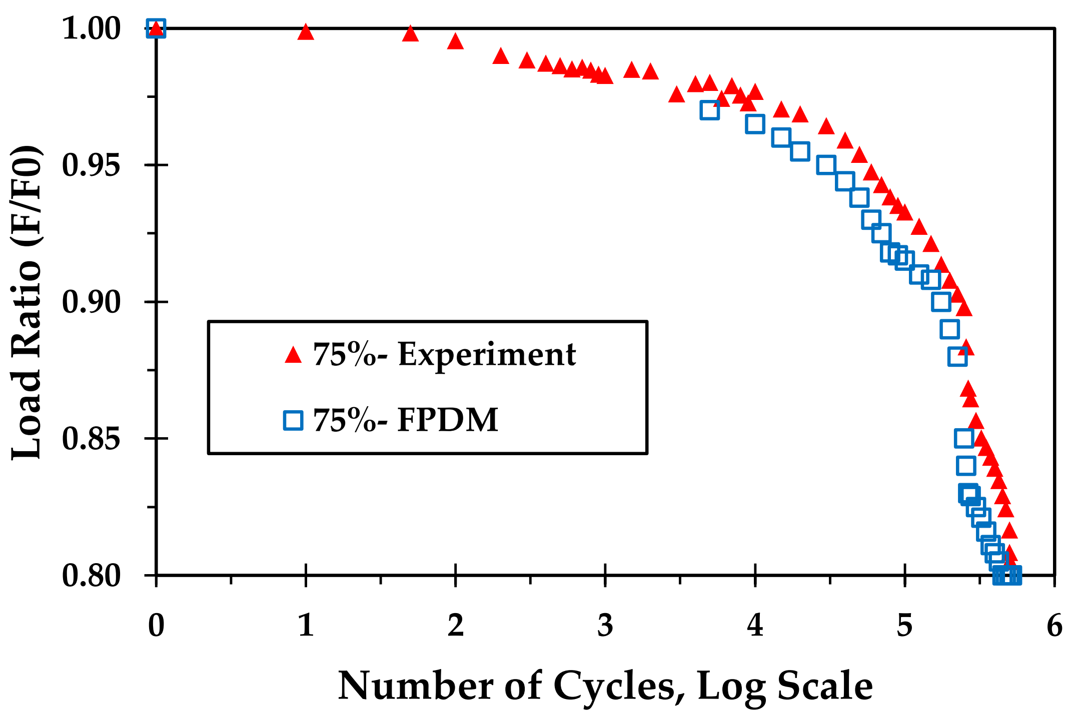

Figure 5-19 Comparison of load ratio reduction curves of experiments and FPDM for 75% of deflection level- 70-Layer Laminates

The next deflection level for 70-Layer laminate was chosen as 75%. The laminate which was tested under 75% deflection level failed at around 520,000 cycles. This laminate was solved for by FPDM and the two sets of results are integrated in Figure 5-19. For this laminate we observe the under estimation of FPDM results with an agreement in the overall trend.

5.3.1.4. LRR for 80-Layer Laminates

In this section, the developed fatigue progressive damage model is examined against the experimental results of 80-Layer laminates which were performed by Wendy Xiong [65]. Different deflection levels are summarized in Table 5-4.

Table 5-4 Four Deflection Levels of $[0]_{80}$ Laminates [65]

Deflection Level	*61%*	*65%*	*70%*	*75%*
R-ratio	*0.1*	*0.1*	*0.1*	*0.1*
U_{ult} (in)	*1.201*	*1.201*	*1.201*	*1.201*
U_{min} (in)	*0.073*	*0.078*	*0.084*	*0.090*
U_{max} (in)	*0.732*	*0.784*	*0.846*	*0.902*

Figure 5-20 to Figure 5-23 show the comparison between the results of load ratio reduction (LRR) of 80-Layer laminates obtained from experiments and FPDM for four deflection levels. All figures show a degree of agreement between the experimental and FPDM results with a margin of under-estimation of experimental results by FPDM results.

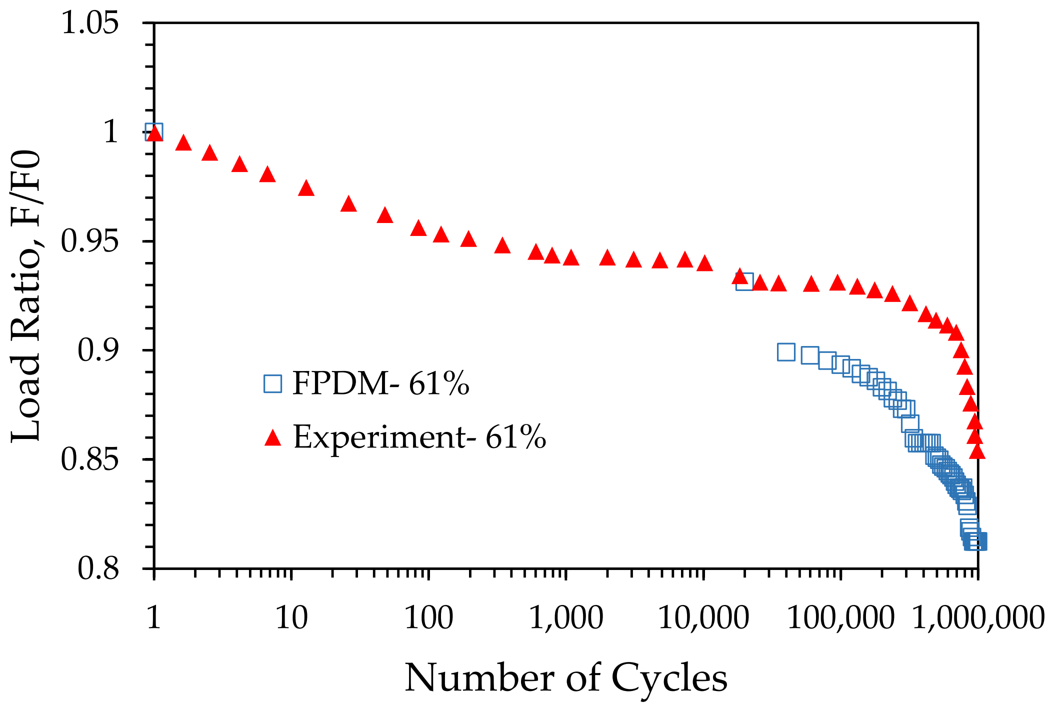

Figure 5-20 Comparison of load ratio reduction curves of experiments and FPDM for 61% of deflection level- 80-Layer Laminates

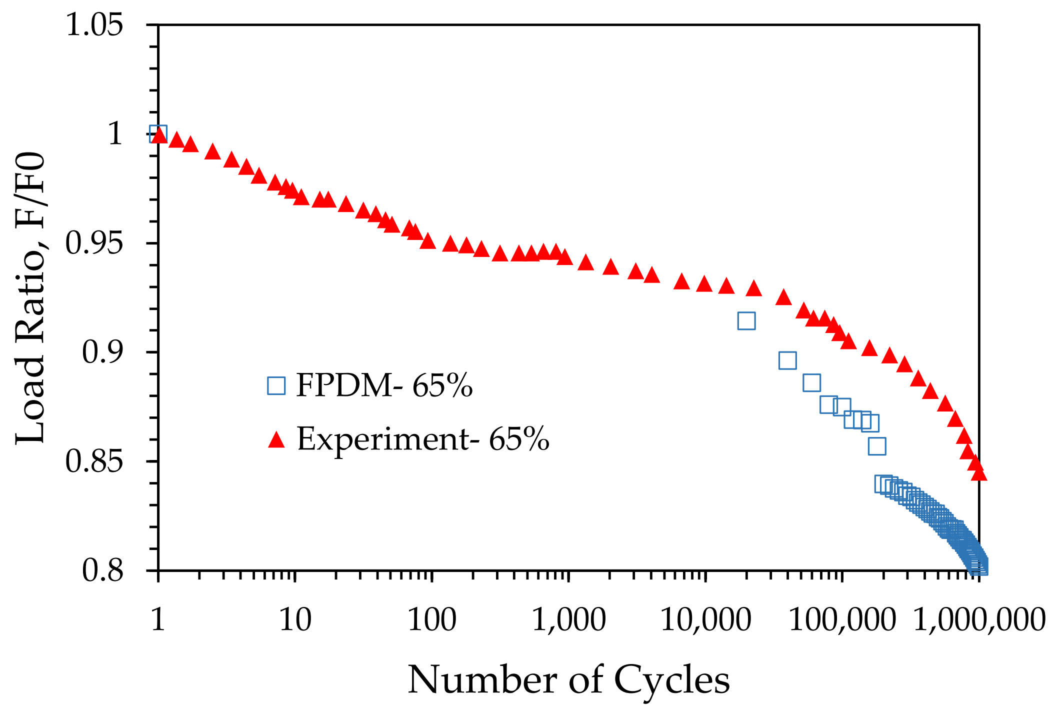

Figure 5-21 Comparison of load ratio reduction curves of experiments and FPDM for 65% of deflection level- 80-Layer Laminates

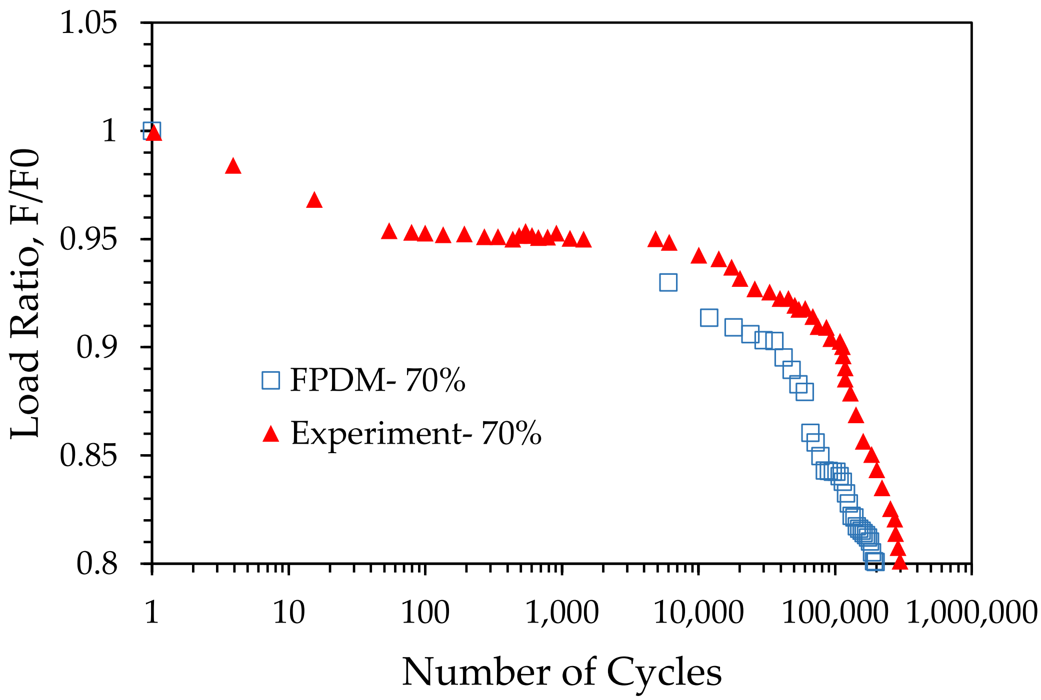

Figure 5-22 Comparison of load ratio reduction curves of experiments and FPDM for 70% of deflection level- 80-Layer Laminates

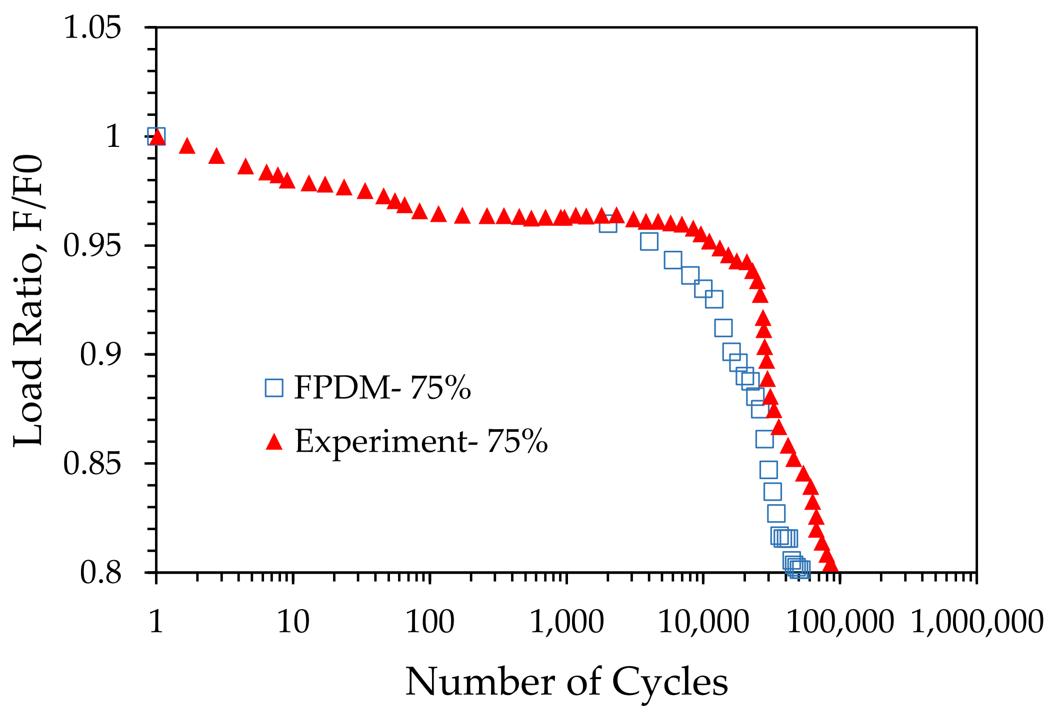

Figure 5-23 Comparison of load ratio reduction curves of experiments and FPDM for 75% of deflection level- 80-Layer Laminates

For four 80-Layer laminates under different deflection levels, the results of load ratio reduction are integrated in Figure 5-24. As shown in Figure 5-24, the fatigue life of the laminates depends mainly on the deflection level of flexural load. The higher is the deflection level, the faster is the reduction in the fatigue life. This fact is closely captured by the fatigue progressive damage modeling. There are two distinguished regions in Figure 5-24. “Region 1” corresponds to the area where load ratio is gradually decreasing. This region is related to damage initiation stage. “Region 2” is related to a sharper decrease in load ratio. “Region 2” corresponds to the damage propagation stage. The number of cycles corresponding to the transfer point of these two regions depends on the deflection level.

Figure 5-25 represents the evolution of failed elements based on the progression of fatigue cycles for all four deflection levels as listed in Table 5-4. Figure 5-25 demonstrates the decreasing of number of un-damaged elements of the finite element model. By the evolution of load cycles under displacement control loading, the load bearing capacity of the laminates decreases as shown in Figure 5-24. The results of finite element progressive damage model show the evolution of damaged elements. The correspondence between these two phenomena, i.e., decreasing of load bearing capacity and decreasing of number of un-damaged elements, shows that the number of un-damaged elements could be taken as an indication of fatigue damage progression in the laminates. This phenomenon is directly related to the stiffness degradation of the laminate.

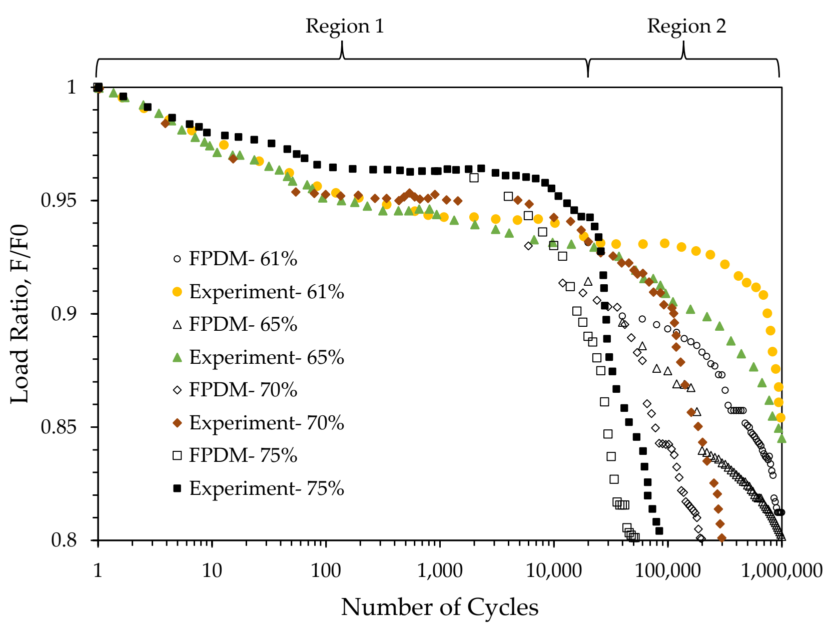

Figure 5-24 Comparison of load ratio reduction curves of experiments and FPDM for all deflection levels

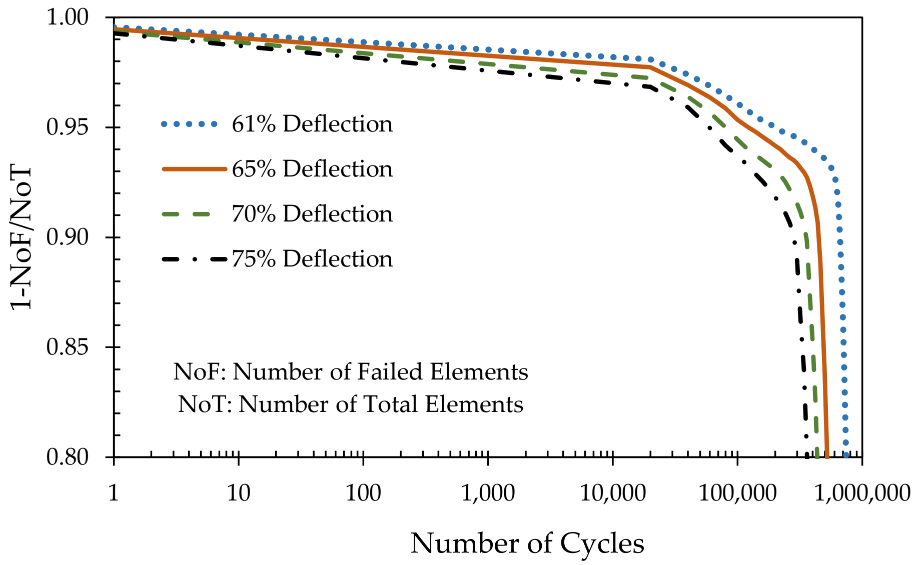

Figure 5-25 Damage progression in terms of reduction of number of un-damaged elements versus number of cycles for [0]$_{80}$ laminates

5.3.2. Dominant Fatigue Failure Mechanism (DFM)

In Section 5.3.1 the results of finite element model as regards of load ratio reduction (LRR) curves were compared with the experimental results. In this section the model is used to visualize the damage initiation and propagation in the thick laminates and to compare it with the experimental results for each thickness group.

As mentioned in Chapter 2, the developed Fatigue Progressive Damage Modeling (FPDM) is capable of distinguishing between the different failure modes. At each load step the information of failed elements as regards of element numbers and the failure mode is recorded. This information is used to visualize the fatigue failure pattern inside the laminates. The results of comparison for the dominant fatigue failure mechanism (DFM) for each thickness group are summarized in the following sections.

After finishing the fatigue tests, failed specimens were cut in different transverse cross sections in order to observe the state of internal cracks. The locations of the transverse cuts are shown in Figure 5-26.

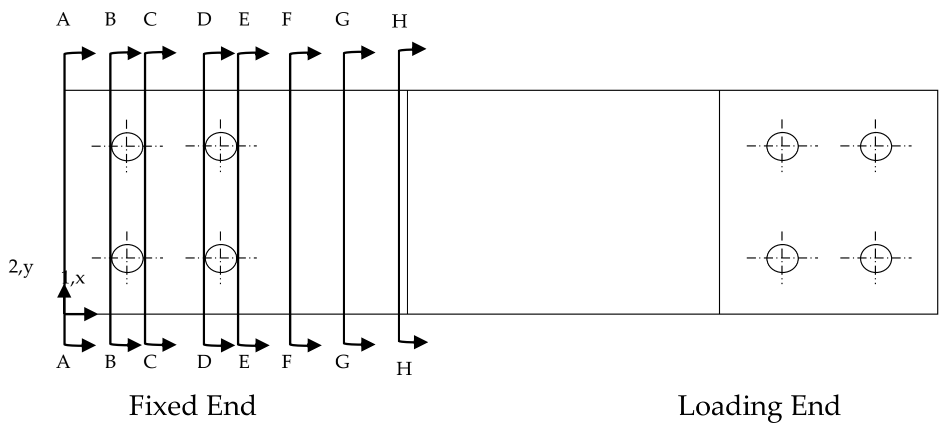

Figure 5-26 Location of Applied Section Cuts on Failed Specimens

5.3.2.1. DFM for 50-Layer Laminates

In Chapter 4, Section 4.2.1.1, the experimental results regarding tested 50-Layer laminate under 60% of deflection level (F50_5) was shown. This specimen did not fail until 1M cycles based on failure indication as reduction of actuator force by more than 20% as compared to the first cycle actuator force. However, the cracks were observed on Side A surface. After the experiment finished, the specimen was cut in transverse directions to observe the internal cracks. Section E-E cut is shown in Figure 5-27 (Upper Picture). The finite element model was solved until 1,000,000 cycles with 20,000 of cycle intervals. The section E-E cut at the end of cycling from FPDM is also presented in Figure 5-27 (Middle Picture). These elements are those failed under delamination failure mode based on failure equations (Equation (2-7)). The comparison of experimental and FPDM results shows that the damage style is captured by FPDM. However the experimental result shows the unsymmetrity of damage style for the reasons that have been discussed in Chapter 4, Section 4.3. The unsymmetrity of the laminate or the loading setup leads to release the energy at one side of the laminate by creating new surfaces. The energy release at one side results in not to create new failure surfaces at the other side of the laminate as shown in Figure 5-27.

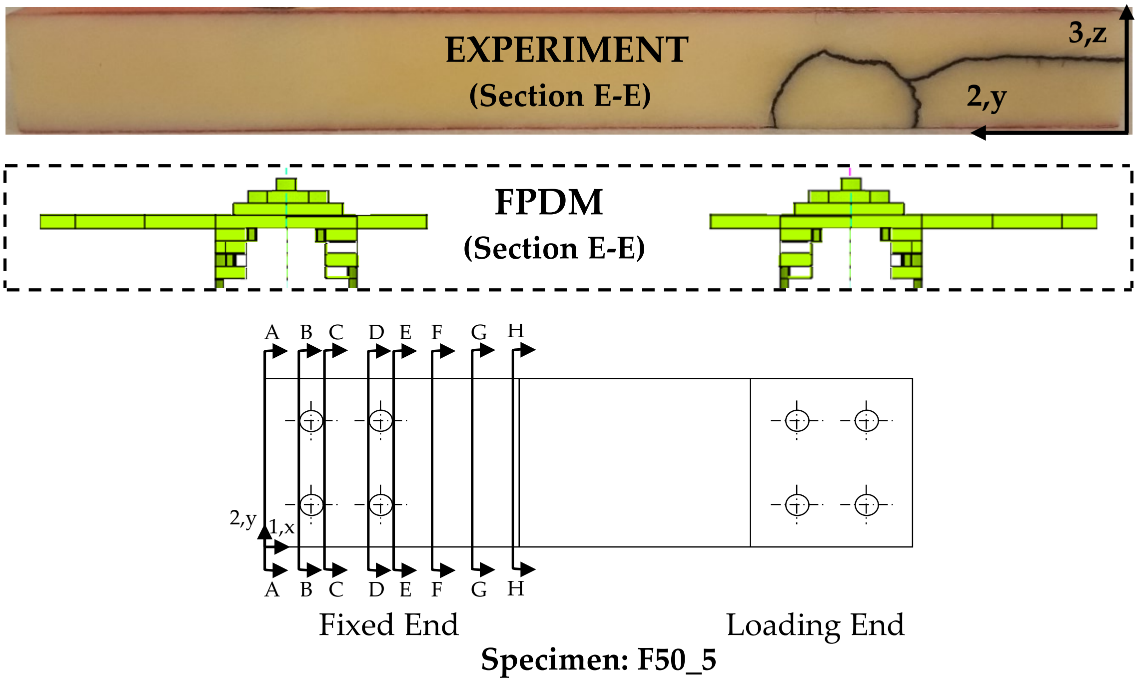

Figure 5-27 Transverse Cuts from the Experiment and FPDM for F50_5 specimen under 60% of deflection level

The progression of delamination failure as the result of FPDM is shown in Figure 5-28. As shown in the figure at 40,000 cycles there are some elements around the second row of the bolt holes at fixed end failed under delamination failure. This could be considered as delamination initiation. The progression of the delamination failure until 1M cycles shows the propagation of the delamination failure towards the fixed end of the laminate.

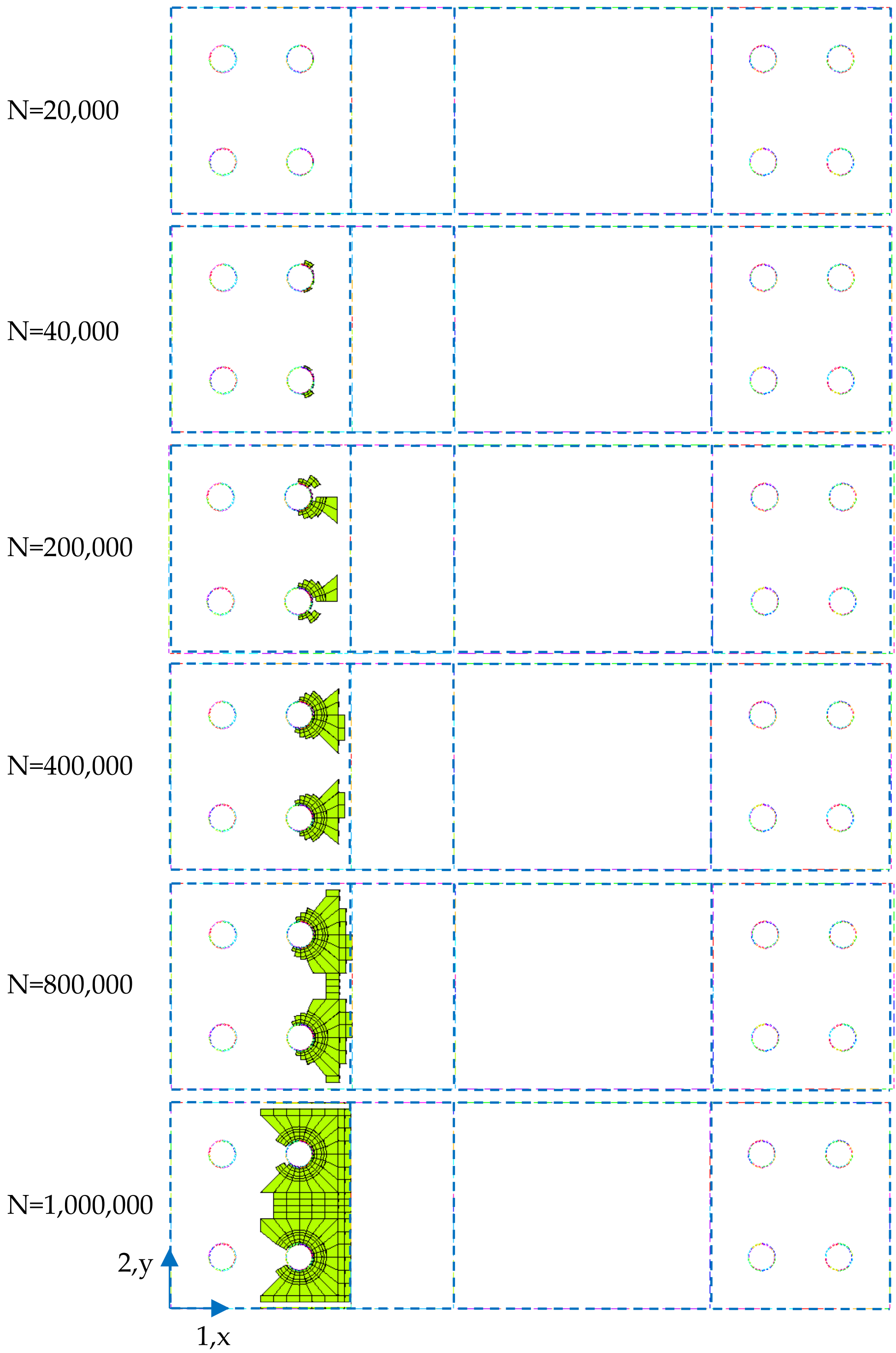

Figure 5-28 Progression of delamination failure in 50-Layer laminate under 60% of deflection level

5.3.2.2. DFM for 60-Layer Laminates

Specimen F60_2 was tested under 60% of deflection level which endured until 1M cycles as presented in Chapter 4, Section 4.2.2.1. The 60-Layer laminate was analyzed in FPDM under the same flexural loading condition until 1M cycles with 20,000 of cycle intervals. The damage mechanism results from both experiment (Upper Picture) and FPDM (Middle Picture) are shown in Figure 5-29. These elements shown in FPDM result are those failed under delamination failure mode based on failure equations (Equation (2-7)). As shown in Figure 5-29 the damage style of the experiment is captured by FPDM. However, the damage style of the experiment shows a degree of unsymmetrity because of the unsymmetrity of the manufactured laminate or the loading setup, as discussed in Chapter 4, Section 4.3.

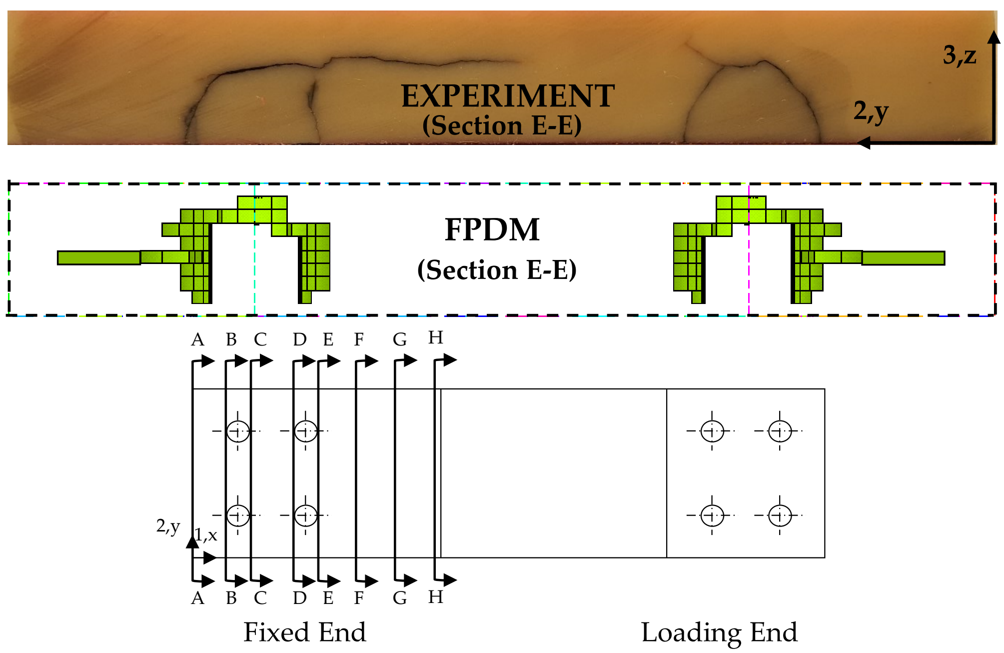

Specimen: F60_2

Figure 5-29 Transverse Cuts from the Experiment and FPDM for F60_2 specimen under 60% of deflection level

The progression of delamination failure for 60-layer laminate (F60_2) is shown in Figure 5-30. The upper picture in this figure shows that failure initiates from the second-row holes. Middle picture at 500,000 cycles shows the propagation of the failure towards the loading end of the laminate. Until 1M cycles the failure does not propagate towards the fixed end of the laminate.

Furthermore, there is no failed elements at the side edges. The damage style corresponds with the experiment as shown in Figure 5-29.

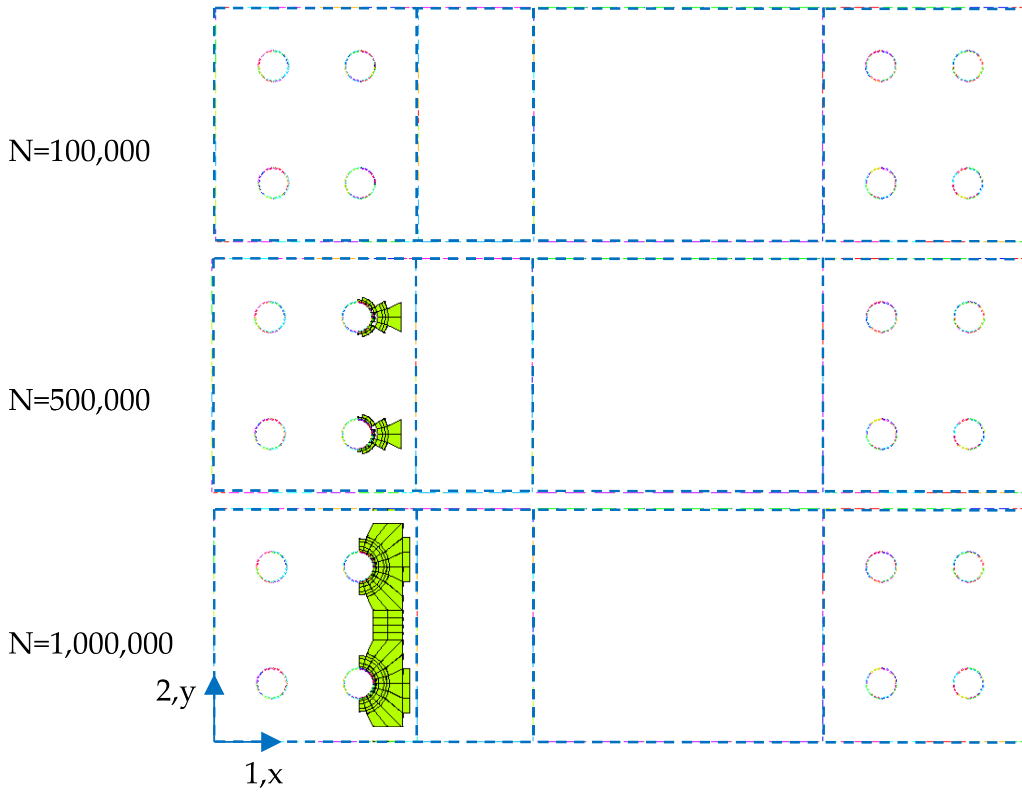

Figure 5-30 Progression of delamination failure in 60-Layer laminate under 60% of deflection level

5.3.2.3. DFM for 70-Layer Laminates

In Chapter 4, the location of the failure initiation was discovered to be the transverse section after the second row of the bolt holes (Section E-E in Figure 5-26). FPDM was examined for the 70-Layer laminates and Figure 5-31 (Middle Picture) shows the transverse cross section corresponding to the failed elements. These elements are those failed under delamination failure mode based on failure equations (Equation (2-7)). The distribution of the failed elements in a parabolic shape from FPDM corresponds with the damage pattern from experiment. These elements are considered as failure initiation elements which happened at around 10,000 cycles for 70_1 specimen under 75% of deflection level.

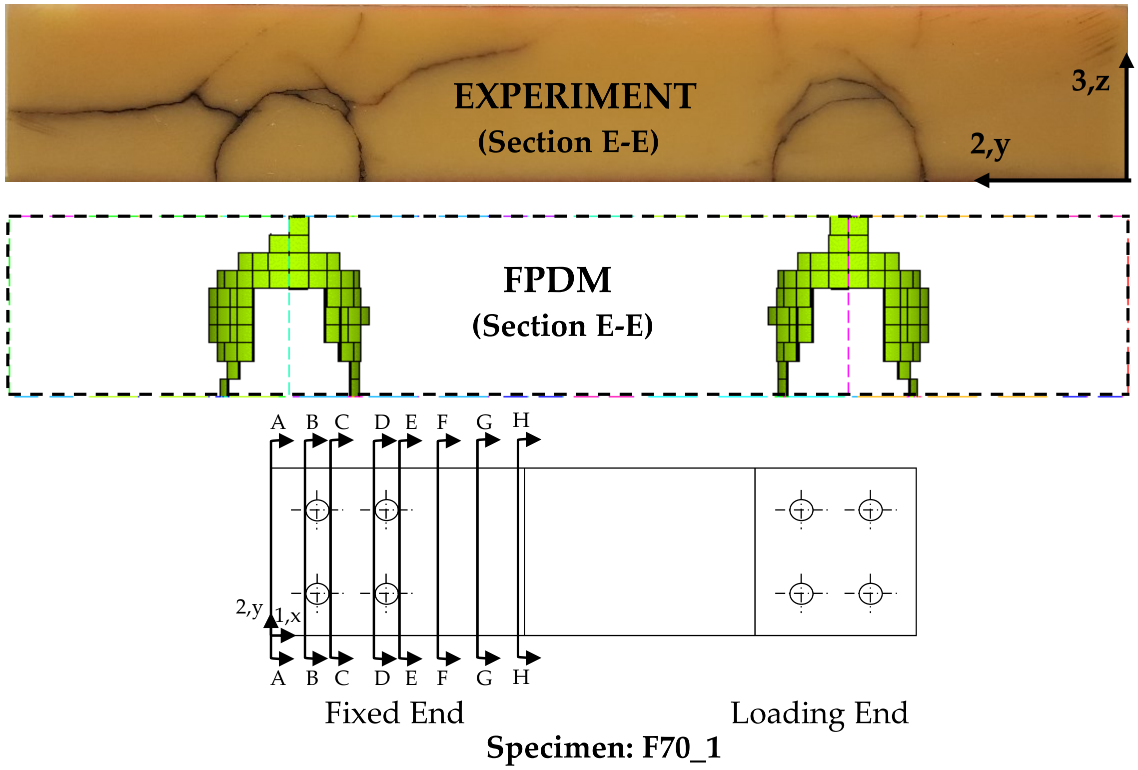

Figure 5-31 Transverse Cuts from the Experiment and FPDM for F70_1 specimen under 75% of deflection level

Figure 5-32 shows the progression of fatigue failure extracted from FPDM for F70_1 laminate which was tested under 75% of deflection level. The figure shows the initiation of failure at the right-hand side of second-row bolt holes at 10,000 cycles. The FPDM was solved until 500,000 cycles as the failure point found from the experiment. Initiated failures propagate towards the loading end of the laminate. However. The failure does not appear on the side surfaces.

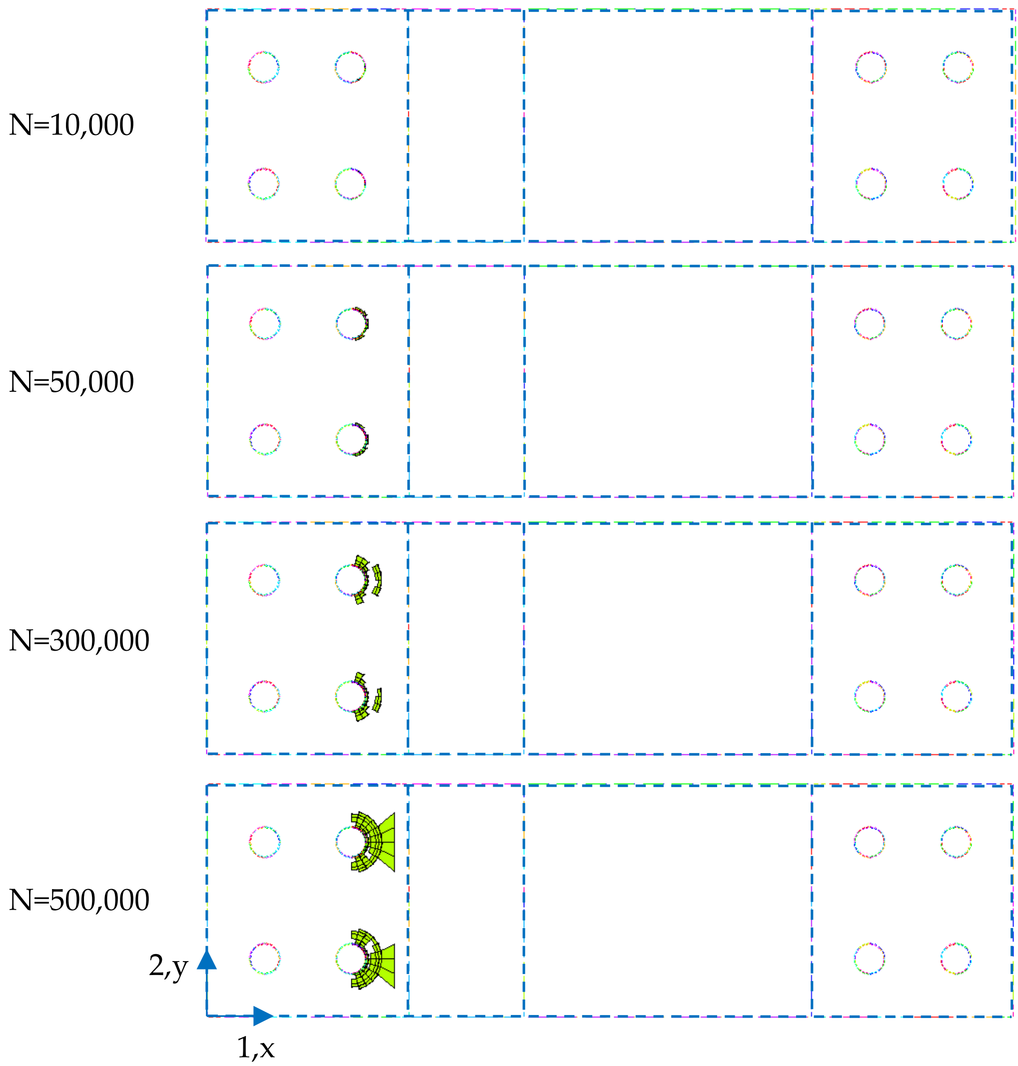

Figure 5-32 Progression of delamination failure in 70-Layer laminate under 75% of deflection level

Figure 5-33 shows three section cuts of F70_5 specimen which failed in fatigue loading under 70% of deflection level. Section D-D is located at the left-hand side of the second row of the bolt holes and Section E-E is located at the right-hand side of the second row of the bolt holes at the fixed end. Section F-F is the section where the crack appears to end. It can be concluded from these sections that the failure initiates from the transverse section at the second row of the bolt holes and it propagates mainly towards the fixed end side (Section A-A) in the form of horizontal delamination. Furthermore, the initiation of delamination from the second row of the bolts corresponds with the damage state which is presented in Figure 5-31.

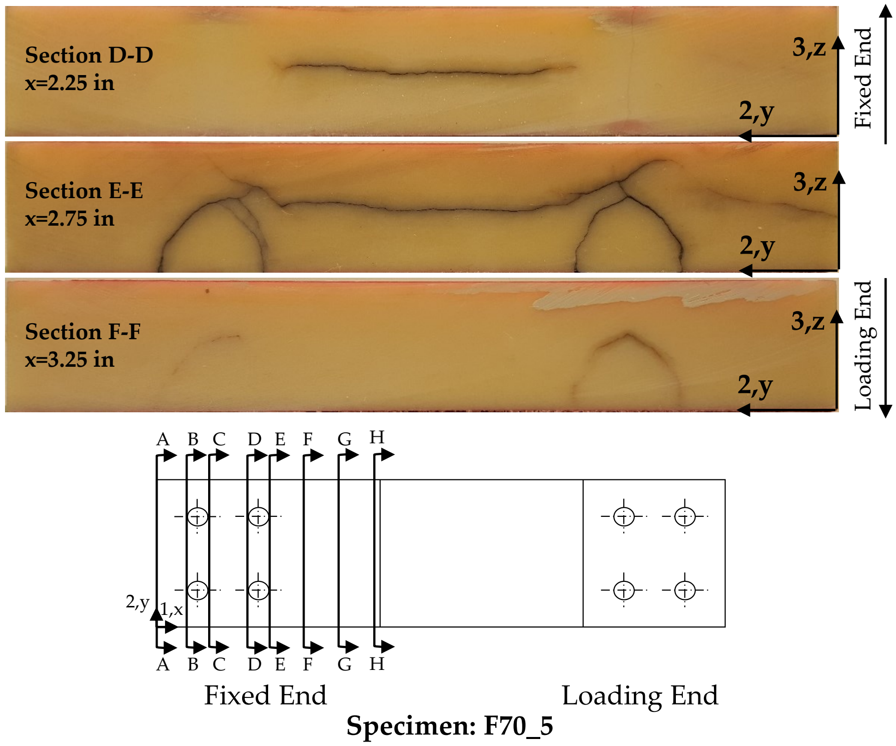

Figure 5-33 Transverse cross sections of F70_5 laminate at three different locations

The section cuts discussed above are used to demonstrate the three-dimensional representation of the internal failure inside the laminate as shown in Figure 5-34. There is a good correspondence between the results of FPDM as mentioned above and the results of experiments as shown in Figure 5-33 and Figure 5-34.

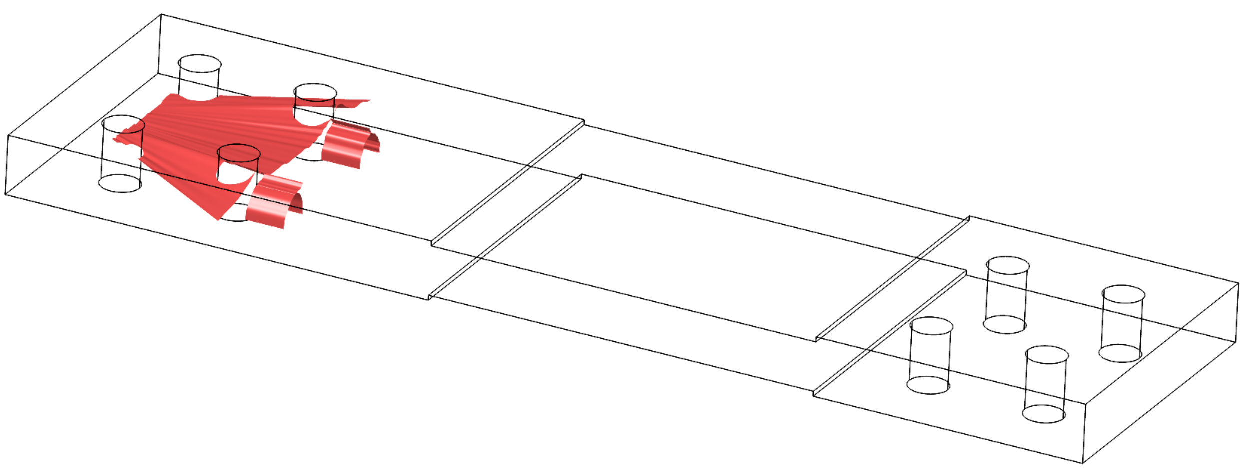

Figure 5-34 Three-dimensional representation of internal cracks for $[0]_{70}$ laminate

5.3.2.4. DFM for 80-Layer Laminates

All deflection levels shown in Table 5-4 are modeled and solved. The average final fatigue life for the largest deflection level of 75% was reported as 110,000 cycles from the experiments. Based on this average final value, the finite element model was solved from 1 to 120,000 cycles with the load step increment of 2,000 cycles. The progression of damage is shown in Figure 5-35. Bolt holes shown in the left of Figure 5-35 are related to the fixed end of the laminate. As indicated in Figure 5-35, at 4,000 cycles, some elements fail around the bolt holes close to the right edge of the steel plate. Based on failure criteria, the majority of elements fail under delamination failure mode. The green elements are those fail under delamination failure mode. The number of failed elements increases until 20,000 cycles. This state of the delamination failure at 20,000 cycles in Figure 5-35 corresponds with the experimental results which showed the first sharp load drop at 20,000 cycles for the laminate under 75% of the deflection level as shown in Figure 5-23. The lower picture in Figure 5-35 shows the state of failed elements at 96,000 cycles which shows the propagation of the delamination towards the fixed end of the laminate.

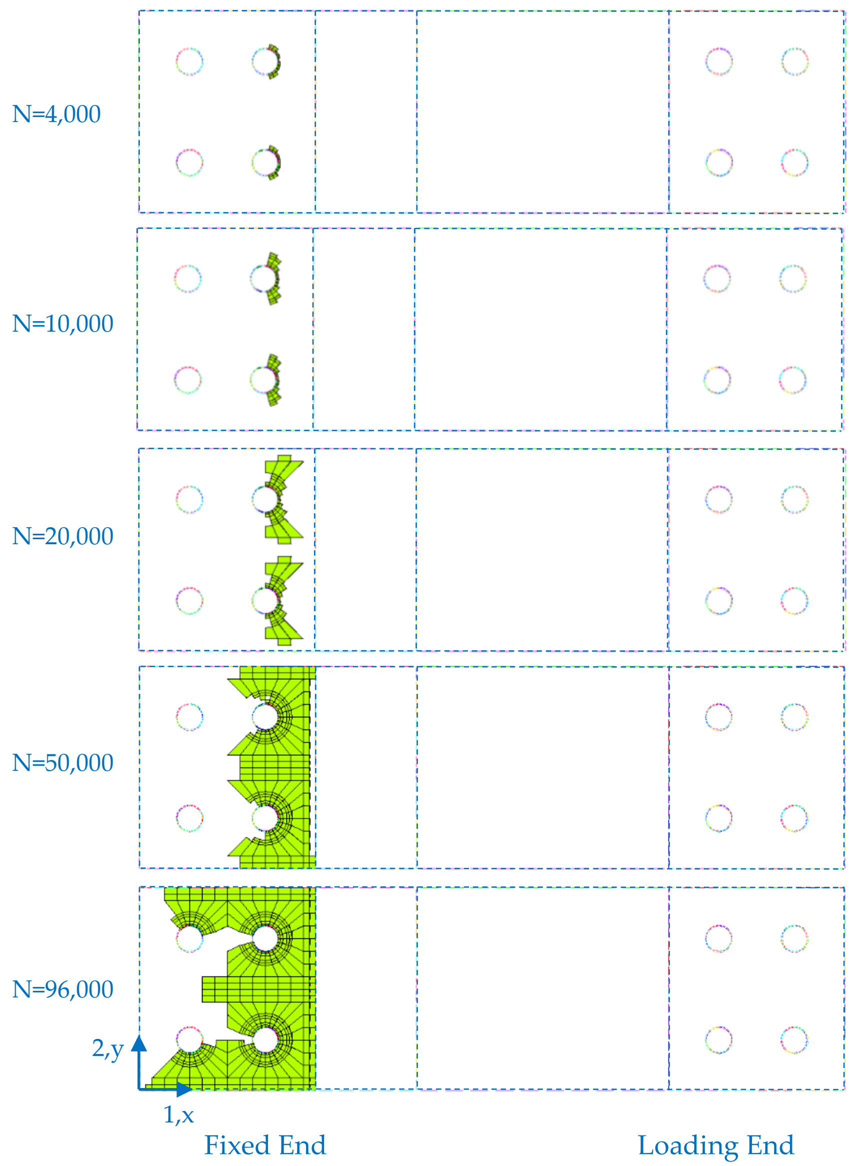

Figure 5-35 Progression of delamination failure in 80-Layer laminate under 75% of deflection level

To explain the reason for occurrence of the delamination in FPDM, one needs to refer back to the Section 2.1.2 Equation (2-7) and Equation (2-8). In numerators of these equations, the stress components are σ_{33} , τ_{13} and $\alpha\alpha\alpha\alpha$. Failure equation stands in the location of maximum stress components as mentioned above. The maximum value for these stress components takes place in the location around the second row of the bolt holes as shown in Figure 5-10. These maximum values for stress components are then applied in the Equation (2-7) and Equation (2-8) which leads to appearance of delamination failure in correspondence with finite element analysis. For this reason, the initiation and propagation of delamination as shown in Figure 5-35 initiates from the second row of the bolt holes.

5.4. Local nature of the cracks

It can be seen from the presented results in current chapter that weak points in the case of thick laminates subjected to bolt load and flexural loading are extremely localized. This is in contrast to the case of thin laminates subjected to fatigue loading where the crack locations may jump from point to point. As such, apart from the shear deformation that needs to be taken into account in the stress analysis, the failure study could be simpler in the thick laminates as compared to the thin laminates. In other words, for the case of thin laminates, the location of failure initiation is not predicted from the beginning of fatigue loading. This makes the failure analysis to be more complicated. In thick laminates however, the probable failure locations are known. This could help to identify the weak locations in order to reinforce them and to have better fatigue loading response.

5.5. Summary

In this chapter the thickness effect was examined by comparing the quasi static and fatigue experimental results of three different thickness-group laminates. The results of quasi static experiments showed that the out-of-plane shear strain on the side surfaces of the laminates increases by increasing of the thickness of the laminates for the same actuator displacement. Furthermore, the finite element analysis of thick laminates under quasi static loading showed that the maximum absolute shear stress in the laminate and maximum out-of-plane normal stress occur around the second row of the bolt holes. Mentioned stress components are the most contributing stress components for the case of delamination failure. Therefore, this area was expected to be the most probable area of fatigue failure initiation.

According to the experimental and numerical results presented in this chapter, following main conclusions can be extracted:

- The numerical results of FPDM for thick laminates show that the dominant failure modes are delamination and shear-out cracks with a localized fashion, corresponding with the results of experiments. The delamination failure also leads to the major drop in the load bearing capacity of the laminates.
- From the experimental results it was observed that for thick laminates the delamination appeared in a range of the thickness from 1/3 to 2/3 of the thickness. The reason was that the maximum values of the out-of-plane normal and shear strain occur in a region between 1/3 and 2/3 of elevation from the bottom.
- The results of finite element progressive damage model show the evolution of damaged elements. The correspondence between these two phenomena, i.e., decreasing of load bearing capacity and decreasing of number of un-damaged elements, shows that the number of un-damaged elements could be taken as an indication of fatigue damage progression in the laminates. This phenomenon is directly related to the stiffness degradation of the whole laminate.
- It can be seen from the above results that weak points in the case of thick laminates subjected to bolt load and flexural loading are extremely localized. This is in contrast to the case of thin laminates subjected to fatigue loading where the crack locations may jump from point to point. As such, apart from the shear deformation that needs to be taken into account in the stress analysis, the failure study could be simpler in the thick laminates as compared to the thin laminates. In other words for the case of thin laminates, the location of failure initiation is not predicted from the beginning of fatigue loading. This makes the failure analysis to be more complicated. In thick laminates however, the probable failure locations are known. This could help to identify the weak locations in order to reinforce them and to have better fatigue loading response.
- Finally, from the agreement between the results of experiments with those of developed fatigue progressive damage model, it is proved that the introduced approach as the application of coupon level fatigue material properties into the 3D finite element model is suitable to study the fatigue behavior of thick composite laminates.

Chapter 6. Summary, Contributions, Publications and Future Work

The aim of this research was experimental and numerical fatigue failure analysis of bolted thick Glass/Epoxy composite laminates for Helicopter Yoke application. The main focus was on the load cycle and location of fatigue failure initiation. Three groups of laminates with different thickness were manufactured and tested under both quasi static and cyclic constant-displacement loading. The behavior of laminates with different thicknesses were examined and compared to determine the thickness effect on the quasi static and fatigue behavior as regards of load bearing capacity and damage mechanisms. Chapter 6 summarizes the main conclusions. Furthermore, the main contributions of this research are stated and the recommendations to proceed the future work are made.

6.1. Summary

According to the research on fatigue behavior of thick composite laminates, following statements are concluded:

- Fatigue life models as the quadratic failure equations can be used for the failure initiation and propagation analysis of thick composite laminates.
- In failure analysis of thick composite laminates, the structural aspect should be taken into account in addition to the material aspect which is in common with thin composite laminates. For this reason, a progressive fatigue damage modeling was developed in order to take both structural and material aspects into account. To respect the material behavior, the material was characterized to find the fatigue behavior of the material itself. For the structural aspect a finite element model was developed to identify the location of failures and damage mechanisms by performing the structural stress analysis in order to find the area of critical locations.
- Hand lay-up and Autoclave manufacturing procedure was used and was able to produce high quality composite laminates. For the case of thick laminates, a suitable bagging procedure was required to be employed. A special bagging procedure was proposed by the industrial partner and employed to manufacture high quality laminates with higher physical and mechanical properties.
- Based on the experiments on thick laminates, the dominant failure modes were observed to be delamination and shear-out cracks in certain locations of the laminates. This means that damage initiation and propagation in thick laminates take place in a localized fashion rather than a global fashion which could happen for thin composite laminates. For the specific laminate structure which was tested in this study, the two dominant failures were observed to initiate from a specific location. The repetition of the same damage style for laminates with different thicknesses proved that for the laminates of the same thickness range, the damage style should be the same. The threshold for the thickness range from thin to thick laminates was not investigated in this research for the specific structure of the laminates. The reason was that the loading setup was not able to read the required higher displacement at 3 (Hz) of frequency for less than 50-layer laminates.

- Based on experimental results, the damage mechanisms of laminates under quasi static loading were different than that of cyclic loadings.
- All Fatigue experiments were performed under displacement control mode. The actuator force versus number of cycles were plotted for all laminates which was called the "load ratio reduction (LRR)" curve. From the load ratio reduction curve, it was observed that the load bearing capacity of the laminates decreased smoothly until damage initiated inside the laminate. From this point the figures showed that the load bearing capacity of the laminates started to decrease drastically until the final failure of the laminates.
- 20% or more decrease in actuator force was taken as indication of a laminate failure. Two other damage initiation indications were first audible sounds during the experiments and second sudden drop in the actuator force.
- Side surface of the laminates under cyclic loading was scanned with thermal camera to obtain the temperature change. There was a drastic temperature increase, i.e. more than 15°C, when the delamination was appeared on the side surface. For temperature changes less than 15°C, delamination was not apparent on the side surface. This concludes that 15°C could be taken as a threshold for the temperature increase above which delamination could appear on the side surface.
- Side surfaces of the laminates were scanned by digital image correlation (DIC) setup. The setup was able to provide all six components of whole field side surface strains. After analyzing the DIC results, among all six available strain components, i.e. three normal and three shear strain components, out-of-plane shear strain seemed to provide useful information about the strain field of the side surfaces.
- It was observed from all fatigue experiments that the maximum out-of-plane shear strain of the side surfaces takes an almost constant trend at the beginning of the cyclic loading and it starts to increase drastically when the delamination reaches the side surface.
- The whole field out-of-plane shear strain contours showed that the maximum region of the shear strain relocates during cyclic loading.
- In most of the experiments the maximum region of the shear strain was well centered on the mid-thickness. However, in some specimens the maximum region of the shear strain

relocated to either upper or lower half-thickness of the laminates where the delamination appeared at the same upper or lower half-thickness.

- In some fatigue experiments the damage pattern in transverse section cuts seemed to be un-symmetric. This fact is because of variabilities that arise in the experiment from either manufacturing or the test setup which makes the failure style to be un-symmetric. The two important variations coming from manufacturing would be first the variation in the thickness of the specimens which could happen because of either non-uniform autoclave pressure on the caul plate at the time of curing or the thickness tolerance of each ply. The second variation could arise from the fact that the drilled holes could be a little off-centered which could lead to have non-uniform bolt-clamping forces. With regards to the test setup, the actuator could be a little off-centered with respect to the longitudinal center line of the specimens. Otherwise the apparent delamination damages shall be completely symmetric. The unsymmetrity of the laminate or the loading setup leads to release of the energy at one side of the laminate by creating new surfaces. The energy release at one side results in no new failure surfaces at the other side of the laminate as shown in the section cuts of tested specimens.
- The results of quasi static experiments showed that the out-of-plane shear strain on the side surfaces of the laminates increases by increasing of the thickness of the laminates for the same actuator displacement. Furthermore, the finite element analysis of thick laminates under quasi static loading showed that the maximum absolute shear stress in the laminate and maximum out-of-plane normal stress occur around the second row of the bolt holes. Mentioned stress components are the most contributing stresses for the case of delamination failure. Therefore, this area was expected to be the most probable area of fatigue failure initiation.
- The numerical results of FPDM for thick laminates show that the dominant failure mode is delamination and shear-out cracks with a localized fashion, corresponding with the results of experiments. The delamination failure also leads to the major drop in the load bearing capacity of the laminates.
- From the experimental results it was observed that for thick laminates the delamination appeared in a range of the thickness from 1/3 to 2/3 of the thickness. The reason was that

the maximum values of the out-of-plane normal and shear strain which occur in a region between 1/3 and 2/3 of elevation from the bottom.

- The thicker the laminate is, the less decrease in load ratio reduction (LRR) is observed for corresponding deflection levels. This could conclude that thicker laminates are less susceptible to degrade under higher deflection levels.
- The “Endurance Deflection Level (EDL)” is higher for thicker laminates. “EDL” is the deflection level below which no damage would initiate inside the laminate.
- The results of finite element progressive damage model show the evolution of damaged elements. The correspondence between these two phenomena, i.e., decreasing of load bearing capacity and decreasing of number of un-damaged elements, shows that the number of un-damaged elements could be taken as an indication of fatigue damage progression in the laminates. This phenomenon is directly related to the stiffness degradation of the whole laminate.
- It can be seen from the results that weak points in the case of thick laminates subjected to bolt load and flexural loading are extremely localized. This is in contrast to the case of thin laminates subjected to fatigue loading where the crack locations may jump from point to point. As such, apart from the shear deformation that needs to be taken into account in the stress analysis, the failure study could be simpler in the thick laminates as compared to the thin laminates. In other words for the case of thin laminates, the location of failure initiation is not predicted from the beginning of fatigue loading. This makes the failure analysis to be more complicated. In thick laminates however the probable failure locations are known. This could help to identify the weak locations in order to reinforce them and to have better fatigue loading response.

6.2. Contributions to the advance of knowledge and technology

The main contributions of this research are:

- A procedure has been developed for the determination of crack initiation of thick composite structures, subjected to fatigue loading. Even though the structure studied is bolted, the analysis can be extended to other support conditions.

- A procedure has been developed for the degradation of the stiffness of thick composite structures, subjected to fatigue loading. Again, even though the structure studied is bolted, the analysis can be extended to other support conditions.

In addition to the main contributions as stated above, following statements summarize the detail contributions to the advance of knowledge and technology:

- A combined material and structural approach was introduced to study the fatigue behavior of thick composite laminates subjected to bolt loads. The first part of the approach comprises the selection of the fatigue life models to study the material aspect of fatigue behavior of thick laminate representing the yoke of helicopter. The second part of the approach comprises a 3D finite element model which takes the structural aspect of fatigue behavior into account. The combination of fatigue material properties, failure equations and the 3D finite element model enables the entire model to include both material and structural aspects in one single fatigue model. From the agreement between the results of experiments with those of developed fatigue progressive damage model, it is proved that the introduced approach as the application of coupon level fatigue material properties into the 3D finite element model is suitable to study the fatigue behavior of thick composite laminates.
- An aerospace grade Glass/Epoxy material was characterized and the quasi static material properties were obtained. Furthermore, the S-N Curves of the material under cyclic loading were obtained and are available to furnish the material properties for further investigations.
- A parametric fatigue progressive damage model (FPDM) was developed and verified against in-house experimental results of 80-layer thick composite laminates. The FPDM as a new model is available to study the fatigue behavior of different lay-up sequence and laminates with different thicknesses. The FPDM is also capable of taking both material and structural aspects into account.
- Different thickness-group laminates were manufactured and tested under quasi static and fatigue loading. The experiments showed that damage mechanisms in thick laminates are presented in a localized fashion which is different than that of thin laminates.

- Effect of thickness on the quasi static and fatigue behavior of the laminates was discussed and the direct relation between the load bearing capacity of the laminates and capability of the laminates to withstand the fatigue flexural loadings was provided.

6.3. Publications

[1] H. Hamidi, W. Xiong*, S.V. Hoa, R. Ganesan*, "Fatigue behavior of thick composite laminates under flexural loading," *Composite Structures,* vol. 200, pp. 277-289, 2018.

[2] H. Hamidi, R. Ganesan, S.V. Hoa, "Thickness effect on fatigue behavior of thick composite laminates under flexural loading,", Composite Science and Technology, To be submitted.

[3] H. Hamidi, S. V. Hoa, R. Ganesan, "Thickness Effect on Dominant Fatigue Failure Mechanisms in Bolted Composite Laminates". MECHCOMP3, 3rd International Conference on Mechanics of Composites, 2017, Italy.

[4] H. Hamidi, S. V. Hoa, R. Ganesan, "Material Characterization for Implementation of Hashin Tri-Axial Fatigue Failure Criteria for Unidirectional Composite Laminates", Proceedings of International workshop on Mechanical behavior of thick composites, Montreal, Canada, DEStech Publications, March 14-15, 2016.

6.4. Future Work

In order to perform further investigation on fatigue failure analysis of thick composite laminates, following research domains are recommended:

- Experimental and numerical fatigue failure analysis of different lay-up sequences than unidirectional laminates which were studied in this research. Common laminates in industry could be selected such as Quasi-Isotropic, Cross–Ply and Angle–ply thick composite laminates.

- Investigating the thickness effect on the fatigue behavior of thick Quasi-Isotropic, Cross–Ply and Angle–ply composite laminates.
- Investigating the effect of loading frequency on fatigue behavior of Unidirectional, Cross-Ply and Angle-Ply thick laminates. This would need to provide a test set-up which is capable of applying different-frequency cyclic loading with respect to large required displacements.
- Investigating the effect of environmental conditioning such as moisture absorption and exposure to higher temperatures in fatigue behavior of thick composite laminates with different thicknesses.

It should be noted that the developed parametric fatigue progressive damage model (FPDM) in this research can be used to analyze different laminate types as mentioned above. However extensive experimental work is required for manufacturing and testing of such laminates.

References

[1] C. Bathias, "An engineering point of view about fatigue of polymer matrix composite materials," *Int. J. Fatigue,* vol. 28, *(10),* pp. 1094-9, 2006. Available: http://dx.doi.org/10.1016/j.ijfatigue.2006.02.008. DOI: 10.1016/j.ijfatigue.2006.02.008.

[2] D. Schutz and J. J. Gerharz, "Fatigue strength of a fibre-reinforced material," *Composites,* vol. 8, *(4),* pp. 245-250, 1977. Available: http://dx.doi.org/10.1016/0010-4361(77)90110-0. DOI: 10.1016/0010-4361(77)90110-0.

[3] Z. Hashin and A. Rotem, "A fatigue failure criterion for fiber reinforced materials," *J. Composite Mater.,* vol. 7, pp. 448-64, 10, 1973.

[4] M. J. Owen and R. J. Howe, "The accumulation of damage in a glass-reinforced plastic under tensile and fatigue loading," *Journal of Physics D (Applied Physics),* vol. 5, *(9),* pp. 1637-9, 1972. Available: http://dx.doi.org/10.1088/0022-3727/5/9/319. DOI: 10.1088/0022-3727/5/9/319.

[5] G. Caprino and A. D'Amore, "Flexural fatigue behaviour of random continuous-fibre-reinforced thermoplastic composites," *Composites Sci. Technol.,* vol. 58, *(6),* pp. 957-65, 1998. Available: http://dx.doi.org/10.1016/S0266-3538(97)00221-2. DOI: 10.1016/S0266-3538(97)00221-2.

[6] C. Bathias, "Fracture and fatigue of high performance composite materials: Mechanisms and prediction," in *Icamp '90,* 1991, Available: http://dx.doi.org/10.1016/0013-7944(91)90234-R. DOI: 10.1016/0013-7944(91)90234-R.

[7] M. N. Bureau and J. Denault, "Fatigue behavior of continuous glass fiber composites: Effect of the matrix nature," in *Polymer Composites '99: International Symposium on Polymer Composites Science and Technology,* 2000, Available: http://dx.doi.org/10.1002/pc.10219. DOI: 10.1002/pc.10219.

[8] M. Hojo *et al*, "Mode I delamination fatigue properties of interlayer-toughened CF/epoxy laminates," *Composites Sci. Technol.,* vol. 66, *(5),* pp. 665-75, 2006. Available: http://dx.doi.org/10.1016/j.compscitech.2005.07.038. DOI: 10.1016/j.compscitech.2005.07.038.

[9] H. Zhuang and J. P. Wightman, "Influence of surface properties on carbon fiber/epoxy matrix interfacial adhesion," *J. Adhesion,* vol. 62, *(1-4),* pp. 213-245, 1997.

[10] H. Thom, "A review of the biaxial strength of fibre-reinforced plastics," *Composites Part A (Applied Science and Manufacturing),* vol. 29A, *(8),* pp. 869-86, 1998. Available: http://dx.doi.org/10.1016/S1359-835X(97)00090-0. DOI: 10.1016/S1359-835X(97)00090-0.

[11] S. V. Hoa, *PRINCIPLES of the MANUFACTURING OF COMPOSITE MATERIALS.* DEStech Publications, 2009.

[12] N. J. Pagano and R. B. Pipes, "The influence of stacking sequence on laminate strength," *J. Composite Mater.,* vol. 5, pp. 50-7, 1971. Available: http://dx.doi.org/10.1177/002199837100500105. DOI: 10.1177/002199837100500105.

[13] J. E. Bailey, P. T. Curtis and A. Parvizi, "On the transverse cracking and longitudinal splitting behaviour of glass and carbon fibre reinforced epoxy cross ply laminates and the effect of Poisson and thermally generated strain," *Proceedings of the Royal Society of London, Series A (Mathematical and Physical Sciences),* vol. 366, *(1727),* pp. 599-623, 1979. Available: http://dx.doi.org/10.1098/rspa.1979.0071. DOI: 10.1098/rspa.1979.0071.

[14] B. Harris, *Fatigue in Composites :Science and Technology of the Fatigue Response of Fibre-Reinforced Plastics.* 2003.

[15] A. P. Mouritz, "A simple fatigue life model for three-dimensional fiber-polymer composites," *J. Composite Mater.,* vol. 40, *(5),* pp. 455-69, 2006. Available: http://dx.doi.org/10.1177/0021998305055199. DOI: 10.1177/0021998305055199.

[16] A. P. Mouritz and B. N. Cox, "A mechanistic interpretation of the comparative in-plane mechanical properties of 3D woven, stitched and pinned composites," *Composites Part A: Applied Science and Manufacturing,* vol. 41, *(6),* pp. 709-728, 2010. Available: http://dx.doi.org/10.1016/j.compositesa.2010.02.001. DOI: 10.1016/j.compositesa.2010.02.001.

[17] A. P. Mouritz, "Review of z-pinned composite laminates," *Composites Part A,* vol. 38, *(12),* pp. 2383-97, 2007. Available: http://dx.doi.org/10.1016/j.compositesa.2007.08.016. DOI: 10.1016/j.compositesa.2007.08.016.

[18] J. Degrieck and W. Van Paepegem, "Fatigue damage modeling of fibre-reinforced composite materials: Review," *Appl Mech Rev,* vol. 54, *(4),* pp. 279-299, 2001.

[19] M. -. R. Jen and C. -. Lee, "Strength and life in thermoplastic composite laminates under static and fatigue loads. I. Experimental," *Int. J. Fatigue,* vol. 20, *(9),* pp. 605-15, 1998. Available: http://dx.doi.org/10.1016/S0142-1123(98)00029-2. DOI: 10.1016/S0142-1123(98)00029-2.

[20] M. -. R. Jen and C. -. Lee, "Strength and life in thermoplastic composite laminates under static and fatigue loads. II. Formulation," *Int. J. Fatigue,* vol. 20, *(9),* pp. 617-29, 1998. Available: http://dx.doi.org/10.1016/S0142-1123(98)00030-9. DOI: 10.1016/S0142-1123(98)00030-9.

[21] T. P. Philippidis and A. P. Vassilopoulos, "Fatigue strength prediction under multiaxial stress," *J. Composite Mater.,* vol. 33, *(17),* pp. 1578-99, 1999. Available: http://dx.doi.org/10.1177/002199839903301701. DOI: 10.1177/002199839903301701.

[22] K. L. Reifsnider and Z. Gao, "A micromechanics model for composites under fatigue loading," *Int. J. Fatigue,* vol. 13, *(2),* pp. 149-56, 1991. Available: http://dx.doi.org/10.1016/0142-1123(91)90007-L. DOI: 10.1016/0142-1123(91)90007-L.

[23] Z. Fawaz and F. Ellyin, "Fatigue failure model for fibre-reinforced materials under general loading conditions," *J. Composite Mater.,* vol. 28, *(15),* pp. 1432-51, 1994. Available: http://dx.doi.org/10.1177/002199839402801503. DOI: 10.1177/002199839402801503.

[24] Y. M. Paramonov, M. A. Kleinhof and A. Y. Paramonova, "Probabilistic model of the fatigue life of composite materials for fatigue-curve approximations," *Mechanics of Composite Materials,* vol. 38, *(6),* pp. 485-92, 2002. Available: http://dx.doi.org/10.1023/A:1021718407399. DOI: 10.1023/A:1021718407399.

[25] K. W. Jeon, K. B. Shin and J. S. Kim, "A study on fatigue life and strength of a GFRP composite bogie frame for urban subway trains," in *11th International Conference on the Mechanical Behavior of Materials, ICM11, June 5, 2011 - June 9,* 2011, Available: http://dx.doi.org/10.1016/j.proeng.2011.04.396. DOI: 10.1016/j.proeng.2011.04.396.

[26] T. Park *et al*, "A nonlinear constant life model for the fatigue life prediction of composite structures," *Advanced Composite Materials,* vol. 23, *(4),* pp. 337-350, 2014. Available: http://dx.doi.org/10.1080/09243046.2013.871172. DOI: 10.1080/09243046.2013.871172.

[27] R. Talreja and C. V. Singh, *Damage and Failure of Composite Materials.* 2012Available: http://dx.doi.org/10.1017/CBO9781139016063. DOI: 10.1017/CBO9781139016063.

[28] R. Talreja, "Fatigue of composite materials: damage mechanisms and fatigue-life diagrams," *Proceedings of the Royal Society of London, Series A (Mathematical and Physical Sciences),* vol. 378, *(1775),* pp. 461-75, 1981. Available: http://dx.doi.org/10.1098/rspa.1981.0163. DOI: 10.1098/rspa.1981.0163.

[29] Z. Hashin, "Fatigue failure criteria for unidirectional fiber composites," *Transactions of the ASME. Journal of Applied Mechanics,* vol. 48, *(4),* pp. 846-52, 1981. Available: http://dx.doi.org/10.1115/1.3157744. DOI: 10.1115/1.3157744.

[30] C. G. Davila, P. R. Camanho and C. A. Rose, "Failure criteria for FRP laminates," *J. Composite Mater.,* vol. 39, *(4),* pp. 323-45, 2005. Available: http://dx.doi.org/10.1177/0021998305046452. DOI: 10.1177/0021998305046452.

[31] C. T. Sun, B. J. Quinn and D. W. Oplinger, "Comparative evaluation of failure analysis methods for composite laminates," Federal Aviation Administration, Tech. Rep. DOT/FAA/AR-95/109, 1996.

[32] A. Puck and H. Schurmann, "Failure analysis of FRP laminates by means of physically based phenomenological models," *Composites Sci. Technol.,* vol. 58, *(7),* pp. 1045-67, 1998. Available: http://dx.doi.org/10.1016/S0266-3538(96)00140-6. DOI: 10.1016/S0266-3538(96)00140-6.

[33] J. A. Epaarachchi and P. D. Clausen, "An empirical model for fatigue behavior prediction of glass fibre-reinforced plastic composites for various stress ratios and test frequencies," *Composites Part A (Applied Science and Manufacturing),* vol. 34A, *(4),* pp. 313-26, 2003. Available: http://dx.doi.org/10.1016/S1359-835X(03)00052-6. DOI: 10.1016/S1359-835X(03)00052-6.

[34] G. P. Sendeckyj, "Fitting models to composite materials fatigue data," American Society for Testing and Materials, USA, Tech. Rep. ASTM STP 734, 1981.

[35] R. J. Huston, "Fatigue life prediction in composites," *Int. J. Pressure Vessels Piping,* vol. 59, *(1-3),* pp. 131-140, 1994.

[36] H. A. Whitworth, "A stiffness degradation model for composite laminates under fatigue loading," *Composite Structures,* vol. 40, *(2),* pp. 95-101, 1997. Available: http://dx.doi.org/10.1016/S0263-8223(97)00142-6. DOI: 10.1016/S0263-8223(97)00142-6.

[37] H. A. Whitworth, "Modeling stiffness reduction of graphite/epoxy composite laminates," *J. Composite Mater.,* vol. 21, *(4),* pp. 362-72, 1987. Available: http://dx.doi.org/10.1177/002199838702100405. DOI: 10.1177/002199838702100405.

[38] C. Wen and S. Yazdani, "Anisotropic damage model for woven fabric composites during tension-tension fatigue," *Composite Structures,* vol. 82, *(1),* pp. 127-31, 2008. Available: http://dx.doi.org/10.1016/j.compstruct.2007.01.003. DOI: 10.1016/j.compstruct.2007.01.003.

[39] W. Zhang *et al*, "A phenomenological fatigue life prediction model of glass fiber reinforced polymer composites," *Materials and Design,* vol. 66, pp. 77-81, 2015. Available: http://dx.doi.org/10.1016/j.matdes.2014.10.036. DOI: 10.1016/j.matdes.2014.10.036.

[40] J. N. Yang *et al*, "A stiffness degradation model for graphite/epoxy laminates," *J. Composite Mater.,* vol. 24, *(7),* pp. 753-69, 1990. Available: http://dx.doi.org/10.1177/002199839002400705. DOI: 10.1177/002199839002400705.

[41] R. Sakin, I. Ay and R. Yaman, "An investigation of bending fatigue behavior for glass-fiber reinforced polyester composite materials," *Materials and Design,* vol. 29, *(1),* pp. 212-217, 2008. Available: http://dx.doi.org/10.1016/j.matdes.2006.11.006. DOI: 10.1016/j.matdes.2006.11.006.

[42] J. Schon, "A model of fatigue delamination in composites," *Composites Sci. Technol.,* vol. 60, *(4),* pp. 553-8, 2000. Available: http://dx.doi.org/10.1016/S0266-3538(99)00156-6. DOI: 10.1016/S0266-3538(99)00156-6.

[43] H. W. Bergmann and R. Prinz, "Fatigue life estimation of graphite/epoxy laminates under consideration of delamination growth," *Int J Numer Methods Eng,* vol. 27, *(2),* pp. 323-341, 1989.

[44] C. Dahlen and G. S. Springer, "Delamination growth in composites under cyclic loads," *J. Composite Mater.,* vol. 28, *(8),* pp. 732-81, 1994.

[45] M. M. Shokrieh and L. B. Lessard, "Multiaxial fatigue behaviour of unidirectional plies based on uniaxial fatigue experiments. I. Modelling," *Int. J. Fatigue,* vol. 19, *(3),* pp. 201-7, 1997. Available: http://dx.doi.org/10.1016/S0142-1123(96)00074-6. DOI: 10.1016/S0142-1123(96)00074-6.

[46] M. M. Shokrieh and L. B. Lessard, "Multiaxial fatigue behaviour of unidirectional plies based on uniaxial fatigue experiments. II. Experimental evaluation," *Int. J. Fatigue,* vol. 19, *(3),* pp. 209-17, 1997. Available: http://dx.doi.org/10.1016/S0142-1123(96)00068-0. DOI: 10.1016/S0142-1123(96)00068-0.

[47] M. M. Shokrieh and L. B. Lessard, "Progressive fatigue damage modeling of composite materials. I. Modeling," *J. Composite Mater.,* vol. 34, *(13),* pp. 1056-80, 2000. Available: http://dx.doi.org/10.1106/NCNX-DXP1-JT6A-E49E. DOI: 10.1106/NCNX-DXP1-JT6A-E49E.

[48] M. M. Shokrieh and L. B. Lessard, "Progressive fatigue damage modeling of composite materials. II. Material characterization and model verification," *J. Composite Mater.,* vol. 34, *(13),* pp. 1081-116, 2000. Available: http://dx.doi.org/10.1106/VVER-UM0W-VVJ2-JGJN. DOI: 10.1106/VVER-UM0W-VVJ2-JGJN.

[49] Wen-Guang Jiang *et al*, "A concise interface constitutive law for analysis of delamination and splitting in composite materials and its application to scaled notched tensile specimens," *Int J Numer Methods Eng,* vol. 69, *(9),* pp. 1982-95, 2007. Available: http://dx.doi.org/10.1002/nme.1842. DOI: 10.1002/nme.1842.

[50] P. W. Harper and S. R. Hallett, "A fatigue degradation law for cohesive interface elements - Development and application to composite materials," *Int. J. Fatigue,* vol. 32, *(11),* pp. 1774-1787, 2010. Available: http://dx.doi.org/10.1016/j.ijfatigue.2010.04.006. DOI: 10.1016/j.ijfatigue.2010.04.006.

[51] M. May and S. R. Hallett, "A combined model for initiation and propagation of damage under fatigue loading for cohesive interface elements," *Composites Part A: Applied Science and Manufacturing,* vol. 41, *(12),* pp. 1787-1796, 2010. Available: http://dx.doi.org/10.1016/j.compositesa.2010.08.015. DOI: 10.1016/j.compositesa.2010.08.015.

[52] M. May and S. R. Hallett, "An advanced model for initiation and propagation of damage under fatigue loading - part I: Model formulation," *Composite Structures,* vol. 93, pp. 2340-2349, 2011. Available: http://dx.doi.org/10.1016/j.compstruct.2011.03.022. DOI: 10.1016/j.compstruct.2011.03.022.

[53] E. Wu and J. R. Reuter, "Crack extension in fiberglass reinforced plastics," University of Illinois, Tech. Rep. 275, 1965.

[54] J. D. Whitcomb, "Analysis of instability- related growth of a through- width delamination," NASA, Tech. Rep. TM 86301, 1984.

[55] N. Blanco *et al*, "Mixed-mode delamination growth in carbon-fibre composite laminates under cyclic loading," *Int. J. Solids Structures,* vol. 41, *(15),* pp. 4219-35, 2004. Available: http://dx.doi.org/10.1016/j.ijsolstr.2003.02.040. DOI: 10.1016/j.ijsolstr.2003.02.040.

[56] (27/01/2011). *Forces Acting on a Helicopter Blade*. Available: http://cesarvandevelde-constructieleer.blogspot.com/2011/01/forces-acting-on-helicopter.html.

[57] A. Gorjipoor *et al*, "**Computational and experimental strain analysis of flexural bending of thick glass/epoxy laminates**," *Composite Structures,* vol. 176, pp. 526-538, 2017.

[58] Z. Hashin, "Failure criteria for unidirectional fiber composites," *Transactions of the ASME. Journal of Applied Mechanics,* vol. 47, *(2),* pp. 329-34, 1980. Available: http://dx.doi.org/10.1115/1.3153664. DOI: 10.1115/1.3153664.

[59] P. Papanikos, K. I. Tserpes and S. Pantelakis, "Modelling of fatigue damage progression and life of CFRP laminates," *Fatigue and Fracture of Engineering Material and Structures,* vol. 26, *(1),* pp. 37-47, 2003. Available: http://dx.doi.org/10.1046/j.1460-2695.2003.00585.x. DOI: 10.1046/j.1460-2695.2003.00585.x.

[60] K. I. Tserpes *et al*, "Strength prediction of bolted joints in graphite/epoxy composite laminates," *Composites Part B: Engineering,* vol. 33, *(7),* pp. 521-529, 2002. Available: http://dx.doi.org/10.1016/S1359-8368(02)00033-1. DOI: 10.1016/S1359-8368(02)00033-1.

[61] T. Kermanidis, G. Labeas and K. Tserpes, "Finite element modeling of damage accumulation in bolted composite joints under incremental tensile loading," in *Proceedings of the Third ECCOMAS Congress, Barcelona,* Spain, 2000, pp. 11-14.

[62] T. Adam *et al*, "Fatigue behaviour of kevlar/carbon hybrid composites." in *International Conference on Fatigue of Engineering Materials and Structures,* 1986, .

[63] T. Adam *et al*, "POWER LAW FATIGUE DAMAGE MODEL FOR FIBRE-REINFORCED PLASTIC LAMINATES," *Proceedings of the Institution of Mechanical Engineers. Part C. Mechanical Engineering Science,* vol. 200, pp. 155-166, 1986.

[64] T. Adam *et al*, "Fatigue life prediction for hybrid composites," *Int. J. Fatigue,* vol. 11, *(4),* pp. 233-7, 1989. Available: http://dx.doi.org/10.1016/0142-1123(89)90306-X. DOI: 10.1016/0142-1123(89)90306-X.

[65] W. Xiong, "Manufacturing and Fatigue Behavior of Thick Glass/Epoxy Composite Beams." , Concordia University, Montreal, QC, Canada, 2017.